IDENTIFICATION, CATEGORIZATION, AND PREDICTION OF DROUGHT IN COLD CLIMATE REGIONS

A Dissertation
Submitted to the Graduate Faculty
of the
North Dakota State University
of Agriculture and Applied Science

By

Mohammad Hadi Bazrkar

In Partial Fulfillment of the Requirements
for the Degree of
DOCTOR OF PHILOSOPHY

Major Department:
Civil and Environmental Engineering

July 2021

Fargo, North Dakota

North Dakota State University
Graduate School

Title

IDENTIFICATION, CATEGORIZATION, AND PREDICTION OF DROUGHT IN COLD CLIMATE REGIONS

By

Mohammad Hadi Bazrkar

The Supervisory Committee certifies that this ***disquisition*** complies with North Dakota State University's regulations and meets the accepted standards for the degree of

DOCTOR OF PHILOSOPHY

SUPERVISORY COMMITTEE:

Dr. Xuefeng Chu
Chair

Dr. Jianglong Zhang

Dr. David R. Steward

Dr. Rhonda Magel

Approved:

July 15, 2021
Date

Dr. Xuefeng Chu
Department Chair

ABSTRACT

To mitigate drought losses, identification, categorization, and prediction of droughts are essential. The objectives of this dissertation research are (1) to improve drought identification in cold climate regions by developing a new hydroclimatic aggregate drought index (HADI) and a snow-based hydroclimatic aggregate drought index (SHADI), (2) to customize drought categorization by considering both spatial and temporal distributions of droughts, and (3) to improve drought prediction by modifying the traditional support vector regression (SVR). R-mode principal component analyses (PCA) are conducted for rainfall, snowmelt, surface runoff, and soil water storage to derive the HADI. Instead of rainfall and snowmelt in the HADI, precipitation and snowpack are used to estimate the SHADI for adding the capability of snow drought identification. Drought frequencies and classes form a bivariate distribution function by applying a joint probability distribution function. A conditional expectation is further used to estimate the probability of occurrence of droughts. To derive variable threshold levels for drought categorization, hierarchical K-means clustering is used. For drought prediction, a change point detection method is employed to split the non-stationary time series into multiple stationary time series. SVR is further performed on each stationary time series to predict drought. The new drought methods were applied to the Red River of the North Basin (RRB). The 1979-2010 and 2011-2016 data obtained from the North American land data assimilation system were used for training and testing, respectively. Precipitation, temperature, and evapotranspiration were selected as the predictors, and the target variables consisted of multivariate HADI and SHADI, bivariate standardized drought indices, and univariate standardized drought indices. The results showed that the new HADI and SHADI, together with the customized drought categorization, were able to provide more accurate drought identification and characterization, especially for cold climate regions. The comparison of the results of the traditional and modified SVR models in the RRB demonstrated better performance of the modified SVR, particularly when drought indices with higher sensitivity to

temperature were used. The methodologies developed in this dissertation research can be used for improving drought identification, categorization, and prediction, as well as further mitigating the potential adverse impacts of droughts.

ACKNOWLEDGEMENTS

First and foremost, I am extremely grateful to Dr. Xuefeng Chu for his invaluable advice, continuous support, and patience during my PhD study. His immense knowledge and plentiful experience have encouraged me in all the time of my academic research and daily life. I would also like to thank my other committee members: Dr. Magel, Dr. Steward, and Dr. Zhang who provided guidance, passion, and support throughout this incredible experience. I am extending many thanks to my friends in the hydrologic modeling group at NDSU, including Mohsen Tahmasebi Nasab, Ning Wang, Lan Zeng, and Kendall Grimm. Additionally, I would like to express gratitude to my friends in Fargo. It is their kind help and support that have made my study and life in the US a wonderful time. Finally, I would like to express my gratitude to my parents, my wife and my children. Without their tremendous understanding and encouragement in the past few years, it would be impossible for me to complete my study.

DEDICATION

To

my family,

Negin, Soren, and Ariana

Without their love and sacrifices

this project would not have been made possible!

TABLE OF CONTENTS

LIST OF TABLES

LIST OF FIGURES

1. GENERAL INTRODUCTION: DROUGHT

Drought with an average annual loss of 9 billion dollars in the U.S. ranks second in natural disasters during the past three decades (NCEI 2019). Thus, drought studies are crucial to water resources planning and management. Drought is defined as anomaly or deviation of hydroclimatic variables from a normal condition (Palmer 1965). Depending on the drought mechanism in each region, different hydroclimatic variables and their anomaly are considered for drought studies. Therefore, selecting the most suitable drought index or indices is important (Staudinger et al. 2014). The values of drought indices, which include a large volume of data, can be converted into drought categories that represent a measure of severity and also facilitate "apple to apple" comparisons over time (NCEI 2019). This conversion facilitates the interpretation of drought indices since it can be easily understood by stakeholders. Drought prediction, which covers a major portion of drought studies, provides early warnings of drought development for stakeholders. Thus, identification, categorization, and prediction of droughts are formed an integrated process that needs to be treated with a holistic view.

1.1. Drought Identification

The first and the most important step in identification of drought is recognition of the drought mechanism (Staudinger et al. 2014). Thus, understanding the dominant hydroclimatic processes and the drought mechanism plays a key role in drought identification. Numerous drought indices have been developed to address different types of drought. Palmer drought severity index (PDSI) (Palmer 1965) is among the first drought indices. PDSI is based on water balance theory considering precipitation, soil moisture, runoff, and potential evapotranspiration. The major drawback of PDSI is its dependency on regional geographical features. Thus, the parameters of PDSI should be calibrated based on regional geographical features (Alley, 1984; Guttman et al., 1992; Karl, 1983, Karl, 1986). To fill this gap and to facilitate the spatial comparisons of PDSI in different regions, a self-calibrating palmer drought

severity index (sc-PDSI) (Wells et al. 2004) was developed. Another shortcoming of PDSI is that it is limited by the shortage of the long-term continuous soil moisture data and the actual evapotranspiration. Moreover, using a two-stage bucket model in calculation of water deficit/surplus conditions is another shortcoming of PDSI. In addition, PDSI is data demanding and computationally intensive. The complicated nature of PDSI necessitates the development of unsophisticated drought indices. The standardized precipitation index (SPI) (McKee 1993) is one of these indices.

SPI developed by McKee (1993) initiated an ongoing cascade of standardized drought indices. SPI is simply calculated by fitting a probability distribution on precipitation time series and further standardizing the cumulative distribution of the best fitted distribution. McKee (1993) suggested the applications of the same methodology to streamflow, reservoir storage, soil moisture, groundwater, and snowpack. Streamflow drought index (SDI) (Nalbantis and Tsakiris 2008), standardized soil moisture index (Xu et al. 2018), and standardized groundwater index (SGI) (Bloomfield and Marchant 2013) were developed accordingly. Standardized runoff index (SRI) (Shukla and Wood 2008), standardized streamflow index (SSFI) (Modarres 2007), and standardized direct runoff index (SDRI) (Bazrkar and Chu 2020) are derivatives of the SDI. Standardized baseflow index (SBFI) (Bazrkar and Chu 2020) was also developed as a representative of the SGI in regions with scarcity of groundwater data. Snow water equivalent as a proxy for snowpack was used in standardized snow water equivalent index (SWEI) developed by Huning and Aghakouchak (2020) to address snow drought. The SWEI or a standardized snowpack drought index can be helpful to monitor drought in cold climate regions, since the dominant hydroclimatic processes in such regions have been neglected in some drought indices such as SPI and PDSI (Guttman et al. 1992 and Dai et al. 2004).

Some studies have been conducted to specifically address drought in cold climate regions (Akinremi and McGinn 1996; Li et al. 2014; Van Loon and Van Lanon 2012; Van Loon et al. 2014; Van Loon et al. 2015; Harpold et al. 2012; Cooper et al. 2016; Dierauer et al. 2019). Cold

climate regions have their unique drought mechanisms. For example, some hydrological droughts that develop in summer can end in summer, but others may continue throughout the winter. In winter, the chances of recovery from a hydrological drought that develops during the previous summer are extremely low, because all precipitation falls as snow, and no water recharge takes place. Therefore, the recession of discharge stays below the threshold until the snowmelt peak in spring. Van Loon and Van Lanen (2012) termed these long multi-season droughts as rain-to-snow-season drought. This type of drought has a larger increase of deficit with duration, especially when snowmelt is delayed. In winter, low temperature and snow, and lack of infiltration, recharge, and discharge result in "cold snow season drought." On the other hand, high temperature in winter and low precipitation (snowfall and rainfall) cause "warm snow season drought." Finally, the lack of snow accumulation due to snowfall deficit or high temperature in winter leads to "snowmelt drought." The effect of seasonality on drought propagation is stronger in cold seasonal climates, where snow accumulation during winter prevents recovery from summer hydrological drought, and deficit increases strongly with duration (Van Loon et al. 2014).

Snowpack, snow accumulation, and snowmelt processes are important for identification of drought in cold climate regions. Snowpack storage was suggested by McKee et al. (1993) for drought analysis. The consideration of snowpack can improve the capability of drought indices for identification of drought especially in cold climates. A deficit in the amount of snowpack causes snow drought. The risk of snow drought has increased due to climate change and global warming so that a shrinkage in average snow cover and montane snowpack has been observed in recent studies (Marty et al. 2017, Sproles et al. 2017, Huning and Aghakouchak, 2018).

The surface water supply index (SWSI) (Shafer and Dezman 1982), aggregate drought index (ADI) (Keyantash and Dracup 2004), standardized melt and rainfall index (SMRI) (Staudinger et al. 2014), and SWEI (Huning and Aghakouchak 2020) consider snowpack, snow water equivalent, and snow melt in identification of hydrologic droughts. SWSI and ADI are

aggregate drought indices. The weighting factors in the SWSI are defined by experts' opinions. The principal component analysis (PCA) is used in the ADI. There are some overlaps among the variables used in the ADI. For example, precipitation and snow water content or streamflow and reservoir storage provide redundant information. The sharp distinction between rainfall and snowfall in cold climate regions is not considered in the ADI. Drought types are ignored in the aggregate drought indices.

1.2. Drought Categorization

Unlike drought identification, a limited number of studies have been conducted on drought categorization. Droughts are categorized based on their intensity and frequency (McKee et al. 1993; Agnew 2000; Svoboda et al. 2002; Steinemann 2003) by defining threshold levels for each drought category. Defining these threshold levels is a crucial process for drought categorization. Arbitrarily-defined (Palmer 1965) or fixed (Nalbantis and Tsakiris 2009) threshold levels based on frequency in time (McKee et al. 1993) and percentile (Svoboda et al. 2002) have been employed in drought studies. Redefining the threshold levels for each region based on the frequencies of the employed drought index and the spatial distribution of droughts is essential (Mishra and Singh 2010; Carrão et al. 2014). Carrão et al. (2014) showed that the drought categorization based on variable threshold levels was more accurate since it considered both geographic locations and time.

1.3. Drought Prediction

Drought prediction is crucial for water resource management. Numerous studies have been done on prediction of drought. Wood et al. (2015) and Hao et al. (2018) reviewed different prospects of drought prediction and concluded that there were fundamental limitations in prediction of onset, termination, and severity of droughts (Wood et al. 2015). According to Hao et al. (2018), drought prediction methods are generally divided into two main categories: dynamical and statistical methods.

Dynamical prediction is to forecast hydroclimatic variables by using predicted climatic variables (e.g. precipitation and temperature) to run the hydrologic models and predict future hydrologic variables (e.g. surface runoff). According to Wood et al. (2015), the current capabilities in climate variables forecast using the North American multi-model ensemble (NMME) showed low skill in summer seasons. Applications of downscaling methods such as Bayesian downscaled climate forecast system version 2 (CFSv2) showed higher correlation and lower errors than ensemble streamflow precipitation (ESP).

Statistical methods include times series, regression, Markov chain, artificial intelligence, conditional probability (Hao et al. 2018). The time series method was employed in different predictors such as 3- and 6-month SPI (Durdu 2010; Mishra and Desai 2005), Palmer drought index (Rao and Padmanabhan 1984), and standardized streamflow index (SSI) (Fernandez et al. 2009; Modarres 2007). The time series method is less attractive due to its major limitation in assuming a linear relationship between predictors and predictands. Despite the existence of the same limitation in linear regression, it was applied to model the relationship between drought indicators and the predictors such as southern oscillation index (SOI) and Pacific decadal oscillation (PDO) in some studies (Barrons and Bowden 2008; Liu and Juarez 2001; Panu and Sharma 2002; Sun et al. 2012). Nonlinear regressions such as locally weighted polynomial regression (LWPR) (Hwang and Carbone 2009; Liu and Hwang 2015) have been developed and applied to remove the shortcoming of linear regression. A logistic regression model can be applied (Hao et al. 2016; Regonda et al. 2006) to predict binary categories of drought (drought/no-drought). In more complex cases (more than two categories like the USDM drought categories: D0 to D4), the ordinal regression model can be used (Hao et al. 2016). Markov chain (MC) was also employed for prediction of drought categories based on the PDSI (Lohani and Loganathan 1997), the SPI (Cancelliere et al. 2007; Paulo and Periera 2007; 2008), and standardized hydrological index (SHI) (Sharma and Panu 2012).

Machine learning or soft computing models have been used for drought prediction to account for the complicated and nonlinear relationships between predictands and predictors. Artificial neural network (ANN) (Mishra and Desai 2006; Mishra et al. 2007; Morid et al. 2007; Barua et al. 2012; Santos et al. 2012; Yang et al. 2015), fuzzy logic (FL), adaptive neuro-fuzzy inference system (ANFIS) (Esfahanian et al. 2016), support vector regression (SVR), support vector machine (SVM) (Ganguli and Reddy 2014), genetic algorithm (GA) or genetic programming (GP), and wavelet transformation (Maity et al. 2016; Ozger et al. 2011) are various types of machine learning.

Local maxima and overfitting are some limitations in ANN. These limitations have been removed in SVM or SVR by using structural risk minimization instead of the empirical one in the ANN. Wavelet transformation method is an alternative method, in which the original series are decomposed into different resolution levels. Different hybrid methods such as wavelet-ANN or SVR (Belayneh et al. 2014; Deo et al. 2016; Kim and Valdes 2003), wavelet-FL (Ozger et al. 2012), and wavelet GP (Mehr et al 2014) have been applied for statistical modeling. Also, there are some other combined models such as ARIMA-ANN (Mishra et al. 2007) and ANN-FL (Bacanli et al. 2009). Ensemble-ANFIS has been employed by Ali et al. (2018) with 10-fold cross validation to forecast the SPI.

Non-stationarity in time series of hydroclimatic variables due to climate change/variability is one of the challenges in drought prediction (Hao et al. 2018). Therefore, it is important to consider non-stationarity to improve drought assessment under climate change (Mukherjee et al. 2018). The performance of drought prediction can be improved by capturing the non-stationary conditions from historical records of hydroclimatic variables (Hao et al. 2018, Brunner et al. 2021).

To assess the predictability skills of drought prediction models, especially the non-categorical models, standard statistical measures are used. Mean absolute error (MAE), mean square error (MSE), root mean square error (RMSE), and coefficient of determination (R2) are

among the performance measures. However, these performance metrics can cause misclassification (or mis-categorization) of droughts since their goals are to reduce the difference between actual and predicted values of drought indices. The predicted mis-categorized drought potentially misleads stakeholders and causes waste of budgets and efforts if they take inappropriate actions against the predicted drought category.

1.4. Research Gaps

To improve drought identification and tailor drought indices to cold climate regions, selection of input hydroclimatic variables need to be customized for such regions. Separation of rainfall and snowfall as well as snowmelt and snowpack need to be considered besides other hydroclimatic variables. To integrate all these hydroclimatic variables, different methodologies have been employed. The copula concept in multivariate standardized drought index (MSDI) (Hao and Aghakouchak 2013), joint deficit index (JDI) (Kao and Govindaraju 2010), and standardized soil moisture index (SSI) (Xu et al. 2018) and P-mode principal component analysis (PCA) in ADI (Keyantash and Dracup 2004) are some examples. In the P-mode PCA, the variations of variables through time are not fully considered. Therefore, the integration methods need to be improved in integrated drought indices. Despite the advantages of the integrated drought indices over the specialized drought indices (Keyantash and Dracup 2004, Van Loon et al. 2016, Bayissa et al. 2018), classification of drought for determination of drought types is neglected in such drought indices. Thus, adding this feature can improve the capabilities of the integrated drought indices.

The frequencies of snow droughts have recently increased due to climate change (Huning and Aghakouchak 2020). However, there are few snow-based drought indices with the capabilities of addressing snow droughts. Moreover, snow-based drought indices and their capabilities for short-term lead prediction of drought are critical under a changing climate (Huning and Aghakouchak 2020; Abel et al. 2018). Livneh and Badger (2020) criticized the

predictability of such snow-based drought indices due to declining future snowpack in a warming climate. Comparison of snow-based drought indices with those that only consider available water can shed lights on this point.

Identification of droughts has been the major focus of drought studies. The application of fixed or arbitrarily-defined threshold levels can result in less accurate drought categorization. The spatial distribution of droughts has been neglected in the existing methodologies for drought categorization. Thus, drought categorization needs to be customized for each location (Mishra and Singh 2010).

Climate change leads to non-stationarity in hydroclimatic time series, which can cause lower predictive skills of drought prediction models (Hao et al. 2018, Brunner et al. 2021). Moreover, application of the standard measures such as MAE, MSE, RMSE, and R2 can result in misclassification in the predicted drought.

1.5. Objectives and Tasks

To fill the gaps in the existing methodologies, the primary objectives of this dissertation research are:

to improve drought identification in cold climate regions

to improve drought categorization

to improve drought prediction under changing climate

To achieve these research objectives, this dissertation research includes the following specific tasks: (1) to develop an integrated hydroclimatic aggregate drought index (HADI) by accounting for the dominant hydroclimatic processes in cold climate regions while considering drought types and target stakeholders; (2) to improve drought identification in cold climate regions and in warming climate by developing a new snow-based hydroclimatic aggregate drought index (SHADI); (3) to customize drought categorization by deriving variable threshold levels, which accounts for both temporal and spatial distributions of droughts; (4) to assess the

impacts of snowpack and snowmelt in drought analyses by comparing SHADI with HADI and PDSI (Palmer 1965); (5) to develop a novel category-based scoring SVR (CBS-SVR); and (6) to improve drought prediction by removing non-stationarity in time series due to a changing climate. The comparisons of the new approaches developed in this dissertation research for drought identification, categorization, and prediction with the existing methods highlight the unique features and new contributions of this research.

1.6. Organization of the Dissertation

The contents of this dissertation are organized into five chapters. Chapter 1 provides a general introduction to identification, categorization, and prediction of droughts. The shortcomings of the available drought indices in identification of drought in cold climate regions and limitations of the existing methodologies for categorization and prediction of drought are presented, which provide a basis for the specific objectives and tasks of this dissertation research.

Chapter 2 introduces two new drought indices, HADI and SHADI. HADI and SHADI are specifically developed to improve drought identification in cold climate regions. In addition to presenting the related methodologies, the capabilities of these two drought indices are tested in the Red River of the North Basin (RRB) and compared with the existing drought indices.

Chapter 3 introduces a novel category-based scoring method for cross validation in a CBS-SVR model and evaluates the impacts of CBS-SVR on the performance of traditional SVR. The application of standard measures for numerical (non-categorical) drought prediction models causes misclassification (mis-categorization). A novel customized drought categorization is developed and used to overcome this shortcoming. The model is applied to the RRB to predict drought. The results of the CBS-SVR are compared with those from the traditional SVR.

Chapter 4 assesses the influences of non-stationarity in temperature datasets due to climate change/variability on drought prediction. A window-based change point detection is

used to identify change points on temperature time series and an ensemble stationary-based SVR (ESSVR) is developed. Finally, the results of ESSVR and SVR are compared.

Lastly, Chapter 5 provides a summary of the conducted studies and highlights the major conclusions, findings, and implications. In addition, future research directions and potential improvements for identification, categorization, and prediction of droughts are briefly discussed.

1.7. References

Agnew CT (2000). Using the SPI to identify drought. Drought Network News. Vol. 12, National Drought Mitigation Center, Lincoln, NE, 6–12. [Available online at http://digitalcommons.unl.edu/cgi/viewcontent.cgi?article51000&context5droughtnetnew]

Akinremi OO, Mcginn SM, Barr AG (1996). Evaluation of the Palmer Drought index on the Canadian prairies. Journal of Climate, 9, 897–905, doi:10.1175/1520-0442(1996)009<0897:EOTPDI>2.0.CO;2

Alley, W.M., (1984). The Palmer drought severity index: limitations and assumptions, J. Clim. Appl. Meteorol., 23 (7), 1100-1109.

Bacanli, U. G., Firat, M., & Dikbas, F. (2009). Adaptive neuro-fuzzy inference system for drought forecasting. Stochastic Environmental Research and Risk Assessment, 23, 1143–1154. https://doi.org/10.1007/s00477-008-0288-5

Barua, S., Ng, A. W. M., & Perera, B. J. C. (2012). Artificial neural network-based drought forecasting using a nonlinear aggregated drought index. Journal of Hydrologic Engineering, 17, 1408–1413. https://doi.org/10.1061/(ASCE)HE.1943-5584.0000574

Bazrkar, M. H. and X. Chu. (2020). A new standardized baseflow index for identification of hydrologic drought in the Red River of the North Basin. Natural Hazards Review, 21(4), 05020011, 1-8, doi:10.1061/(ASCE)NH.1527-6996.0000414.

Belayneh, A., Adamowski, J., Khalil, B., & Ozga-Zielinski, B. (2014). Long-term SPI drought forecasting in the Awash River basin in Ethiopia using wavelet neural networks and wavelet support vector regression models. Journal of Hydrology, 508, 418–429. https://doi.org/10.1016/j.jhydrol.2013.10.052

Bloomfield JP, Marchant BP (2013). Analysis of groundwater drought building on the standardised precipitation index approach, Hydrology and Earth System Sciences. 17(12), 4769–4787, doi:10.5194/hess-17-4769-2013

Brunner, MI, Slater, L, Tallaksen, LM, Clark, M. Challenges in modeling and predicting floods and droughts: A review. WIREs Water. (2021). 8:e1520. https://doi.org/10.1002/wat2.1520

Cancelliere, A., Di Mauro, G., Bonaccorso, B., & Rossi, G. (2007). Drought forecasting using the standardized precipitation index. Water Resources Management, 21(5), 801–819. https://doi.org/10.1007/s11269-006-9062-y

Carrão H, Singleton A, Naumann G (2014). An optimized system for the classification of meteorological drought intensity with applications in drought frequency analysis. Journal of Applied Meteorology and Climatology, 53(8), 1943–1960, doi:10.1175/JAMC-D-13-0167.1

Cattell RB (1952). Factor Analysis: An Introduction and Manual for the Psychologist and Social Scientist. 462, Greenport Press, Westport, Conn

Cooper, M. G., Nolin, A. W., & Safeeq, M. (2016). Testing the recent snow drought as an analog for climate warming sensitivity of Cascades snowpacks. Environmental Research Letters, 11(8), 084009.

Deo, R. C., Tiwari, M. K., Adamowski, J. F., & Quilty, J. M. (2016). Forecasting effective drought index using a wavelet extreme learning machine (W-ELM) model. Stochastic Environmental Research and Risk Assessment, 31(5), 1211–1240.

Dierauer, J. R., Allen, D. M., & Whitfield, P. H. (2019). Snow drought risk and susceptibility in the western United States and southwestern Canada. Water Resources Research, 55. doi: 10.1029/2018WR023229.

Durdu, Ö. F. (2010). Application of linear stochastic models for drought forecasting in the Büyük Menderes River basin, western Turkey. Stochastic Environmental Research and Risk Assessment, 24, 1145–1162. https://doi.org/10.1007/s00477-010-0366-3

Fernández, C., Vega, J. A., Fonturbel, T., & Jiménez, E. (2009). Streamflow drought time series forecasting: A case study in a small watershed in North West Spain. Stochastic Environmental Research and Risk Assessment, 23, 1063–1070. https://doi.org/10.1007/s00477-008-0277-8

Ganguli, P., & Reddy, M. J. (2014). Ensemble prediction of regional droughts using climate inputs and the SVM–copula approach. Hydrological Processes, 28(19), 4989–5009. https://doi.org/10.1002/hyp.9966

Guttman, N. B., J. R. Wallis, and J. R. M. Hosking, (1992). Spatial comparability of the Palmer drought severity index. Water Resour. Bull., 28, 1111–1119.

Hao, Z., Hao, F., Xia, Y., Singh, V. P., Hong, Y., Shen, X., & Ouyang, W. (2016). A statistical method for categorical drought prediction based on NLDAS-2. Journal of Applied Meteorology and Climatology, 55(4), 1049–1061. https://doi.org/10.1175/JAMC-D-15-0200.1

Hao, Z., Singh, V. P., and Xia, Y. (2018). Seasonal Drought Prediction: Advances, Challenges, and Future Prospects. Reviews of Geophysics, 56(1), 108–141, doi: 10.1002/2016RG000549

Harpold, A., et al. (2012). Changes in snowpack accumulation and ablation in the intermountain west, Water Resour. Res., 48, W11501, https://doi.org/10.1029/2012WR011949.

Huning, S. L. and Aghakouchak, A. (2018). Mountain snowpack response to different levels of warming, Proceedings of the National Academy of Sciences, 115(43), 10932-10937.

Hwang, Y., & Carbone, G. J. (2009). Ensemble forecasts of drought indices using a conditional residual resampling technique. Journal of Applied Meteorology and Climatology, 48, 1289–1301. https://doi.org/10.1175/2009JAMC2071.1

Karl T.R. (1986). The sensitivity of the Palmer drought severity index and Palmer's Z-index to their calibration coefficients including potential evapotranspiration, J. Clim. Appl. Meteorol., 25 (1) 77-86.

Karl, T.R. (1983). Some spatial characteristics of drought duration in the United States, J. Clim. Appl. Meteorol., 22 (8) 1356-1366.

Keyantash, J. A., and Dracup, J. A. (2004). An aggregate drought index: Assessing drought severity based on fluctuations in the hydrologic cycle and surface water storage. Water Resources Research, 40(9), 1–14.

Li B, Liang Z, Yu Z, Acharya K (2014). Evaluation of drought and wetness episodes in a cold region (Northeast China) since 1898 with different drought indices. Natural Hazards, 71(3), 2063–2085, doi: 10.1007/s11069-013-0999-x

Liu, Y., & Hwang, Y. (2015). Improving drought predictability in Arkansas using the ensemble PDSI forecast technique. Stochastic Environmental Research and Risk Assessment, 29(1), 79–91. https://doi.org/10.1007/s00477-014-0930-3

Lohani, V. K., & Loganathan, G. (1997). An early warning system for drought management using the Palmer drought index. Journal of the American Water Resources Association, 33(6), 1375–1386. https://doi.org/10.1111/j.1752-1688.1997.tb03560.x

Maity, R., Suman, M., & Verma, N. K. (2016). Drought prediction using a wavelet based approach to model the temporal consequences of different types of droughts. Journal of Hydrology, 539, 417–428. https://doi.org/10.1016/j.jhydrol.2016.05.042

Marty, C., Schlögl, S., Bavay, M., and Lehning, M. (2017). How much can we save? Impact of different emission scenarios on future snow cover in the Alps, The Cryosphere, 11, 517-529, doi:10.5194/tc-11-517-2017.

McKee TB, Doesken NJ, Kleist J (1993). The relationship of drought frequency and duration to time scales. AMS 8th Conference on Applied Climatology, 179–184.

Mishra AK, Singh VP (2010). A review of drought concepts. Journal of Hydrology, 391(1), 202-216, doi:10.1016/j.jhydrol.2010.07.012

Mishra, A., & Desai, V. (2005). Drought forecasting using stochastic models. Stochastic Environmental Research and Risk Assessment, 19, 326–339. https://doi.org/10.1007/s00477-005-0238-4

Mishra, A., & Desai, V. (2006). Drought forecasting using feed-forward recursive neural network. Ecological Modelling, 198, 127–138. https://doi.org/10.1016/j.ecolmodel.2006.04.017

Mishra, A., Desai, V., & Singh, V. P. (2007). Drought forecasting using a hybrid stochastic and neural network model. Journal of Hydrologic Engineering, 12, 626–638. https://doi.org/10.1061/(ASCE)1084-0699(2007)12:6(626)

Modarres, R. (2007). Streamflow drought time series forecasting. Stochastic Environ. Res. Risk Assess. 21 (3): 223–233. https://doi.org/10.1007/s00477-006-0058-1.

Morid, S., Smakhtin, V., & Bagherzadeh, K. (2007). Drought forecasting using artificial neural networks and time series of drought indices. International Journal of Climatology, 27, 2103–2111. https://doi.org/10.1002/joc.1498

Mukherjee S., Mishra A., Trenberth K. E. (2018). Climate Change and Drought: a Perspective on Drought Indices, Current Climate Change Reports, 4:145–163, doi: 10.1007/s40641-018-0098-x

Nalbantis I, Tsakiris G (2009). Assessment of hydrological drought revisited. Water Resources Management, 23(5), 881–897, doi:10.1007/s11269-008-9305-1

NCEI (2019). DROUGHT: Monitoring Economic, Environmental, and Social Impacts., National Centers for Environmental Information, <https://www.ncdc.noaa.gov/news/drought-monitoring-economic-environmental-and-social-impacts> (November 25, 2019).

Özger, M., Mishra, A. K., & Singh, V. P. (2012). Long lead time drought forecasting using a wavelet and fuzzy logic combination model: A case study in Texas. Journal of Hydrometeorology, 13, 284–297. https://doi.org/10.1175/JHM-D-10-05007.1

Palmer WC (1965). Meteorological drought. U.S. Weather Bureau, research paper no. 45

Paulo, A. A., & Pereira, L. S. (2008). Stochastic prediction of drought class transitions. Water Resources Management, 22, 1277–1296. https://doi.org/10.1007/s11269-007-9225-5

Rao, A. R., & Padmanabhan, G. (1984). Analysis and modeling of Palmer's drought index series. Journal of Hydrology, 68(1-4), 211–229. https:// doi.org/10.1016/0022-1694(84)90212-9

Regonda, S. K., Rajagopalan, B., & Clark, M. (2006). A new method to produce categorical streamflow forecasts. Water Resources Research, 42, W09501.

Santos, J. F., Portela, M. M., & Pulido-Calvo, I. (2014). Spring drought prediction based on winter NAO and global SST in Portugal. Hydrological Processes, 28(3), 1009–1024. https://doi.org/10.1002/hyp.9641

Shafer, B. A., and Dezman, L. E. (1982). Development of a surface water supply index (SWSI) to assess the severity of drought conditions in snowpack runoff areas. proceedings of the 50th Annual Western Snow Conference, 164–175.

Sharma, T. C., & Panu, U. S. (2012). Prediction of hydrological drought durations based on Markov chains: Case of the Canadian prairies. Hydrological Sciences Journal, 57, 705–722. https://doi.org/10.1080/02626667.2012.67274

Shukla S, Wood AW (2008). Use of a standardized runoff index for characterizing hydrologic drought. Geophysical Research Letters, 35(2), 1–7, doi:10.1029/2007GL032487

Sproles, E. A., Roth, T. R., and Nolin, A. W. (2017). Future snow? A spatial-probabilistic assessment of the extraordinarily low snowpacks of 2014 and 2015 in the Oregon Cascades, The Cryosphere, 11, 331-341, doi:10.5194/tc-11-331-2017.

Staudinger M, Stahl K, Seibert J (2014). A drought index accounting for snow. Water Resour Res 50(10):7861–7872. https://doi.org/10.1002/2013WR015143

Steinemann A (2003). Drought indicators and triggers: A stochastic approach to evaluation. Journal of American Water Resources Association, 39(5), 1217–1233, doi:10.1111/j.1752-1688.2003.tb03704.x

Sun, M., Ph, D., and Kim, G. (2016). Quantitative Monthly Precipitation Forecasting Using Cyclostationary Empirical Orthogonal Function and Canonical Correlation Analysis. Journal of Hydrologic Engineering, 21(1), 1–13.

Svoboda M, LeComte D, Hayes M, Heim R, Gleason K, Angel J, Rippey B, Tinker R, Palecki M, Stooksbury D, Miskus D, Stephens S (2002). The drought monitor. Bulletin of the American Meteorological Society, 83(8), 1181–1190, doi:10.1175/1520-0477(2002)083<1181:TDM>2.3.CO;2

Van Loon AF, Laaha G (2015). Hydrological drought severity explained by climate and catchment characteristics. Journal of Hydrology, 526, 3–14, doi:10.1016/j.jhydrol.2014.10.059

Van Loon AF, Stahl K, Di Baldassarre G, Clark J, Rangecroft S, Wanders N, Gleeson T, Van Dijk AIJM, Tallaksen LM, Hannaford J, Uijlenhoet R, Teuling AJ, Hannah DM, Sheffield J, Svoboda M, Verbeiren B, Wagener T, Van Lanen HAJ (2016). Drought in a human-modified world: Reframing drought definitions, understanding, and analysis approaches. Hydrology and Earth System Sciences, 20(9), 3631–3650, doi:10.5194/hess-20-3631-2016

Van Loon AF, Van Lanen HAJ (2012). A process-based typology of hydrological drought. Hydrology and Earth System Sciences, 16(7), 1915–1946, doi:10.5194/hess-16-1915-2012, 2012

Van Loon, A. F., E. Tijdeman, N.Wanders, H. A. J. Van Lanen, A.J. Teuling, and R. Uijlenhoet (2014). How climate seasonality modifies drought duration and deficit, J. Geo-phys. Res. Atmos., 119, 4640–4656,doi:10.1002/2013JD020383.

Wells N., S. Goddard, M.J. Hayes. (2004). A self-calibrating Palmer drought severity index, J. Clim., 17 (12) 2335-2351.

Wood, E. F., Schubert, S. D., Wood, A. W., Peters-Lidard, C. D., Mo, K. C., Mariotti, A., and Pulwarty, R. S. (2015). Prospects for Advancing Drought Understanding, Monitoring, and Prediction. Journal of Hydrometeorology, 16(4), 1636–1657.

Xu Y, Wang L, Ross KW, Liu C, Berry K (2018). Standardized soil moisture index for drought monitoring based on soil moisture active passive observations and 36 years of North American Land Data Assimilation System data: A case study in the Southeast United States. Remote Sensing, 10(2), doi:10.3390/rs10020301

Yang, T., Zhou, X., Yu, Z., Krysanova, V., & Wang, B. (2015). Drought projection based on a hybrid drought index using artificial neural networks. Hydrological Processes, 29(11), 2635–2648. https://doi.org/10.1002/hyp.10394

2. DROUGHT IDENTIFICATION IN COLD CLIMATE REGIONS

2.1. Hydroclimatic Aggregate Drought Index (HADI): A New Approach for Identification and Categorization of Drought in Cold Climate Regions [1]

2.1.1. Abstract

Drought identification is crucial to water resources management and planning. Different drought indices have been developed and their complexity and applicability vary. The objectives of this research are to develop a new integrated drought index with the capability of identification of drought and to further customize drought categorization for cold climate regions. Specifically, a new hydroclimatic aggregate drought index (HADI) is developed by coupling with a grid-based hydrologic model and applying the R-mode correlation-based principal component analysis. The HADI is a composite drought index, which assesses the anomalies of rainfall, surface runoff, snowmelt, and soil moisture in the root zone. Furthermore, joint probability distribution function of drought frequencies and classes as well as conditional expectation are used for drought categorization. The HADI was applied to the Red River of the North Basin (RRB) and its performance was evaluated by comparing with the Palmer Drought Severity Index (PDSI) and the U.S. Drought Monitor (USDM) products. Based on the impacts of drought on agriculture, the HADI outperformed the PDSI in identification of droughts in the RRB. Although the HADI and USDM showed a good agreement in identification of drought periods, the drought area coverages for each drought category from the two methods differed. The new customized drought categorization based on variable threshold levels accounted for the variations in both time and geographical locations. The new HADI, together with the customized

[1] The material in this chapter was co-authored by Mohammad Hadi Bazrkar, Dr. Jianglong Zhang, and Dr. Xuefeng Chu. Mohammad Hadi Bazrkar had primary responsibility for developing the new drought index and drought analyses. Mohammad Hadi Bazrkar was the primary developer of the conclusions that are advanced here. Mohammad Hadi Bazrkar also drafted and revised all versions of this chapter. Dr. Xuefeng Chu and Dr. Jianglong Zhang served as proofreader and checked analysis conducted by Mohammad Hadi Bazrkar.

drought categorization, is able to provide more accurate drought identification and characterization, especially for cold climate regions.

2.1.2. Introduction

Drought has many definitions due to its complex nature; however, there is a common phrase in most of them: anomaly or deviation from a normal condition (Palmer 1965). There has been a continuing negotiation on determination of such a normal condition in different places and time periods because of the diversity in climates. For example, normal conditions in cold regions are substantially different from those in other regions. Therefore, in each region, the first and the most important step in identification of drought is recognition of the drought mechanism (Staudinger et al. 2014). Figure 2.1 shows the interactions of different variables in a hydroclimatic system for understanding the mechanisms of different types of drought. In the system, precipitation (rainfall and snowfall) is the main climatic variable and the major variables include snowpack, surface runoff, and soil moisture. Temperature is another climatic variable, and its abnormal rising or falling trends can cause meteorological drought. High temperature increases evaporation from ponding water and reduces surface runoff. Moreover, it enhances evapotranspiration and reduces soil moisture. High temperature also increases snowmelt and surface runoff. After a certain delay, the impacts of climatic variables on surface runoff and soil moisture emerge, which respectively induce hydrologic and agricultural droughts. The red lines in Figure 2.1 show the lag in occurrence of these types of droughts. The sign of (+) or (-) defines direct or inverse relation between variables. The sign of (+) between snowpack and snowmelt indicates that snowpack potentially is a source of snowmelt. Thus, understanding the dominant hydroclimatic processes and the drought mechanism in cold climate regions is crucial to defining normal conditions and further identifying droughts in such regions.

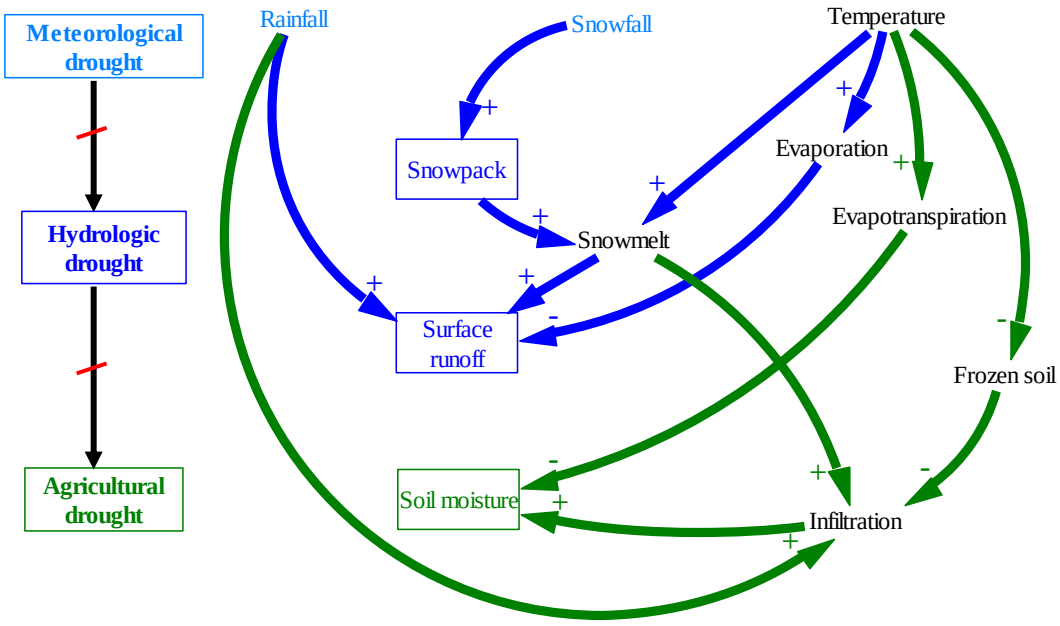

Figure 2.1. Mechanism of different types of droughts and the associated interactions of hydroclimatic variables (signs (+) and (-) respectively refer to direct and inverse relationships between the variables; the red line indicates a delay in the occurrence of droughts, and colors of light blue, dark blue, and green are associated with meteorological, hydrologic, and agricultural drought types).

Some studies have been conducted for drought identification specifically for cold climate regions. Akinremi and McGinn (1996) evaluated the performance of the Palmer drought severity index (PDSI) (Palmer 1965) for the Canadian Prairies. Li et al. (2014) evaluated the performance of different drought indices in a cold climate region in Northeast China. Van Loon and Van Lanon (2012) and Van Loon et al. (2015) qualitatively analyzed drought in cold climates and reframed drought classification based on drought drivers. For instance, a prolonged rainfall deficit causes “classical rainfall deficit drought”. A rainfall deficit in summer and winter besides low temperature during winter that causes surface and subsurface water shortage brings about “rain to snow season drought.” In winter, low temperature and snow, and lack of infiltration, recharge, and discharge result in “cold snow season drought.” On the other hand, high temperature in winter and low precipitation (snowfall and rainfall) cause “warm snow season drought.” Finally, the lack of snow accumulation due to snowfall deficit or high temperature in

winter leads to “snowmelt drought.” Such a drought class accentuates the importance of snowpack in identification of drought in the cold regions with snow accumulation and snowmelt processes. In addition, snowpack storage was suggested by McKee et al. (1993) for drought analysis by employing the same method. The consideration of snowpack can improve the capability of drought indices in identification of drought especially in cold climates.

The surface water supply index (SWSI, Shafer and Dezman 1982) is among the first attempts to consider snowpack in the identification of hydrologic droughts. Although this index accounts for snowpack besides precipitation, streamflow, and reservoir storage, it does not consider soil moisture and evaporative losses. Keyantash and Dracup (2004) developed the aggregate drought index (ADI) by considering not only snowpack but also precipitation, evapotranspiration, streamflow, reservoir storage, and soil moisture content. Snow water content is the representative of snowpack in the ADI. Shukla and Wood (2008) developed the standardized runoff index (SRI) for the regions with snowmelt. Moreover, snow, as a dominant type of precipitation in cold climate regions, should not be neglected in drought identification because of its impact on available water. Thus, the investigations of anomalies of rainfall and precipitation substantially differ. To solve this problem, Staudinger et al. (2014) developed a standardized melt and rainfall index (SMRI) calculated by employing the same methodology as the SPI. But it was based on the daily sum of snowmelt and rain. Daily snowmelt values were obtained by a snow model, which simulated (1) snow accumulation based on a threshold temperature and (2) snowmelt based on a degree-day approach. In addition to the SMRI, the Sahelian standardized rainfall index (Ali and Lebel 2009), rainfall anomaly index (RAI) (Tilahun 2006), and the modified RAI (Hänsel et al. 2016) are also rainfall-related drought indices.

Drought is a multi-temporal phenomenon. If a drought index is solely based on one climatic driver, consideration of different time scales (e.g., 3-month, 6-month, 9-month, 12-month) is inevitable to compensate the lag between the onset of the drought driver and the

observations of the drought impacts on different hydroclimatic variables. For example, the 3-month SPI is based on the accumulated values of precipitation for a sequence of three months. In this index, the impacts of precipitation deficit on other hydrologic variables such as streamflow and soil moisture are reflected indirectly using time scales. In addition, the employment of statistical distributions requires long-term time series (at least 30 years, McKee et al. 1993). Wu et al. (2005) showed that the SPI values were different when different lengths of data were used. Furthermore, none of the specialized drought indices can individually identify a drought and its severity, onset, and duration (Keyantash and Dracup 2004, Van Loon et al. 2016, Bayissa et al. 2018). Therefore, integrated (combined) drought indices can be employed to overcome these limitations. Two approaches are generally used to develop integrated indices: (1) composite (hybrid) indices and (2) aggregate indices.

Composite drought indices are a combination of different indices such as hybrid drought index (HDI) (Karamouz et al. 2009) and multivariate standardized drought index (MSDI) (Hao and Aghakouchak 2013). The HDI combined the SPI, SWSI, and PDSI and different weighting factors were determined based on the magnitude of damage to the surrounding environment caused by drought (Karamouz et al. 2009). The copula concept was used for calculation of the MSDI, which was based on the SPI and the standardized soil moisture index (SSI) (Xu et al. 2018). However, calculations of these two separate indices (i.e., SPI and SSI) and their combined index (i.e., MSDI) make the index-based drought assessment more complicated. Figure 2.2 shows the classification of drought indices based on the number and type of components and their employed methodologies.

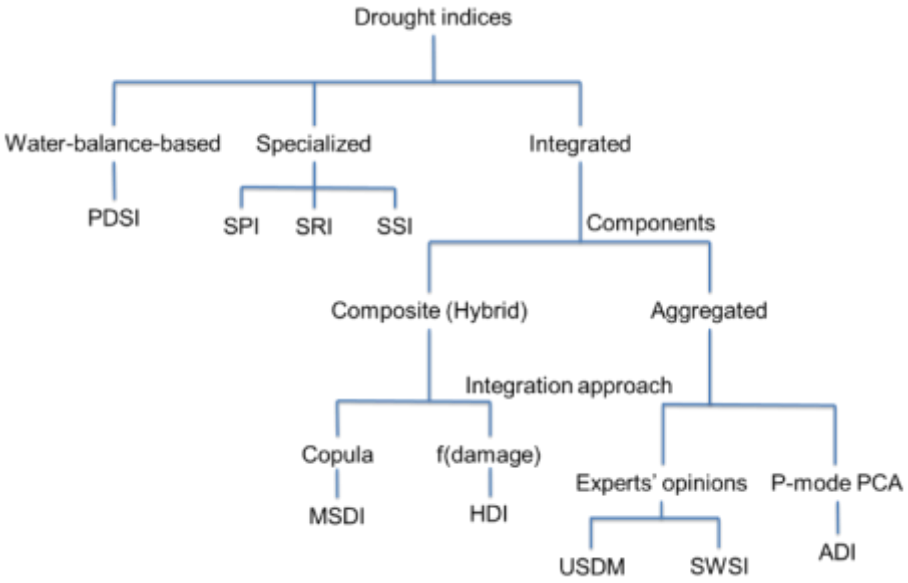

Figure 2.2. Classification of drought indices based on their components and methodologies

In the aggregation approach, the original values (e.g., copula-based joint deficit index (JDI), Kao and Govindaraju 2010), or the probability of non-exceedance (e.g., SWSI, Shafer and Dezman 1982), or the standardized anomalies (e.g., ADI, Keyantash and Dracup 2004) of different hydroclimatic variables are integrated to derive one index. The methodology employed for aggregation and the weighting factors in the derivation are of great importance. Precipitation and streamflow data are used for the JDI estimated by the copula approach (Kao and Govindaraju 2010). The weighting factors were defined by experts' opinions and used in the SWSI after adjusting to the actual situation and fitting to the normal distribution (Shafer and Dezman 1982). The principal component analysis (PCA) is another methodology to reduce dimensions. There are six basic operational modes of the PCA (i.e., O, P, Q, R, S, and T), each of which addresses a different combination of time, objects, and attributes (variables) (Richman 1986). The P-mode PCA (time versus attributes) is used in the ADI. The attributes in the ADI are standardized anomalies of the hydroclimatic variables including precipitation, evapotranspiration, streamflow, reservoir storage, soil moisture content, and snow water content. In the P-mode PCA, the variations of variables through time are not fully considered. In

this method, the weighting coefficients are defined by conducting the PCA for the variables on a specific month in different years. In addition, there are some overlaps among the variables used in the ADI. Although the PCA is responsible for removing redundant information, the user can avoid this overlap in input data before implementing the PCA. For example, precipitation and snow water content or streamflow and reservoir storage provide redundant information. Moreover, the selection of input data in the ADI focuses on general types of water resources rather than available ones. For instance, the sharp distinction between rainfall and snowfall in cold climate regions is not considered in the ADI.

Based on the types of impacts or the related variables, drought can also be classified into meteorological drought, hydrologic drought, agricultural drought, and socio-economic drought (Zargar et al. 2011). Each drought type has a different time scale (Wilhite and Grantz, 1985; Mishra and Singh, 2010) and each specialized drought index accounts for a specific drought type. For example, the SPI addresses precipitation-related meteorological droughts. Thus, simultaneous applications of different drought indices are common in drought analyses. For example, Sawada et al. (2014) quantified the meteorological, agricultural, and hydrological droughts by using three different indices. Integrated drought indices can also be used to simultaneously address different types of droughts. However, drought types, which are defined for the targeted stakeholders, are ignored in the process of integration. For example, the HDI or SWSI provides more general information about droughts rather than a specific drought type. Therefore, finding a solution to address drought types in integrated drought indices can be helpful in improving classification of droughts.

The major focus of drought studies has been on improving identification of droughts by using various indices rather than drought categorization (drought threshold levels). Droughts can be categorized based on their intensity and frequency (McKee et al. 1993, Agnew 2000, Svoboda et al. 2002, Steinemann 2003). For drought severity categorization, defining a threshold is a crucial process. Fixed threshold levels are often employed in drought studies. For

example, McKee et al. (1993) and Palmer (1965) categorized droughts into mild, moderate, severe, and extreme levels according to their frequencies using “arbitrarily-defined” threshold levels (McKee et al. 1993). McKee et al. (1993) used the SPI frequency threshold values of 2.3%, 4.4%, 9.2%, and 24% to respectively define extreme, severe, moderate, and mild drought categories. Wilhite et al. (2000) found that these threshold levels were acceptable and in accordance with water planning. For example, they argued that the occurrence of about 2 to 3 times for the SPI values less than -2.00 over 100 years was acceptable for the extreme drought category. The SPI values of -1.50, -1.00, and 0 were respectively the thresholds for severe, moderate, and mild drought categories. Wilhite et al. (2000) also considered the consistency of the frequencies in defining drought categories for any time and location as one of the advantages of the SPI. Following Wilhite et al. (2000), Nalbantis and Tsakiris (2009) used the similar threshold levels for drought categorization for a basin in Greek. However, their proposed threshold levels were defined based on the frequencies of SPI values, which were derived by McKee et al. (1993) in Fort Collins, Colorado, USA. It is essential to redefine the threshold levels for each region based on the frequencies of the employed drought index. Furthermore, the spatial distribution of droughts was implicitly considered in deriving the fixed threshold levels since the frequency in time varies with locations. Thus, in addition to the temporal distribution of droughts, an explicit consideration of the spatial distribution can result in higher accuracy in drought categorization. Although the long-established and time-honored drought categorization should not be considered as the ultimate standard (Keyantash and Dracup, 2004), other drought analyses followed the same procedure (e.g., Shukla and Wood 2008). In the U.S. drought monitor (USDM), Svoboda et al. (2002) employed the percentile method to define the category thresholds, which is easy to interpret and similar to the rating method for hurricanes. For example, D1 is for less intense and more common drought, while D4 represents the most severe and rare drought. Although these available drought categorization approaches and their related thresholds are frequently employed in drought studies, the threshold levels should be

customized for different hydroclimatic regions (Mishra and Singh 2010; Carrão et al. 2014). Tabular accuracy index (TAI) showed that the drought categorization based on variable threshold levels, instead of the fixed ones, was more useful since it considered both geographic locations and time (Carrão et al. 2014). Carrão et al. (2014) employed the Fisher_Jenks algorithm in their new optimized categorization approach.

To fill the aforementioned gaps in drought analyses, developing a new methodology to integrate different hydrologic processes unique to cold climate regions is inevitable. In this regard, there is room for improvement in selection of input hydroclimatic variables, the integration methodologies, characteristics of drought types, and drought categorization, especially for cold climate regions. The objectives of this research are (1) to develop an integrated hydroclimatic aggregate drought index (HADI) by considering the dominant hydroclimatic processes in cold climate regions while considering drought types and target stakeholders, and (2) to customize drought categorization by deriving variable threshold levels, which accounts for both temporal and spatial distributions of droughts.

2.1.3. Methodology

In this study, the HADI was developed to investigate the anomalies of available water. The variables selected for the HADI include rainfall, surface runoff, snowmelt, and soil moisture, which are directly associated with meteorological, hydrologic, and agricultural droughts in cold climate regions (Zargar et al. 2011). The input data for calculating HADI are listed in Table 2.1. Precipitation is the water source of a hydrologic system. Rainfall is selected since it is an accessible source of water. Since the water of snowpack can be accessible later in spring after it melts down, snowmelt was considered in the derivation of the HADI. Surface runoff is routed to streams. Soil water storage is the water source of plants in agriculture. Therefore, anomalies of rainfall, snowmelt, surface runoff, and soil water storage were investigated. These input data of the HADI were obtained from a macro-scale grid-based

hydrologic model (GHM) (Chu et al. 2018). The GHM simulated the dominant hydroclimatic processes in cold climate regions such as snow, snow accumulation, frozen soil, and snowmelt (Chu et al. 2018) and provided the outputs with a 4-km spatial resolution (i.e., 4 × 4 km grid) and a daily time interval. The daily outputs of the GHM were converted to monthly time series, which were further used for drought analysis. Figure 2.3 shows the flowchart of the HADI calculation, which consists of three main steps: preparation of input data (GHM simulation), calculation of the HADI, and drought categorization.

Table 2.1. Input data for calculating HADI

Variable	**Acronym**
Rainfall	RF
Snowmelt	SM
Soil water storage	SWS
Surface runoff	R

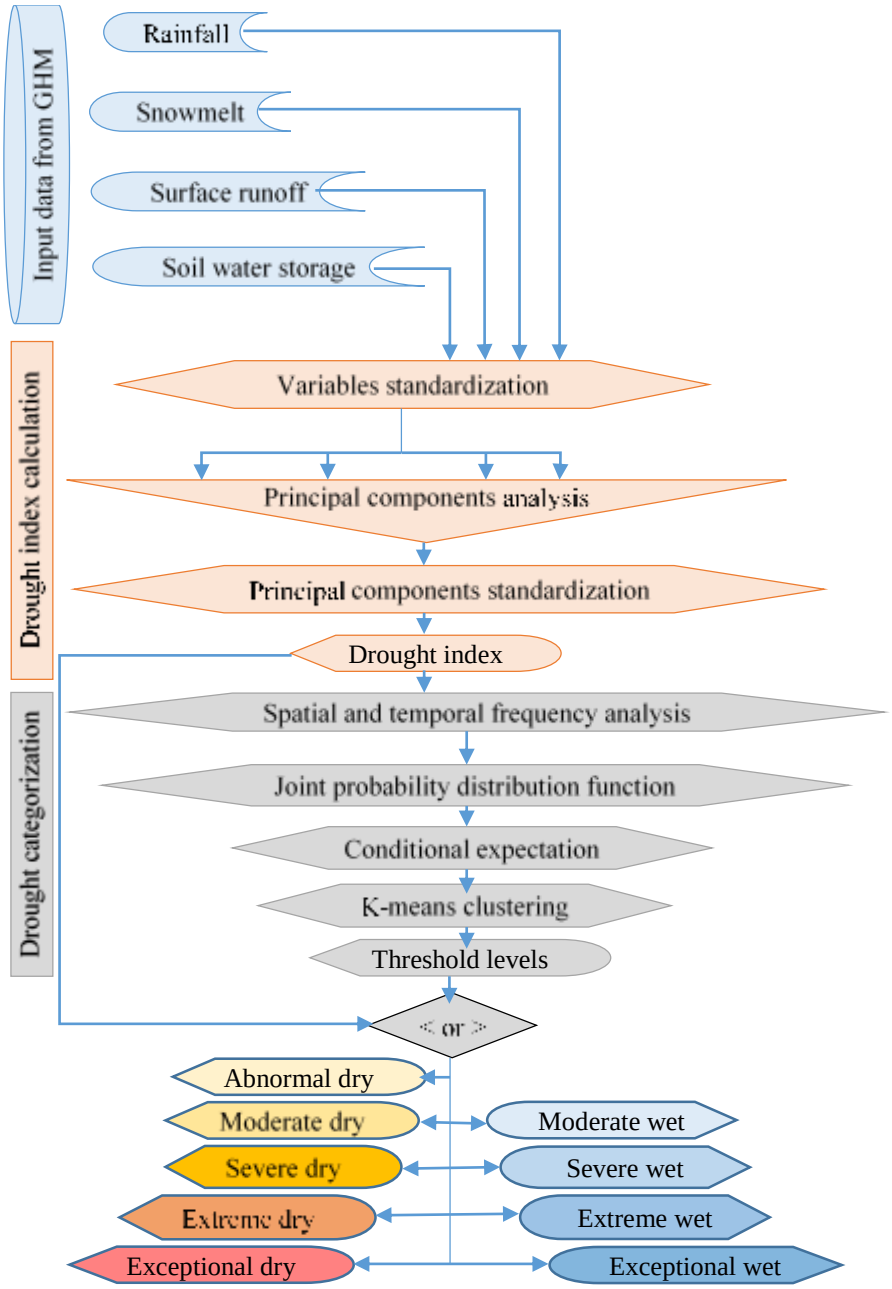

Figure 2.3. Flowchart for the HADI calculation and drought categorization

2.1.3.1. Study Area

The Red River of the North Basin (RRB) (Figure 2.4) is located in the Northern Glaciated Plains ecoregion in the central and eastern part of North Dakota (ND), central and western part of Minnesota (MN), and the northern part of South Dakota (SD). The climate of the Northern Glaciated Plains is categorized within the continental climate with warm summers and cold

winters (Tollerud et al. 2018). The average annual precipitation in the Northern Glaciated Plains ecoregion varies from 380 to 760 mm and exhibits an increasing spatial pattern from northwest to southeast (HPRCC 2018). Figure 2.4 shows the RRB and its location in the U.S. as well as its associated climate divisions (CDs) in ND, MN, and SD. Cultivated areas, grasslands, wetlands, and water are the main land use and land covers in the area. In addition, a major portion of the area is within the Prairie Pothole Region (PPR) (Habtezion et al. 2016; Tahmasebi Nasab et al. 2018). Agricultural land is the most common land use (about 60% of the RRB (within the US), Fry et al. 2011), which can be affected by drought. According to the U.S. drought portal and the USDM, a long drought occurred from 2002 to 2005 for 162 weeks. The basin was also prone to floods due to heavy snowmelt in early spring (Tahmasebi Nasab et al. 2018). Because of the abovementioned hydroclimatic features, the RRB is particularly prone to the risks of both flood and drought and, hence, the analysis of extreme climate conditions is essential to the RRB. Thus, the RRB and the period of 2003 to 2007 were selected to evaluate the performance of the HADI in identification of droughts in the cold climate region. Figures 2.4b – 2.4f show the average annual precipitation distributions in 2003-2007, respectively. The lowest amount of precipitation occurred in 2003 and 2006. In addition, the precipitation in the western part of the RRB was lower than that of the eastern part. Figures 2.4g – 2.4k show the spatial distributions of mean annual temperature in 2003-2007. The lowest and highest temperatures were recorded in 2004 and 2006, respectively.

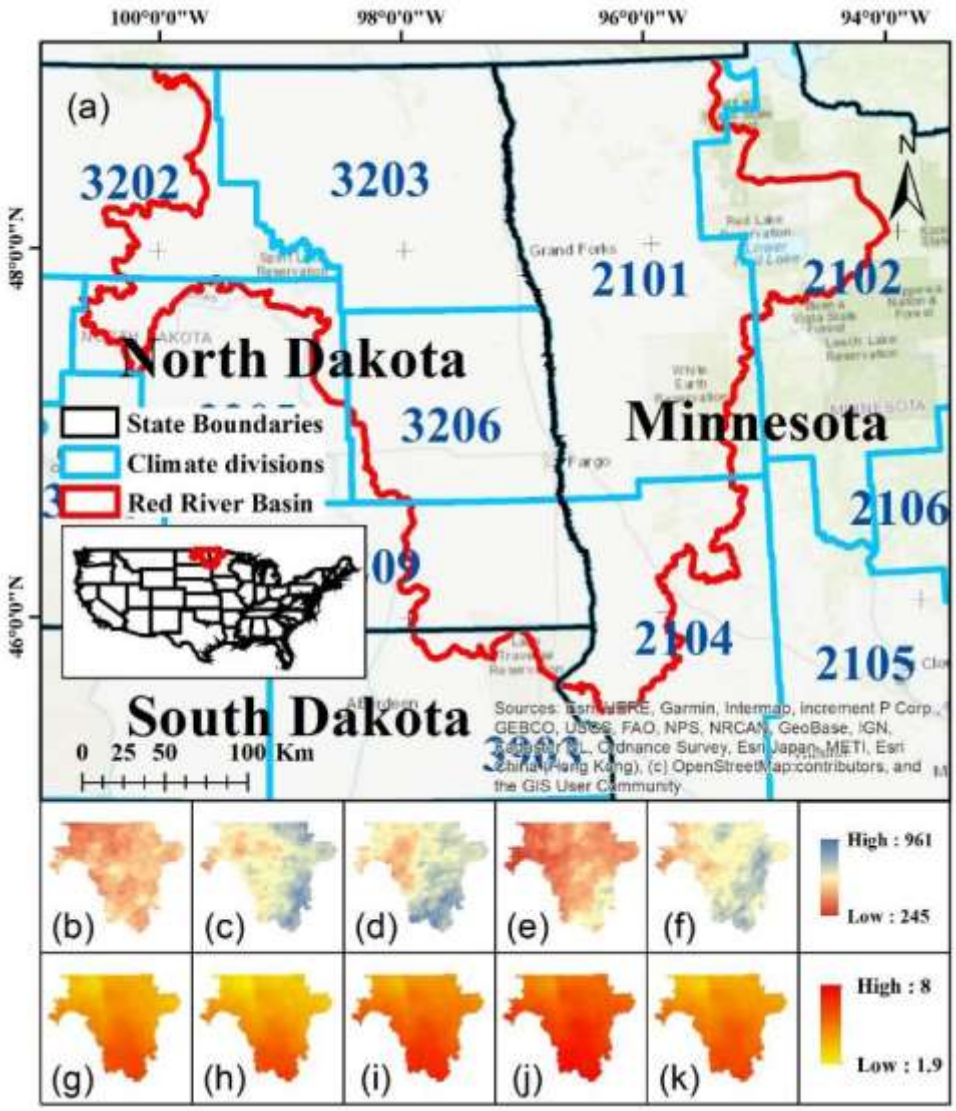

Figure 2.4. (a) RRB, its location in the U.S., and its associated climate divisions, (b-f) average annual precipitation (mm), and (g-k) mean annual temperature (°C) from 2003 to 2007

2.1.3.2. Introduction to GHM

As the main water source in the hydrologic cycle, precipitation is one of the most important variables considered in most of the available drought indices. However, one fact, which is essential especially in cold climates, has been neglected in previous studies (e.g., SPI, McKee et al. 1993). The major portion of precipitation in cold climates is snow. It accumulates in the snowpack, and it is out of reach for usage until it melts in spring. In the GHM, precipitation is separated into snowfall and rainfall by considering a user-defined single temperature

threshold (Chu et al. 2018). The total monthly rainfall data were used in the calculation of the HADI.

In the GHM, snowmelt was simulated by using a degree-day method. Snowmelt initiates when the mean temperature is higher than a user-defined threshold temperature (Chu et al. 2018). The snowmelt amount may deviate from the normal condition due to the lack of snow in the entire winter or occurrence of snowmelt in an inappropriate time in spring (earlier or later than the usual time). In this research, the accumulated monthly snowmelt was used to evaluate the anomaly in snowmelt.

Surface runoff, another source of available water, is employed for identification of hydrologic drought in the HADI. The water mass balance of the surface zone used in the GHM for each grid and each daily time step can be expressed as (Chu et al. 2018):

$$\Delta S_{d\,j,t} = RS_{j,t} + SM_{j,t} - R_{j,t} - I_{j,t} - E_{j,t} \tag{2.1}$$

where $RS_{j,t}$ is the total rainfall reaching the soil surface (mm), $SM_{j,t}$ is the snowmelt (mm), $R_{j,t}$ is surface runoff (mm), $I_{j,t}$ is the infiltration (mm), $\Delta S_{d_{j,t}}$ is the change in depression storage (mm), and $E_{j,t}$ is the evaporation from ponded water (mm) in grid j at daily time step t. The monthly surface runoff, obtained from the summation of the daily surface runoff simulated by the GHM, was applied for the derivation of the HADI. Note that surface runoff anomalies from the normal condition were assessed in the SRI and the NLDAS with a 1/8th-degree spatial resolution was employed (Shukla and Wood 2008). In the current research, the GHM provides surface runoff with a higher resolution.

The identification of agricultural drought is based on the anomalies in soil moisture in this study. The water mass balance of the root zone in the GHM can be written as (Chu et al. 2018):

$$\Delta S_{rz\,j,t} = Per_{ts\,j,t} - ET_{j,t} - Per_{vz\,j,t} \tag{2.2}$$

where $\Delta S_{rz_{j,t}}$ is the soil water storage change in the root zone, $Per_{ts_{j,t}}$ and $Per_{vz_{j,t}}$ are the percolations from the surface zone to the root zone and from the root zone to the deep vadose zone, respectively, and $ET_{j,t}$ is the evapotranspiration in grid j and at daily time step t. The average monthly soil water storage in the root zone was employed for calculating the HADI.

2.1.3.3. Hydroclimatic Aggregate Drought Index

To derive the HADI, a correlation-based dimension reduction technique of the PCA (Cattell, 1952) was used. The variables can be spread out further on the mean and a better analysis is obtained by the PCA, which is the same as weighted averaging (Rencher and Christensen 2012). The PCA reduces dimensions and introduces a linear combination of variables with the maximum variances instead of the original variables. In other words, the most important information from the hydroclimatic condition is represented in the first principal components (PCs). To account for the temporal variations, a R-mode PCA was used. In the P-mode PCA as used in the ADI (Keyantash and Dracup 2004), its accuracy depends on the correlation coefficient matrix of the input variables. Therefore, the study period has to cover at least 30 years for proper characterization of drought using the PCA approach. For the R-mode PCA (spaces (grids) and attributes (variables)), however, a long time series is not required.

The PCA is not scale invariant. Thus, the units of the variables to be estimated need to be carefully considered. It is recommended to express all the variables in the same units (Rencher and Christensen 2012). If this assumption is satisfied, no standardization of the variables is required. However, if the variables have widely disparate variances, the variables should be standardized before extracting the corresponding eigenvalues and eigenvectors. To standardize the variables in each grid, their average and standard deviation values through time were calculated in this study. Then, each variable was standardized by division of the difference between each value and its average to its standard deviation, as shown below:

$$SY_{i,j} = \frac{y_{i,j} - \mu_j}{\sigma_j} \tag{2.3}$$

where $SY_{i,j}$ is the standardized value of each variable ($y_{i,j}$) in grid j at month i; and μ_j and σ_j are the mean and standard deviation of each variable in grid j over the entire study period. Then, the R-mode PCA was employed for the standardized values. The PCs are estimated by Equations (2.4), (2.5), and (2.6).

$$z_i = A_i \, SY_i \tag{2.4}$$

$$z_i = \begin{bmatrix} z_{1,i} \\ z_{2,i} \\ z_{3,i} \\ z_{4,i} \end{bmatrix} \tag{2.5}$$

$$A_i = \begin{bmatrix} a_{1,i} \\ a_{2,i} \\ a_{3,i} \\ a_{4,i} \end{bmatrix} \tag{2.6}$$

where z_i is the PC vector; $z_{1,i}$ to $z_{4,i}$ are the first to fourth PCs; SY_i is the matrix of the standardized variables; and A_i is the normalized eigenvector in month i. The elements of the eigenvector ($a_{1,i}$- $a_{4,i}$) are unequal weights in the PCs in month i. The unequal weights, which are based on the highest variances among the variables, define drought types. For instance, based on the covariance matrix in a given month, if the variance of soil water storage is higher than others, higher weights are allocated to soil water storage and agricultural drought occurs in that grid at that time. Drought indices need to be regardless of time and place. Thus, they can be used in a different place and at a different time and they are comparable for any given condition with the normal condition. Therefore, the PCs should be standardized to derive the HADI. To standardize the PCs, the average and standard deviation values of the PCs in each grid were calculated. Then, the PCs in each grid and month were standardized by division of the difference between each value and its average to its standard deviation, as shown below:

$$HADI_{i,j} = \frac{PC_{i,j} - \mu_{PC_j}}{\sigma_{PC_j}} \tag{2.7}$$

where $HADI_{i,j}$ is the HADI in grid j at month i; $PC_{i,j}$ is the PC in grid j at month i; and μ_{PC_j} and σ_{PC_j} are the mean and standard deviation of each PC in grid j.

2.1.3.4. Customized Drought Categorization

In the customized drought categorization proposed in this study, variable threshold levels were derived based on both spatial and temporal distributions of drought. The range of the HADI values was defined. The HADI values were divided into a defined number of classes, based on which the HADI values were classified. The higher the number of classes, the more precise threshold levels. To estimate the spatial and temporal frequencies of the HADI, a cell-by-cell based analysis was performed. The frequency of each drought class during the study period was estimated for each cell. Figure 2.5 shows a schematic illustration of the process, in which x, y, and z are drought classes. Note that during a three-month period, the frequency of class x in the magnified grid is 1.

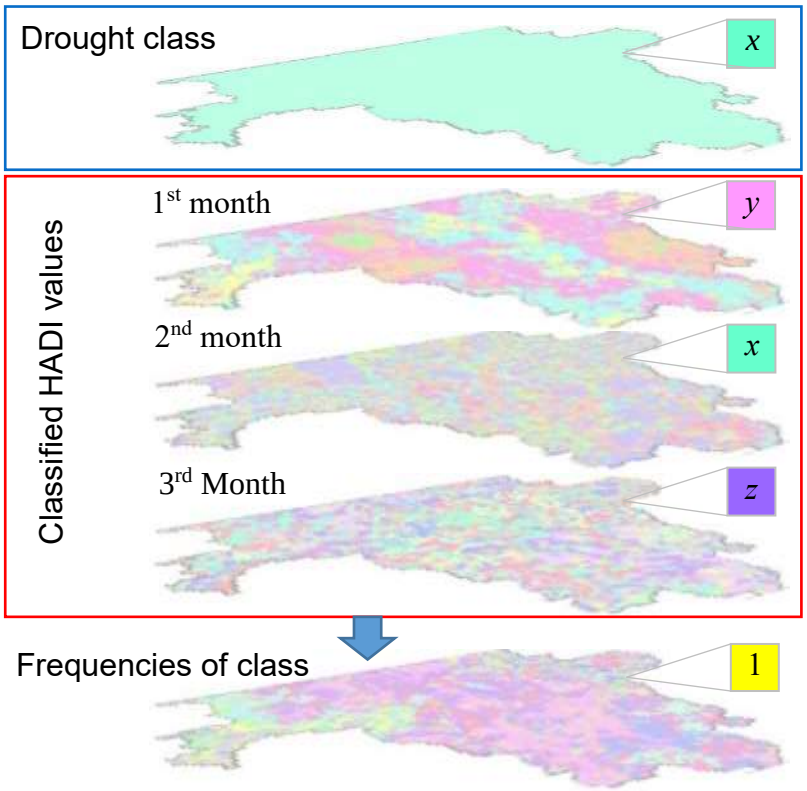

Figure 2.5. Schematic illustration of spatial and temporal frequencies analyses (x, y, and z are different classes of the HADI)

To obtain the spatial distribution, temporal frequencies of all drought classes for all cells were estimated. The spatial and temporal frequencies analysis provided a table, showing the number of grids with the same temporal frequencies. Then, a discrete joint probability distribution function (JPDF) was employed to find an appropriate threshold for each drought category (Table 2.2).

Table 2.2. Joint probability distribution of drought class and frequency

		Drought classes (Lower Class Limit (LCL)-Upper Class Limit (UCL))			
		1 (LCL-UCL)	2 (LCL-UCL)	…	n (LCL-UCL)
Frequency (f)	0	$g(0,1)$	$g(0,2)$	…	$g(0,n)$
	1	$g(1,1)$	$g(1,2)$	…	$g(1,n)$
	⋮	⋮	⋮	…	⋮
	m	$g(\mathrm{m},1)$	$g(\mathrm{m},2)$	…	$g(\mathrm{m},n)$
$\boldsymbol{g(c)}$		$g(1) = \sum g(f,1)$	$g(2) = \sum g(f,2)$	…	$g(n) = \sum g(f,n)$

The frequency (f), which is the number of times the HADI values occur in each class and the drought classes (c) form a bivariate matrix, the element of which represents the number of grids with equal frequencies throughout the entire period. The conditional expectation (CE) values are equal to the average values of probabilities for each drought class (Table 2.3). The lowest CE represents the most intense drought and the highest CE is associated with a normal condition. The conditional JPDF and CE of the frequencies for each class can be estimated by Equations 2.8 and 2.9, respectively (Hogg and Craig, 1978).

$$g(f \mid c) = {g(f,c)}\Big/{g(c)} \tag{2.8}$$

$$E(f \mid c) = \sum f \,.\, g(f \mid c) \tag{2.9}$$

where $g(f,c)$ is the JPDF of frequency and drought class; $g(c)$ is the probability distribution function of drought class; $g(f \mid c)$ and $E(f \mid c)$ are respectively the conditional probability and the conditional expectation of different frequencies for each associated class.

Table 2.3. Conditional probability distribution of drought class and frequency

		Drought classes (Lower Class Limit (LCL)-Upper Class Limit (UCL))			
		1 (LCL-UCL)	2 (LCL-UCL)	…	n (LCL-UCL)
Frequency (f)	0	$g(0 \mid 1)$	$g(0 \mid 2)$	…	$g(0 \mid n)$
	1	$g(1 \mid 1)$	$g(f \mid c)$	…	$g(1 \mid n)$
	⋮	⋮	⋮	…	⋮
	m	$g(\mathrm{m} \mid 1)$	$g(\mathrm{m} \mid 2)$	…	$g(\mathrm{m} \mid n)$
$\boldsymbol{E(f \mid c)}$		$E(f \mid 1)$	$E(f \mid 2)$		$E(f \mid n)$

2.1.3.4.1. K-Means Clustering

Cluster analysis is a multivariate technique used to seek for an optimal grouping, in which each cluster has as similar observations as possible. To derive the threshold levels for each drought category, a nonhierarchical k-means clustering (MacQueen, 1967) was used in this study. In the k-means clustering, the number of clusters was defined. The same numbers of drought categories as those of the USDM (six categories) (Svoboda et al. 2002) were used to account for the creeping nature of drought (slow emergence and recession). They included exceptional, extreme, severe, moderate, and abnormal dry categories as well as the normal condition. To categorize the wet conditions, four wet classes (including exceptional, extreme, severe, moderate wet) were considered. Finally, the customized drought categorization was conducted based on these ten dry and wet clusters. Ten points (X: lower class limit (LCL), Y: conditional expectation (CE)) that were mutually farthest apart were selected as initial seeds in the k-means clustering. Instead of choosing arbitrarily-defined threshold levels (e.g. McKee et al. 1993), these values were defined based on the cluster analysis. In this approach, the threshold levels for the normal condition were associated with the highest probability. The threshold levels for other categories of drought were associated with lower probability and based on the grouping results by the cluster analysis. That is, rational-and-statistical threshold levels were used in this study. These thresholds, based on spatial and temporal distributions, are helpful for

more precise and reliable drought categorization. Moreover, this method fulfils the essence of improving threshold definition, as emphasized by Mishra and Singh (2010).

2.1.3.5. Comparison of HADI with PDSI, Gross Domestic Production (GDP), and USDM

To test the performances of the HADI and the new customized drought categorization, the HADI was compared with the PDSI, GDP, and USDM. The monthly and annual values of the PDSI and GDP were used to assess the performance of the HADI in drought identification. The new customized drought categorization was further tested by comparison of the monthly drought area coverages identified by the HADI and USDM.

2.1.3.5.1. PDSI

The PDSI (Palmer 1965) is a well-established drought index. However, it has some limitations such as geographic biases, complex empirical formulations, and ignorance of the most dominant process in cold climates (e.g., snowfall, frozen soil, snowpack, and snowmelt) (Keyantash and Dracup 2004). Furthermore, the PDSI has a water-balance-based nature, and hence different hydroclimatic variables need to be taken into account. The HADI also considers different hydroclimatic variables and accounts for the dominant processes in cold climates. Thus, the PDSI is an appropriate index to test the performance of the HADI. The PDSI data were obtained from the NOAA's National Centers for Environmental Information (NOAA's NCEI 2019).

2.1.3.5.2. GDP

The GDP is an index for estimation of drought impacts especially in watersheds with agriculture-based economy. In the previous studies (e.g., Bachmair et al. 2015 and 2018), the performances of the SPI and Standardized Precipitation Evapotranspiration Index (SPEI) (Vicente-Serrano et al. 2010) were evaluated by considering drought impacts. Since the study

area is agriculture-dominated and about 60% of the area is covered by cultivated lands, the agriculture-based GDP can be a good indicator for the impact of droughts in the area. Thus, the GDP was also selected to compare with the HADI and PDSI. The agriculture-based GDP data for North Dakota were obtained from the Bureau of Economic Analysis (BEA), U.S. Department of Commerce (BEA 2019).

2.1.3.5.3. USDM

The mean monthly values of the USDM time series (USDM 2019) were compared with the HADI results. The comparison involved the main aspects of droughts such as onset, termination, and drought area coverage in each category of drought. Note that the USDM is "a composite product" developed from different indices, models, and the input of experts (Svoboda et al. 2002). Based on the Objective Drought Indicator (ODI) Blends, the USDM (Svoboda et al. 2002) is a blend of six main drought indicators and other objectively-selected ancillary indices. The six main indicators include the PDSI, CPC soil moisture model (percentiles), USGS weekly streamflow (percentiles), percent of normal, SPI, and satellite vegetation. The other ancillary indices (e.g., SWSI) add the information about the conditions of crop moisture, surface soil moisture, forests' fire risk, relative humidity and temperature deviation from normal, levels of surface water bodies and groundwater, and snowpack. The USDM provides a broad range of useful information related to droughts. Soil moisture is considered in the input data of both USDM and HADI. Observed streamflow is used in the USDM, while simulated surface runoff is used in the HADI. Although precipitation and snowpack are taken into account in the derivation of the USDM products, separation of rainfall and snowfall and snowmelt are ignored in the USDM. In contrast, the HADI accounts for these dominant hydroclimatic processes in cold climate regions.

The threshold levels for drought categorization in the USDM are based on percentile. Subjective adjustments of these threshold values based on drought impacts are essential due to

the complex nature of drought and these threshold values provide "consistent and replicable standard" for drought categorization (Svoboda et al. 2002). However, these threshold levels do not correlate completely to the appropriate percentiles for all geographical locations (Svoboda et al. 2002). The approach of one-weight-fits-all can be a limitation of the USDM in weighting coefficients of the involved indices and in the representation of seasonal changes. In contrast, the variable threshold levels were used in the HADI. The customized categorization in the HADI was adjusted by geographic locations and the time periods. Moreover, by using the PCA, the weighting coefficients for different hydroclimatic variables in the HADI were derived based on the employed time series, instead of the fixed coefficients used in the USDM.

The weekly USDM products incorporate the advices from about 450 experts across the U.S. Although such efforts can be considered a burden on creating the USDM products, the information added to the USDM by these experts is highly valued. Therefore, the USDM was selected as a benchmark in this study to evaluate the performance of the HADI. Note that since the study focuses on a cold climate region in a mostly dry period and the methodology and input data are different from the USDM, it is expected to have certain discrepancies in these two drought indicators. Moreover, in comparison of drought indices, a perfect corroboration should not be expected or desired (Keyantash and Dracup, 2004). The widely-used drought indices should not be taken as the ultimate standard (Keyantash and Dracup, 2004).

2.1.4. Results and Discussion

In this research, all the four variables, including rainfall, surface runoff, snowmelt, and soil water storage had the same unit (mm). However, the variance analysis of these variables in this research indicated high covariances among different variables. To cope with this issue, each variable was standardized before extracting the eigenvalues and eigenvectors. The highest proportion (47.00% to 98.98%) of variances was represented in the first PCs. The first PC for February 2003 (Figure 2.6a) had 98.98 % of the information and the last PC layer (Figure 2.6d)

showed less information. In June 2006, the percentage of information in the first PC (Figure 2.6e) was about 47% and was not much higher than that for the second PC layer (Figure 2.6f). However, the first PC still had the highest information compared with the other PC layers.

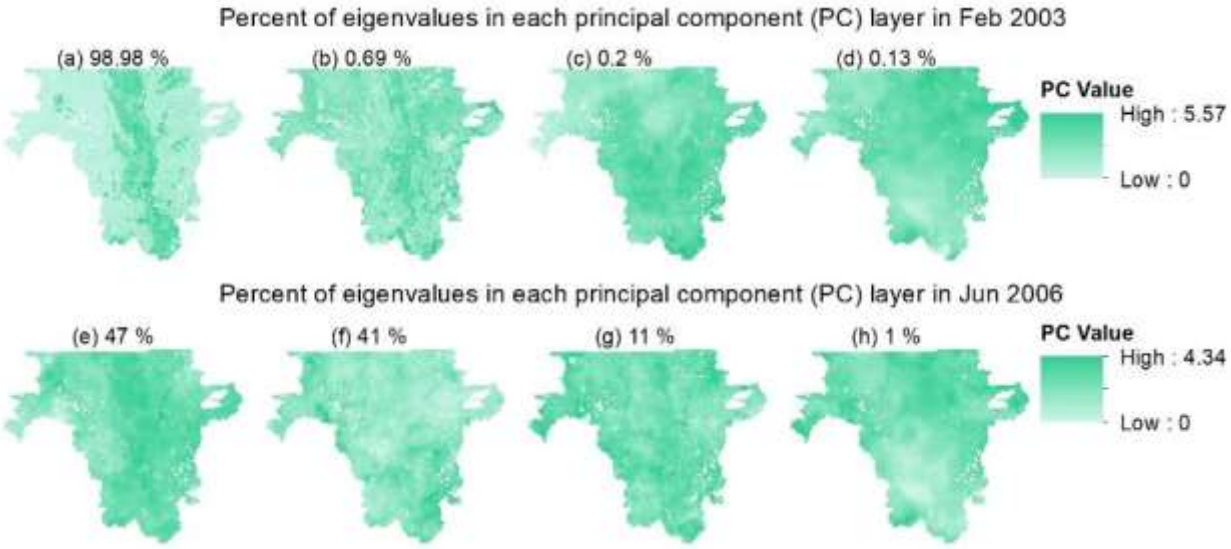

Figure 2.6. Percent of eigenvalues in each principal component layer in February 2003 (a-d: the first to the last principal component layers) and in June 2006 (e-h: the first to the last principal component layers)

Figure 2.7 shows the scree plot and variance explained by each PC. For February 2006 (Figures 2.7a and 2.7b), the scree plot slope is the highest for the first PC, while it is almost flat for the other PCs. In Figures 2.7c and 2.7d, the scree plot slope is higher for the first and second PCs, but based on Figure 2.7d, the highest proportion of variance is still explained by the first PC. In addition, the seasonally averaged percentage of information is above 65% for the first PC (Figure 2.8). Therefore, only the first PC was considered for the derivation of the HADI.

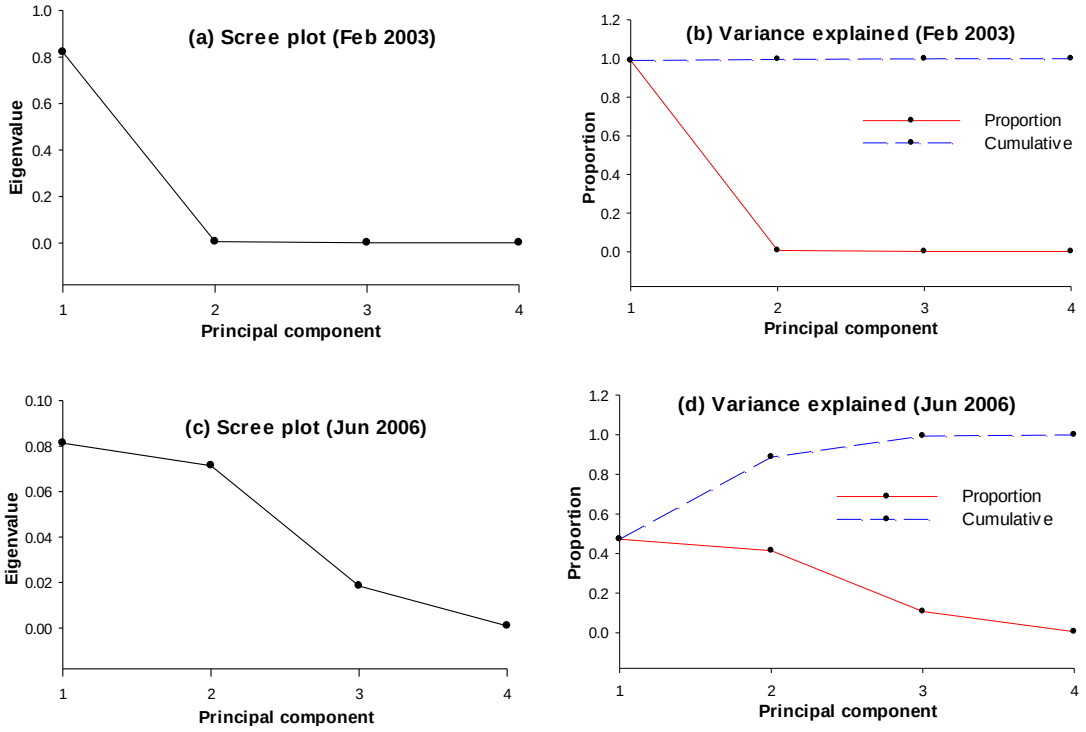

Figure 2.7. Scree plot and variance explained by each principal component in February 2003 and June 2006

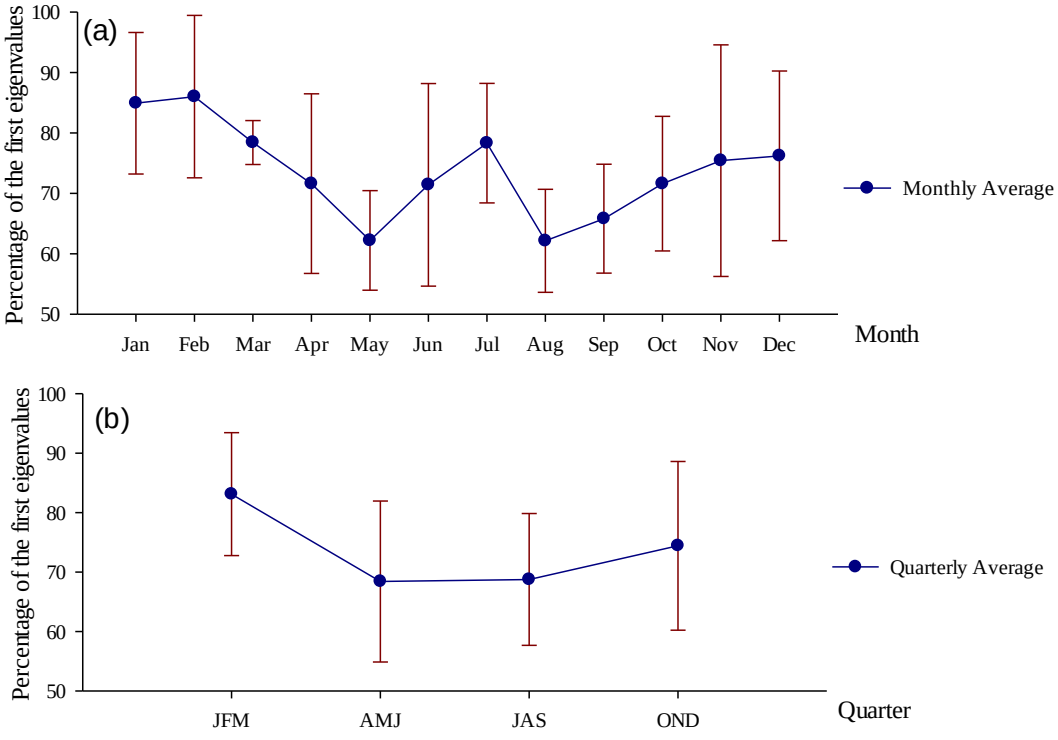

Figure 2.8. Monthly and quarterly average and standard deviation of percentages of the first eigenvalues in the study period (2003-2007)

Although this research focuses on the principal components corresponding to the larger eigenvalues, the principal components corresponding to the smaller eigenvalues can also provide important information. If the last eigenvalue is close to zero, it signifies the presence of a collinearity among the variables. Collinearity is a condition in which some of the independent variables are highly correlated. The values of correlation between rainfall and surface runoff in February 2003 and June 2006 were 0.32 and 0.49, respectively. Therefore, the collinearity was apparent in June 2006, which justifies the low value of the first eigenvalue (0.08) and the lower percentage of the first eigenvalue in this month. In addition, the lowest and highest average values of the percentages of the first eigenvalues in different months were observed in August and February, respectively. March showed the lowest standard deviation value (3.65), while the highest standard deviation was observed in November (19.16). Based on the same analysis for different quarters of a year, the first quarter (JFM) showed the highest average (83.1) and the lowest standard deviation (10.33). The lowest average values were observed in the second quarter (AMJ: 68.4) and third quarter (JAS: 68.75) of the year. The lowest and highest standard deviations were associated with JFM (10.33) and the fourth quarter (OND) (14.18), respectively. Therefore, the second and third quarters of the year (i.e., spring and summer) had lower percentages of the first eigenvalues due to collinearity. Figures 2.8a and 2.8b respectively show the monthly and quarterly average and standard deviation values.

Figure 2.9 shows the conditional expectation distributions of the HADI in the 60 months (2003-2007) over the entire RRB. The results showed a remarkably mixture distribution of two normal distributions with different means and variances (N1 (μ_1 , σ_1) and N2 (μ_2 , σ_2)). Since all the values of the HADI, which either belong to dry or wet, were gathered in one population, the distribution of the population was obtained as a mixture distribution of the two normal distributions, which represented wet and dry classes. The highest conditional expectation occurred for negative values (LCL= -1.1), which indicated a normal condition. In previous studies, the arbitrarily-defined and fixed threshold levels of the normal condition were derived

around zero (e.g., McKee et al. 1993). However, depending on the study periods and the geographic locations, the threshold levels for a normal condition should be different. The Q-Q plot was also used to show the normality of the HADI and other hydroclimatic variables. The Q-Q plot shows the quantiles of the normal distribution and the empirical distribution of the dataset. The deviation of the scattered points from the 1:1 line indicates the normality and skewness of the dataset. The Q-Q plots shown in Figure 2.10 also confirm that the areal averages of precipitation (Figure 2.10b), rainfall (Figure 2.10c), snowpack (Figure 2.10d), snowmelt (Figure 2.10e), surface runoff (Figure 2.10f), and the HADI (Figure 2.10h) are positively skewed. The means of these hydroclimatic variables and the HADI are located on the right side of the peaks of their distributions. In contrast, temperature (Figure 2.10a) and soil water storage (Figure 2.10g) are negatively skewed.

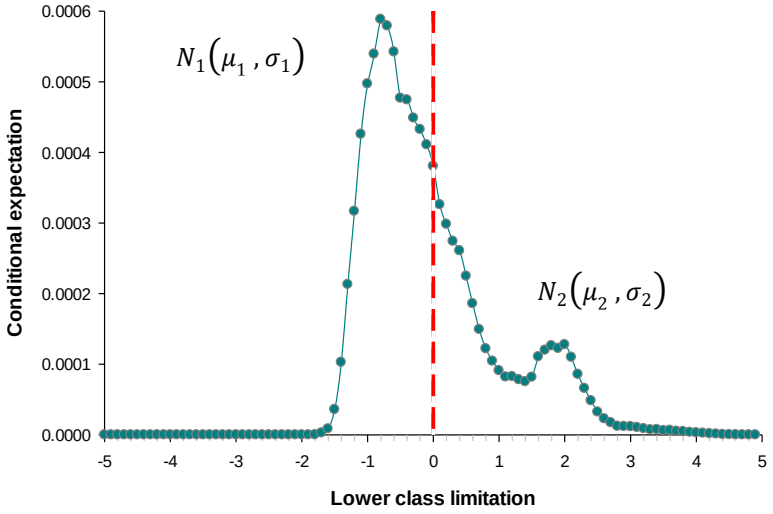

Figure 2.9. Conditional expectation of relative frequency of the HADI given each lower class limitation

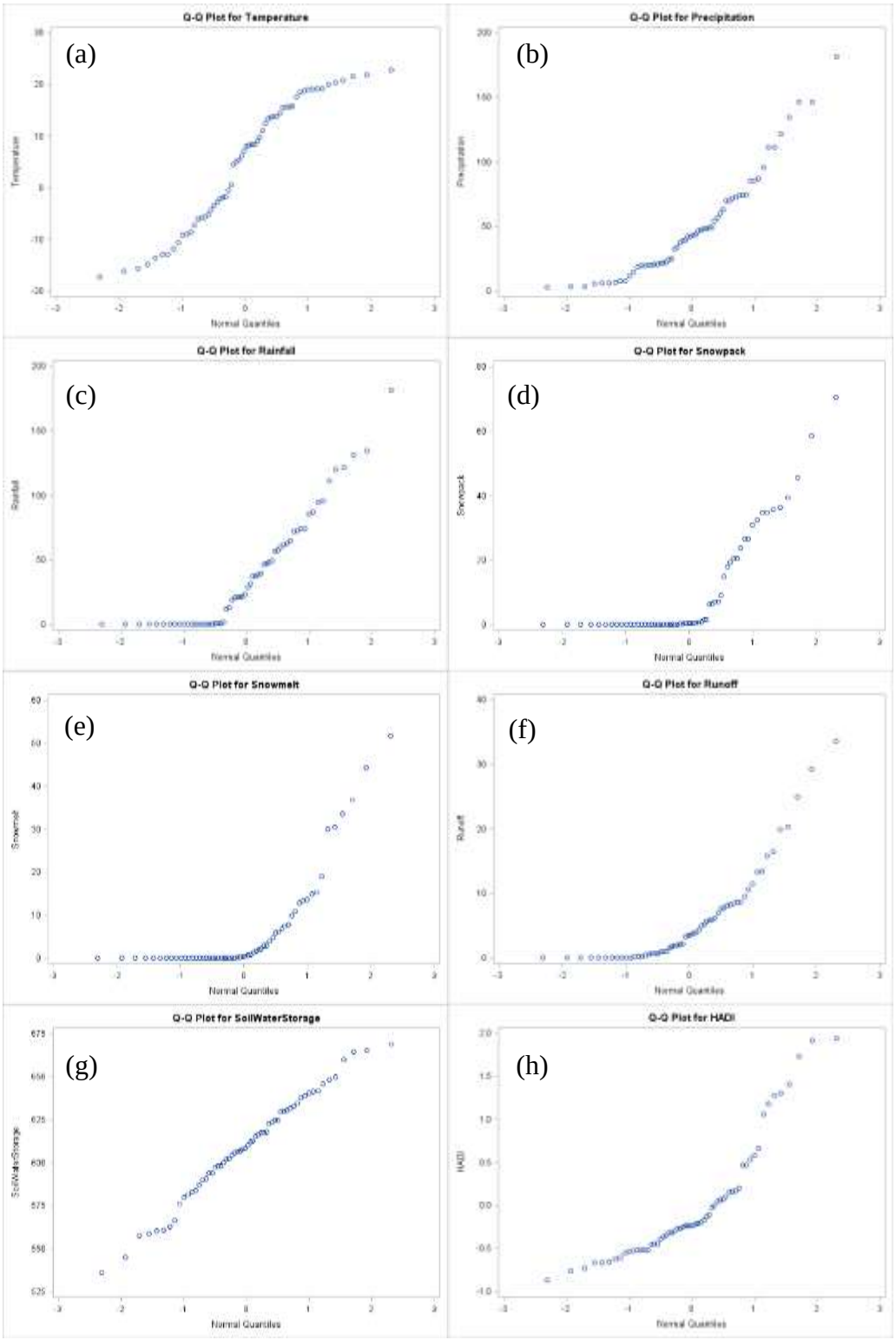

Figure 2.10. Q-Q plots of areal averages of hydroclimatic variables (temperature, precipitation, rainfall, snowpack, snowmelt, surface runoff, and soil water storage) and the HADI in RRB

Based on the K-means clustering results, the CE and LCL were grouped into ten clusters. Normal conditions for both negative and positive LCL were defined in clusters with high probabilities. Other clusters with lower values of LCL were considered as abnormally dry, moderate, severe, and extreme drought. The positive values of LCL were categorized as moderate, severe, and extreme wet categories. Table 2.4 shows the derived variable threshold levels for the categorization of drought and wet conditions.

Table 2.4 HADI-based drought categories

HADI values	Category	Symbol
HADI > 4.6	Exceptional wet condition	W4
2.9 < HADI < 4.6	Extreme wet condition	W3
1.3 < HADI < 2.9	Severe wet condition	W2
0.2 < HADI < 1.3	Moderate wet condition	W1
- 1.1 < HADI < 0.2	Normal condition	N
- 1.4 < HADI < - 1.1	Abnormal drought	D0
- 1.5 < HADI < - 1.4	Moderate drought	D1
- 1.7 < HADI < - 1.5	Severe drought	D2
- 1.8 < HADI < - 1.7	Extreme drought	D3
HADI < -1.8	Exceptional drought	D4

2.1.4.1. Assessment of HADI in Identification and Categorization of Drought

To evaluate the performance of the HADI, it was compared with the PDSI and the agriculture-based GDP in CD 3206 (Figure 2.5). As shown in Figure 2.11a, apparent discrepancies between the results of the HADI and PDSI can be observed. Both the Pearson correlation coefficient (0.02) (original data) and the Spearman correlation coefficient (0.04) (based on the data ranks in time series) were noticeably low. There was an obvious difference between the HADI and PDSI in 2005. Ignoring the flash wet periods, the HADI showed the onset of drought in 2004 and its termination in 2007. In contrast, although the PDSI identified the dry year in 2003, it identified an extreme wet condition started from the middle of 2004 and ended by the beginning of 2006. However, the agriculture-based GDP was in contradiction with

the PDSI results (Figure 2.11b). The GDP during 2003 was relatively high, indicating that 2003 was a wet year. The HADI average value for 2003 was 0.43, which also indicated a relatively wet year. However, the PDSI value was very low (0.04). In addition, the GDP had a decreasing trend from 2004 to 2006 and the HADI showed a dry condition in these years. Conversely, the PDSI results identified an increasing trend and showed a wet condition in these years. Both HADI and PDSI identified 2007 as a wet year that was in accordance with the GDP result. Therefore, it can be concluded that the HADI outperformed the PDSI since the HADI results were in accordance with the agriculture-based GDP.

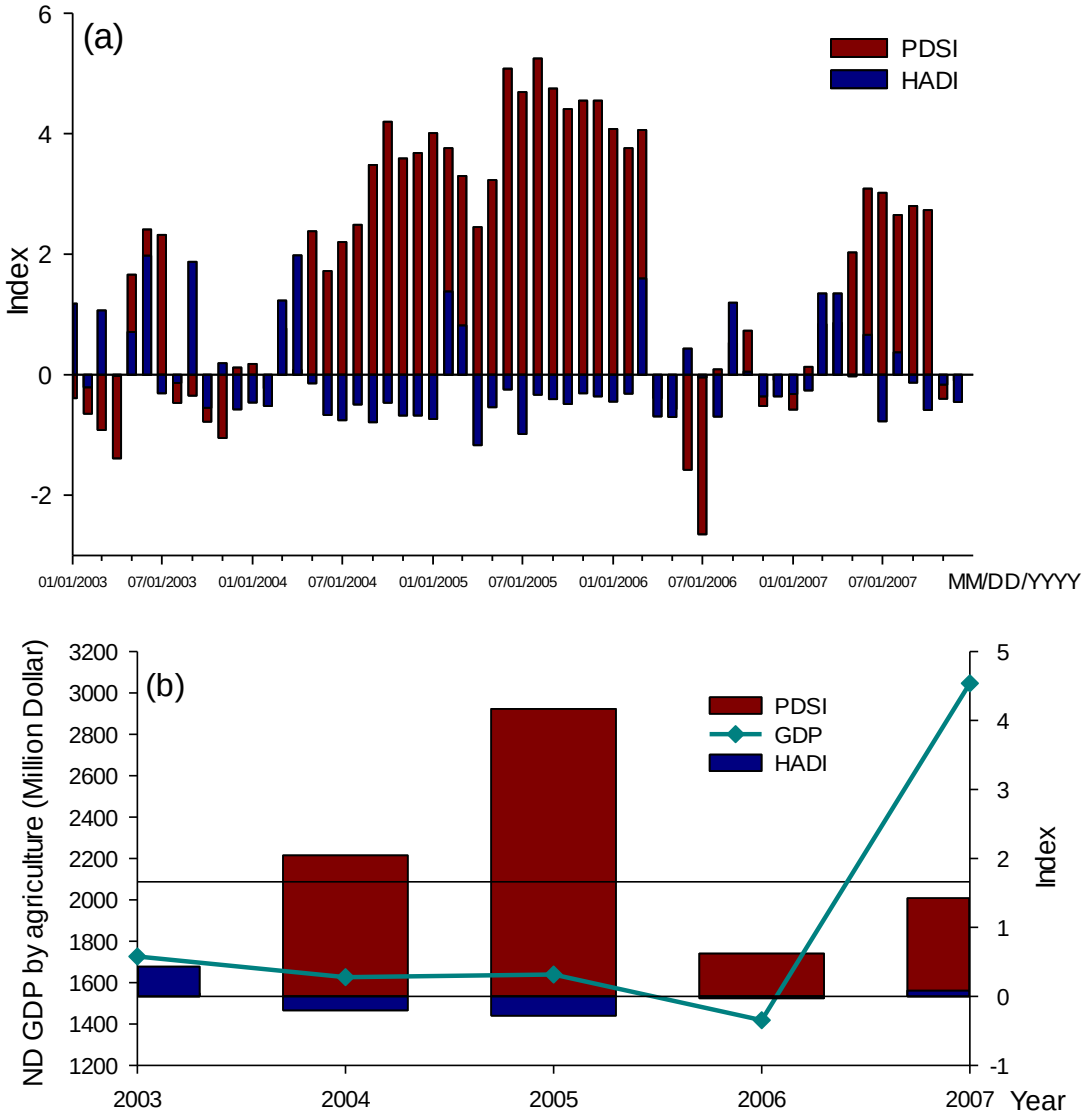

Figure 2.11 Comparison of (a) the monthly PDSI and HADI values and (b) annual values of the PDSI, HADI, and ND agriculture-based GDP

Figures 2.12 to 2.14 show the comparison of the percentages of area affected by different categories of drought identified by the HADI and USDM in CDs 2101, 3203, and 3206 (Figure 2.5). The drought area coverage is the ratio of the areas influenced by a specific intensity of drought to the entire area. For instance, the abnormally dry condition (D0) illustrates the percentage of the areas covered by a range of drought intensities from abnormally dry to exceptional drought. According to Figure 2.12a, both the HADI and USDM identified an abnormally dry condition in northwestern MN but the drought area coverage identified by the

USDM was smaller. The HADI indicated that an abnormal dry condition initiated from March 2003, progressed, and covered almost 40% of CD 2101 in June 2004. After a recession, the area coverage of this category of drought increased and reached its highest level in June 2005. After some flash droughts with small coverage and a wet period in the end of 2006 and the beginning of 2007, the same percentage of abnormally drought coverage happened in this CD. Figure 2.12b shows that the HADI, unlike the USDM, did not identify a great proportion of this CD with moderate drought. However, regardless of the area coverage, both HADI and USDM indicated moderate drought in the same months except July in 2005. The HADI did not indicate the existence of severe (Figure 2.12c) and extreme (Figure 2.12d) droughts in the end of 2006 and the beginning of 2007.

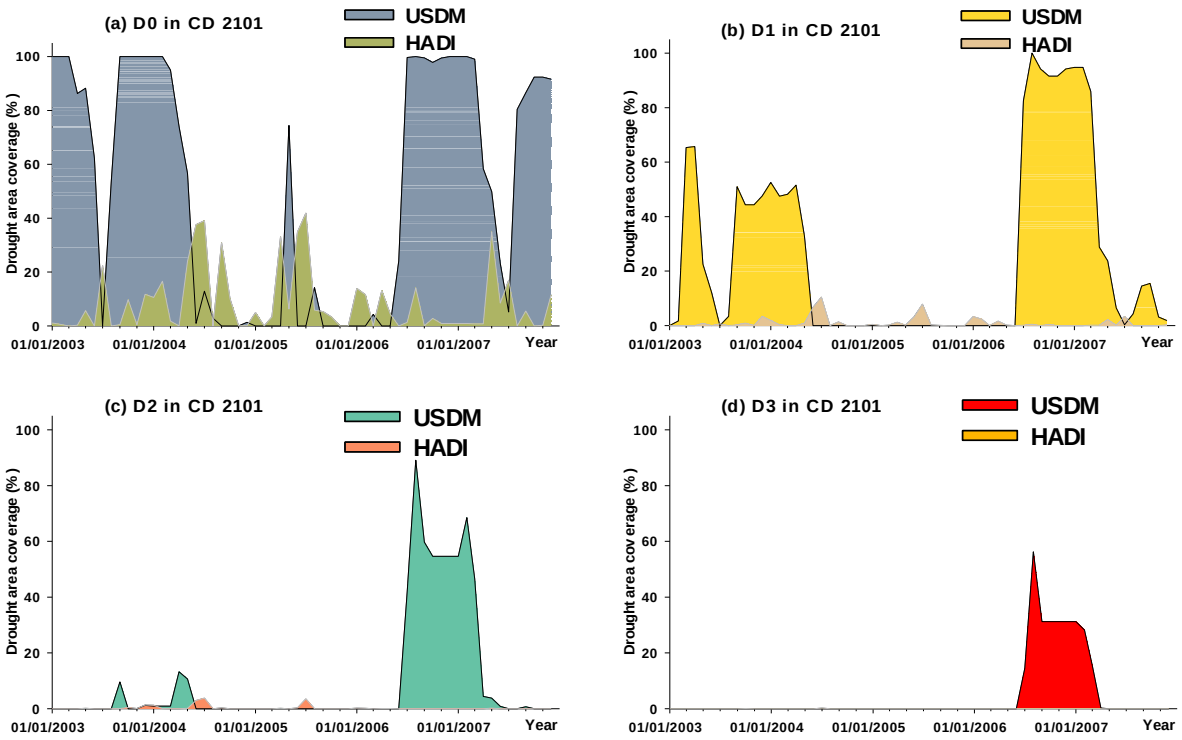

Figure 2.12. Comparison of the HADI and USDM for climate division 2102

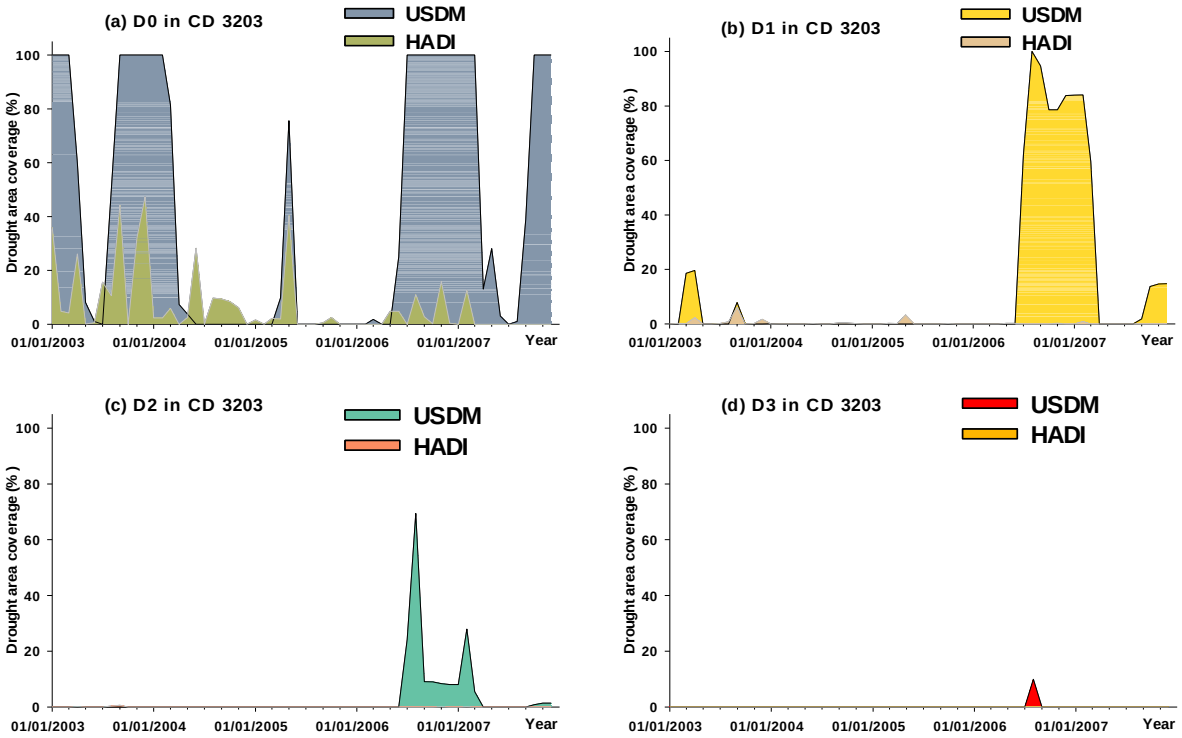

Figure 2.13. Comparison of the HADI and USDM for climate division 3203

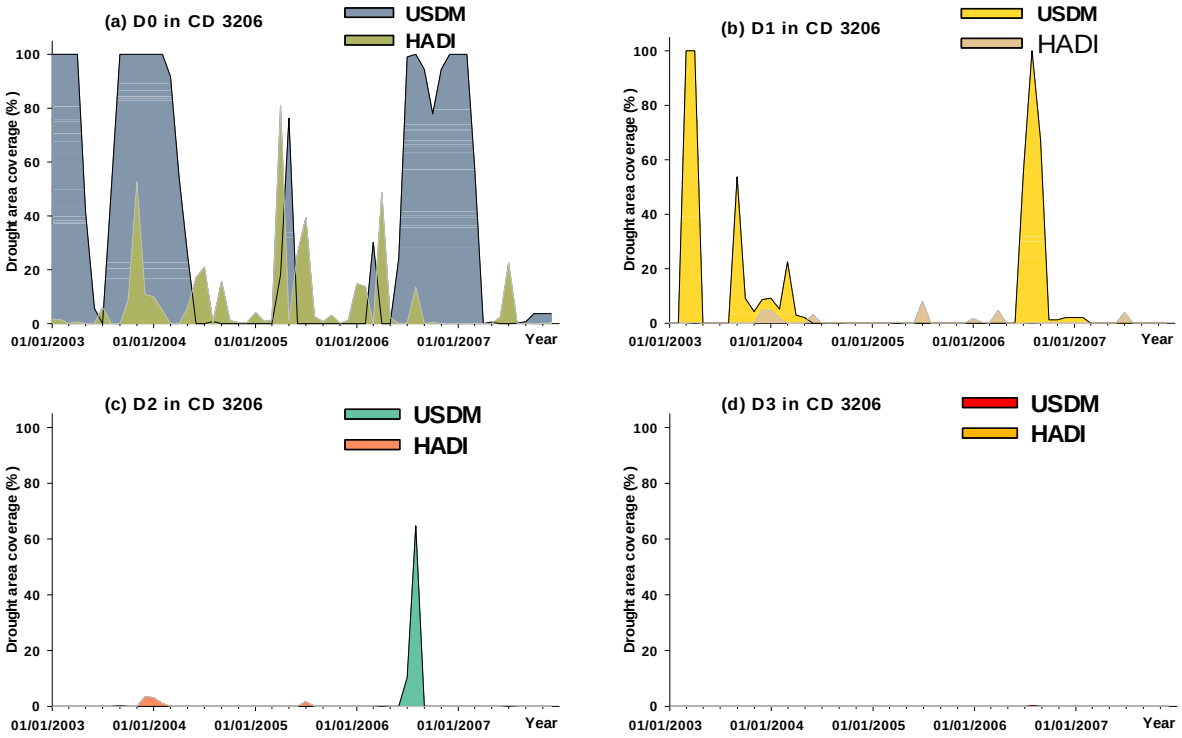

Figure 2.14. Comparison of the HADI and USDM for climate division 3206

As shown in Figure 2.13a, the HADI and USDM indicated that CD 3203 experienced the same trend of abnormally dry and moderate drought conditions. However, the HADI did not identify any severe or extreme drought in this CD (Figure 2.13b-d). In CD 3206, both indices categorized the drought in April and May 2005 as abnormally dry with the same area of coverage (Figure 2.14a). However, the area coverages at the end of 2003 and 2005 were different. In addition, in December 2003 and July 2005, the same categories of drought were found by both indices as D1, D2, and D3 (Figure 2.14b-d). However, like two other CDs, the drought area coverages detected by the HADI were different from those from the USDM in the end of 2006 and the beginning of 2007. The discrepancy in the identification and categorization of drought can be attributed to two reasons. First, different numbers and types of hydroclimatic variables were utilized in the HADI and USDM. For example, the HADI considered the dominant hydroclimatic processes for cold climate regions such as separation of rainfall and snowfall as well as snowmelt. In contrast, the USDM neither accounted for this distinction nor directly considered snowmelt. Moreover, the adopted variable threshold levels in the customized drought categorization were different in the HADI since a dry period was intentionally chosen to test the proposed index. Thus, these discrepancies in the results were expected.

2.1.4.2. Assessment of HADI by Its Correlation with Hydroclimatic Variables

To further assess the performance of the HADI, its correlation with each hydroclimatic variable was analyzed. Table 2.5 shows the Pearson correlation coefficients and the related p-values. The variables with positive correlation coefficients and p-values below 0.05 tend to increase with the HADI. The variables with negative correlation coefficients and p-values below 0.05 tend to decrease as the HADI increases. The p-values greater than 0.05 imply no significant relationship between the pair of datasets. Since the p-values for all the variables except snowmelt are greater than 0.05, it can be concluded that only the correlation of the HADI and snowmelt was significant. However, the null hypothesis of existence of any correlation

between the HADI and other variables was totally rejected. The PCA looks for the unique properties of the climate that strongly differ from other properties to avoid any redundant information in the derivation of the HADI. In this case, it is snowmelt, from which the HADI was extracted. Therefore, it is concluded that the HADI represents a drought condition mainly based on snowmelt, whenever applicable. The Pearson correlation results also indicated that rainfall, surface runoff, and soil moisture were not the main indicators of drought conditions in the regions with cold climates such as the RRB. Note that this does not mean that these variables had no impact on the HADI, but their influences were indirect and/or lower than snowmelt. The scatterplot matrix in Figure 2.15 confirms the results of correlations of different hydroclimatic variables and the HADI.

Table 2.5. Pearson correlation coefficients and the corresponding P-values

Period		Temperature	Rainfall	Snowmelt	Runoff	Soil water storage	HADI
Total	Temperature	1.00	0.75	-0.24	0.34	0.41	-0.03
			<.0001	0.067	0.007	0.001	0.81
	Rainfall		1.00	-0.25	0.72	0.47	-0.01
				0.056	<.0001	0.0002	0.93
	Snowmelt			1.00	0.34	-0.25	0.34
					0.008	0.055	0.008
	Runoff				1.00	0.34	0.09
						0.009	0.52
	Soil water storage					1.00	-0.18
							0.16
	HADI						1.00
Warm seasons		**Temperature**	**Rainfall**	**Snowmelt**	**Runoff**	**Soil water storage**	**HADI**
	Temperature	1.00	0.31	-0.70	-0.03	0.24	-0.23
			0.1	<.0001	0.89	0.20	0.22
	Rainfall		1.00	-0.34	0.82	0.38	-0.05
				0.06	<.0001	0.04	0.77
	Snowmelt			1.00	0.07	-0.13	0.10
					0.71	0.51	0.61
	Runoff				1.00	0.41	-0.14
						0.02	0.48
	Soil water storage					1.00	-0.26
							0.17
	HADI						1.00
Cold seasons		**Temperature**	**Rainfall**	**Snowmelt**	**Runoff**	**Soil water storage**	**HADI**
	Temperature	1.00	0.71	0.23	0.41	0.21	-0.01
			<.0001	0.22	0.02	0.27	0.96
	Rainfall		1	0.19	0.57	0.21	-0.02
				0.32	0.001	0.27	0.91
	Snowmelt			1.00	0.88	-0.22	0.58
					<.0001	0.23	0.0007
	Runoff				1.00	-0.03	0.48
						0.87	0.008
	Soil water storage					1.00	-0.13
							0.48
	HADI						1.00

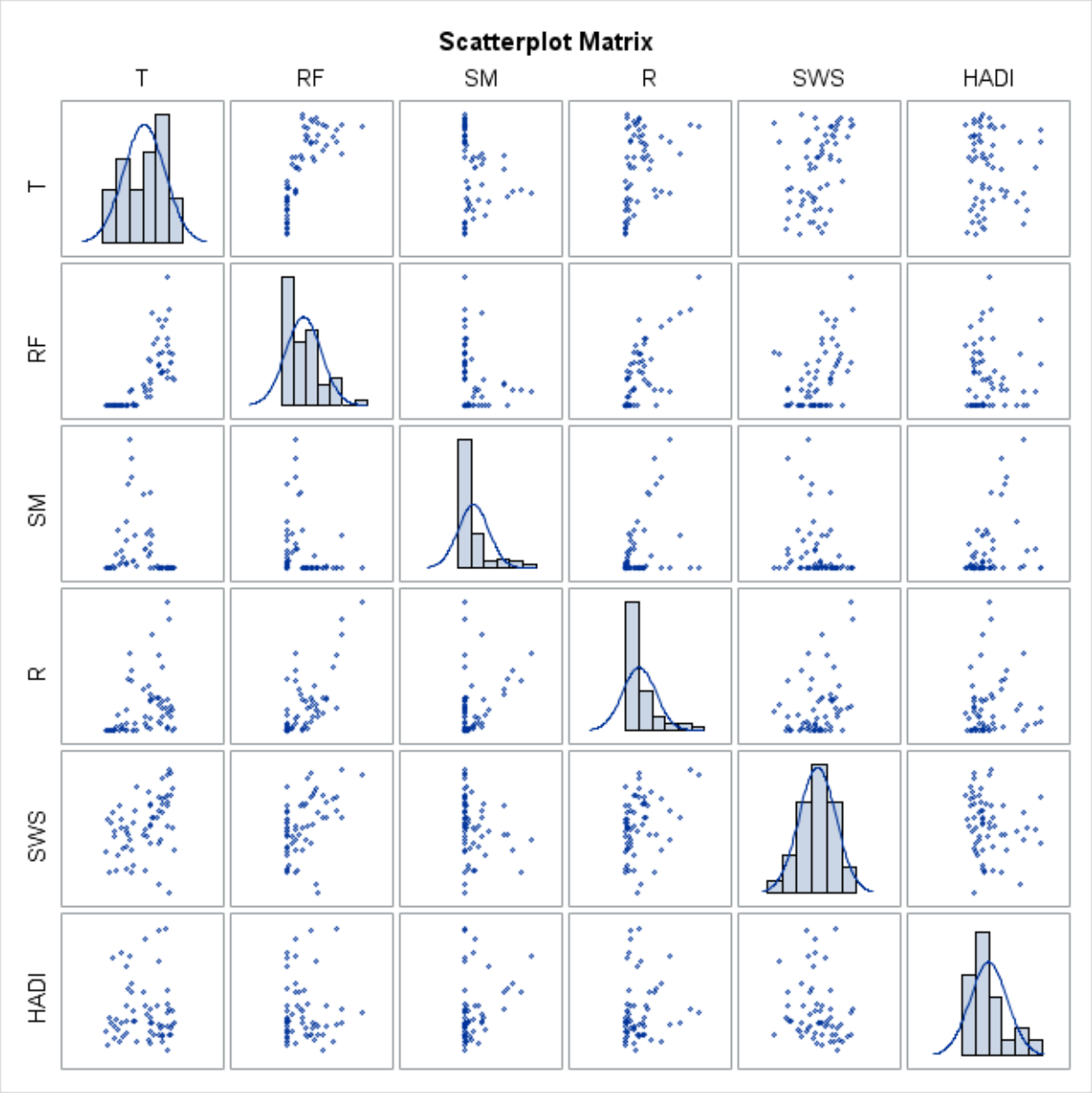

Figure 2.15. Scatterplot matrix for temperature (T), input data (rainfall (RF), snowmelt (SM), surface runoff (R), soil water storage (SWS)), and the HADI

The results of correlation between the HADI and the hydroclimatic variables in warm (April to September) and cold (October to March) seasons were also shown in Table 2.4. According to the p-values, no correlation test was significant during the warm seasons. It can be justified by the lower percentage of the first eigenvalues due to the collinearity among variables in the warm seasons. Ignoring the unacceptable p-value, the highest correlation was observed

between the HADI and soil water storage, indicating that the HADI values were mostly based on soil water storage during the warm seasons. In contrast, the acceptable p-values were observed for the correlation test between the HADI and snowmelt and surface runoff in the cold seasons, which emphasizes the dominant role of snowmelt and surface runoff in the identification of droughts in the cold seasons.

2.1.4.3. Classification of Drought Types

Loadings in the PCA are weighting coefficients of the variable in weighted average, based on which the PCs are estimated. The greater values of the loadings, the higher effects on the PC values. Therefore, drought types can be defined by comparing the loadings of the hydroclimatic variables. For example, if the loading of rainfall is higher than those of others, the impact of rainfall on drought is higher. In other words, drought occurs mainly due to rainfall deficit and thus the drought can be classified as meteorological drought. Table 2.6 shows the absolute values of loadings of the first PC in the long period. The longest red band in each row indicates the highest loading of the hydroclimatic variables. For instance, the loading of surface runoff is the highest from May to July in 2004, indicating the occurrence of hydrologic drought in this period. In addition, as shown in Table 2.6, the longest blue band, which indicates the wet condition, is related to snowmelt in April 2004, implying that snowmelt played a key role in keeping this month in a wet condition.

Table 2.6. Absolute values of loadings (weighting coefficients) of the first principal component (The blue and red bands indicate wet and dry periods, respectively.)

Month-Year	Rainfall	Snowmelt	Surface runoff	Soil water storage	Drought type
Mar-04	0.15	0.38	0.91	0.02	–
Apr-04	0.13	0.90	0.05	0.43	–
May-04	0.20	0.03	0.98	0.04	H
Jun-04	0.41	0.01	0.86	0.29	H
Jul-04	0.67	0.02	0.74	0.07	H
Aug-04	0.85	0.02	0.45	0.26	M
Sep-04	0.38	0.01	0.92	0.10	H
Oct-04	0.55	0.15	0.82	0.09	H
Nov-04	0.07	0.07	0.03	0.99	A
Dec-04	0.11	0.28	0.15	0.94	A
Jan-05	0.06	0.00	0.16	0.99	A
Feb-05	0.00	0.88	0.48	0.02	–
Mar-05	0.01	0.44	0.89	0.09	–
Apr-05	0.00	0.97	0.12	0.21	H
May-05	0.32	0.01	0.87	0.37	H
Jun-05	0.20	0.00	0.98	0.06	H
Jul-05	0.36	0.01	0.92	0.16	H
Aug-05	0.35	0.01	0.92	0.18	H
Sep-05	0.48	0.02	0.76	0.43	H
Oct-05	0.26	0.89	0.23	0.28	H
Nov-05	0.03	0.09	0.17	0.98	A
Dec-05	0.04	0.48	0.31	0.82	A
Jan-06	0.01	0.04	0.13	0.99	A
Feb-06	0.00	0.00	0.11	0.99	A
Mar-06	0.05	0.77	0.63	0.05	–

[a] H = Hydrologic drought
[b] M = Meteorological drought
[c] A = Agricultural drought

2.1.4.4. Drought Characteristics in the Cold Climate RRB

According to the results, starting from April 2004, a long dry period initiated in the RRB. The highest areal average of the HADI occurred in July 2004 (Figure 2.16a). As shown in Figure 2.16b, a large area of the basin was covered by an abnormal dry condition. A part of the basin especially in the downstream area (CDs 2101 and 3203) experienced higher intensities of drought such as moderate or severe drought. There also exist evidences of extreme drought in

the north part of CD 2101. Although there was a short wet period (February and March in 2005) in the middle of this long dry period, the drought continued until the beginning of 2006. Figure 2.16c shows how drought disappeared in the RRB in March 2006. In this month, except CD 3203 that suffered from the impacts of antecedent drought, almost the entire basin was in a moderate to extreme wet condition.

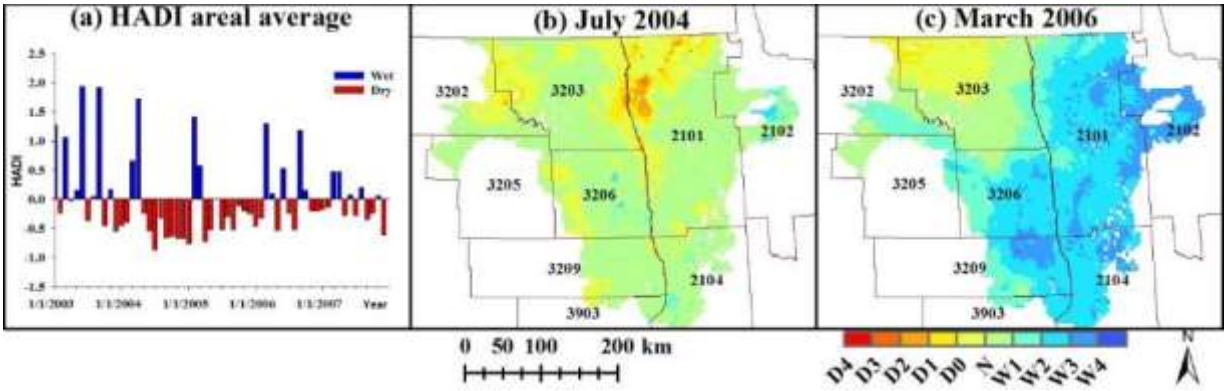

Figure 2.16. (a) Areal average of the HADI values in Red River of the North Basin; spatial distributions of the HADI in (b) July 2004 and (c) March 2006

The droughts in the RRB were further analyzed from the perspective of the Van Loon and Van Lanon (2012) drought classification. According to the results (Figure 2.17h), the HADI identified a long dry period initiated from October 2003 and lasted for years (ignoring the flash wet periods, which lasted only one or two months) until the end of 2007. This long dry period can be characterized as four different classes of drought. In the first period from fall 2003 to the end of winter 2004, the temperature decreased to -17.28°C in January 2004, the lowest temperature in the entire study period (Figure 2.17a). This temperature was about 5°C below the mean monthly temperature of these 5 years (red dashed line in Figure 2.17a). As a result, a major portion of the precipitation was in form of snow in these two cold seasons (fall 2003 and winter 2004) (Figure 2.17b and 2.17c). As a result, snow was accumulated in the snowpack (Figure 2.17d) and it was not melted until February 2004 (Figure 2.17e). The surface runoff generation was decreased (Figure 2.17f). The frozen soil significantly reduced infiltration and soil moisture storage recharge. Thus, soil water storage was below the mean monthly value in

this period (Figure 2.17g). The negative values of the HADI in Figure 2.17h indicated drought in this period. This period can be characterized as “cold snow season drought.” The highest temperature in January occurred in 2006, which was -5.23°C, i.e. 8°C above the mean monthly temperature for this month (Figure 2.17a). In this period, the low precipitation (both rainfall and snowfall) caused “warm snow season drought.” “Snowmelt drought” was another probable type of the 2006 drought, provided high temperature led to low snowfall in winter or early snowmelt, which reduced snow accumulation. Figure 2.17d shows high level of snowpack, but it is not possible to conclude about early or late snowmelt based on the monthly data. The third period of drought occurred because of rainfall deficit and was classified as “classical rainfall deficit drought.” The last period was similar to the first one. However, the rainfall deficit in the previous summer and winter seasons exacerbated the situation and led to a shortage in surface and subsurface water resources. Therefore, this period can be characterized as “rain to snow season drought.”

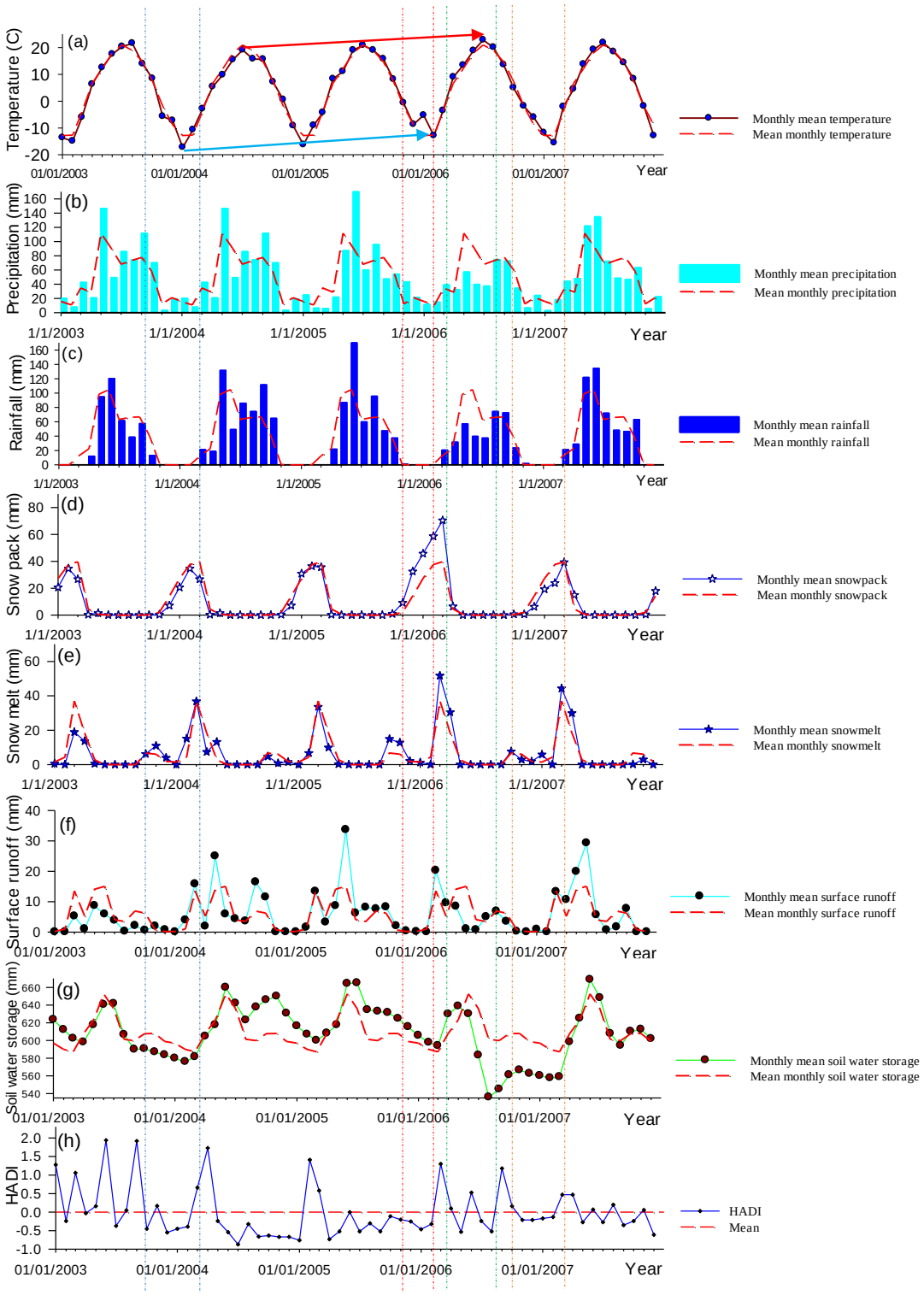

Figure 2.17. Areal average of hydroclimatic variables (temperature (a), precipitation(b), rainfall (c), snowpack (d), snowmelt (e), surface runoff (f), soil water storage (g)) and HADI (h) in Red River of the North Basin

In the first and second dry periods, low temperature was the main cause of the dry condition during cold seasons in the RRB in different ways. First, a decrease in the temperature caused snowfall rather than rainfall. Second, the frozen soil, which reduced infiltration and soil moisture storage, was another consequence of the low temperature. It also delayed or stopped the process of surface runoff generation. Due to low temperature, snow was accumulated and stored in the snowpack and it could not be melted until the temperature increased. Overall, the uniqueness of the drought drivers in cold climates entitled these types of regions to have special drought indices such as the HADI.

2.2. A Snow-based Hydroclimatic Aggregate Drought Index for Identification, Categorization, and Short-Term Lead Drought Prediction in Cold Climate Regions[1]

2.2.1. Abstract

Climate change has increased the risk of snow drought, which is associated with the deficit in snowfall and snowpack. The objectives of this research are to improve drought identification in warming climate by developing a new snow-based hydroclimatic aggregate drought index (SHADI) and to assess the impacts of snowpack and snowmelt in drought analyses. To derive the SHADI, an R-mode principal component analysis is performed on precipitation, snowpack, surface runoff, and soil water storage. Then, a joint probability distribution function of drought frequencies and drought classes, conditional expectation, and k-means clustering are used to categorize droughts. The SHADI was applied to the Red River of the North Basin (RRB), a typical cold climate region, to characterize droughts in a mostly dry period from 2003 to 2007. The SHADI was compared with the Palmer drought severity index (PDSI), the hydroclimatic aggregate drought index (HADI), and the U.S. drought monitor (USDM) data. The SHADI showed the capabilities of identifying both dry and warm snow droughts, while the PDSI was able to identify dry snow drought but failed to identify dry/wet spells and warm snow drought due to its simplification in the separation of snowfall and rainfall, frozen soil, and snow accumulation processes in cold climate regions. Particularly, the SHADI facilitated a 2-month lead prediction of drought. The major differences between SHADI and HADI were observed in cold seasons and in transition periods (dry-to-wet or wet-to-dry). The derived variable threshold levels for different categories of drought based on the SHADI were close to, but different from those of the HADI. Due to the use of these variable thresholds,

[1] The material in this chapter was co-authored by Mohammad Hadi Bazrkar and Dr. Xuefeng Chu. Mohammad Hadi Bazrkar had primary responsibility for developing the new drought index and drought analyses. Mohammad Hadi Bazrkar was the primary developer of the conclusions that are advanced here. Mohammad Hadi Bazrkar also drafted and revised all versions of this chapter. Dr. Xuefeng Chu served as proofreader and checked analysis conducted by Mohammad Hadi Bazrkar.

despite similarities in drought onset and termination, drought area coverages for each drought category identified by SHADI and HADI were different from that of USDM. The SHADI can be used for a short-term lead prediction of droughts in cold climates regions and, in particular, can provide an early warning for drought in the warming climate.

2.2.2. Introduction

Climate change and global warming have caused temperature variability, a warming climate, and consequently a shrinkage in average snow cover and montane snowpack (Marty et al. 2017, Sproles et al. 2017, Huning and Aghakouchak, 2018). The function of snowpack is similar to a seasonal natural reservoir; where snowmelt leads the equivalent stored water to be released by an increase in temperature. The magnitude and occurrence timing of temperature and precipitation have been affected by climate change, which has increased the risk of snow drought.

Snow drought and its impact on water resources availability were introduced by Schneider & Matson (1977) and Wiesnet (1981). Snow drought is referred to "a period of abnormally little snowpack for the time of year, reflecting either below-normal cold-season precipitation or a lack of snow accumulation despite near-normal precipitation, usually when warm temperatures prevent precipitation from falling as snow or result in unusually early snowmelt" (American Meteorological Society 2019). Based on the definition of snow drought, the drought drivers include (1) quantity and (2) timing. The first drought driver is associated with the deficit in the amount of precipitation and/or high or low levels of temperatures, while the second drought driver is characterized by an early or late occurrence of hydroclimatic processes such as snowfall and snowmelt. Snow drought can also be divided into temperature-driven or precipitation-driven categories (Harpold et al. 2012; Van Loon et al. 2015; Cooper et al. 2016). Harpold et al. (2017) also classified snow drought into dry snow drought and warm snow drought based on these climatic drivers. Dry snow droughts are caused by a deficit in

winter precipitation. While above-normal winter temperatures (consequently, late onset of snow season), midseason snowmelt or rainfall events, and early spring snowmelt cause warm snow drought (Dierauer et al. 2019). For instance, a temperature threshold of -3.1 °C - 1.4 °C led to a rapid increase in the risk of warm snow drought in southwestern Canada (Dierauer et al. 2019). Therefore, the first step of drought identification is to understand the dominant hydroclimatic processes and drought drivers and types (Mote 2003). This essential step ensures to use the right tools or drought indices (Staudinger et al. 2011).

Each region has its own distinct drought drivers (Van Loon et al. 2015). For example, low precipitation, high temperature, and low initial soil moisture caused a considerable reduction in snowmelt runoff in the Canadian prairies (Fang and Pomeroy 2007). Generally, a low amount of precipitation (snowfall and rainfall) because of high temperature in winter may bring about "warm snow season drought." Moreover, in regions where the winter temperatures normally are far below zero for a long time (e.g., more than 6 months of a year), a mild anomaly in winter temperature may affect snow accumulation, snow water equivalent, and streamflow. In such areas, a lack of snow accumulation due to snowfall deficit or high temperature in winter provokes a shift in the timing of snowmelt and causes "snowmelt drought" (Van Loon and Van Lanon 2012; Van Loon et al. 2015). These drought classes accentuate the necessity of consideration of snow storage and release (snowmelt) in identification of drought in the regions with snow accumulation and snowmelt processes.

Snow drought can cause some challenges for water resource management in cold climate regions. On the one hand, the lack of snowpack causes a reduction in available water resources in warm seasons and, on the other hand, a substitution of rain for snow in unusually warm winters leads to a higher risk of flood in mountainous regions. Correspondingly, snow drought can cause serious ecological and socioeconomic impacts (Dierauer et al. 2019). For example, the agricultural losses of the 2015 dry snow drought in the Sierra Nevada region of the U.S. were estimated to be about $1.84 billion for a reduction of 20 - 60% in the normal precipitation

(Howitt et al. 2015). In this region, extreme early season precipitation, frequent rain-on-snow events, and low-precipitation years were the main causes of snow drought (Hatchett and McEvoy 2018). Therefore, understanding the mechanisms of droughts and their drivers in cold climate regions is important to identification of snow droughts and mitigation of their impacts.

To mitigate the impacts of droughts in the changing climate, a special drought index for the identification of snow droughts is essential. There exist a few drought indices, which account for the anomalies of snowpack. Huning and Aghakouchak, (2020) developed a standardized snow water equivalent index (SWEI) by considering snow water equivalent (SWE) to assess global snow drought. Since a below normal SWE in cold seasons can be compensated by a high antecedent soil water storage or an upcoming rainfall events in warm seasons, consideration of other hydroclimatic variables can provide more information about drought. The surface water supply index (SWSI) (Shafer and Dezman 1982) and aggregate drought index (ADI) (Keyantash and Dracup 2004) account for snowpack amounts in addition to other hydroclimatic variables. In contrast, there are some other indices, which account for available water, instead of the stored water sources. For example, the standardized snowmelt and rainfall index (SMRI) (Staudinger et al. 2014) and hydroclimatic aggregate drought index (HADI) (Bazrkar et al. 2020) consider snowmelt and rainfall. Some studies demonstrated the critical roles of snow-based drought indices (Huning and Aghakouchak, 2020) and their capabilities for short-term lead prediction of drought (Abel et al. 2018) in a changing climate. However, some researchers (Livneh and Badger 2020) found drought less predictable by using snow-based approaches under declining future snowpack in a warming climate. The objectives of this research are (1) to improve drought identification in cold climate regions and in the warming climate by developing a new snow-based hydroclimatic aggregate drought index (SHADI) and (2) to assess the impacts of snowpack and snowmelt in drought analyses by comparing SHADI with HADI and Palmer drought severity index (PDSI) (Palmer 1965).

2.2.3. Methodology

2.2.3.1. Study Area

The Red River of the North Basin (RRB) (Figure 2.18) is located in the Northern Glaciated Plains and covers over 90,000 km^2 in the states of Minnesota, North Dakota, and South Dakota. In the RRB, cold and dry winters are common due to a strong continental climate, a very low amount of air moisture, and cold intrusions from the polar and arctic regions (NDAWN, 2014). Remarkably, the precipitation in the six cold months from October through March accounts for only about 22% of the annual precipitation. In contrast, a slow transition in low-level wind flow brings about a high amount of moisture from the Gulf of Mexico in spring. Therefore, springs and summers are generally warm and wet (NDAWN, 2014). The climate divisions (CDs) in the RRB are shown in Figure 2.18.

A large portion of the Great Plains was hit by the 1930s devastating drought, known as the Great Drought or Dust Bowl. It led to a steady drop in the population of the area, especially in North Dakota due to poor crop yields. The culmination of the Great Drought occurred in 1936. The winter of that year was recorded as the most severe cold season in the area (NDAWN, 2014). That drought lasted a long time until the emergence of the cool and wet summer of 1942, and the driest years were recorded in 1934 and 1936. According to the 118-year data (1901 - 2019), the mean discharge of the Red River is 12.77 m^3/s and the minimum and maximum discharges at the Fargo Station are 0.045 m^3/s (1937) and 226.8 m^3/s (1998), respectively (USGS 2020).

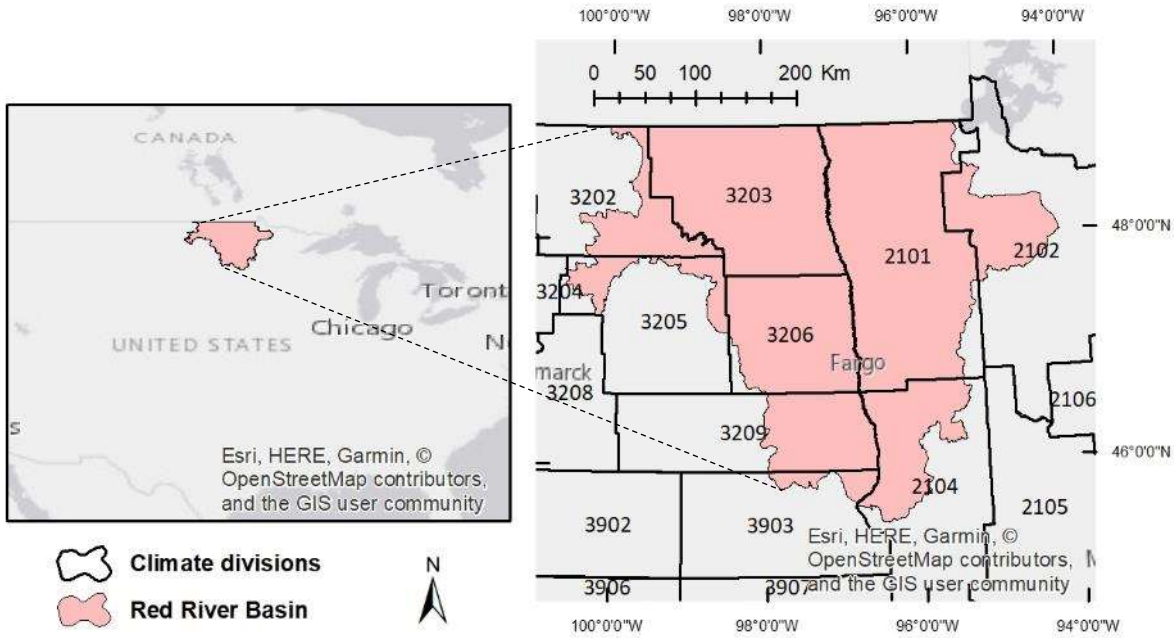

Figure 2.18. Red River Basin (RRB) and its associated climate divisions

Figures 2.19a and 2.19b depict the precipitation amounts in the warm season (April through September) and cold season (October through March) at the Grand Forks Station, ND from 1920 to 2018. Figure 2.19a shows that the lowest precipitation in the warm seasons occurred in 1934 and 1936 over this long period. However, as shown in Figure 2.19b, the precipitation in the cold seasons was not among the lowest in these two years. The heatmaps (Figure 2.19a and 2.19b) indicate that the precipitation values with the highest frequencies in 1930's for the warm and cold seasons were 300-350 mm and 100-125 mm, respectively. Similarly, the temperatures (Figure 2.20a and 2.20b) for the warm and cold seasons were 15 °C to 17.5 °C and -7.5 °C to -5 °C, respectively. Thus, the Great Drought was induced mainly by the low precipitation in the warm seasons (Figure 2.19a), unusually low temperature in the cold seasons (Figure 2.20b), and abnormally high temperature in the warm seasons (Figure 2.20a). The lowest precipitation and the highest temperature in the cold seasons occurred in 1990's (Figure 2.19b), which can be referred to as snow drought. The precipitation in the cold seasons in the last two decades was relatively low. Therefore, a drought index with the capability of addressing snow drought is required. To test the performance of the SHADI, it was applied to

the RRB for a period from 2003 to 2007, the longest dry period after 2000 in the area (USDM 2019).

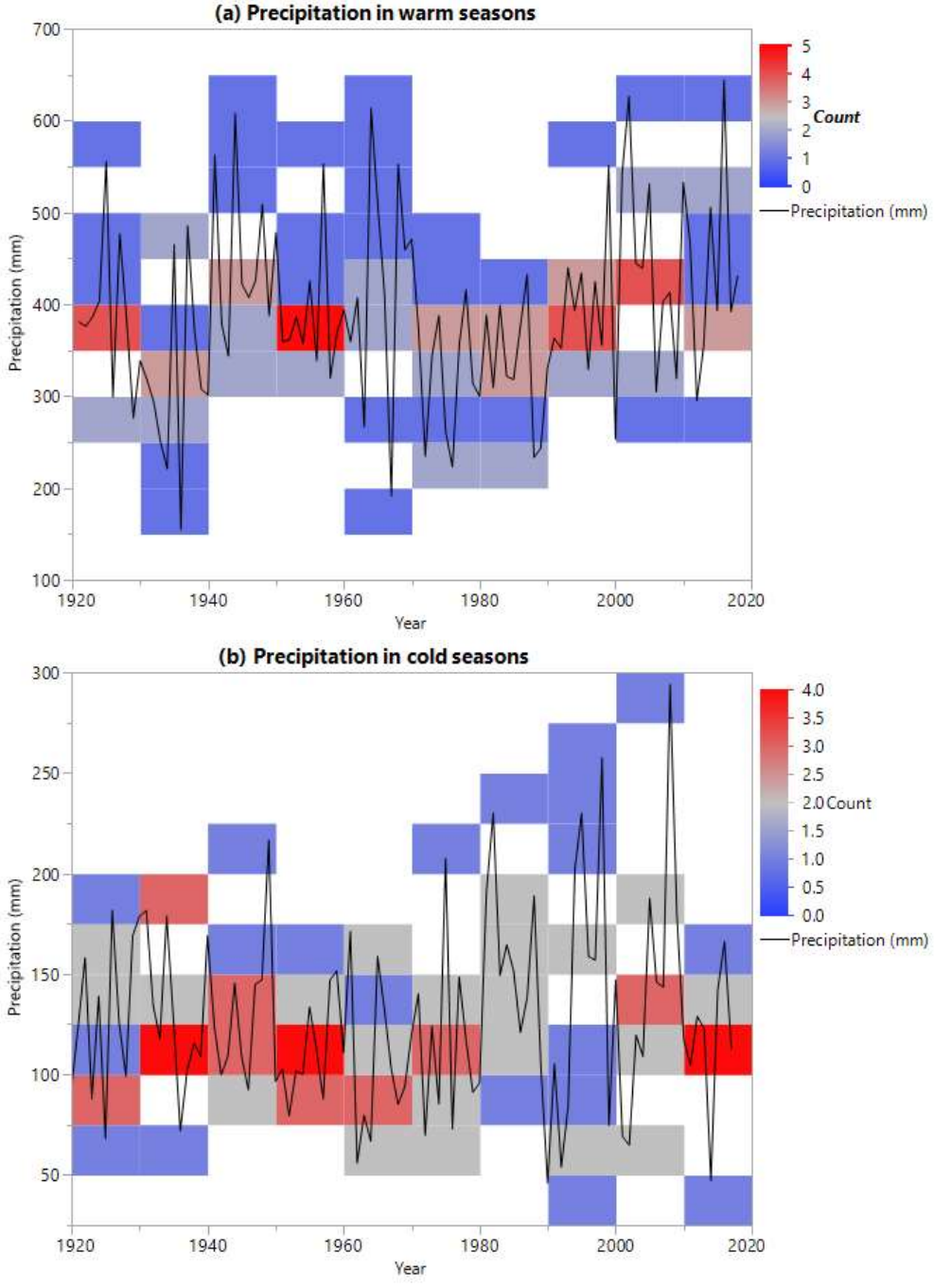

Figure 2.19. Heatmap of total annual precipitation at Grand Forks station: (a) warm seasons and (b) cold seasons

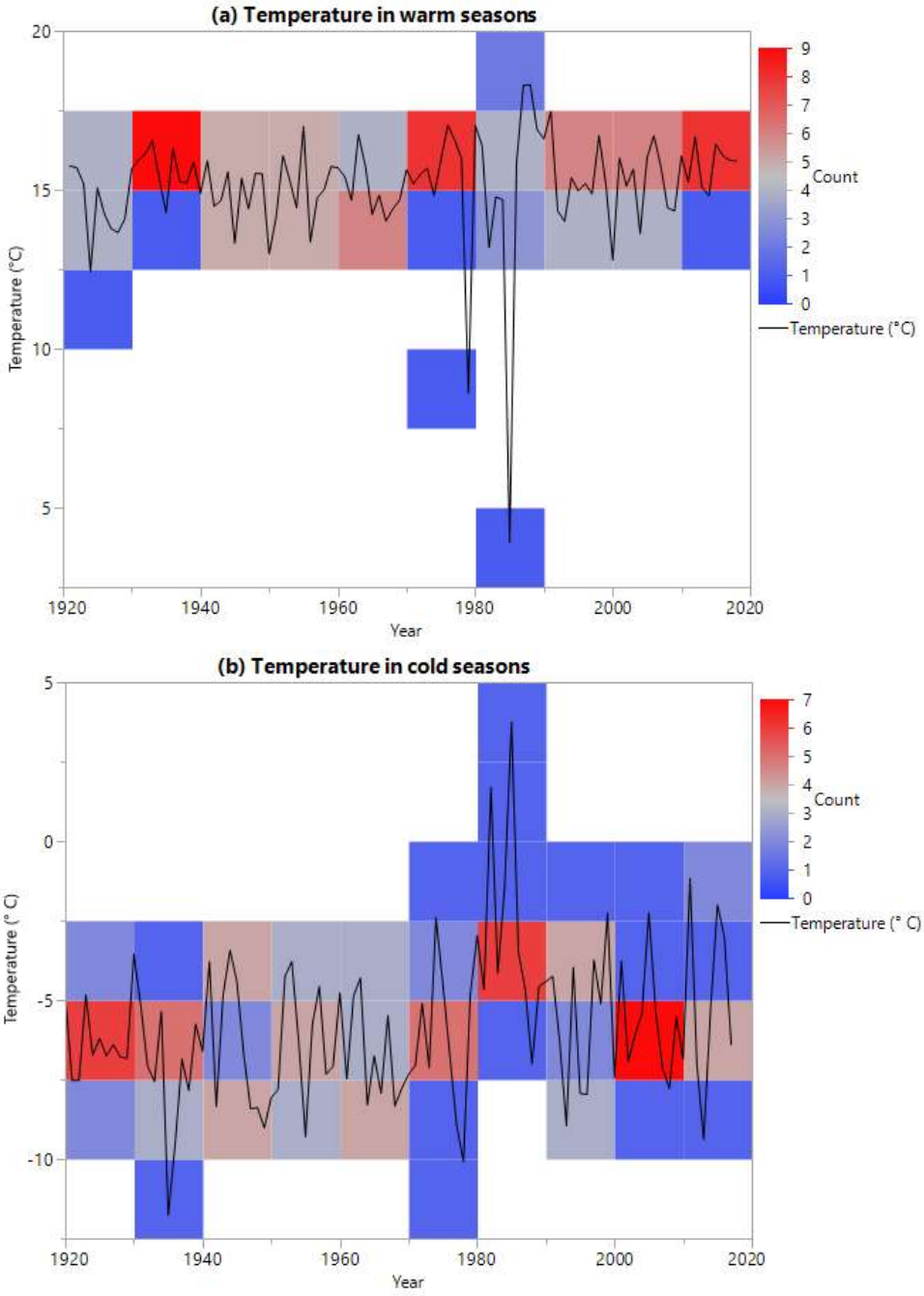

Figure 2.20. Heatmap of average annual temperature at Grand Forks station: (a) warm seasons and (b) cold seasons

2.2.3.2. SHADI

Precipitation, snowpack, surface runoff, and soil water storage of the root zone are used to derive the SHADI. The input data and variables for calculating SHADI are listed in Table 2.7. Snowpack is the primary variable in the identification of snow drought. Thus, the SHADI can

potentially address the anomalies in stored water as a snow drought index. The other hydroclimatic variables (i.e., precipitation, surface runoff, and soil water storage) are also integrated to address other types of drought.

Table 2.7. Input data and variables for calculating SHADI

Variables	Acronym
Precipitation	P
Snowpack	SP
Surface runoff	R
Soil water storage	SWS

Similar to the HADI (Bazrkar et al. 2020), the SHADI accounts for the impacts of available water or stored water on drought characterization. However, the SHADI uses precipitation and snowpack, instead of rainfall and snowmelt in the HADI. The daily snowpack, surface runoff, and soil water storage simulated by a grid-based hydrologic model (GHM) (Chu et al. 2018) are used after being converted to monthly values. To overcome the high covariance of these variables, they are standardized by:

$$P_{i,j}^{stz} = \frac{P_{i,j} - \mu_j^P}{\sigma_j^P} \tag{2.10}$$

$$SP_{i,j}^{stz} = \frac{SP_{i,j} - \mu_j^{SP}}{\sigma_j^{SP}} \tag{2.11}$$

$$R_{i,j}^{stz} = \frac{R_{i,j} - \mu_j^R}{\sigma_j^R} \tag{2.12}$$

$$SWS_{i,j}^{stz} = \frac{SWS_{i,j} - \mu_j^{SWS}}{\sigma_j^{SWS}} \tag{2.13}$$

where $P_{i,j}^{stz}$, $SP_{i,j}^{stz}$, $R_{i,j}^{stz}$, and $SWS_{i,j}^{stz}$ are the standardized values of precipitation, snowpack, surface runoff, and soil water storage of grid j in month i, respectively; $P_{i,j}$, $SP_{i,j}$, $R_{i,j}$, and $SWS_{i,j}$ are the precipitation, snowpack, surface runoff, and soil water storage of grid j in month i, respectively; μ_j^P, μ_j^{SP}, μ_j^R, and μ_j^{SWS} are the mean values of precipitation, snowpack, surface runoff, and soil water storage of grid j in the entire period, respectively; and σ_j^P, σ_j^{SP}, σ_j^R, and

σ_j^{SWS} are the standard deviation values of precipitation, snowpack, surface runoff, and soil water storage of grid j in the entire period, respectively. By performing a correlation-based R-mode principal component analysis (PCA) (Cattell, 1952) on the standardized variables, the SHADI is estimated for grid j and month i. The principal components (PCs) are given by (Cattell, 1952):

$$\begin{bmatrix} PC_{i,j}^{1} \\ PC_{i,j}^{2} \\ PC_{i,j}^{3} \\ PC_{i,j}^{4} \end{bmatrix} = \begin{bmatrix} a_i^{11} & a_i^{12} & a_i^{13} & a_i^{14} \\ a_i^{21} & a_i^{22} & a_i^{23} & a_i^{24} \\ a_i^{31} & a_i^{32} & a_i^{33} & a_i^{34} \\ a_i^{41} & a_i^{42} & a_i^{43} & a_i^{44} \end{bmatrix} \cdot \begin{bmatrix} P_{i,j} \\ SP_{i,j} \\ R_{i,j} \\ SWS_{i,j} \end{bmatrix} \tag{2.14}$$

where $(PC_{i,j}^{1})$ to $(PC_{i,j}^{4})$ are the first to fourth PCs for grid j in month i; and a_i^{11} to a_i^{14}, a_i^{21} to a_i^{24}, a_i^{31} to a_i^{34}, and a_i^{41} to a_i^{44} are respectively the normalized eigenvectors of the first, second, third, and forth PC in month i. The elements of the eigenvector are unequal weights in the PCs for month i. The drought types can be determined by these unequal weights, which are based on the highest variances among the variables. The drought type is defined by the highest absolute values of loadings of the first PC, since the effect of the corresponding hydroclimatic variable on the PC values is greater. If the absolute value of the loading of precipitation is the highest, the drought is classified as a meteorological drought. Since the anomalies in snowpack, snowmelt, and surface runoff represent hydrologic drought, if the absolute values of the loadings of one of these variables are among the highest, the drought is classified as a hydrologic drought. If the absolute value of the loading of soil water storage is the highest, agricultural drought is determined.

The PCs should be standardized to be independent of time and space, and thus comparable for any normal conditions. The mean and standard deviation values of the first PCs throughout the study period in each grid are calculated. The SHADI is computed by standardization of the first PCs for each grid and month or the ratio of the difference between each first PC value and its mean to its standard deviation:

$$SHADI_{i,j} = \frac{PC_{i,j}^{1} - \mu_{PC_j^1}}{\sigma_{PC_j^1}} \tag{2.15}$$

where $SHADI_{i,j}$ is the SHADI of grid j in month i; $PC_{i,j}^{1}$ is the first PC of grid j in month i; and $\mu_{PC_j^1}$ and $\sigma_{PC_j^1}$ are the mean and standard deviation of the first PC of grid j. The first PC is selected for estimation of the SHADI since a high proportion of information is found in the first PC.

To categorize droughts, a customized drought categorization based on variable threshold levels (Bazrkar et al. 2020) is implemented. According to the range of the SHADI values, they are divided into a defined number of classes. To estimate the spatial and temporal frequencies of the SHADI, a cell-by-cell based analysis is performed. The frequency of each drought class during the study period is estimated for each cell and the temporal frequencies of all drought classes for all cells are also estimated. The frequency and class of droughts form a bivariate function. Thus, a joint probability distribution function (JPDF) is determined. To find the probability of the occurrence of each class of drought, the conditional expectation is calculated. The lower the conditional expectation, the lower the probability of occurrence and the higher risk of rare drought. The conditional expectation for each class of drought is given by (Hogg and Craig 1978):

$$g(f|c) = \frac{g(f,c)}{g(c)} = \begin{bmatrix} g(0|1) & g(0|2) & \dots & g(0|n) \\ g(1|1) & g(1|2) & \dots & g(1|n) \\ \dots & \dots & \dots & \dots \\ g(m|1) & g(m|2) & \dots & g(m|n) \end{bmatrix} \tag{2.16}$$

in which

$$\mathrm{g}(f,c) = \begin{bmatrix} g(0,1) & g(0,2) & \dots & g(0,n) \\ g(1,1) & g(1,2) & \dots & g(1,n) \\ \dots & \dots & \dots & \dots \\ g(m,1) & g(m,2) & \dots & g(m,n) \end{bmatrix} \tag{2.17}$$

$$g(c) = \sum_{c=1}^{n} \sum_{f=1}^{m} g(f,c) \tag{2.18}$$

where $g(f,c)$ is the JPDF of frequency f and drought class c; $g(c)$ is the probability distribution function of drought class c; and $g(f \mid c)$ is the conditional probability. The conditional expectation of different frequencies for each associated class, P_c or $E(f \mid c)$ can be expressed as:

$$P_c = E(f|c) = \sum_{f=1}^{m} (f \cdot g(f|c)) \tag{2.19}$$

To derive the threshold levels for different drought categories, the k-means clustering method (MacQueen, 1967) is used. The k-means clustering employs a partitioning approach, in which the observations are separated into n clusters without using a hierarchical method. Partitioning is the most commonly used method among nonhierarchical methods of clustering. The specific procedures for determining the variable threshold levels using k-means include (MacQueen, 1967): (1) select n items to serve as seeds (i.e., initial cluster centroids); (2) assign each observation in the dataset to the cluster with the nearest seed/centroid based on the squared Euclidean distance; (3) recalculate the centroid for each cluster (i.e., the mean vector of all observations in the cluster); and (4) repeat steps 2 and 3 until no observations move to different clusters.

To account for the slow emergence and recession of drought, Svoboda et al. (2002) used six categories (exceptional, extreme, severe, moderate, abnormal, and normal) in the USDM. The same numbers of drought categories in the USDM are used in this study. Four wet classes (including exceptional, extreme, severe, moderate wet) are also considered to categorize the wet conditions. Thus, the customized drought categorization is based on these ten dry and wet clusters. Ten points that are mutually farthest apart are selected as initial seeds in the k-means clustering. The observation vector can be expressed as:

$$\begin{cases} \boldsymbol{y_1} = (c_1, P_1) \\ \boldsymbol{y_2} = (c_2, P_2) \\ \quad \vdots \\ \boldsymbol{y_n} = (c_n, P_n) \end{cases} \tag{2.20}$$

where c_1 is the representative of lower class limit for class 1 of the SHADI; and P_1 is the expected value of probability of occurrence of class 1. The k-means method clusters these n observations into ten groups. The initial centroids are the ten observations that are farthest apart. The procedure starts by calculating the squared Euclidean distance between each pair of observations:

$$\begin{cases} d^2(\boldsymbol{y_k}, \boldsymbol{y_{k+1}}) = (c_k - c_{k+1})^2 + (P_k - P_{k+1})^2 \\ d^2(\boldsymbol{y_k}, \boldsymbol{y_{k+2}}) = (c_k - c_{k+2})^2 + (P_k - P_{k+2})^2 \\ \vdots \\ d^2(\boldsymbol{y_{k+1}}, \boldsymbol{y_{k+2}}) = (c_{k+1} - c_{k+2})^2 + (P_{k+1} - P_{k+2})^2 \\ \vdots \\ d^2(\boldsymbol{y_{n-2}}, \boldsymbol{y_n}) = (c_{n-2} - c_n)^2 + (P_{n-2} - P_n)^2 \\ d^2(\boldsymbol{y_{n-1}}, \boldsymbol{y_n}) = (c_{n-1} - c_n)^2 + (P_{n-1} - P_n)^2 \end{cases} \quad (2.21)$$

where $d^2(\boldsymbol{y_k}, \boldsymbol{y_{k+1}})$ is squared Euclidean distance between $\boldsymbol{y_k}$ and $\boldsymbol{y_{k+1}}$ observation vectors for k (k=1, …, n). Ten points with the longest pairwise distances are selected as the initial seeds. The distances from each observation to the initial seeds are calculated. Then, the centroid of each cluster and the distance from each observation to each centroid are calculated. These processes are repeated until the cluster assignments in the last step are the same as those in the previous step.

2.2.3.3. Assessment of SHADI in Identification and Categorization of Droughts

To assess the performance of the SHADI in identification of droughts, it was compared with the well-established, water-balance-based PDSI, ND agriculture-based gross domestic production (GDP), and HADI for CD 3206 (Figure 2.18). A great portion of CD 3206 is covered by agricultural lands; therefore, drought impacts on the agriculture-based GDP can be observed. The PDSI and GDP data were obtained from the NOAA's National Centers for Environmental Information (NOAA's NCEI 2019) and the Bureau of Economic Analysis (BEA), U.S. Department of Commerce (BEA 2019), respectively. After the assessment of the SHADI, the new customized drought categorization was applied to the RRB. The drought classification results based on the SHADI and HADI were further compared and their performances were evaluated for the entire RRB and separately for CDs 2101, 3203, and 3206 (Figure 2.18).

The SHADI, HADI, and USDM (Svoboda et al. 2002; USDM 2019) were compared in the form of drought severity and coverage index (DSCI) (Akyuz, 2017). The USDM (Svoboda et al. 2002) is "a composite product" based on the Objective Drought Indicator (ODI) Blends. The USDM product is a blend of six main drought indicators and other objectively-selected ancillary

indices including the PDSI, CPC soil moisture model (percentiles), USGS weekly streamflow (percentiles), percent of normal, SPI, and satellite vegetation (Svoboda et al. 2002). Additional information about the conditions of soil moisture and snowpack is added by other ancillary indices (e.g., SWSI).

There are some differences in the derivations of USDM, HADI, and SHADI. Soil moisture and observed streamflow are used in the USDM, while the simulated surface runoff and soil water storage in the root zone are used in the SHADI and HADI. Although precipitation and snowpack are considered in the derivation of the USDM products, separation of rainfall and snowfall and snowmelt are ignored in the USDM. In contrast, the SHADI and HADI account for these dominant hydroclimatic processes in cold climate regions (precipitation and snowpack in SHADI and rainfall and snowmelt in HADI).

The drought severity and drought coverage index (DSCI) (Akyuz, 2017) turned the USDM categorical drought into one value. The DSCI is used to compare both severity and coverage of drought in the USDM, SHADI, and HADI. The DSCI is given by (Akyuz, 2017):

$$DSCI = \sum_{i=0}^{4}(i+1) \times ACD(i) \tag{2.22}$$

where *ACD (i)* is the percentage of area coverage of drought in category *i*.

Finally, the outputs of the cluster analysis for precipitation, rainfall, snowpack, snowmelt, surface runoff, and soil water storage (i.e., inputs of the HADI and SHADI) were compared with their corresponding indices. In the k-means clustering for these hydroclimatic variables, to avoid complexity, only two clusters (dry/wet) were defined.

2.2.4. Results and Discussion

2.2.4.1. Comparison of SHADI and HADI with PDSI and ND Agriculture-based GDP

To evaluate the performances of the HADI and SHADI, they were compared with the PDSI and the agriculture-based GDP for CD 3206 (Figure 2.21). Notable discrepancies between

the monthly values of these three indices were observed. Both HADI and SHADI showed that a drought commenced in 2004 and terminated in 2007, and particularly, SHADI provided a one- or two-month lead drought prediction. The feasibility of short-term lead prediction for short term drought warning using the standardized precipitation index (McKee et al. 1993) and standardized runoff index (SRI) (Shukla and Wood 2008) was examined by Li et al. (2016). The same 2-month lead prediction was obtained by using the SHADI. This capability can be attributed to its consideration of snowpack. Abel et al. (2018) also found that the predictability of drought was increased by considering snow water equivalent. Although Livneh and Badger (2020) suggested to find alternatives for snow-based forecasting for water management due to a warmer future and reduced snowpack, the results of this study demonstrated that the snow-based forecasting can be helpful for short-term early warning of drought.

Consistency is one of the significant characteristics of a drought index. Since the HADI and SHADI have a monthly time scale, they can be influenced by short-duration events. The flash wet periods (e.g., February and March 2005, Figure 2.21a) were the results of such short events. Ignoring these flash wet periods, the HADI and SHADI exhibited a long dry period in 2003 to 2007. However, the PDSI identified an extreme wet condition started from the middle of 2004 and ended by the beginning of 2006 (Figure 2.21a). Thus, the HADI and SHADI demonstrated more consistency than the PDSI. In addition, the agriculture-based GDP was in contradiction with the PDSI results (Figure 2.21b). The GDP during 2003 was relatively high, indicating that 2003 was a wet year. The average values of the HADI and SHADI for 2003 were 0.43 and 0.27, respectively, which also indicated a relatively wet year. However, the PDSI value was much lower (0.04). Guttman et al. (1992) also found more severe PDSI for normal climate conditions in the Great Plains, where the RRB is located.

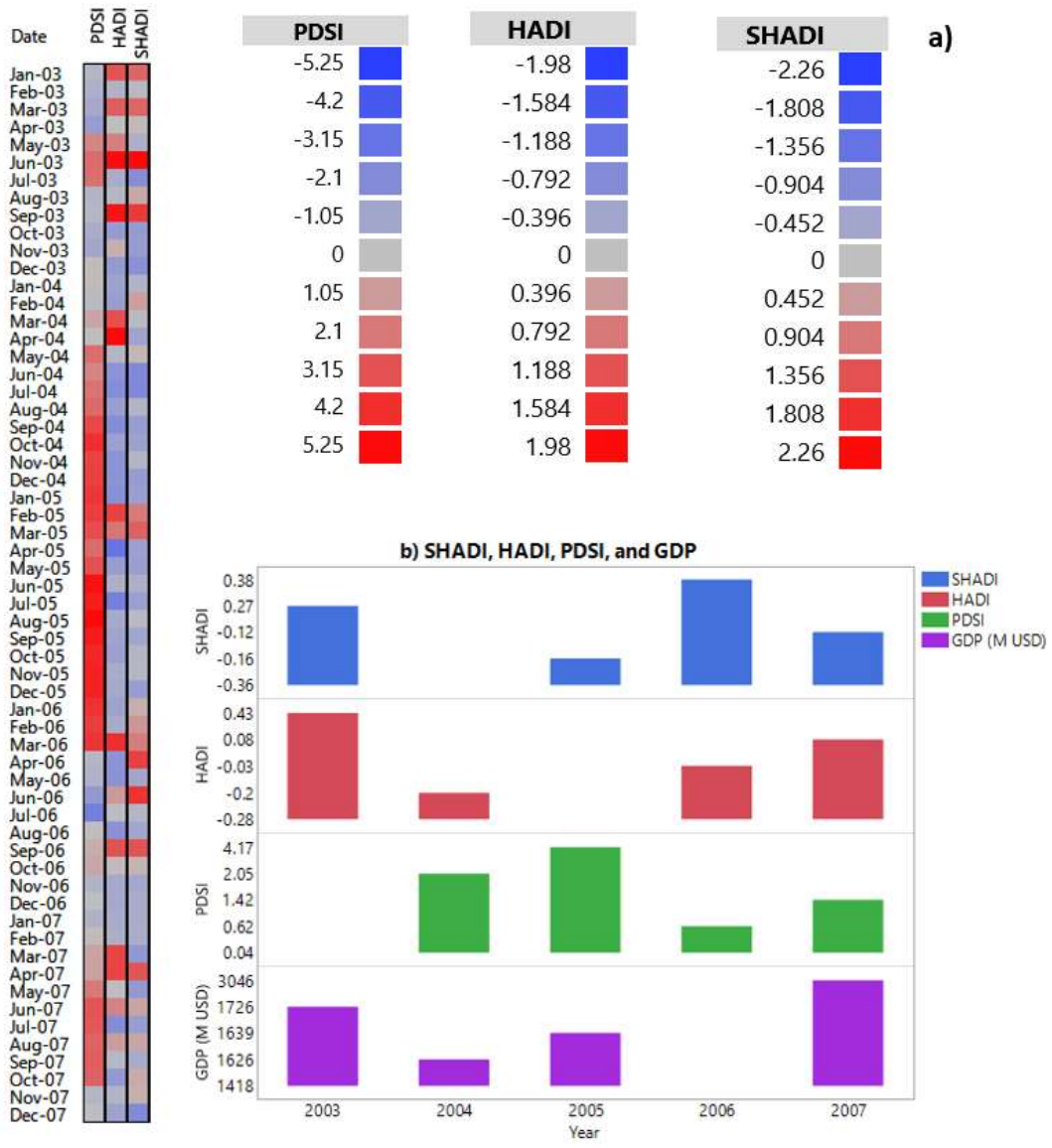

Figure 2.21. PDSI, HADI, SHADI, and ND agriculture-based GDP in climatic division 3206: (a) monthly and (b) annual

The GDP in 2004 decreased by $100 million, which can be related to the drought. The areal average values of HADI (- 0.20) and SHADI (- 0.36) in 2004 showed a dry condition, while the PDSI (2.05) showed a wet condition. The PDSI for 2005 (4.17) also indicated a wet year with a high intensity. However, the HADI (- 0.28) and SHADI (- 0.16) for 2005 remained negative (i.e., a dry condition). The differences between the PDSI and the HADI and SHADI can mainly be attributed to the fact that in the PDSI precipitation is assumed as immediately available

rainfall (i.e., no distinction between rainfall and snowfall) (Dai et al. 2004) and snowpack and snowmelt are not considered. In 2005, the GDP slightly increased to $1,639 million, which was about half of the GDP in 2007. Both HADI and PDSI identified 2007 as a wet year, which was in accordance with the GDP ($3,046 million). This was the highest GDP over the study period. In contrast, the GDP in 2006 ($1,418 million) is the lowest. This can be interpreted as a result of the antecedent long dry period started from 2004. The HADI value in 2006 (- 0.03) was still negative, while the PDSI (0.62) and SHADI (0.38) were positive. The positive value of the SHADI can be attributed to the consideration of snowpack and its consequent capability of lead prediction of the upcoming wet condition in 2007.

The Pearson correlation coefficient between soil moisture and PDSI was 0.48. This value can be mostly associated with the good correlation of the PDSI with soil moisture content during warm seasons. For instance, the lowest value of the PDSI (-2.65) was obtained in summer 2006, when the soil moisture reached its lowest in the study period (Figure 2.29g). However, similar to the results of Dai et al. (2004), the PDSI was not able to show the soil moisture trend due to its poor reflection of soil moisture conditions in frozen soil during winter and early spring months. Therefore, it can be concluded that the PDSI is not always a good measure of soil moisture and thus agricultural droughts. Besides, the PDSI was not in good agreement with the GDP. In contrast, the HADI demonstrated a trend similar to that of the GDP. Thus, the HADI outperformed the PDSI since the HADI results were in accordance with those from the agriculture-based GDP. The HADI and SHADI had the same values until November 2003 (Figure 2.21a). According to the SHADI, a long dry period started in November 2003, while the HADI showed that the drought commenced in December 2003. The slight discrepancies between the SHADI and GDP in 2006 and 2007 can be related to the reflection of the future condition in the SHADI. Again, the SHADI exhibited the capability of a short-term lead prediction of droughts. Unlike HADI, the SHADI and PDSI can be relatively weak in the

identification of agricultural droughts. However, SHADI can provide an earlier warning for the upcoming drought.

Two typical snow droughts (Harplod et al. 2017), dry snow drought and warm snow drought, were observed in 2003 and 2005 water years, respectively. The precipitation amounts in October, November, and December of 2003 were respectively 22.9, 2.3, and 5.3 mm below the monthly average. Correspondingly, a smaller snowpack was observed, which signified a drought potential in such a dry cold season. This dry snow drought reflected abnormal high temperatures in the cold season in 2003, which was further intensified by the lack of winter precipitation. This early snowpack deficit signaled a possibility of drought in the coming late spring and summer. In 2005, temperature in most of the months of the cold season was likewise above the average. For instance, the temperatures in October, November, January, and February were 0.7, 1.2, 7.5, and 0.1 °C above the average. The precipitation in November 2005, on the other hand, was notably above average (25.7 mm above the average). Early snowmelt in this month (7.6 mm above its average) caused an increase in the surface runoff (1.4 mm above the average), which led to an earlier-than-normal arrival of the streamflow. However, the spring snowmelt in February 2005 was 3.4 mm below the average. The warm snow drought in 2005 reflected the lack of snow accumulation similarly due to the high temperature that increased the rainfall and melted snowpack, despite the above-average or near-normal precipitation. Both HADI and SHADI were able to identify these dry and warm snow droughts. The only minor discrepancy was observed in November 2003, when the HADI value turned slightly positive due to an earlier-than-normal snowmelt in that month (3.5 mm above normal). Despite a contradiction in December 2003 and January 2004, the PDSI was able to identify the dry snow drought in other months in the cold season since the dry snow drought was mainly due to the precipitation deficit and the PDSI did account for precipitation. However, the PDSI failed to identify the warm snow drought in 2005. The PDSI indicated an extreme wet condition in this

CD. Therefore, the HADI and SHADI outperformed the PDSI in the identification of warm snow drought.

2.2.4.2. Categorization and Classification of Droughts by SHADI and HADI

The droughts in the study period were characterized by using the customized drought categorization method for both SHADI and HADI. The threshold levels for different categories of drought based on the SHADI and HADI were close (Table 2.8). Since the study period and the study area remained unchanged, the threshold levels did not alter. This similarity can confirm the variability of the derived threshold levels by time and geographic locations. Figure 2.22 shows the percentage of drought area coverage in the RRB. In this figure, D0-D4 and D4 depict the abnormal dry condition and exceptional drought, respectively. Both the SHADI (Figure 2.22a) and HADI (Figure 2.22b) identified a long abnormal dry period.

The major difference in the area coverage of an abnormal dry condition based on the SHADI and HADI was the percentage of drought at the end of 2003. In this year, the percentage of the abnormal dry area coverage by the SHADI was much higher than that of the HADI. The drought area coverage percentages of the other categories of drought were almost the same throughout the study period except in 2007, when the SHADI identified a more severe drought. In addition, the SHADI preidentified a moderate to severe drought at the end of 2003. The HADI also identified a moderate drought in the beginning of 2006. However, the SHADI did not recognize any kind of drought at that time. Despite the similar variable threshold levels, the drought characterizations differed in some cases because these drought indices address the deficiency in different forms of water (stored/available water).

Table 2.8. Variable threshold levels and drought categories based on the SHADI

SHADI values	***HADI values***	***Category***	***Symbol***
SHADI > 4.7	*HADI > 4.6*	*Exceptional wet*	*W4*
2.9 < SHADI < 4.7	*2.9 < HADI < 4.6*	*Extreme wet*	*W3*
1.3 < SHADI < 2.9	*1.3 < HADI < 2.9*	*Severe wet*	*W2*
0.2 < SHADI < 1.3	*0.2 < HADI < 1.3*	*Moderate wet*	*W1*
−1.2 < SHADI < 0.2	*−1.1 < HADI < 0.2*	*Normal condition*	*N*
−1.5 < SHADI < −1.2	*−1.4 < HADI < −1.1*	*Abnormal drought*	*D0*
−1.6 < SHADI < −1.5	*−1.5 < HADI < −1.4*	*Moderate drought*	*D1*
−1.8 < SHADI < −1.6	*−1.7 < HADI < −1.5*	*Severe drought*	*D2*
−1.9 < SHADI < −1.8	*−1.8 < HADI < −1.7*	*Extreme drought*	*D3*
SHADI < −1.9	*HADI < −1.8*	*Exceptional drought*	*D4*

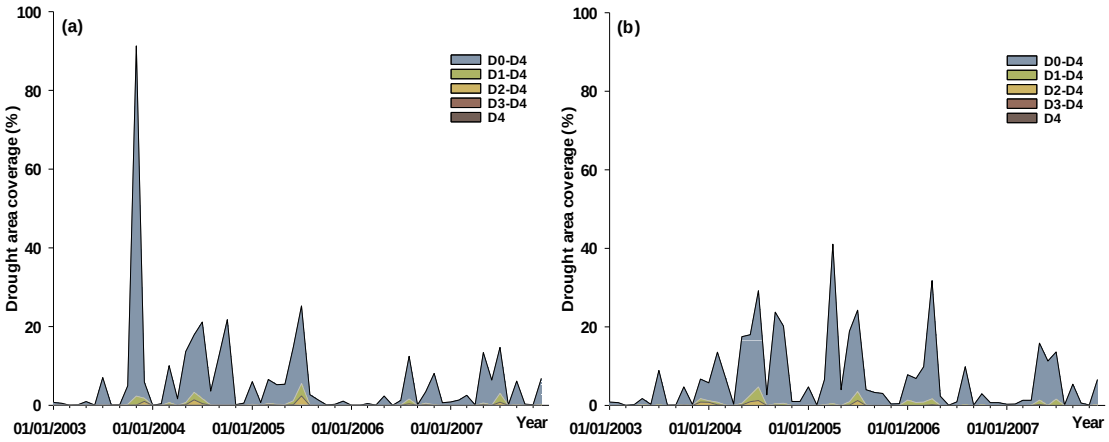

Figure 2.22. Drought area coverage based on (a) SHADI and (b) HADI in RRB (D0-D4 and D4 depict the abnormal dry condition and exceptional drought, respectively.)

Drought classifications, which determine the drought types and the targeted stakeholders, were compared for the HADI and SHADI. The loadings (weighting coefficients) of the hydroclimatic variables in the first PC can determine drought types. As shown in Table 2.9, the longest red band in each row indicates the highest loading of the hydroclimatic variables. Despite the resemblance in the drought classification results, the HADI demonstrated to be more consistent in identification of drought types since it is based on the available water sources.

Table 2.9. Absolute values of loadings (weighting coefficients) of the first principal component in SHADI and HADI (the blue and red bands indicate wet and dry periods, respectively.)

Month-Year	SHADI					HADI				
	Precipitation	Snowpack	Surface runoff	Soil Water Storage	Drought Type	Rainfall	Snowmelt	Surface runoff	Soil water storage	Drought type
Mar-04	0.18	0.39	0.90	0.01	–	0.15	0.38	0.91	0.02	–
Apr-04	0.22	0.03	0.10	0.97	A	0.13	0.90	0.05	0.43	–
May-04	0.23	0.01	0.97	0.07	H	0.20	0.03	0.98	0.04	H
Jun-04	0.43	0.01	0.86	0.29	H	0.41	0.01	0.86	0.29	H
Jul-04	0.74	0.02	0.66	0.08	H	0.67	0.02	0.74	0.07	H
Aug-04	0.87	0.04	0.43	0.24	M	0.85	0.02	0.45	0.26	M
Sep-04	0.47	0.02	0.88	0.11	H	0.38	0.01	0.92	0.10	H
Oct-04	0.54	0.02	0.84	0.08	H	0.55	0.15	0.82	0.09	H
Nov-04	0.07	0.02	0.03	1.00	A	0.07	0.07	0.03	0.99	A
Dec-04	0.05	0.31	0.14	0.94	A	0.11	0.28	0.15	0.94	A
Jan-05	0.15	0.97	0.01	0.21	H	0.06	0.00	0.16	0.99	A
Feb-05	0.06	0.93	0.37	0.04	–	0.00	0.88	0.48	0.02	–
Mar-05	0.01	0.31	0.94	0.10	–	0.01	0.44	0.89	0.09	–
Apr-05	0.02	0.01	0.15	0.99	A	0.00	0.97	0.12	0.21	H
May-05	0.37	0.01	0.86	0.36	H	0.32	0.01	0.87	0.37	H
Jun-05	0.21	0.00	0.98	0.06	H	0.20	0.00	0.98	0.06	H
Jul-05	0.37	0.02	0.91	0.16	H	0.36	0.01	0.92	0.16	H
Aug-05	0.83	0.02	0.56	0.06	M	0.35	0.01	0.92	0.18	H
Sep-05	0.54	0.03	0.73	0.41	H	0.48	0.02	0.76	0.43	H
Oct-05	0.01	0.02	0.68	0.73	A	0.26	0.89	0.23	0.28	H
Nov-05	0.07	0.16	0.18	0.97	A	0.03	0.09	0.17	0.98	A
Dec-05	0.12	0.99	0.01	0.13	H	0.04	0.48	0.31	0.82	A
Jan-06	0.12	0.99	0.04	0.11	H	0.01	0.04	0.13	0.99	A
Feb-06	0.06	1.00	0.05	0.02	H	0.00	0.00	0.11	0.99	A
Mar-06	0.05	0.16	0.98	0.05	–	0.05	0.77	0.63	0.05	–

Notes: A: agricultural drought; H: hydrologic drought; and M: meteorological drought.

In addition, the main differences were observed in July 2004 and August 2005, where the HADI identified a hydrologic drought while the SHADI showed a meteorological drought. Correspondingly, the HADI identified agricultural droughts in January 2005, December 2005, January 2006, and February 2006, while the SHADI identified hydrologic droughts, indicating that the role of consideration of available water sources is similar to the multiscalar drought indices approach. Therefore, the drought classification based on the HADI is more reliable.

2.2.4.3. Comparison of the Results of SHADI and HADI in the RRB

The Pearson and Spearman correlation coefficients of the SHADI and HADI (Figure 2.23a) were 0.75 and 0.78, respectively. The Spearman correlation coefficient indicated that the intensities of dry or wet conditions identified by the HADI and SHADI and their corresponding ranks among different months in the study period were close in the warm seasons. The Pearson correlation coefficient showed the similarity between the HADI and SHADI values in most of the months especially in the warm seasons. In fact, the differences were negligible in May to September in all years. However, notable dissimilarities were observed in the cold seasons and in the dry-wet or wet-dry transitions. The maximum difference between the HADI (1.73) and SHADI (-0.46) was observed in April 2004, featuring a transition from wet to dry conditions. Another transition period from dry to wet occurred in January 2006 (HADI = -0.46; SHADI = 0.23). In this month, the HADI remained negative, while the SHADI preidentified the upcoming wet condition. Moreover, in the middle of the long dry period (2004-2006), the HADI (1.41) identified a high-intensity wet condition in February 2005 (Figure 2.23c and Figure 2.23e). In contrast, the SHADI (0.47) showed a wet condition with a considerably less intensity in this month (Figure 2.23a and Figure 2.23d), indicating that the SHADI exhibited fewer fluctuations than the HADI.

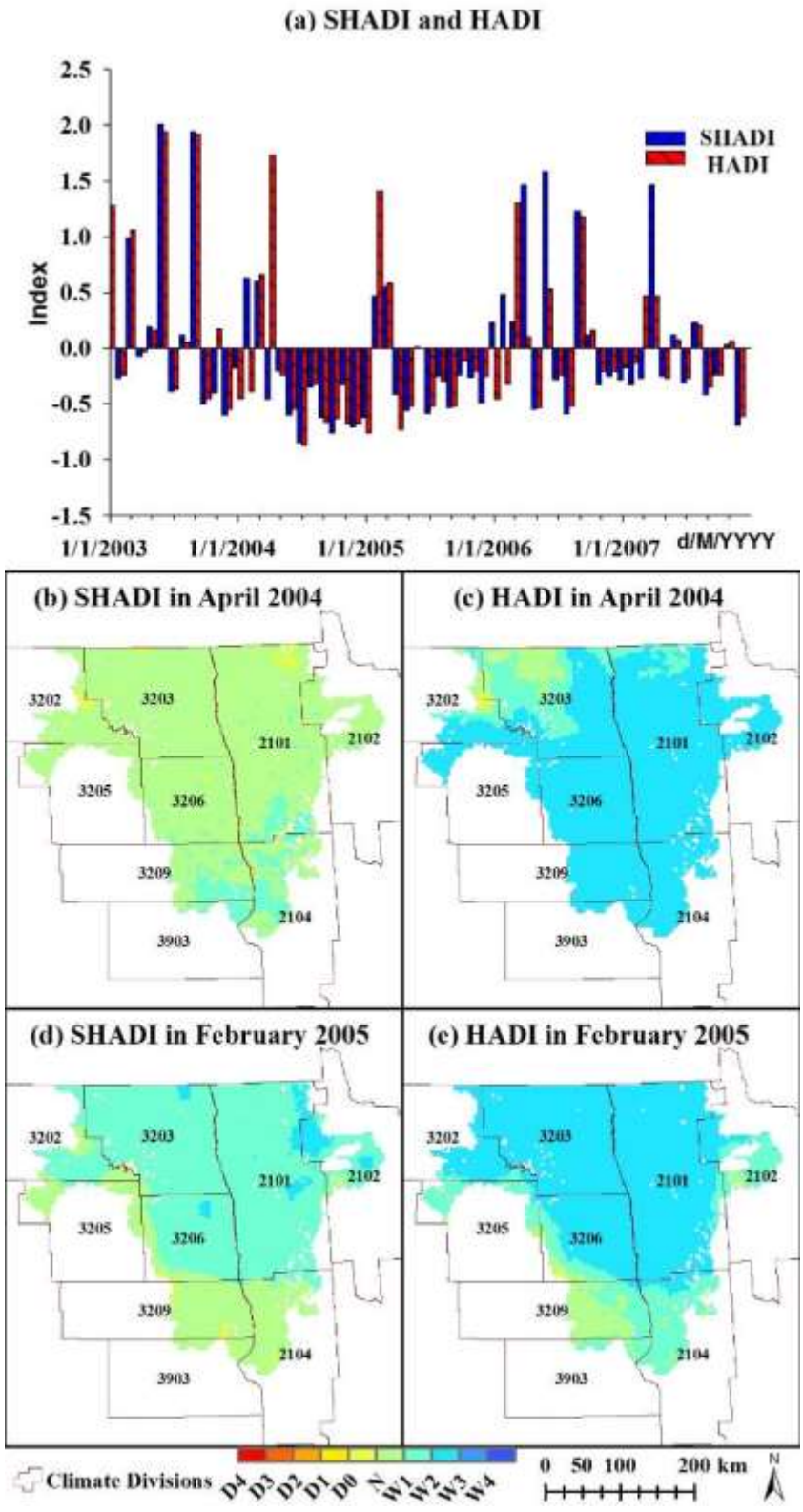

Figure 2.23. Comparison of temporal and spatial distributions of HADI and SHADI

The analysis of the dissimilarities in the spatial distributions of the HADI and SHADI helps determine the sensitivity of the indices to drought drivers (e.g., temperature-driven or precipitation-driven droughts). There was a minor difference between HADI and SHADI for 2003 (Figures 2.24a and 2.24f) and 2007 (Figures 2.24e and 2.24j). However, major differences were observed between HADI and SHADI in 2004 (Figures 2.24b and 2.24g), 2005 (Figures 2.24c and 2.24h), and 2006 (Figures 2.24d and 2.24i). These significant differences were in the upper RRB in 2004, the lower RRB in 2005, as well as the upper and northeast part of the RRB in 2006. As shown in Figure 2.25, the HADI and SHADI had similar values in 2003 (Figure 2.25a and 2.25f) and 2007 (Figures 2.25e and 2.25j). However, the SHADI indicated more intense droughts in the upper RRB in 2003 (Figures 2.25b and 2.25g) and in the lower RRB in 2004 (Figures 2.25c and 2.25h). By the end of the 2004 - 2006 drought (Figures 2.25d and 2.25i), the SHADI identified a wetter condition in the upper and northeast part of the RRB. The lowest annual precipitation occurred in 2003 (Figure 2.25k) and 2006 (Figure 2.25n). In addition, the western side of the RRB had a lower amount of precipitation than that of the eastern side. Figures 2.25p – 2.25t show the spatial distribution of the mean annual temperatures from 2003 to 2007. The lowest and the highest temperatures occurred in 2004 and 2006, respectively. 2004 was the coldest year in the study period. However, the high temperature in the upper RRB caused rainfall, instead of snow. Thus, the SHADI identified a dry condition with higher drought intensity due to the lack of snowpack (Figure 2.25b and Figure 2.25g). Both precipitation and temperature in the lower RRB in 2005 were relatively low and the intensity of drought based on the SHADI was higher (Figures 2.25c and 2.25h). The low precipitation and high temperature in the upper and northeast part of the RRB in 2006 led to high-intensity drought based on the HADI (Figures 2.25d and 2.25i). Therefore, it can be concluded that the SHADI is more sensitive to low temperature and the intensity of drought identified by the SHADI can be higher in cold climate conditions.

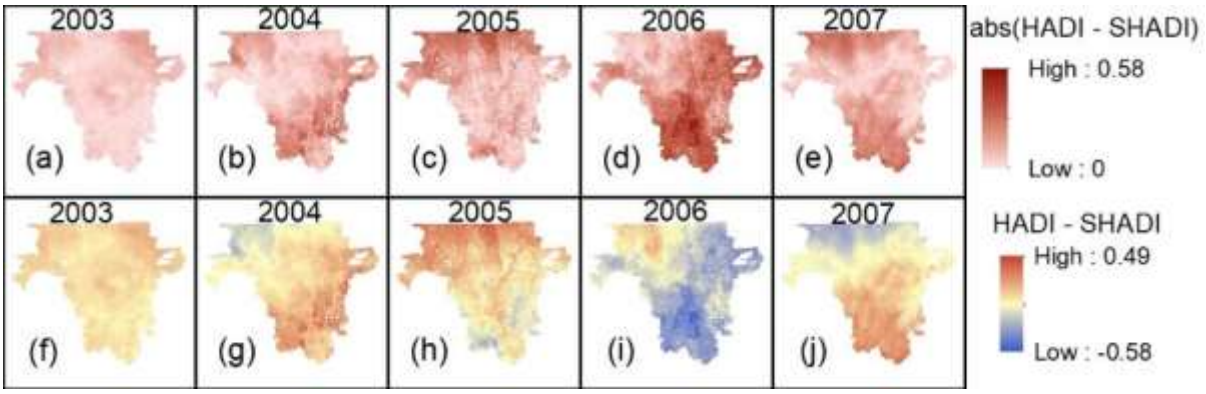

Figure 2.24 Differences between HADI and SHADI in the RRB

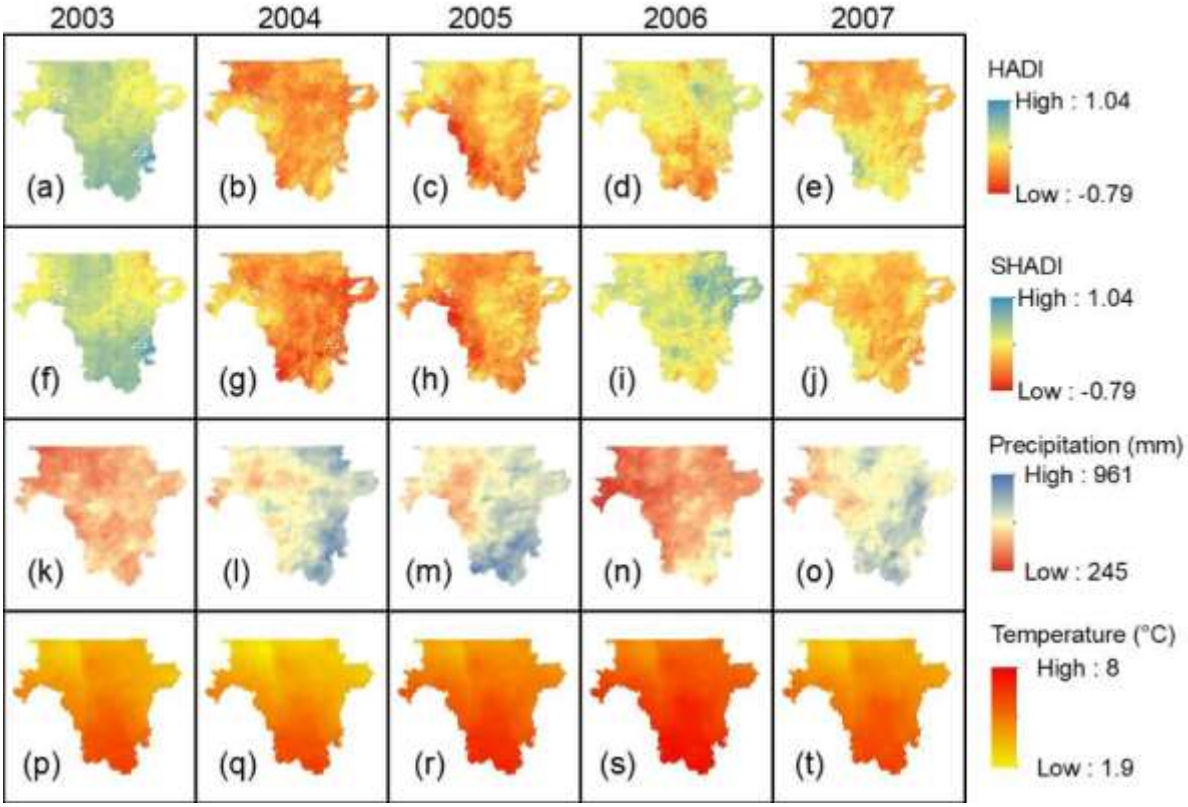

Figure 2.25 Spatial and temporal distributions of HADI, SHADI, temperature, and precipitation in the RRB

2.2.4.4. Performances of the SHADI and HADI in Different Climate Divisions

To evaluate the performances of the HADI and SHADI under different climate conditions, the areal averages of the SHADI and HADI were compared for several selected climate divisions (CDs) (including 2101, 3203, and 3206) (Figure 2.18) by considering their corresponding inputs and temperatures. The identified long dry period from the end of 2003 to

the beginning of 2007 was divided into three periods based on the main drought drivers. In the first period (Figure 2.26), the monthly temperature was lower than the mean monthly temperature in CD 2101, especially in the cold seasons (Figure 2.26a). As a result, the precipitation was in the form of snowfall (Figure 2.26b and Figure 2.26c) and the snowpack increased over time, reaching its capacity by the end of the cold season in February 2004 (Figure 2.26d). Then, the snowmelt process initiated by a temperature increase in March 2004 (Figure 2.26e). The snowmelt-induced surface runoff (Figure 2.26f) and soil water storage (Figure 2.26g) increased with a one-month delay. The SHADI identified this dry period two months earlier than the HADI (in October 2003) (Figure 2.26h and Figure 2.26i).

In the second period (Figure 2.26), the monthly temperature was higher than the mean monthly temperature in the cold seasons (Figure 2.26a). Therefore, the majority of precipitation was in the form of rainfall. Although the rainfall was higher than that in the other years in the study period, both HADI and SHADI identified a dry condition in this period. The snowpack and snowmelt were relatively low. The scatter plot matrix in Figure 2.27b shows certain relationship between the HADI and snowmelt. Therefore, the drought identified by the HADI can be justified by the low snowmelt in this period. However, there was no direct correlation between the SHADI and temperature, precipitation, snowpack, surface runoff, and soil water storage (Figure 2.27a). This can be verified by the similar loadings of the PCs or the weighting coefficients of all inputs. Thus, the SHADI represented a combination of all hydroclimatic variables. Due to the relatively low values of these variables, the SHADI identified a dry condition in this period.

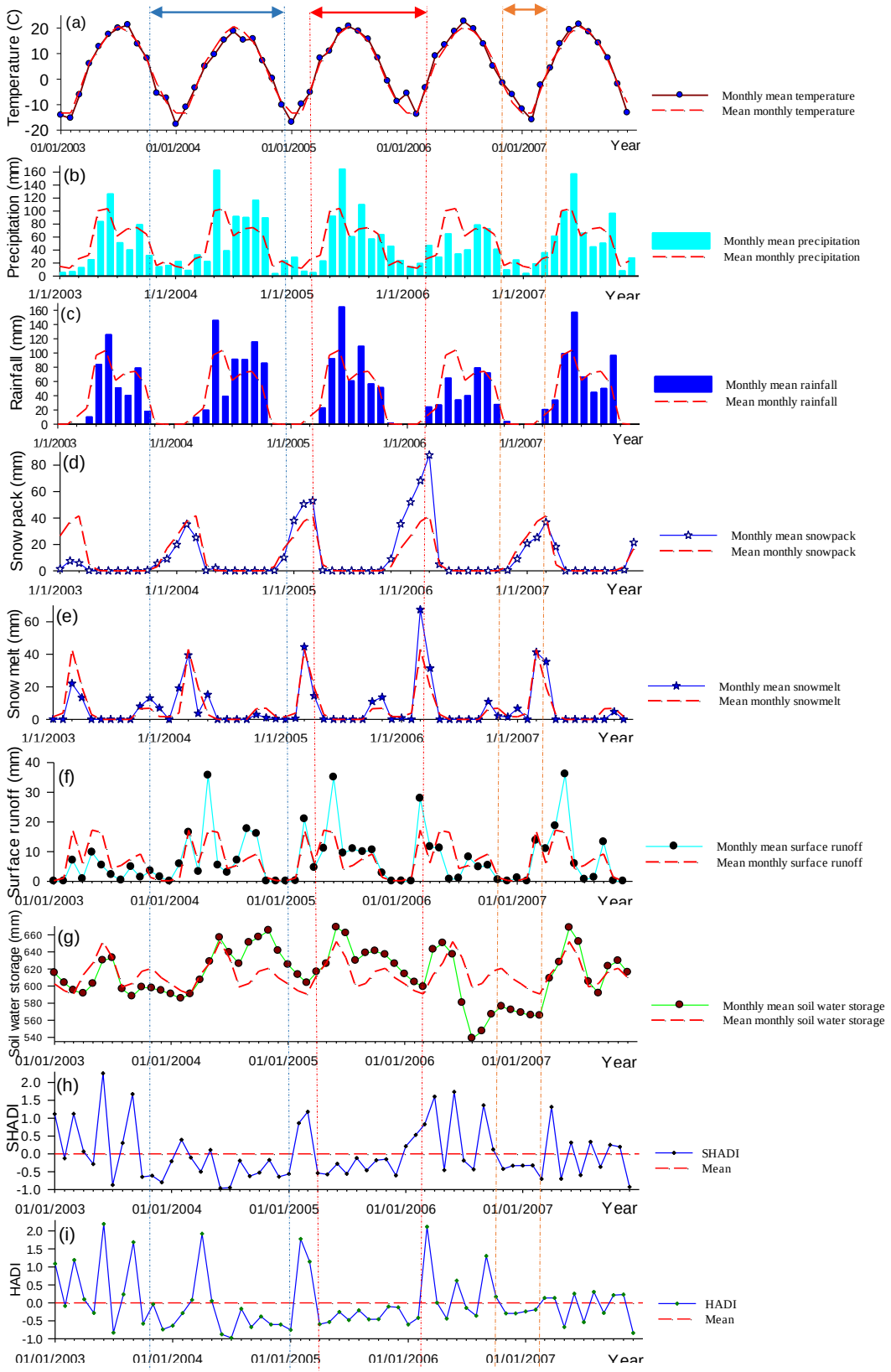

Figure 2.26. Hydroclimatic variables, SHADI, and HADI in climatic division 2101

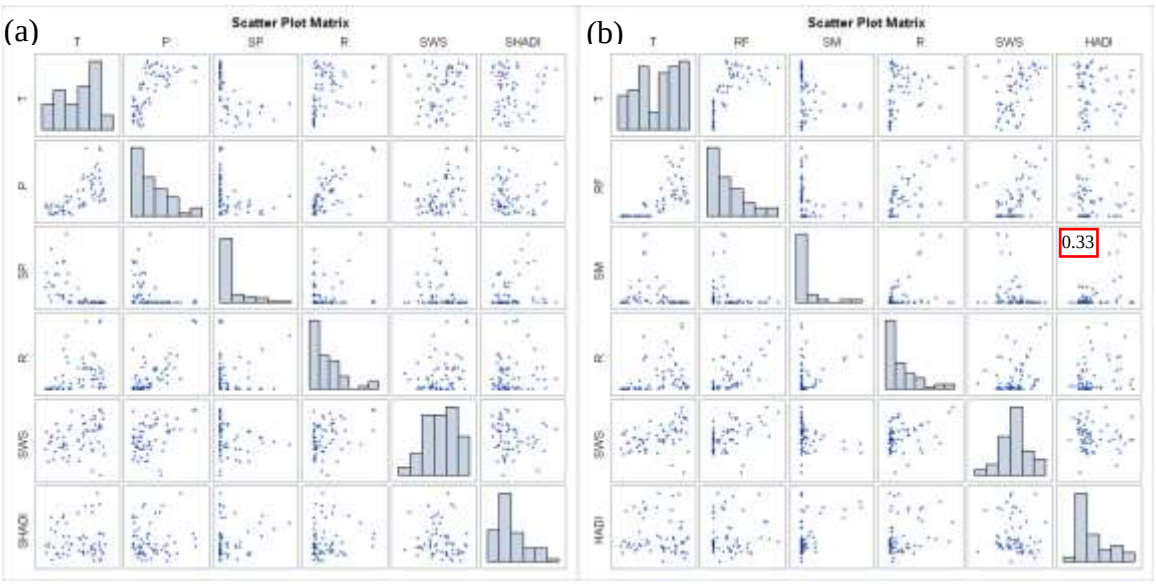

Figure 2.27. Scatter plot matrix of (a) SHADI, its inputs, and temperature, (b) HADI, its inputs, and temperature in climate division 2101 (notes: T: monthly mean temperature; P: monthly mean precipitation; SP: monthly mean snowpack; R: monthly mean surface runoff; SWS: monthly mean soil water storage; RF: monthly mean rainfall; and SM: monthly mean snowmelt)

The third period was a short dry period from the end of 2006 to March 2007 (Figure 2.26). In this period, both HADI and SHADI identified a dry spell with below-normal precipitation and soil water storage. The deficit in the antecedent precipitation during 2006 led to a decrease in the available soil moisture. Thus, this drought can be categorized as a classical rainfall deficit drought.

Figure 2.28 and Figure 2.29 show the temperatures and the inputs of the HADI and SHADI for CDs 3203 and 3206, respectively. The drought intensity based on the SHADI (Figure 2.29h) was higher than that of the HADI (Figure 2.29i) in CD 3203 in November 2003. This can be justified by the lower temperature in CD 3203 than that in CD 2101 (Figure 2.26a) and CD 3206 (Figure 2.29a). In addition, the SHADI exhibited more consistency in the second dry period than the HADI in CD 3203. For example, the HADI identified a wet condition in October 2005 (middle of the second dry period) due to an increase in snowmelt, while the SHADI remained negative in this month.

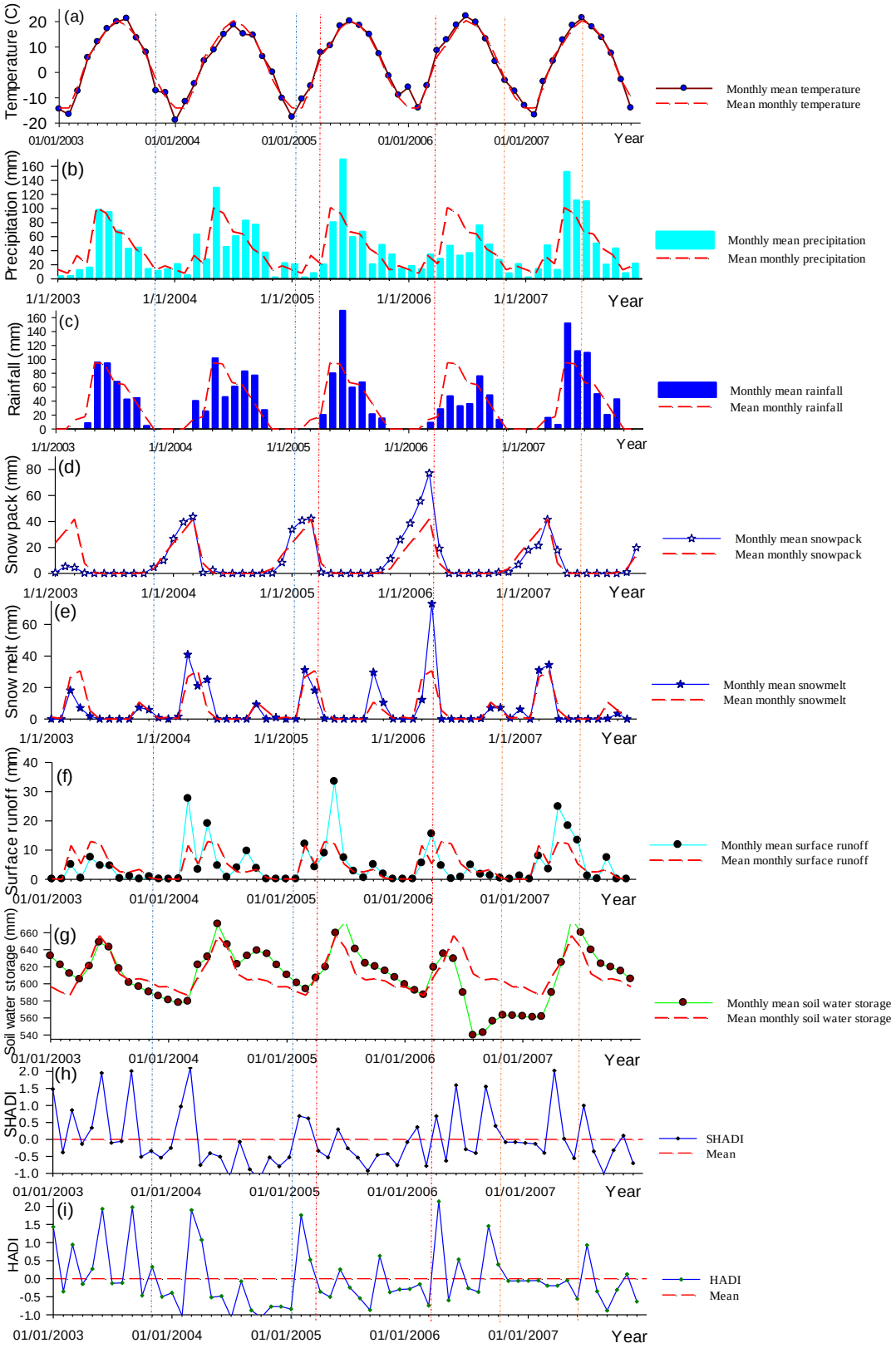

Figure 2.28. Hydroclimatic variables, SHADI, and HADI in climatic division 3203

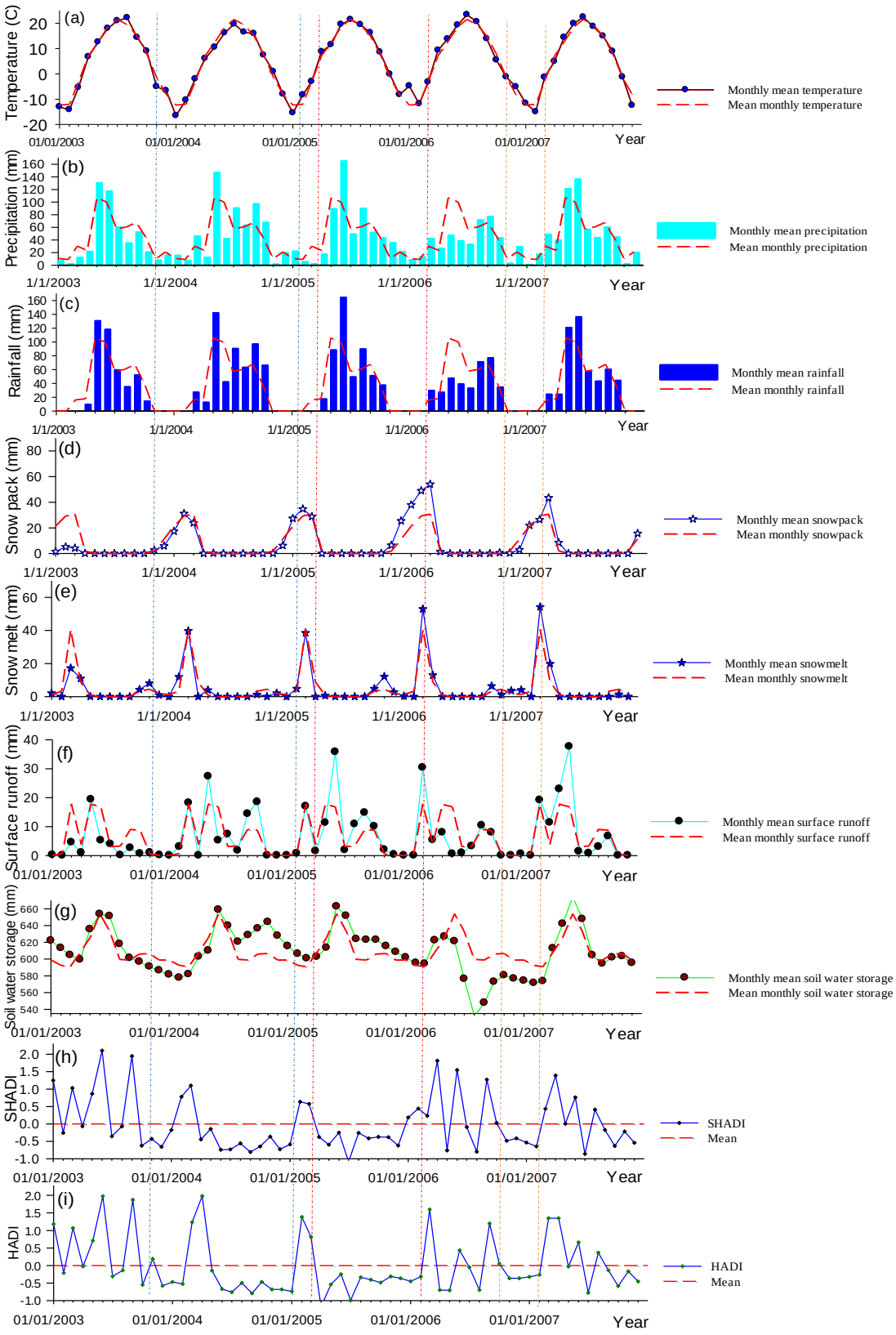

Figure 2.29. Hydroclimatic variables, SHADI, and HADI in climatic division 3206

Two types of major differences were observed between HADI and SHADI in CD 3206 (Figure 2.29h and Figure 2.29i). First, in some months the HADI values were positive, while the SHADI values were negative. For instance, the HADI values were 0.19 and 0.77 in November 2003 and February 2004, respectively. However, the SHADI values were -0.43 and -0.52. Comparing with the HADI (1.98) that showed a high-intensity wet condition in April 2004, the SHADI (-0.44) identified a dry condition in this month, which can be interpreted as a short-term lead prediction of the forthcoming dry period by the SHADI. Second, in some months close to the end of the 2004-2006 dry period the SHADI turned to positive values, whereas the HADI remained negative. For example, the SHADI values were 0.18, 0.44, and 1.81 in January, February, and April 2006, respectively. However, the HADI values were -0.45, -0.31, and -0.69 for these months. In fact, by the end of this long dry period, the SHADI preidentified a wet condition in January 2006, two months prior to the HADI since SHADI is based on snowpack and precipitation, rather than available water such as rainfall and snowmelt used in the HADI.

2.2.4.5. Comparison of SHADI, HADI, and USDM in the Form of DSCI

To compare the DSCIs of the SHADI, HADI, and USDM, the dry span in the study period was divided into three short dry spells: (1) from the end of 2003 to the end of 2004, (2) from the beginning of 2005 until the end of 2005, and (3) from the beginning of 2006 to the beginning of 2007. As shown in Figure 2.30, despite the differences in the values of DSCI of the USDM, SHADI, and HADI, they identified the first dry spell at the same time in all CDs. The DSCIs of the USDM were higher than those of the HADI in all CDs. In contrast, the DSCIs of the SHADI were higher than those of the USDM in CDs 2101 and 3203. The peak DSCIs of the HADI and SHADI occurred with a shorter delay than the DSCI of the USDM in the second dry spell. The DSCI of the SHADI was higher than those of the USDM and HADI in the first two CDs (2101 and 3203). The DSCIs of the USDM and HADI were close to or higher than the DSCI of the SHADI

in CD 3206. The DSCI of the USDM was noticeably higher than those of the SHADI and HADI in the third dry spell.

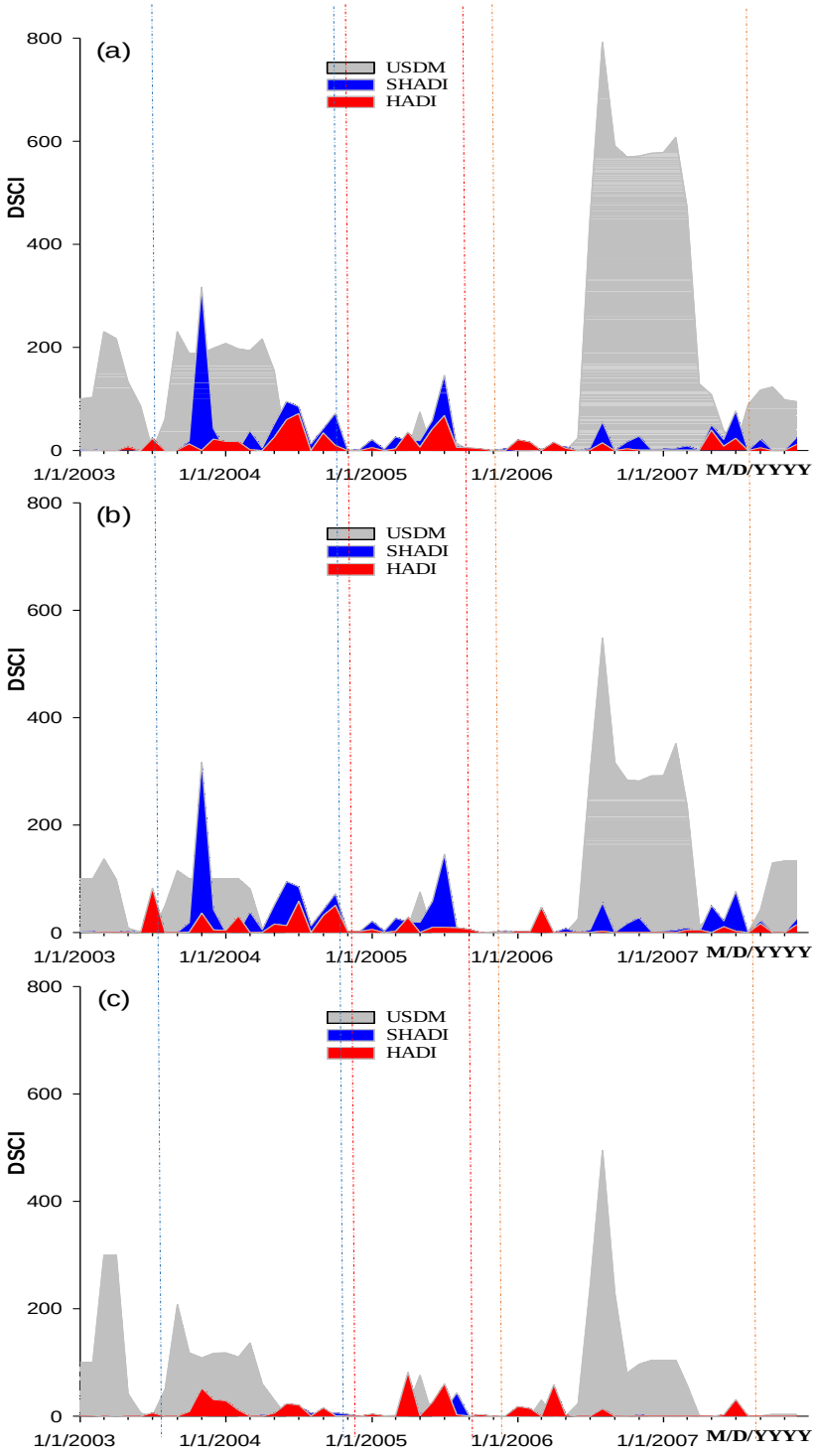

Figure 2.30. Severity and coverage drought index of the USDM, SHADI, and HADI in climate divisions (a) 2101, (b) 3203, and (c) 3206

The dissimilarities among the results of the SHADI, HADI, and USDM can be associated with three main reasons. First, different numbers and types of inputs were used for the derivation of these indices. The SHADI accounted for snowpack and snow drought and the HADI considered snowmelt and rainfall. However, the USDM did not consider the separation of rainfall and snowfall, snow accumulation, and snowmelt as the dominant hydroclimatic processes in cold climate regions. Second, the approach of one-weight-fits-all can be a limitation of the USDM in weighting coefficients of the involved indices and in the representation of seasonal changes. However, by using the PCA, the weighting coefficients for different hydroclimatic variables in the HADI were derived based on the employed time series, instead of the fixed coefficients used in the USDM. Third, in this research, the variable threshold levels were used in drought categorization for the HADI and SHADI, instead of the fixed threshold levels based on the percentages for the USDM. Since a dry period was intentionally chosen to test the SHADI and HADI, these discrepancies in the results were expected. The main purpose for the derivation and utilization of variable threshold levels in drought categorization is to fulfil the necessity of consideration of both spatial and temporal distributions of droughts (Mishra and Singh 2010). Hence, different thresholds for each drought category would be expected if different periods were selected. Therefore, the properties of the HADI and SHADI, which were incorporated to improve drought identification and categorization, resulted in these discrepancies among the indices.

2.2.4.6. Cluster Analyses of the Inputs of HADI and SHADI

Figure 2.31 shows the HADI and SHADI and the clustering analysis results based on their associated inputs in CD 2101 (14 Figure 2.31a and 2.31b), CD 3203 (Figure 2.31c and 2.31d), and CD 3206 (Figure 2.31e and 2.31f). The SHADI and cluster analysis identified the same dry/wet conditions in 47%, 72%, and 68% of times for CDs 2101, 3203, and 3206, respectively. Results of the HADI and cluster analysis for identification of dry/wet conditions

agreed in 43%, 53%, 52% of times for CDs 2101, 3203, and 3206, respectively. The longest similarity between the indices and the clustering results on their inputs was observed from January to December of 2005 in CD 3206 for the SHADI (Figure 2.31f). Thus, the results of the SHADI were closer to those from the cluster analysis especially for CD 3203. It can be concluded that despite some discrepancies, the results of cluster analysis verified the results of the HADI and SHADI in most cases.

The Q-Q plot was also used to compare the normality and skewness of the HADI, SHADI, and their associated hydroclimatic variables in different CDs by showing the quantiles of the normal distribution and the empirical distribution of the dataset. The deviation of the scattered points from the 1:1 line indicates the normality and skewness of the dataset. The Q-Q plots (Figures 2.32 - 2.34) also confirm that the areal averages of precipitation (Figures 2.32b, 2.33b, and 2.34b), rainfall (Figures 2.32c, 2.33c, and 2.34c), snowpack (Figures 2.32d, 2.33d, and 2.34d), snowmelt (Figures 2.32e, 2.33e, and 2.34e), surface runoff (Figures 2.32f, 2.33f, and 2.34f), SHADI (Figures 2.32h, 2.33h, and 2.34h), and HADI (Figures 2.32i, 2.33i, and 2.34i) are positively skewed. The mean values of these hydroclimatic variables and the HADI are located on the right side of the peaks of their distributions. In contrast, temperature (Figures 2.32a, 2.33a, and 2.34a) and soil water storage (Figures 2.32g, 2.33g, and 2.34g) are negatively skewed. Since all the variables of CD 3206 are less skewed, good agreement between the cluster analysis of the inputs and HADI and SHADI can be justified.

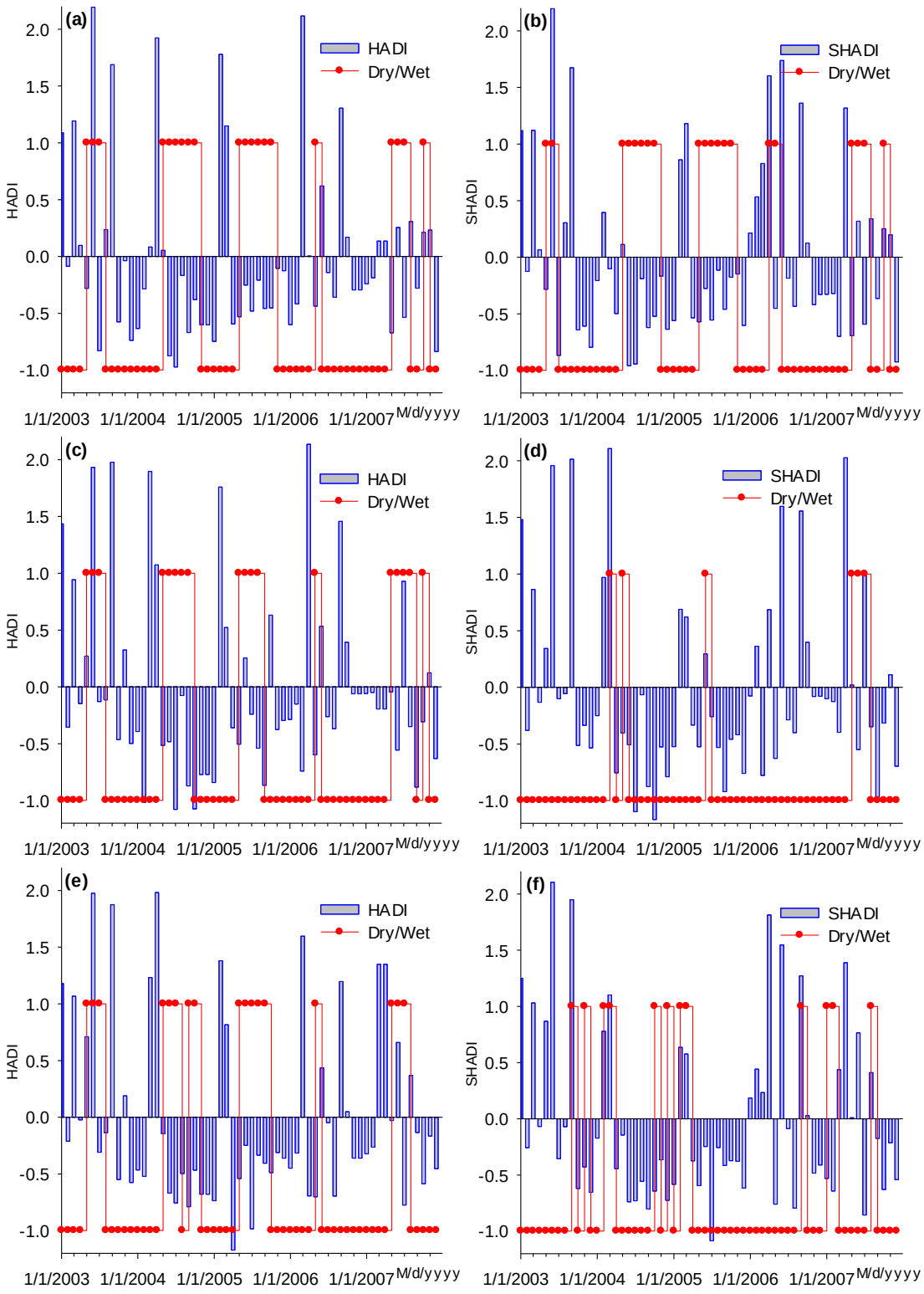

Figure 2.31. Clustering results based on the inputs of the HADI and SHADI and their comparisons with their associated indices in climate divisions (a and b) 2101, (c and d) 3203, and (e and f) 3206

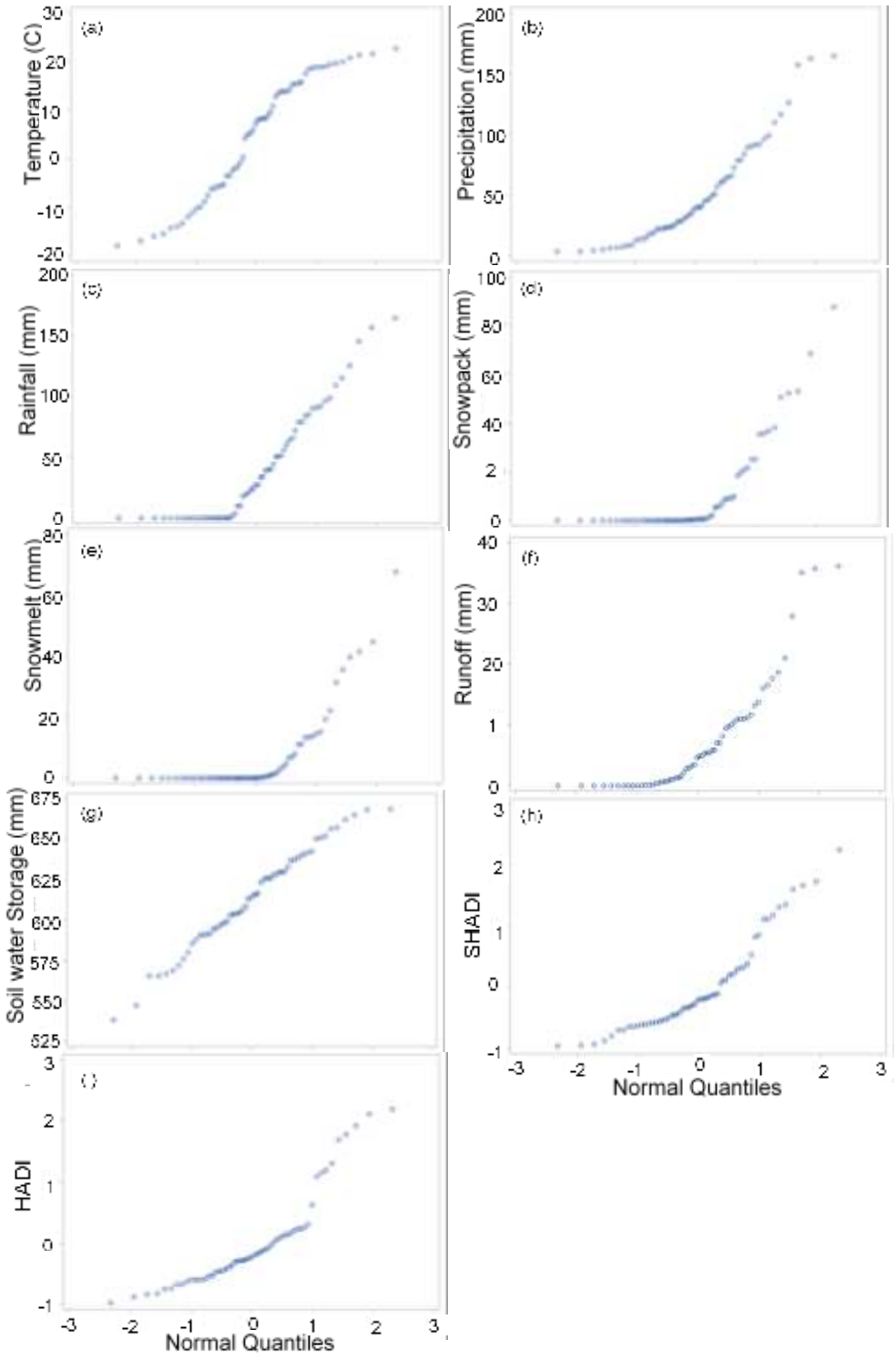

Figure 2.32. Q-Q plots of SHADI and HADI and their associated variables in climate divisions 2101

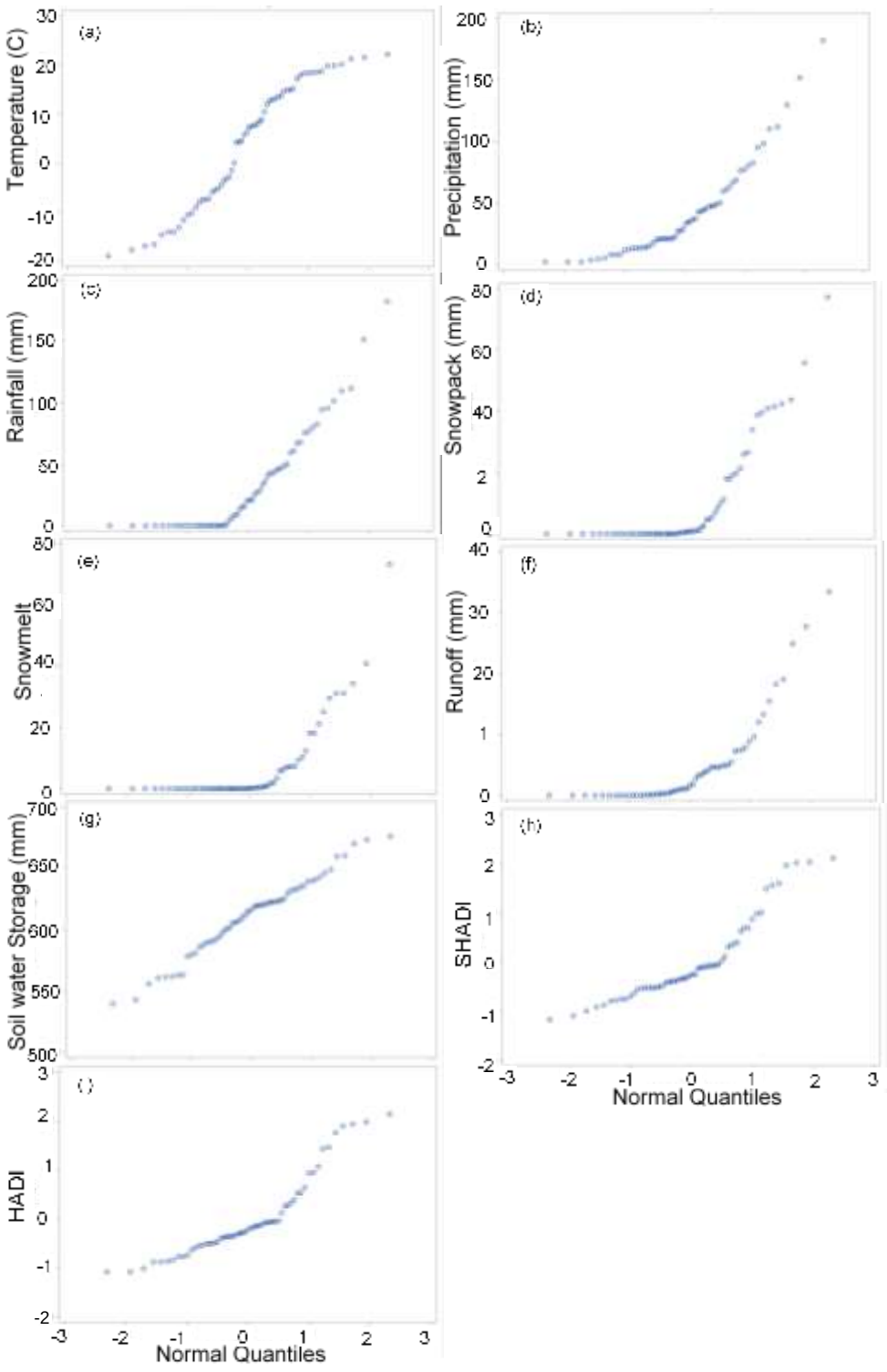

Figure 2.33. Q-Q plots of SHADI and HADI and their associated variables in climate division 3203

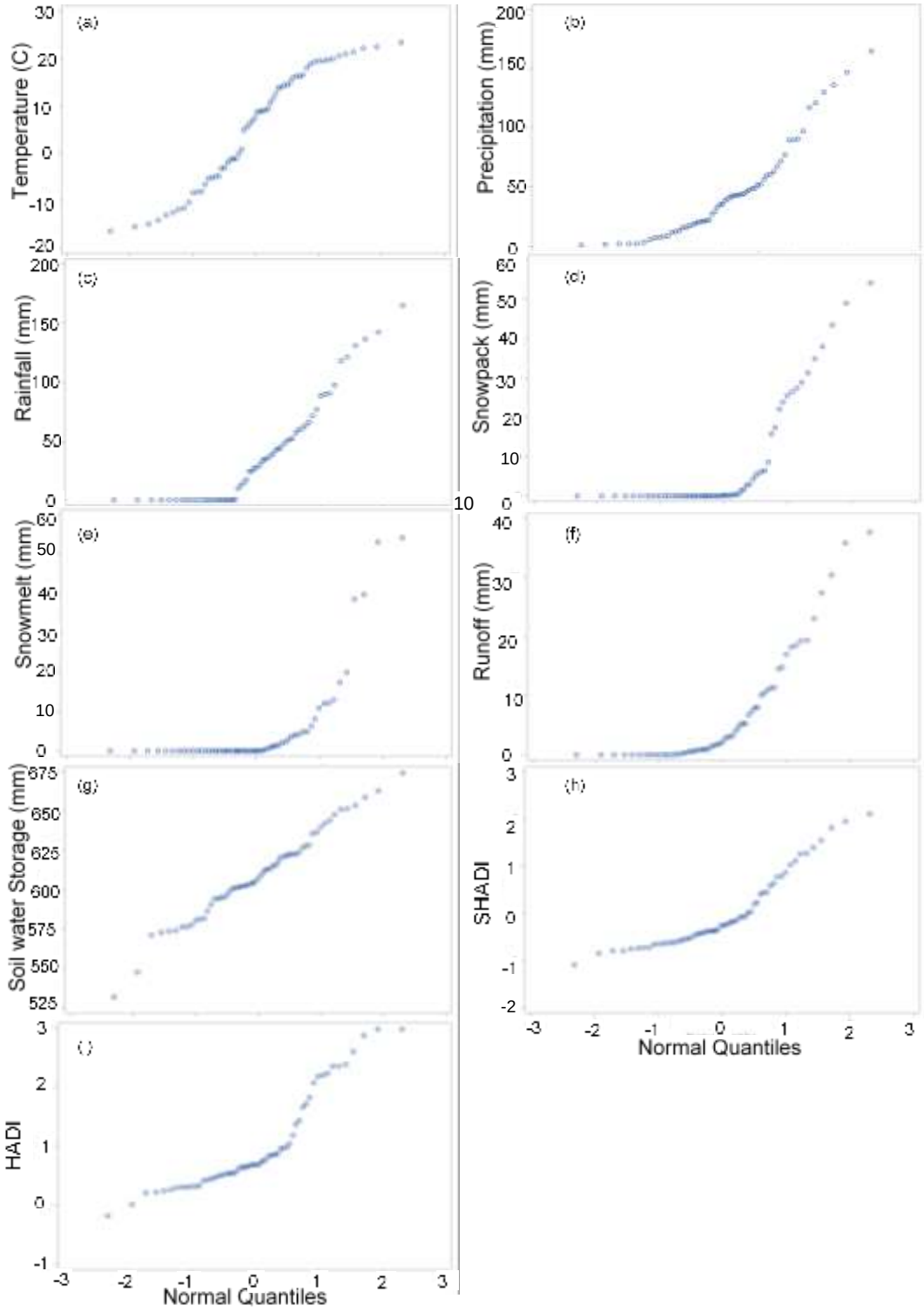

Figure 2.34. Q-Q plots of SHADI and HADI and their associated variables in climate division 3206

2.3. Summary and Conclusions

An integrated index, the HADI, was developed to identify and assess droughts in cold climate regions. The GHM was used to simulate the main hydrologic processes in such regions such as snow accumulation, frozen soil, and snowmelt, which were further utilized to derive the HADI. To evaluate the performance of the HADI, it was applied to the RRB, a depression-dominated cold climate region with distinctive hydroclimatic characteristics and unique drought drivers, and compared with the USDM.

Higher percentages of the first eigenvalues were observed in the cold seasons due to collinearity among hydroclimatic variables of the HADI in the warm seasons. The higher correlation between the HADI and snowmelt confirmed that the snowmelt played an important role in drought identification in this cold climate region. Snowmelt and surface runoff had higher correlation with the HADI in the cold seasons. In contrast, soil water storage had higher correlation with the HADI during the warm seasons. Therefore, snowmelt and surface runoff during cold seasons and soil water storage through warm seasons were the key factors in the identification of droughts by the HADI. The HADI outperformed the PDSI since the results of the HADI were in accordance with the drought impacts quantified by the ND agriculture-based GDP in the RRB. The time-scale-based drought indices (e.g., SPI) require larger time scales (3-month to 12-month or longer) to reflect the impacts of precipitation deficit on other hydrologic processes (e.g., soil water storage). However, the HADI, benefitted from the modeling, considers the main hydrologic processes at a monthly scale. Since the HADI, as an integrated drought index, was based on the status of different types of water resources in the hydroclimatic system, it was able to consider the effects of wet or dry conditions of preceding and succeeding years. Therefore, the estimated drought onset and termination were more reliable. Moreover, drought categorization is crucial to the mitigation of drought impacts. In this research, drought categorization was reanalyzed for cold climates and both spatial and temporal distributions of droughts were explicitly considered by means of variable threshold levels, instead of the

arbitrarily-defined threshold levels (e.g., McKee et al. 1993) or the fixed threshold levels (e.g., Nalbantis and Tsakiris 2009). This reanalysis was a process of customization of the HADI to the cold climate regions, which improved the accuracy in the identification of drought intensity and area coverage. In the new customized approach, a mixture distribution of two normal distributions with different means and variances (N1 ($\mu1$=-1.1 , $\sigma1$) for dry conditions and N2 ($\mu2$=2 ,$\sigma2$) for wet conditions) were observed, instead of only one normal distribution with mean around zero in the previous studies (e.g., McKee 1993; Nalbantis and Tsakiris 2009). In the customized drought categorization, the variable threshold levels varied with time and geographic locations, which overcame the challenge in the definition of the normal condition (Palmer 1965).

The HADI identified 2004 - 2006 as a long dry period in the RRB during the study period. The USDM also showed a dry condition in this period. Note that unlike the HADI, the USDM employed the experts' advices in its drought assessment. The discrepancies between the HADI and USDM were also associated with the selection of a mostly dry period (2003-2007) for the purpose of testing the HADI. In addition to the variable threshold levels, the USDM products used the one-weight-fits-all approach, while the HADI utilized variable weighting coefficients of different hydroclimatic variables as a result of the application of the PCA, which can be another reason for these discrepancies. The long dry period (2004-2006) identified by the HADI was "warm snow season drought" or "snowmelt drought." A dry condition in cold seasons was referred to "cold snow season drought" or "rain to snow season drought." Therefore, rain to snow season drought, cold snow season drought, warm snow season drought, and snowmelt drought are the most prevalent drought types in such a cold climate area (i.e., RRB). Drought types can distinguish the associated stakeholders and provide the appropriate stakeholders with the corresponding drought analyses results. Therefore, drought types should not be neglected in the process of integration. Unlike the previous integrated drought indices

(e.g., MSDI, SWSI, HDI, ADI), the HADI is able to identify drought types and the target stakeholders taking advantage of the loadings in the PCA.

One of the main purposes of developing the HADI was to identify droughts in cold climate regions where snow accumulation, snowmelt process, and frozen soil are dominant. This new index can also be applied to other climates since the PCA automatically adjusts the weighting coefficients of the effective hydroclimatic variables. As an integrated index, the HADI considers the most effective factors in the identification of different types of drought. Due to the important roles of human drivers, such indices can be improved by accounting for the related impacts. One of the limitations of this study is that the study area and period are limited to a specific type of climate region (i.e., cold climate) and a mostly dry period (2003-2007). Therefore, one of the potentials for the future studies is to test the HADI and the customized drought categorization for a longer period (including both wet and dry) and in other climate regions. The low ratio of the explained variances during summer due to collinearity can be another limitation of this index. Moreover, despite the advantage of PCA in reducing the redundant information it may omit certain useful information. To overcome this limitation, considering the second PC in calculation of the drought index can be considered in the future studies. In addition to drought identification, the HADI can also be used to improve drought prediction in cold climate regions.

In this study, a new snow-based hydroclimatic aggregate drought index (SHADI) was also developed. The loadings of the first PC were utilized to determine the drought type and the targeted stakeholder in the SHADI. As a result of the use of the customized drought categorization, the SHADI and HADI yielded similar DSCI values, which were different from those of the USDM. These discrepancies can be attributed to the incorporation of effective hydroclimatic variables in cold climate regions, implementation of different methods for derivation of weighting coefficients, and application of variable threshold levels in the SHADI and HADI for drought identification and categorization.

To evaluate the performance of the SHADI, it was compared with the HADI, PDSI, and the ND agriculture-based GDP. The SHADI was in good agreement with the GDP in most cases. The slight differences between the SHADI and GDP can be related to the SHADI's capability in reflection of an upcoming dry or wet spell. Accounting for snowpack in SHADI facilitated a 2-month lead prediction of drought, which also was demonstrated by Abel's et al. (2018). Thus, the SHADI can be used for a short-term lead prediction of any upcoming drought to mitigate the drought impacts. This study demonstrated the capability of the SHADI for the snow-based drought forecasting. Since this snow-based drought index has relatively simpler nature than sophisticated statistical predictions, it is suggested that the statistical methods (e.g., machine learning techniques) be used to leverage snow-based forecasting. Thus, the anomalous snowpack and snow-based drought indices can provide early warning of drought.

Some discrepancies were observed between the SHADI and HADI in cold seasons and in dry-wet or wet-dry transitions, which can be attributed to the effects of consideration of available water in HADI and stored water sources in SHADI. Similar to the findings by Guttman et al. (1992) and Dai et al. (2004), the SHADI identified the same trend as soil moisture especially in cold seasons since it accounted for the separation of snowfall and rainfall, frozen soil, and snow accumulation processes in cold climate regions. The SHADI was able to identify both dry and warm snow droughts, while the PDSI failed to identify warm snow drought in case of above-normal precipitation and temperature in cold seasons. Thus, the SHADI is particularly suitable for identification of snow droughts. Specifically, an abnormally warm late winter results in a warm snow drought and dry snow drought occurs in case of below normal rainfall and snowmelt in early spring.

2.4. References

Agnew CT (2000). Using the SPI to identify drought. Drought Network News. Vol. 12, National Drought Mitigation Center, Lincoln, NE, 6–12. [Available online at http://digitalcommons.unl.edu/cgi/viewcontent.cgi?article51000&context5droughtnetnew]

Akinremi OO, Mcginn SM, Barr AG (1996). Evaluation of the Palmer Drought index on the Canadian prairies. Journal of Climate, 9, 897–905, doi:10.1175/1520-0442(1996)009<0897:EOTPDI>2.0.CO;2

Akyuz, F. A. (2017). Drought Severity and Coverage Index. United States Drought Monitor. https://droughtmonitor.unl.edu/AboutUSDM/AbouttheData/DSCI.aspx

Ali A, Lebel T (2009). The Sahelian standardized rainfall index revisited. International Journal of Meteorology, 29(12), 1705–1714, doi:10.1002/joc.1832

American Meteorological Society, (2019). Snow Drought. Glossary of Meteorology. [Available online at http://glossary.ametsoc.org/wiki/Snow_drought].

Bachmair S, Kohn I, Stahl K (2015). Exploring the link between drought indicators and impacts, Nat. Hazards Earth Syst. Sci., 15, 1381–1397, doi:10.5194/nhess-15-1381-2015

Bachmair S, Tanguy M, Hannaford J, K Stahl (2018). How well do meteorological indicators represent agricultural and forest drought across Europe? Environ. Res. Lett. 13 034042, doi:10.1088/1748-9326/aaafda

Bayissa Y, Maskey S, Tadesse T, Andel V, Moges SJ, Van Griensven SA, Solomatine D (2018). Comparison of the Performance of Six Drought Indices in Characterizing Historical Drought for the Upper Blue Nile Basin. Ethiopia, Geosciences, 8(3), 81, doi:10.3390/geosciences8030081

Bazrkar, M. H., J. Zhang, and X. Chu. (2020). Hydroclimatic aggregate drought index (HADI): A new approach for identification and categorization of drought in cold climate regions. Stochastic Environmental Research and Risk Assessment, 34(11), 1847-1870, doi:10.1007/s00477-020-01870-5.

Bloomfield JP, Marchant BP (2013). Analysis of groundwater drought building on the standardised precipitation index approach, Hydrology and Earth System Sciences. 17(12), 4769–4787, doi:10.5194/hess-17-4769-2013

Bureau of Economic Analysis (BEA), U.S. Department of Commerce (2019)〈 https://apps.bea.gov/regional/histdata/releases/0609gsp/index.cfm〉(Nov. 12, 2019)

Carrão H, Singleton A, Naumann G (2014). An optimized system for the classification of meteorological drought intensity with applications in drought frequency analysis. Journal of Applied Meteorology and Climatology, 53(8), 1943–1960, doi:10.1175/JAMC-D-13-0167.1

Cattell RB (1952). Factor Analysis: An Introduction and Manual for the Psychologist and Social Scientist. 462, Greenport Press, Westport, Conn

Chu, X., Lin, Z., Tahmasebi Nasab, M., Zeng, L., Grimm, K., Bazrkar, M. H., Wang, N., Liu, X., Zhang, X., Zheng, H. (2018). “Macro-scale grid-based and subbasin-based hydrologic modeling: joint simulation and cross-calibration.” Journal of Hydroinformatics. jh2018026. doi: 10.2166/hydro.2018.026

Cooper, M. G., Nolin, A. W., & Safeeq, M. (2016). Testing the recent snow drought as an analog for climate warming sensitivity of Cascades snowpacks. Environmental Research Letters, 11(8), 084009.

Dai, A., K.E. Trenberth, and T. Qian, (2004). A Global Dataset of Palmer Drought Severity Index for 1870–2002: Relationship with Soil Moisture and Effects of Surface Warming. J. Hydrometeor., 5, 1117–1130, https://doi.org/10.1175/JHM-386.1

Dierauer, J. R., Allen, D. M., & Whitfield, P. H. (2019). Snow drought risk and susceptibility in the western United States and southwestern Canada. Water Resources Research, 55. doi: 10.1029/2018WR023229.

Fang, X., Pomeroy, W. (2007). Snowmelt runoff sensitivity analysis to drought on the Canadian prairies, Hydrological Processes, 21, 2594-2609.

Fry JA, Xian G, Jin S, Dewitz JA, Homer CG, Yang L, Barnes CA, Herold ND, Wickham JD (2011). Completion of the 2006 national land cover database for the conterminous united states. Photogrammetric Engineering and Remote Sensing, 77(9), 858–864

Guttman, N. B., J. R. Wallis, and J. R. M. Hosking, (1992). Spatial comparability of the Palmer drought severity index. Water Resour. Bull., 28, 1111–1119.

Habtezion N, Tahmasebi Nasab M, Chu X (2016). How does DEM resolution affect microtopographic characteristics, hydrologic connectivity, and modeling of hydrologic processes? Hydrology Process, 30(25), 4870–4892, doi:10.1002/hyp.10967

Hänsel S, Schucknecht A, Matschullat J (2016). The Modified Rainfall Anomaly Index (mRAI)—is this an alternative to the Standardised Precipitation Index (SPI) in evaluating future extreme precipitation characteristics? Theoretical and Applied Climatology, 123(3–4), 827–844, doi:10.1007/s00704-015-1389-y

Hao Z, AghaKouchak A (2013). Multivariate Standardized Drought Index: A parametric multi-index model. Advances in Water Resources, 57, 12–18, doi:10.1016/j.advwatres.2013.03.009

Harpold, A. A., Dettinger, M., & Rajagopal, S. (2017). Defining snow drought and why it matters. Eos Transactions American Geophysical Union, 98. https://doi.org/10.1029/2017EO068775.

Harpold, A., et al. (2012). Changes in snowpack accumulation and ablation in the intermountain west, Water Resour. Res., 48, W11501, https://doi.org/10.1029/2012WR011949.

Hatchett, B.J. and McEvoy, D.J. (2018). Exploring the Origins of Snow Drought in the Northern Sierra Nevada, California. Earth Interact., 22, 1–13, https://doi.org/10.1175/EI-D-17-0027.1

Hogg RV, Craig AT (1978) Introduction to Mathematical Statistics. Macmillan Publishing Co., Inc. New York, Fourth edition

Howitt, R., MacEwan, D., Medellín-Azuara, J., Lund, J., &Sumner, D. (2015). Economic analysis of the 2015 drought for California agriculture. UC Davis Center for Watershed Sciences. Retrieved March2018 from

https://watershed.ucdavis.edu/files/biblio/Final_Drought%20Report_08182015_Full_Report_WithAppendices.pdf

HPRCC (2018). 30-year climate normals (1981–2010). High Plains Regional Climate Center. 〈https://hprcc.unl.edu/maps.php?map5Normals〉 (Dec. 12, 2018)

Huning, S. L. and Aghakouchak, A. (2018). Mountain snowpack response to different levels of warming, Proceedings of the National Academy of Sciences, 115(43), 10932-10937.

Huning, S. L. and Aghakouchak, A. (2020). Global snow drought hot spots and characteristics, Proceedings of the National Academy of Sciences Aug 2020, 117 (33) 19753-19759; DOI: 10.1073/pnas.1915921117

Kao SC, Govindaraju RS (2010). A copula-based joint deficit index for droughts. Journal of Hydrology, 380(1–2), 121–134, doi:10.1016/j.jhydrol.2009.10.029

Karamouz M, Rasouli K, Nazif S (2009). Development of a Hybrid Index for Drought Prediction: Case Study. Journal of Hydrologic Engineering, 14(6), 617–627, doi:10.1061/(ASCE)HE.1943-5584.0000022

Keyantash, J. A., and Dracup, J. A. (2004). An aggregate drought index: Assessing drought severity based on fluctuations in the hydrologic cycle and surface water storage. Water Resources Research, 40(9), 1–14.

Li B, Liang Z, Yu Z, Acharya K (2014). Evaluation of drought and wetness episodes in a cold region (Northeast China) since 1898 with different drought indices. Natural Hazards, 71(3), 2063–2085, doi: 10.1007/s11069-013-0999-x

Li, J., Zhou, S., and Hu, R. (2016). Hydrological Drought Class Transition Using SPI and SRI Time Series by Loglinear Regression, Water Resources Management, 30:669–684, doi: 10.1007/s11269-015-1184-7

Livneh, B., Badger, A.M. (2020). Drought less predictable under declining future snowpack. Nat. Clim. Chang. 10, 452–458. Doi: 10.1038/s41558-020-0754-8

MacQueen JB (1967). Some Methods for classification and Analysis of Multivariate Observations. Proceedings of 5-th Berkeley Symposium on Mathematical Statistics and Probability, Berkeley, University of California Press, 1, 281-297

Marty, C., Schlögl, S., Bavay, M., and Lehning, M. (2017). How much can we save? Impact of different emission scenarios on future snow cover in the Alps, The Cryosphere, 11, 517-529, doi:10.5194/tc-11-517-2017.

McKee, T. B., Doesken, N. J., and Kleist, J. (1993). "The relationship of drought frequency and duration to time scales." AMS 8th Conference on Applied Climatology, 179–184.

Mishra AK, Singh VP (2010). A review of drought concepts. Journal of Hydrology, 391(1), 202-216, doi:10.1016/j.jhydrol.2010.07.012

Mote, P. W. (2003). Trends in snow water equivalent in the Pacific Northwest and their climatic causes, Geophys. Res. Lett., 30, 1601, doi:10.1029/2003GL017258, 12.

Nalbantis I, Tsakiris G (2009). Assessment of hydrological drought revisited. Water Resources Management, 23(5), 881–897, doi:10.1007/s11269-008-9305-1

NDAWN. (2014). "The Drought of the 1930s." 〈https://www.ndsu.edu/ndscoblog/?p=626〉 (July 3, 2014).

NOAA's National Centers for Environmental information (NOAA's NCEI) Climate at a Glance: Divisional Time Series. published November 2019, retrieved on November 9, 2019 from https://www.ncdc.noaa.gov/cag/

Palmer WC (1965). Meteorological Drought. U.S. Weather Bureau, Res. Pap. No. 45

Rencher AC, Christensen WF (2012). Methods of Multivariate Analysis. 3rd edition. John Wiley & Sons

Richman MB (1986). Rotation of principal components. Journal of Climatology, 6(3), 293–335, doi:10.1002/joc.3370060305

Sawada Y, Koike T, Jaranilla-Sanchez PA (2014). Modeling hydrologic and ecologic responses using a new eco-hydrological model for identification of droughts. Water Resour. Res., 50, 6214– 6235, doi:10.1002/2013WR014847

Schneider, S. R., and Matson, M. (1977). Satellite observations of snowcover in the Sierra Nevadas during the great California drought. Remote sensing of environment. No.4. Netherlands. P.327-334.

Shafer, B. A., and Dezman, L. E. (1982). Development of a surface water supply index (SWSI) to assess the severity of drought conditions in snowpack runoff areas. proceedings of the 50th Annual Western Snow Conference, 164–175.

Shukla S, Wood AW (2008). Use of a standardized runoff index for characterizing hydrologic drought. Geophysical Research Letters, 35(2), 1–7, doi:10.1029/2007GL032487

Sproles, E. A., Roth, T. R., and Nolin, A. W. (2017). Future snow? A spatial-probabilistic assessment of the extraordinarily low snowpacks of 2014 and 2015 in the Oregon Cascades, The Cryosphere, 11, 331-341, doi:10.5194/tc-11-331-2017.

Staudinger M, Stahl K, Seibert J (2014). A drought index accounting for snow. Water Resources Research, 50(10), 7861–7872, doi:10.1002/2013WR015143

Staudinger, M., Stahl, K., Seibert, J., Clark, M. P., and Tallaksen, L. M. (2011). Comparison of hydrological model structures based on recession and low flow simulations, Hydrol. Earth Syst. Sci., 15, 3447–3459, doi:10.5194/hess-15-3447-2011.

Steinemann A (2003). Drought indicators and triggers: A stochastic approach to evaluation. Journal of American Water Resources Association, 39(5), 1217–1233, doi:10.1111/j.1752-1688.2003.tb03704.x

Svoboda M, LeComte D, Hayes M, Heim R, Gleason K, Angel J, Rippey B, Tinker R, Palecki M, Stooksbury D, Miskus D, Stephens S (2002). The drought monitor. Bulletin of the American Meteorological Society, 83(8), 1181–1190, doi:10.1175/1520-0477(2002)083<1181:TDM>2.3.CO;2

Tahmasebi Nasab M, Grimm K, Bazrkar MH, Zeng L, Shabani A, Zhang X, Chu X (2018). SWAT Modeling of Non-Point Source Pollution in Depression-Dominated Basins under Varying Hydroclimatic Conditions. International Journal of Environmental Research and Public Health, 15(11), 2492, doi:10.3390/ijerph15112492

Tilahun K (2006). Analysis of rainfall climate and evapo-transpiration in arid and semi-arid regions of Ethiopia using data over the last half a century. Journal of Arid Environments, 64(3), 474–487, doi:10.1016/j.jaridenv.2005.06.013

Tollerud H, Brown J, Loveland T, Mahmood R, Bliss N (2018). Drought and Land-Cover Conditions in the Great Plains. Earth Interactions, American Meteorological Society, 22(17), 1–25, doi:10.1175/EI-D-17-0025.1

US Drought Portal (2018). 〈https://www.drought.gov/drought/states/north-dakota〉 (Nov. 13, 2018).

US Geological Survey (2020). 〈https://waterdata.usgs.gov/nd/nwis/uv?site_no=05054000〉 (Mar. 3, 2020).

USDM (2019). United States Drought Monitor. <https://droughtmonitor.unl.edu/Data/Timeseries.aspx> (June 27, 2019).

Van Loon AF, Laaha G (2015). Hydrological drought severity explained by climate and catchment characteristics. Journal of Hydrology, 526, 3–14, doi:10.1016/j.jhydrol.2014.10.059

Van Loon AF, Stahl K, Di Baldassarre G, Clark J, Rangecroft S, Wanders N, Gleeson T, Van Dijk AIJM, Tallaksen LM, Hannaford J, Uijlenhoet R, Teuling AJ, Hannah DM, Sheffield J, Svoboda M, Verbeiren B, Wagener T, Van Lanen HAJ (2016). Drought in a human-modified world: Reframing drought definitions, understanding, and analysis approaches. Hydrology and Earth System Sciences, 20(9), 3631–3650, doi:10.5194/hess-20-3631-2016

Van Loon AF, Van Lanen HAJ (2012). A process-based typology of hydrological drought. Hydrology and Earth System Sciences, 16(7), 1915–1946, doi:10.5194/hess-16-1915-2012, 2012

Van Loon, A. F., Ploum, S. W., Parajka, J., Fleig, A. K., Garnier, E., Laaha, G., and Van Lanen, H. (2015). Hydrological drought types in cold climates: quantitative analysis of causing factors and qualitative survey of impacts, Hydrol. Earth Syst. Sci., 19, 1993-2016, doi:10.5194/hess-19-1993-2015.

Van Loon, A.; Laaha, G.; Van Lanen, H.; Parajka, J.; Fleig, A. K.; Ploum, S. (2015). Drought and Snow: Analysis of Drivers, Processes and Impacts of Streamflow Droughts in Snow-Dominated Regions. American Geophysical Union, Fall Meeting 2015, abstract id. H13I-1699.

Vicente-Serrano Sergio M, Santiago Beguería Juan I López-Moreno (2010). A Multiscalar Drought Index Sensitive to Global Warming, The Standardized Precipitation Evapotranspiration Index. J. Climate, 23, 1696–1718, doi:10.1175/2009JCLI2909.1

Wiesnet, D. (1981). Winter snow drought. Eos, Transactions American Geophysical Union, 62(14), 137-137.

Wilhite DA, Glantz MH (1985). Understanding the drought phenomenon: The role of definitions. Water International, 10(3), 111-120, doi:10.1080/02508068508686328

Wilhite DA, Hayes MJ, Svoboda MD (2000). Drought monitoring and assessment: status and trends in the United States. In: Vogt JV, Somma F (eds) Drought and drought mitigation in Europe. Advances in Natural and Technological Hazards Research, Springer, Dordrecht Kluwer, Dordrecht, 14, 149–160, doi:10.1007/978-94-015-9472-1_11

Wu H, Hayes M, Wilhite JDA, Svoboda MD (2005). The effect of the length of record on the standardized precipitation index calculation, International Journal of Climatology, 25(4), 5050-520, doi:10.1002/joc.1142

Xu Y, Wang L, Ross KW, Liu C, Berry K (2018). Standardized soil moisture index for drought monitoring based on soil moisture active passive observations and 36 years of North American Land Data Assimilation System data: A case study in the Southeast United States. Remote Sensing, 10(2), doi:10.3390/rs10020301

Zargar A, Sadiq R, Naser B, Khan FI (2011). A review of drought indices. Environmental Reviews, 19, 333–349, doi:10.1139/a11-013

3. DEVELOPMENT OF CATEGORY-BASED SCORING SUPPORT VECTOR REGRESSION (CBS-SVR) FOR DROUGHT PREDICTION [1]

3.1. Abstract

Using the existing performance measures for tuning hyperparameters in cross-validation of numerical (non-categorical) prediction models can cause misclassification of droughts. In categorical drought prediction, the drought category thresholds play key roles and the existing fixed thresholds are not applicable. The objectives of this research are (1) to determine the best drought categorization method by comparing different clustering methods to derive variable thresholds, and (2) to develop a category-based scoring support vector regression (CBS-SVR) method to overcome misclassification in drought prediction. To derive variable threshold levels for drought categorization, K-means (KM) and Gaussian mixture (GM) clustering are compared with the traditional drought categorization. For drought prediction, CBS-SVR is performed by using the best categorization method. The new drought prediction model was applied to the Red River of the North Basin (RRB) in the U.S. The 1979-2010 and 2011-2016 data obtained from the North American Land Data Assimilation System were respectively used for model training and testing. Precipitation, temperature, and actual evapotranspiration were selected as the predictors, and the target variables consisted of multivariate drought indices, as well as bivariate and univariate standardized drought indices. Results indicated that, unlike GM, KM clustering generated the same variable thresholds for all standardized drought indices. The best categorization method was different for each drought index. The CBS-SVR outperformed the support vector classification. The new CBS-SVR demonstrated its improvement over the traditional SVR in drought prediction by avoiding overfitting and mis-categorization.

---

[1] The material in this chapter was co-authored by Mohammad Hadi Bazrkar and Dr. Xuefeng Chu. Mohammad Hadi Bazrkar had primary responsibility for developing the new drought prediction model and drought analyses. Mohammad Hadi Bazrkar was the primary developer of the conclusions that are advanced here. Mohammad Hadi Bazrkar also drafted and revised all versions of this chapter. Dr. Xuefeng Chu served as proofreader and checked analysis conducted by Mohammad Hadi Bazrkar.

3.2. Introduction

Drought prediction provides early warnings of drought development and valuable drought mitigation information for stakeholders. The data-driven methods widely used for drought prediction include time series analysis (Durdu 2010, Mishra and Desai 2005, Rao and Padmanabhan 1984, Fernández et al. 2009, Modarres 2007), linear regression (Barros & Bowden 2008, Liu & Juárez 2001, Panu & Sharma 2002, Sun et al. 2012) and nonlinear regression (Hwang & Carbone 2009, Liu & Hwang 2015), artificial neural network (ANN) (Mishra and Desai 2006, Mishra et al. 2007, Morid et al. 2007, Barua et al. 2012, Santos et al. 2014, Yang et al. 2015), Markov chain analysis (Lohani and Loganathan 1997, Cancelliere et al. 2007, Paulo and Periera 2007, 2008, Sharma and Panu 2012), and probabilistic forecasting (Madadgar and Moradkhani 2013, Hao and Singh 2016).

Regression models are used if the predictand (drought index) is continuous. For drought prediction, support vector machine (SVM) for regression or support vector regression (SVR) has been suggested since it has some advantages over other prediction models. For example, the SVR can overcome some limitations of ANN such as local maxima and overfitting and outperform ANN to some extent for drought prediction (Ganguli & Reddy 2014). It also has the ability to learn from much smaller dataset for training and is capable of handling a large number of variables (Hao et al. 2018).

There are various hyperparameters in an SVR model. Penalty factor determines the tradeoff between the model complexity and training error (Joachims 2002). Parameter epsilon controls the width of the epsilon-insensitive zone, which is used to fit the training data. The optimal value of epsilon scales linearly with gamma (Schölkopf and Smola 2002), a Kernel parameter used to reduce the model space and control the complexity of the solution (Kisi and Cimen 2011). Therefore, tuning these hyperparameters is crucial in defining decision boundaries and success of an SVR model. These hyperparameters have been selected by trial and error in some studies for drought prediction (Feng et al. 2019, Belayneh et al. 2014). Cross-validation

methods have been also used for tuning these hyperparameters. Grid search (Larochelle et al. 2007) is one of the well-accepted cross-validation methods in SVR (Bergstra and Bengio 2012) for drought prediction (Deo et al. 2017, Deo et al. 2016a, Deo et al. 2016b).

To assess the prediction skill of a regression model, the regression results are commonly compared with a reference (i.e., actual values). Mean absolute error (MAE), mean square error (MSE), root mean square error (RMSE), and coefficient of determination (R^2) are among the performance measures. Although these performance metrics enhance the preciseness and predictive skills of models, they may cause misclassification (hereafter mis-categorization). For instance, the objective in a cross-validation effort for tuning hyperparameters in SVR is to select the values of hyperparameters so that lower MAE, MSE, and RMSE or higher R^2 are achieved. Although it can reduce the difference between the actual and predicted values of drought indices and increase mathematical preciseness of the prediction model, it may also lead to mis-categorization of the predicted drought. This provides misinformation for stakeholders and causes waste of budgets and efforts, while they take inappropriate actions for preparedness and mitigation for the predicted drought category.

Drought categorization converts a large volume of data (drought indices) into a category that represents a measure of severity and facilitates “apple to apple” comparisons over time (NCEI 2019). Comparing with drought indices values, interpretation of drought categories is simple and can easily be understood by stakeholders. Thus, stakeholders such as decision makers mostly care about drought categories rather than the values of drought indices. Any mis-categorization in drought studies can mislead the stakeholders. Thus, defining a threshold level for drought categorization is a crucial process (Bazrkar 2020).

One can avoid drought mis-categorization by using classification framework such as SVM for classification (SVC) and logistic regression. A logistic regression model works for a binary drought category (drought or wet). Since most of the existing drought information systems are based on multiple drought categories, the logistic regression model needs to be

modified to be employed for drought prediction (Hao, Hao, Xia, Singh et al. 2016; Hao et al. 2016, Regonda et al. 2006). However, the potential limitation is the large number of parameters for prediction of multiple drought categories (Hao et al. 2018).

Accurate predictions of drought categories are crucial for stakeholders to decide on how to be prepared for potential upcoming droughts. However, using the existing standard performance metrics such as RMSE to account for the difference between the actual and predicted values for tuning hyperparameters in cross-validation of SVR-based drought prediction models potentially leads to mis-categorization of droughts. This study aims to fill this gap by developing a new category-based scoring approach for tuning hyperparameters and improving the prediction model training by accounting for the differences in drought categories, rather than the values of drought indices. Specifically, the objective of this study is to use the concept of classification in cross-validation of an SVR model to avoid mis-categorization in drought prediction. A novel category-based scoring SVR (CBS-SVR) method is developed and compared with the traditional SVR and SVC.

3.3. Materials and Methods

3.3.1. Introduction to SVR

SVR was developed by Vapnik (1995) to reduce the generalization error by using the structural risk minimization. A regression function for a set of sampled points from input and target vectors is estimated by tuning hyperparameters. There exist different Kernel functions that can be used to increase the dimensional space in SVR. Depending on the employed Kernel function, different hyperparameters need to be tuned. The nonlinear radial basis function (RBF) was used in this study. Thus, the hyperparameters included gamma (γ), cost (C), and epsilon (ε). Parameter C determines the tradeoff between the model complexity and training error. Parameter ε controls the width of the ε-insensitive zone, and can affect the number of support vectors used to construct the regression function. Parameter γ reduces the model space and

controls the complexity of the solution (Kisi and Cimen 2011). Cross-validation is widely used to select the values of these hyperparameters. In this method, a combination of hyperparameters is selected based on a specific type of scoring. In this study, a novel category-based scoring was developed and used in CBS-SVR.

3.3.2. Development of CBS-SVR

Training, validation, and testing are three phases in the development of an SVR-based prediction model. Training is conducted on the training dataset. If the evaluation of performance on the validation dataset is successfully proceeds, final evaluation can be done on the testing dataset. There are two major problems if the dataset is divided into three parts: (1) a decrease in the number of samples by wasting too much data, and (2) dependence of the results on the random choice for the training and validation datasets. K-fold cross-validation solves these problems by dividing the dataset into training and testing sets. The training set is further divided into k folds and the validation process is repeated k times so that k-1 folds are used for training and 1-fold is used for the primary evaluation. The averaged value of performance measures in the k loops is the performance measure of k-fold cross-validation (k was equal to 5 in this study as shown in Figure 3.1). Among a number of combinations of hyperparameters that go through the cross-validation, the value with the lowest error is selected and set for the testing period of the model (Figure 3.1).

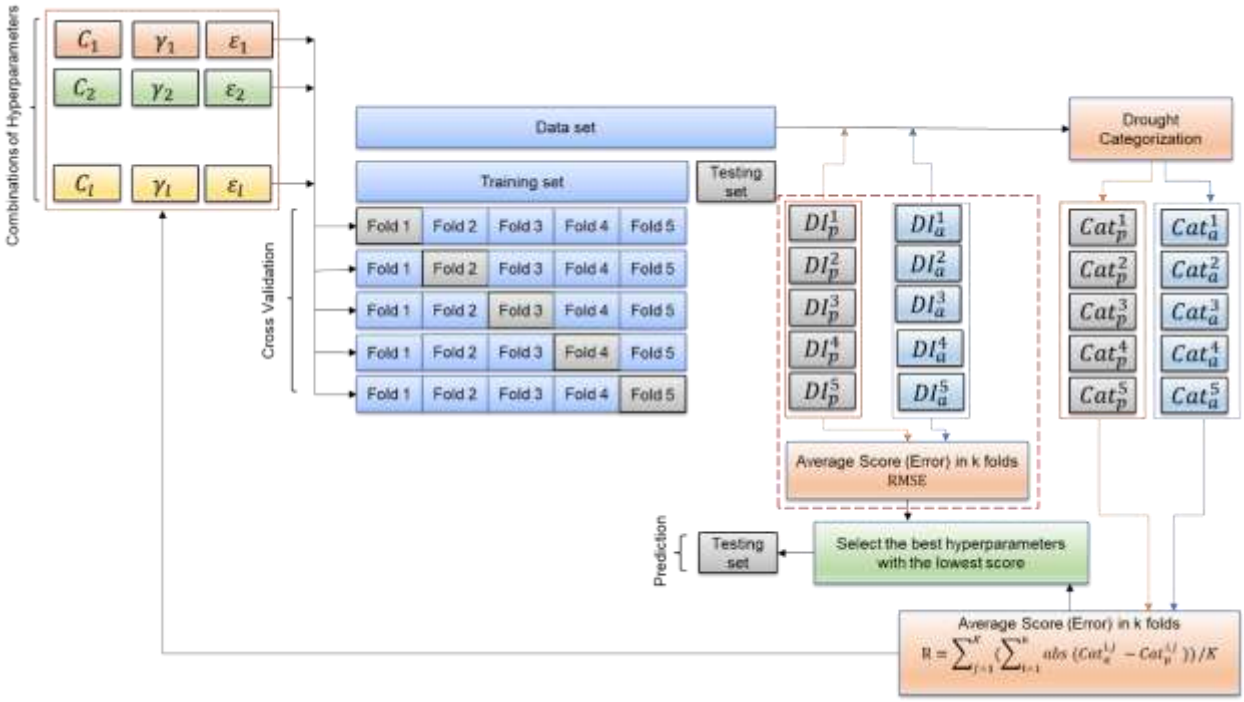

Figure 3.1. 5-fold cross-validation in CBS-SVR and SVR

In the traditional cross-validation for SVR, scoring is based on numerical statistical measures (RMSE in Figure 3.1). In this way, the hyperparameters are selected if they have the lowest difference between the actual and predicted values of drought indices. However, in the CBS-SVR, scoring is based on categorical discrepancies. Therefore, the risk of mis-categorization is potentially lower. Risk or R scoring is defined by:

$$R = \frac{\sum_{j=1}^{K}\sum_{i=1}^{n}\left|Cat_a^{i,j} - Cat_p^{i,j}\right|}{K} \tag{3.1}$$

where $Cat_a^{i,j}$ is the actual category at time i and in fold j; $Cat_p^{i,j}$ is the predicted category at time i and fold j; n is the total number of time steps; and K is the total number of folds.

The selected combination of hyperparameters is used in SVR to define the weights and intercept. Figure 3.2 shows two cases of mis-categorization by using RMSE and how CBS-SVR can avoid this issue. D4, D3, D2, D1, and D0 are exceptional, extreme, severe, moderate, and abnormal droughts, respectively; N indicates a normal condition; and W0, W1, W2, W3, and W4 are representatives of abnormal, moderate, severe, extreme, and exceptional wet conditions,

respectively. The thresholds are selected based on the traditional drought categorization. In case 1, the value predicted by SVR using the RMSE scoring is closer to the actual value but it is in a different drought category. The value predicted by CBS-SVR has a higher RMSE but it is in the same category as that of the actual value. In case 2, as a result of overfitting in other cases (e.g., case 1), the difference between the predicted value by SVR and the actual value is larger than that of the value predicted by CBS-SVR. Thus, the RMSE scoring causes mis-categorization, while CBS-SVR successfully avoids this problem.

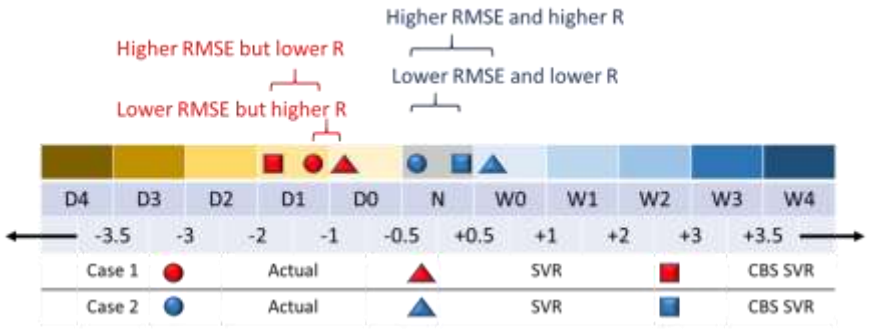

Figure 3.2. Risk of mis-categorization in SVR and more accurate categorization by CBS-SVR

3.3.3. Drought Categorization

Drought categorization plays a crucial role in this study since it determines the hyperparameters for SVR and thus impacts drought prediction. Traditional categorization is based on fixed threshold levels, which need to be varied by time and location (Mishra and Singh 2010, Bazrkar 2020). Bazrkar et al. (2020) proposed a customized drought categorization (CDC) and employed a cell-by-cell based analysis to incorporate both spatial and temporal distributions of drought. A joint probability distribution and conditional expectation were used to estimate the average probability of occurrence of each drought category. K-means clustering (KM) was further used in the CDC to derive variable thresholds. Two normal distributions (one for dry and another for wet) were observed in their study. A Gaussian mixture (GM) model is suggested when two normal distributions are combined. Therefore, GM can be employed for drought categorization in the CDC. Traditional drought categorization (McKee et al. 1993) is

based on the normal distribution (N). Svoboda et al. (2002) employed the percentile method to define the categories thresholds. The same categories were used in this study, including exceptional, extreme, severe, moderate, and abnormal dry conditions as well as the normal condition. In the traditional drought categorization, drought indices values of -3.00, -2.00, -1.00, and -0.50 are respectively the thresholds for extreme, severe, moderate, and abnormal drought categories. 0.50, 1.00, 2.00, and 3.00 are used for abnormal, moderate, severe, and extreme wet categories, respectively. The values between -0.50 and 0.50 are categorized as a normal category. -3.50 and 3.5 are used as the thresholds for exceptional dry and wet categories. The variable threshold levels for drought categories in the CDC were developed to vary by time and geographic locations and were determined by KM or GM for these eleven categories. In this study, the performance of KM was compared to the traditional categorization (McKee 1993) and GM. Since a long time series was required to find the exceptional drought and wet categories, 3.5 and -3.5 were set as the thresholds for these two categories.

3.3.4. Assessment of CBS-SVR

To assess the performance of CBS-SVR, it was first compared with the traditional SVR with the RMSE-based scoring. Then, CBS-SVR was compared with SVC. To measure and compare the performances of the models, a confusion matrix was extended from binary-class to multi-class and then different performance metrics were used.

3.3.4.1. Comparison of the CBS-SVR with SVR and SVC

RMSE has been widely used as scoring in cross-validation for tuning hyperparameters in SVR and for evaluation of the performances of other drought prediction models. However, there is a risk of mis-categorization if hyperparameters are selected based on RMSE. The traditional RMSE-based SVR was modified to overcome the issue of mis-categorization by developing CBS-SVR in this study. Due to its classification nature, SVC is potentially capable of avoiding mis-

categorization. To quantize the predictive skills of each model, the performance of CBS-SVR was compared with those of SVR and SVC.

There are some major differences between SVR and SVC. First, the main goal of SVR is to fit as many points as possible in the decision boundary or ε-tube. However, the primary goal of SVC is to separate the points by maximizing the margin or minimizing the dot product of the coefficients in Equation (3.2). Unlike SVR, in SVC, the fewer points in the boundary margin (ε-tube in SVR), the better. Therefore, the ideal is to satisfy Equation (3.3) for all samples (Vapnik 1995).

$$\|\omega\|^2 = \omega^T\omega \tag{3.2}$$

$$y_i(\omega^T\phi(x_i) + b) \geq 1 \tag{3.3}$$

where ω is the coefficient vector of the predictor x; $\omega^T$is the transpose of ω; $\| \|$ indicates dot product; y_i is predictand i; b is the intercept; and ϕ is the kernel function, which implicitly maps the training vectors into a higher dimensional space. In this study, the nonlinear radial basis function (RBF) kernel is used in the SVR and SVC.

Since the satisfaction of Equation (3.3) is not possible, some samples are allowed to be at a specific distance from their correct margin boundary, defined as a slack variable. However, these points are penalized by a penalty term (regularization parameter). Only one slack variable in SVC is defined so that it is greater than 1 if the point is above the hyperplane (blue line in Fig. 1 with y = 0) and less than 1 if the point is below the hyperplane (Figure 3.3). Therefore, the objective function in SVC is given by (Vapnik 1995):

$$Min\ \left[\frac{1}{2}\|\omega\|^2 + C\sum_{i=1}^{n}\xi_i\right] \tag{3.4}$$

$Subject\ to$:

$$y_i(\omega^T\phi(x_i) + b) \geq 1 - \xi_i, \xi_i \geq 0, i = 1, \dots, n \tag{3.5}$$

where C is the regularization parameter; and ξ_i is the slack variable i in SVC.

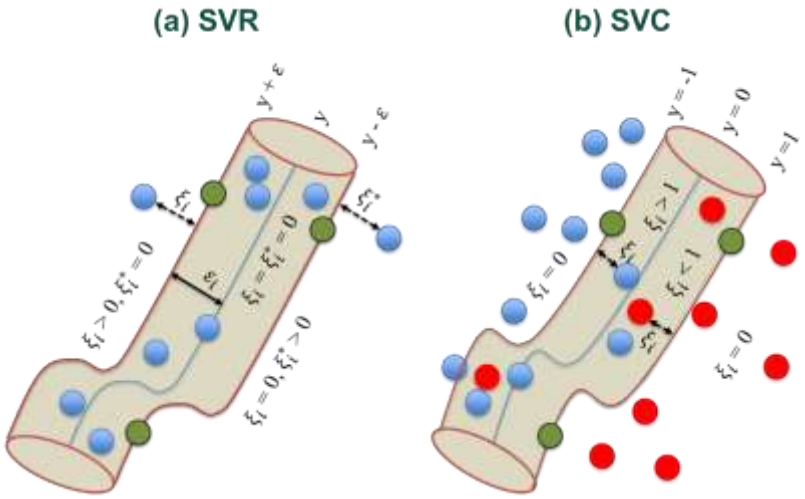

Figure 3.3. SVR and SVC

There are two slack variables (ξ_i , ξ_i^*) for SVR. Depending on the location of the points, these slack variables have different values. If the points are above the ε-tube, ξ_i is greater than zero and ξ_i^* is equal to zero; If the points are below the ε-tube, ξ_i is equal to zero and ξ_i^* is greater than zero; and if the points are inside the ε-tube, both ξ_i and ξ_i^* are equal to zero (Figure 3.3). Thus, the objective function for SVR is defined as (Vapnik 1995):

$$Min\ \left[\frac{1}{2}\|\omega\|^2 + C\sum_{i=1}^{n}(\xi_i + \xi_i^*)\right] \tag{3.6}$$

Subject to:

$$y_i - \omega^T\phi(x_i) - b \leq \varepsilon + \xi_i, \tag{3.7}$$

$$\omega^T\phi(x_i) + b - y_i \leq \varepsilon + \xi_i^*, \xi_i, \xi_i^* \geq 0, i = 1, \ldots, n \tag{3.8}$$

where ε is the radius of the ε-tube. The samples penalize the objective by ξ_i or ξ_i^* above or below the ε-tube, respectively (Figure 3.3). In other words, the samples whose predictions are at least ε away from their true targets are penalized.

The main difference between SVR and SVC is in their loss functions. The loss function in SVC just assures that the prediction is greater than 1 if predicted value is positive and less than -1 if predicted value is negative (Figure 3.3). However, instead of minimizing the observed

training error, the loss function in the SVR tries to minimize the generalization error bound so that a generalized performance is achieved.

3.3.5. Confusion Matrix and Accuracy Measures for Evaluation of the Prediction Models

The confusion matrix (Stehman 1997) and accuracy measures such as the area under the curve of a receiving operating characteristic (AUC-ROC) were originally developed for two-category or binary models. Various approaches have been used to extend the original binary models to multiclass models. One versus all approach (Provost and Domingos 2000) was used in this study to evaluate the performances of the multi-category drought prediction models. Figure 3.4 shows how a confusion matrix for two categories (dry/wet) is extended to the one for eleven drought categories. The AUC-ROC and micro, macro, and weighted average (Fawcett 2001 and 2006) of F1 score were used to obtain overall performances of CBS-SVR, SVR, and SVC.

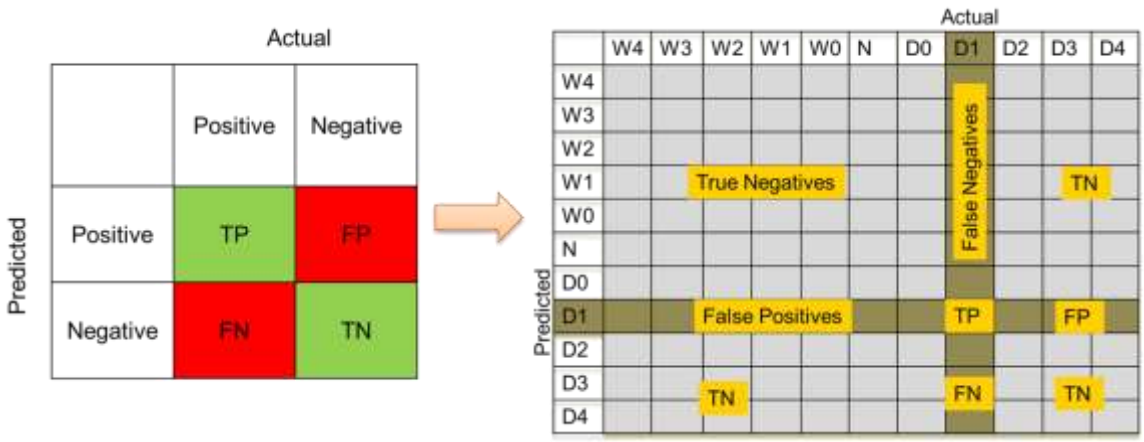

Figure 3.4. Confusion matrix for evaluation of binary and multiclass drought prediction models

If the model predicts a correct category of drought, it is "True Positive (TP)." If the model predicts an incorrect category or categories, it is "True Negative (TN)." Type I error occurs if the model predicts a specific category of drought but in reality, it is not right. This type of error in the confusion matrix is "False Positive (FP)." Type II error occurs if the model predicts that a

specific type of drought does not occur but the prediction is false. This type of error is "False Negative (FN)" in the confusion matrix (Wang and Zheng 2013). Recall, which indicates the correctness of the model prediction, is calculated by (Ting 2011):

$$Recall = \frac{TP}{TP+FN} \tag{3.9}$$

Precision represents the number of actually positive cases out of the positive classes that a model is able to predict correctly and is given by (Ting 2011):

$$Precision = \frac{TP}{TP+FP} \tag{3.10}$$

F1 score is used to make two models with low and high precision comparable. Therefore, to account for these cases, F1 score is used for evaluation of the performances of the models. F1 score is calculated by (Zhang and Zhang 2009):

$$F1\ score = \frac{2\times Recall\times Precision}{Recall+Precision} \tag{3.11}$$

AUC-ROC is also used for comparison of the models' performances. The higher the AUC-ROC, the better the model. The ROC curve is plotted with true positive rate (TPR) against false positive rate (FPR). TPR is defined the same as recall or sensitivity. FPR is calculated by (Ting 2011):

$$FPR = \frac{FP}{TN+FP} \tag{3.12}$$

3.3.6. Setup of CBS-SVR Model

Precipitation, temperature, actual evapotranspiration, and a deficit variable (DFCT) were selected as the predictors. The DFCT was defined as the difference between precipitation and actual evapotranspiration. The target variables consisted of three types of drought indices at different time scales (monthly, seasonally, and semiannually) including (1) multivariate hydroclimatic aggregate drought index (HADI) (Bazrkar et al. 2020) and snow-based hydroclimatic aggregate drought index (SHADI) (Bazrkar and Chu 2021), (2) bivariate standardized drought indices based on the difference between precipitation and actual evapotranspiration (SPEI) and the summation of snowmelt and rainfall, and (3) univariate

standardized drought indices based on precipitation, surface runoff, baseflow (BF), soil moisture, snowpack, and snow water equivalent (SWE). In an application to the Red River of the North Basin (RRB), the North American Land Data Assimilation System (NLDAS) (Xia et al 2012) data in 1979-2010 and 2011-2016 were respectively used for the training and testing of the CBS-SVR model.

3.3.7. Drought Indices

In this study, ten CBS-SVR models were developed, in which ten drought indices were used as the target variables. The multivariate HADI and SHADI (Bazrkar et al. 2020; Bazrkar and Chu 2021) distinguished drought and snow drought in cold climate regions. The R-mode correlation-based principal component analysis (PCA) was employed to aggregate rainfall (RF), snowmelt (SM), surface runoff (R), and soil water storage (SWS) in the calculation of HADI. Precipitation and snowpack (SP) were used, instead of rainfall and snowmelt in HADI, to calculate SHADI to enhance the capability of identifying snow drought (Bazrkar and Chu 2021). Two bivariate standardized drought indices were also used. The standardized difference between precipitation and potential evapotranspiration was used to develop SPEI by Vicente-Serrano (2010). Homdee et al. (2016) and Joetzjer et al. (2013) argued that the use of actual evapotranspiration showed higher consistency with hydrological drought indices and it considered land use and vegetation cover. In this study, actual evapotranspiration was used to calculate SPEI. The standardized snowmelt and rainfall index (SMRI) (Staudinger 2014) was also estimated. The univariate standardized drought indices used in this study included standardized precipitation index (SPI) (McKee 1993), standardized runoff index (SRI) (Shukla and Wood 2008), standardized soil moisture index (SSMI) (Xu et al. 2018), standardized snowpack index (SSPI), standardized snow water equivalent index (SSWEI) (Huning and Aghakouchak 2018), and standardized baseflow index (SBFI) (Bazrkar and Chu 2020). These

drought indices cover a wide range of hydroclimatic variables and different types of drought indices and hence using all of them can reassure the capability of the CBS-SVR model.

3.3.8. Predictors

Depending on the specific drought index used as the target variable in the prediction model, different types of predictor(s) were used. Table 3.1 shows the predictands and their associated predictors. Precipitation (P) was used as a predictor for prediction of all drought indices. Temperature (T) was added for prediction of SPEI, SMRI, SSPI, and SSWEI, where besides precipitation, temperature also played a key role in the identification of drought. Actual evapotranspiration (ET) and the DFCT were also added in the prediction of HADI, SHADI, SSMI, SRI, and SBFI.

Table 3.1. Predictands and predictors

Predictands	Type	Input	Method of calculation	Predictors
HADI	Multivariate	RF, SM, R, SWS	PCA	P, T, ET, DFCT
SHADI	Multivariate	P, SP, R, SWS	PCA	P, T, ET, DFCT
SSMI	Univariate	SWS	Standardized	P, T, ET, DFCT
SRI	Univariate	R	Standardized	P, T, ET, DFCT
SBFI	Univariate	BF	Standardized	P, T, ET, DFCT
SPEI	Bivariate	P, ET	Standardized	P, T
SMRI	Bivariate	SM, RF	Standardized	P, T
SSPI	Univariate	SP	Standardized	P, T
SSWEI	Univariate	SWE	Standardized	P, T
SPI	Univariate	P	Standardized	P

Notes: P: Precipitation, T: Temperature, ET: Evapotranspiration, RF: Rainfall, SM: Snowmelt, R: Runoff, SWS: Soil moisture, SP: Snowpack, BF: Baseflow, SWE: Snow water equivalent, DFCT: difference between precipitation and evapotranspiration, PCA: Principal component analysis

3.3.9. Study Area

The U.S. part of the RRB (Figure 3.5) is a typical cold climate region in the Northern Great Plain, which covers over 90,000 km2 in the states of Minnesota (MN), North Dakota

(ND), and South Dakota (SD). According to the NCEI data (2021), the cold season of 2020 was the driest and the 10th warmest cold season and March 2021 was the driest and the 4th warmest March in the last 127 years in most of climate divisions (CDs) in ND. This sets an alarm for more severe droughts in the RRB. According to Palmer Z-index for March 2021 (Figure 3.5), CDs 3202, 3203, and 3205 were the driest and CD 2101 was the wettest in the RRB. However, according to the five-year mean of Z-index, CD 2101 was also among the driest CDs in the RRB, besides CDs 3202, 3203, and 3205.

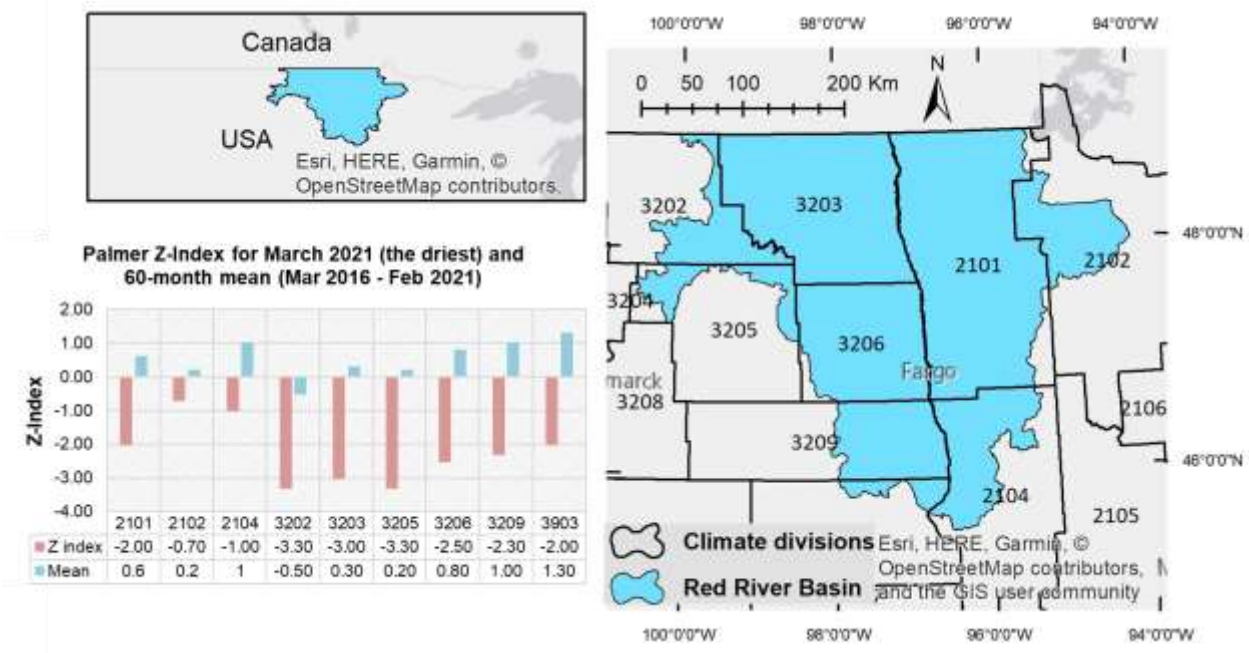

Figure 3.5. RRB, its associated climate divisions, and Palmer Z-Index

A great portion of the RRB is covered by cultivated croplands. Therefore, drought has significant socio-economic impacts on the population in the RRB. One of the devastative droughts in the RRB occurred in 1990's. That drought was referred to as a snow drought since the RRB experienced the lowest precipitation and the highest temperature in the cold seasons in that dry decade. However, the 1930's drought known as the Great Drought was due to low precipitation in the warm seasons (Bazrkar and Chu 2021). Therefore, different drought indices

with the capabilities of addressing different types of drought are required. In this study, the performances of different drought indices were assessed in the CBS-SVR model in the RRB.

3.4. Results and Discussions

To select the best categorization method, the traditional categorization based on the normal distribution, and the CDC with KM and GM clustering methods based on the ten drought indices were compared. The RMSE scoring was used for cross validation of these models. Table 3.2 shows the best, worst, and average of AUC-ROCs and the weighted, micro, and macro F1 scores for these models. A categorization method was selected as the best If the majority of performance measures showed the highest values for that specific categorization method. KM was selected as the best for SHADI and SMRI. Traditional categorization was selected as the best for SPEI, SPI, SRI, SSMI, and SBFI. For HADI, AUC-ROC and the micro F1 score suggested traditional categorization, while the weighted and macro F1 scores showed KM as the best categorization method. Unlike other indices, the best results for SSPI were obtained when GM clustering was applied. According to the results, a slight to significant improvement was achieved by changing the employed categorization method. For instance, a significant increase (0.18) in the weighted F1 score was observed when GM was switched to KM in the categorization of drought based on SRI. The most significant improvement (0.21) was obtained for the same measure and index when the traditional normal categorization was used instead of GM. There was also an improvement in the performance of the model (an increase of 0.08 in the micro F1 score) when the traditional normal drought categorization based on SSPI was changed to GM. It was concluded that depending on the selected drought index or indices, different performances and results were obtained when different drought categorization methods were employed.

Table 3.2. Selection of the best categorization method

Drought Index	Clustering model	AUC-ROC (Micro)	F1 Score (Weighted)	F1 Score (Micro)	F1 Score (Macro)
HADI	N	0.75	0.41	0.54	0.08
	KM	0.72	0.43	0.50	0.10
	GM	0.72	0.38	0.50	0.08
SHADI	N	0.67	0.27	0.40	0.08
	KM	0.71	0.38	0.47	0.10
	GM	0.68	0.35	0.41	0.11
SPEI	N	0.81	0.65	0.66	0.34
	KM	0.80	0.63	0.64	0.36
	GM	0.80	0.63	0.64	0.35
SMRI	N	0.88	0.79	0.79	0.40
	KM	0.89	0.80	0.80	0.43
	GM	0.88	0.77	0.77	0.41
SPI	N	0.99	0.97	0.97	0.55
	KM	0.99	0.97	0.97	0.57
	GM	0.99	0.97	0.97	0.57
SRI	N	0.74	0.52	0.52	0.23
	KM	0.73	0.49	0.51	0.23
	GM	0.64	0.31	0.35	0.10
SSMI	N	0.66	0.34	0.37	0.15
	KM	0.64	0.32	0.35	0.15
	GM	0.60	0.27	0.27	0.12
SSPI	N	0.74	0.58	0.53	0.21
	KM	0.76	0.57	0.56	0.21
	GM	0.79	0.64	0.61	0.20
SSWEI	N	0.73	0.56	0.51	0.19
	KM	0.75	0.54	0.54	0.20
	GM	0.73	0.54	0.52	0.20
SBFI	N	0.71	0.43	0.47	0.11
	KM	0.68	0.40	0.41	0.11
	GM	0.65	0.35	0.36	0.10

Table 3.3 shows the variable thresholds for the drought categories based on the drought indices. Different variable thresholds were obtained for each drought index. The clustering method was used to derive these variable thresholds based on the probabilities of occurrences of those values considering both spatial and temporal distributions of droughts. For example, the lower and upper class limits for the normal category in the traditional categorization were -0.5 and 0.5, respectively. However, the lower class limits for the normal category were as low as -

1.05 for SHADI and -1.03 for SSPI and the upper class limit was as low as -0.33 for SSPI when GM was used for clustering. Since the range of each drought index was different, these different variable thresholds reassured that each drought category was defined based on the temporal and spatial frequencies of the drought index values.

Table 3.3. Variable threshold levels for all drought indices based on different categorization methods

Class No.	Clustering	N	KM			GM									
	Class	DIs	SDIs	HADI	SHADI	SPI	SRI	SSMI	SBFI	SSPI	SSWEI	SPEI	SMRI	HADI	SHADI
0	W4	3.5	3.5	3.5	3.5	3.5	3.5	3.5	3.5	3.5	3.5	3.5	3.5	3.5	3.5
1	W3	3.00	2.37	2.75	2.75	2.27	2.57	2.37	2.27	2.37	2.37	2.57	2.47	2.65	2.55
2	W2	2.00	1.67	1.85	1.85	1.47	1.87	1.77	1.27	1.47	1.57	1.87	1.67	1.75	1.65
3	W1	1.00	0.97	0.95	1.05	0.77	0.97	1.07	0.47	0.57	0.87	1.07	0.87	0.95	0.75
4	W0	0.50	0.27	0.05	0.15	0.17	0.17	0.47	-0.23	-0.33	0.17	0.37	-0.03	0.25	-0.15
5	N														
6	D0	-0.50	-0.53	-0.95	-0.85	-0.63	-0.83	-0.23	-0.83	-1.03	-0.53	-0.43	-0.73	-0.65	-1.05
7	D1	-1.00	-1.33	-1.85	-1.75	-1.43	-1.63	-0.93	-1.43	-1.73	-1.13	-1.33	-1.33	-1.65	-1.95
8	D2	-2.00	-2.13	-2.75	-2.65	-2.23	-2.33	-1.83	-2.23	-2.33	-1.93	-2.13	-2.03	-2.55	-2.75
9	D3	-3.00	-2.93	-3.45	-3.45	-2.93	-2.93	-2.93	-2.93	-2.93	-2.93	-2.93	-2.93	-3.45	-3.45
10	D4	-3.50	-3.50	-3.50	-3.50	-3.50	-3.50	-3.50	-3.50	-3.50	-3.50	-3.50	-3.50	-3.50	-3.50

Notes: DI: Drought index; and SDI: Standardized drought index.

The best categorization method for each drought index was selected and, then, SVR based on RMSE and CBS-SVR based on R scoring were compared for the drought indices. The results of this comparison are shown in Table 3.4. Unlike the results for SRI, SSMI, SSPI, and SSWEI, better results were obtained when R was used, instead of the traditional RMSE for cross-validation of SVR based on HADI, SHADI, SPEI, SMRI, SPI, and SBFI.

Table 3.4. Comparison of the performances of RMSE (SVR) and R (CBS-SVR)

Drought Index	Selected Clustering Model	Performance Measure	AUC-ROC (Micro)	F1 Score (Weighted)	F1 Score (Micro)	F1 Score (Macro)
HADI	N	RMSE	0.747	0.410	0.540	0.082
		R	0.761	0.457	0.566	0.110
SHADI	KM	RMSE	0.708	0.377	0.469	0.102
		R	0.723	0.415	0.497	0.124
SPEI	N	RMSE	0.813	0.647	0.660	0.337
		R	0.814	0.651	0.663	0.333
SMRI	KM	RMSE	0.892	0.796	0.803	0.432
		R	0.896	0.804	0.812	0.435
SPI	N	RMSE	0.986	0.973	0.975	0.550
		R	0.987	0.975	0.977	0.551
SRI	N	RMSE	0.737	0.515	0.521	0.234
		R	0.735	0.512	0.519	0.232
SSMI	N	RMSE	0.656	0.339	0.375	0.150
		R	0.656	0.337	0.374	0.150
SSPI	GM	RMSE	0.786	0.643	0.611	0.199
		R	0.749	0.593	0.543	0.203
SSWEI	KM	RMSE	0.748	0.543	0.542	0.197
		R	0.643	0.324	0.351	0.151
SBFI	N	RMSE	0.706	0.434	0.466	0.106
		R	0.708	0.434	0.469	0.106

Although the overall results (areal average) for all grids showed that R scoring was better than RMSE for the drought prediction models based on most drought indices (6 out of 10), four cases occurred for different grids: (1) R scoring performed better than RMSE; (2) RMSE performed better than R scoring; (3) there was no difference in the performances of R scoring and RMSE based on AUC-ROC; and (4) there was no difference in the performances of R scoring and RMSE based on the standard performance measures (i.e., R^2, MAE, MSE, and RMSE). Figure 3.6 shows the AUC-ROC for the eleven categories of drought in the SVR model based on SRI for grid 466, where R outperformed RMSE with the highest degree among all grids (an example for case 1). The micro average of AUC-ROC increased from 0.66 to 0.73 when R scoring was used for cross-validation of SVR for SRI. Table 3.6 also shows an increase in R^2 (from 0.63 for R scoring to 0.70 for RMSE) and decreases in MAE, MSE, and RMSE for grid 466. When RMSE was used (Figure 3.10), it caused overfitting in some months and underfitting in other months (e.g., March 2011, September 2011, and September 2015). The value of the actual SRI in February 2015 was -0.47, indicating a normal condition based on the best categorization method for SRI (i.e., traditional normal). The predicted value by the R scoring for

the same month was 0.41 and still in a normal condition. However, the predicted value by using RMSE was 0.54 and in an abnormal wet condition. This was an example of mis-categorization caused by using RMSE. However, the CBS-SVR model avoided this kind of mis-categorization by using R scoring.

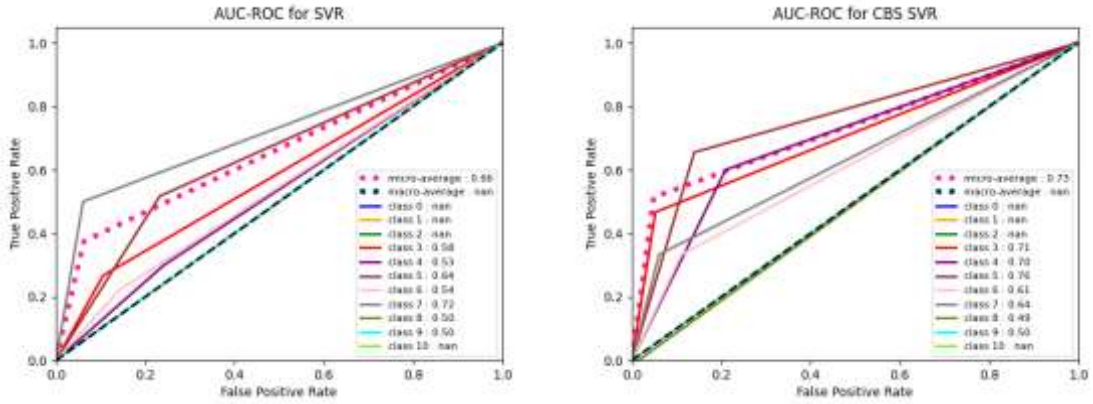

Figure 3.6. AUC-ROC for 11 categories of drought in SVR (left) and CBS-SVR (right) based on SRI for grid 466

The micro- and macro-averages of a specific metric are slightly different in their calculations. In the macro-average computation, the metric is computed independently for each class and then the average is taken by treating all classes equally. However, in the micro-average computation, the contributions of all classes are aggregated to compute the average metric. Therefore, the values of "nan" for macro-average in Figures 3.6 - 3.9 were attributed to the severer dry/wet categories that did not occur in the study area and period and thus their AUC-ROC were indicted as "nan." Ignoring these values of nan, the AUC-ROC values for moderate wet (0.58 - 0.71), abnormal wet (0.53 - 0.70), normal (0.64 - 0.76), and abnormal dry (0.54 - 0.61) increased when R scoring was used. For moderate dry, a decrease in AUC-ROC from 0.72 to 0.64 and for severe drought a slight decrease from 0.50 to 0.49 were observed. The same value for AUC-ROC (0.5) for extreme drought was observed for both RMSE and R scoring. The highest type I and type II errors occurred for normal and abnormal wet categories, respectively (Table 3.5). However, the magnitudes of errors in R scoring were lower than those of RMSE. For

these categories both precision and recall increased when R scoring was used. For abnormal wet, the precision and recall values increased from 0.87 to 0.92 and from 0.76 to 0.79, respectively. For normal category, higher increases in precision (from 0.70 to 0.79) and recall (from 0.77 to 0.86) were observed.

Table 3.5. Confusion matrices for different drought categories in grids 466, 399, 400, and 401

			Actual															
			466				399				400				401			
			RMSE		R		RMSE		R		RMSE		R		RMSE		R	
			P	N	P	N	P	N	P	N	P	N	P	N	P	N	P	N
Predicted	Class 0	P																
		N																
	Class 1	P																
		N																
	Class 2	P	71	0	71	0	70	1	70	1			71	0				
		N	1	0	1	0	1	0	1	0			1	0				
	Class 3	P	51	11	54	8	58	4	57	8	56	5	58	8	60	7	60	7
		N	6	4	3	7	2	8	3	4	3	8	1	5	2	3	2	3
	Class 4	P	47	7	49	4	52	7	49	11	51	7	51	8	52	2	52	2
		N	15	3	13	7	7	6	10	2	8	6	8	5	10	8	10	8
	Class 5	P	33	14	37	10	33	6	27	10	29	6	29	6	35	7	35	7
		N	10	15	6	19	11	22	17	18	13	24	13	24	13	17	12	18
	Class 6	P	54	7	56	6	59	5	59	4	59	7	58	6	51	8	52	7
		N	9	2	7	3	6	2	6	3	5	1	6	2	10	3	10	3
	Class 7	P	62	3	62	4	63	5	61	4	63	7	62	4	57	9	57	9
		N	4	3	4	2	2	2	4	3	2	0	3	3	1	5	1	5
	Class 8	P	70	2	69	2	69	0	69	2	69	1	71	1	70	2	70	2
		N	0	0	1	0	0	3	0	1	2	0	0	0	0	0	0	0
	Class 9	P	71	1	71	1	71	1	71	1			71	0	71	1	71	1
		N	0	0	0	0	0	0	0	0			1	0	0	0	0	0
	Class 10	P																
		N																

Figure 3.7 shows the AUC-ROC for grid 399, where RMSE outperformed R with the highest degree among all grids (an example for case 2). The micro-average of AUC-ROC for RMSE decreased from 0.78 to 0.69 when R scoring was used. The exceptional dry and wet and

extreme wet categories were not observed and thus their associated values were depicted as nan in Figure 3.7. The AUC-ROC values for severe wet (0.49) and extreme dry (0.5) categories remained unchanged. Except for the abnormal dry and moderate dry categories, decreases in the AUC-ROC values were observed for all other drought categories. The highest type I and type II errors occurred for abnormal wet and normal categories, respectively (Table 3.4). However, the magnitudes of errors in R scoring were higher than those of RMSE. For these categories both precision and recall decreased when R scoring was used. For abnormal wet, precision and recall decreased from 0.88 to 0.82 and from 0.88 to 0.83, respectively. For normal category, higher decreases in precision (from 0.85 to 0.73) and recall (from 0.75 to 0.61) were observed. According to Figure 3.10, the major differences were related to April 2011, 2012, and 2013, as well as March 2014, when the predictions based on RMSE were closer to the actual values. Table 3.6 also shows that R^2 increased and MAE, MSE, and RMSE decreased after the application of RMSE.

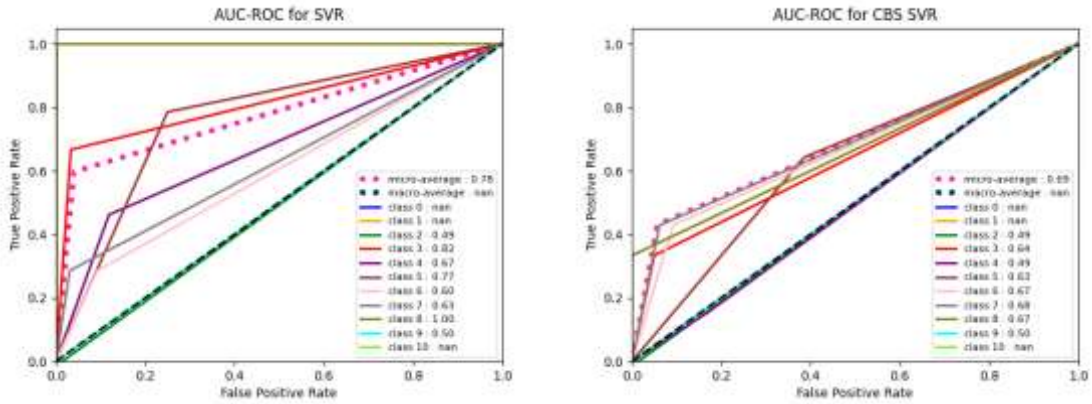

Figure 3.7. AUC-ROC for 11 categories of drought in SVR (left) and CBS-SVR (right) based on SRI for grid 399

Figure 3.8 shows the AUC-ROC for grid 400, where the same AUC-ROC was obtained when the performances of RMSE and R were compared (an example for case 3). However, except for the normal category, the AUC-ROC varied for different drought categories. Increases in the AUC-ROC values from 0.52 to 0.58, from 0.48 to 0.69, and from 0.49 to 0.50 were observed for abnormal, moderate, and severe drought categories, respectively. In contrast, the

AUC-ROC values decreased for moderate (from 0.78 to 0.68) and abnormal wet (from 0.66 to 0.62) categories. Table 3.5 shows that the highest type II error occurred with the same value (13 out of 72 months) in the normal category. This means that 13 out of 72 months were categorized as a normal condition but the model predicted a different category. The precision (0.83) and recall (0.69) had the same value in this category. When RMSE was used, the highest type I error occurred in the abnormal wet/dry and moderate dry categories with a value of 7 out of 72. However, when R scoring was used, the highest type I error occurred in the abnormal and moderate wet categories with a value of 8. Based on Figure 3.10, the major difference was related to March 2014, when R scoring performed better than RMSE. Table 3.5 also shows that based on R^2, MAE, MSE, and RMSE, SVR was better than CBS-SVR.

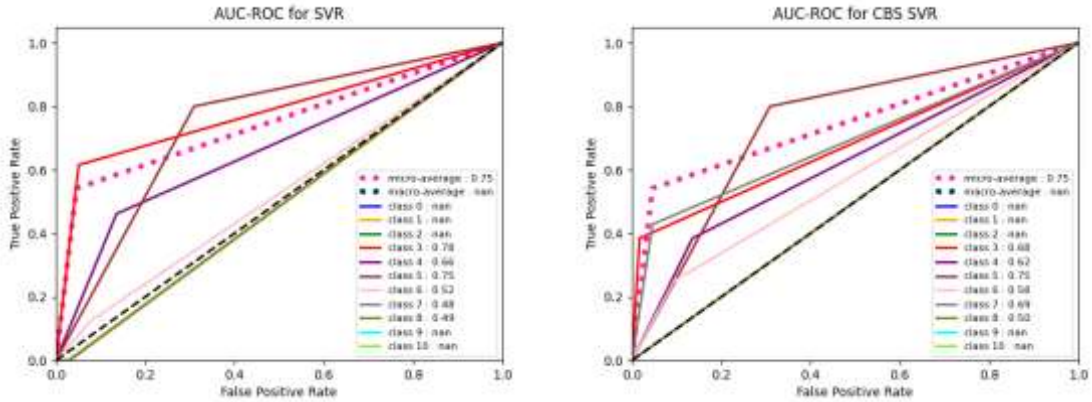

Figure 3.8. AUC-ROC for 11 categories of drought in SVR (left) and CBS-SVR (right) based on SRI for grid 400

Figure 3.9 shows the AUC-ROC for grid 401, where R^2, MAE, MSE, and RMSE were equal when the performances of RMSE and R scoring were compared (an example for case 4). Although the R^2, MAE, MSE, and RMSE values were the same, there was a slight difference between AUC-ROCs. AUC-ROC increased from 0.72 to 0.73 when R scoring was used. This difference was attributed to the slight increases in AUC-ROC of the normal and abnormal drought categories, while AUC-ROC was exactly the same for all other drought categories. The highest type I and II errors also occurred in the same categories (i.e., moderate dry and normal,

respectively). Table 3.6 indicates that the values of R^2, MAE, MSE, and RMSE were exactly the same. Figure 3.10 also shows the similar values of SRI in gird 401.

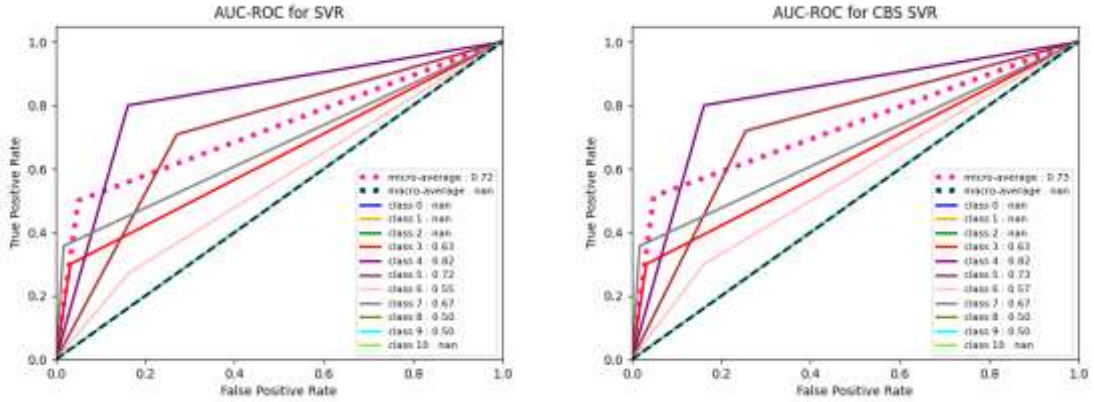

Figure 3.9. AUC-ROC for 11 categories of drought in SVR (left) and CBS-SVR (right) based on SRI for grid 401

Table 3.6. Performance measures for predictions of SRI at grids 466, 399, 400, and 401

RMSE/R	Grid No.	R^2	MAE	MSE	RMSE
RMSE	466	0.63	0.46	0.35	0.59
	399	0.75	0.40	0.29	0.54
	400	0.53	0.48	0.37	0.61
	401	0.63	0.45	0.37	0.61
R	466	0.70	0.40	0.29	0.54
	399	0.64	0.48	0.42	0.65
	400	0.48	0.47	0.41	0.64
	401	0.63	0.45	0.37	0.61

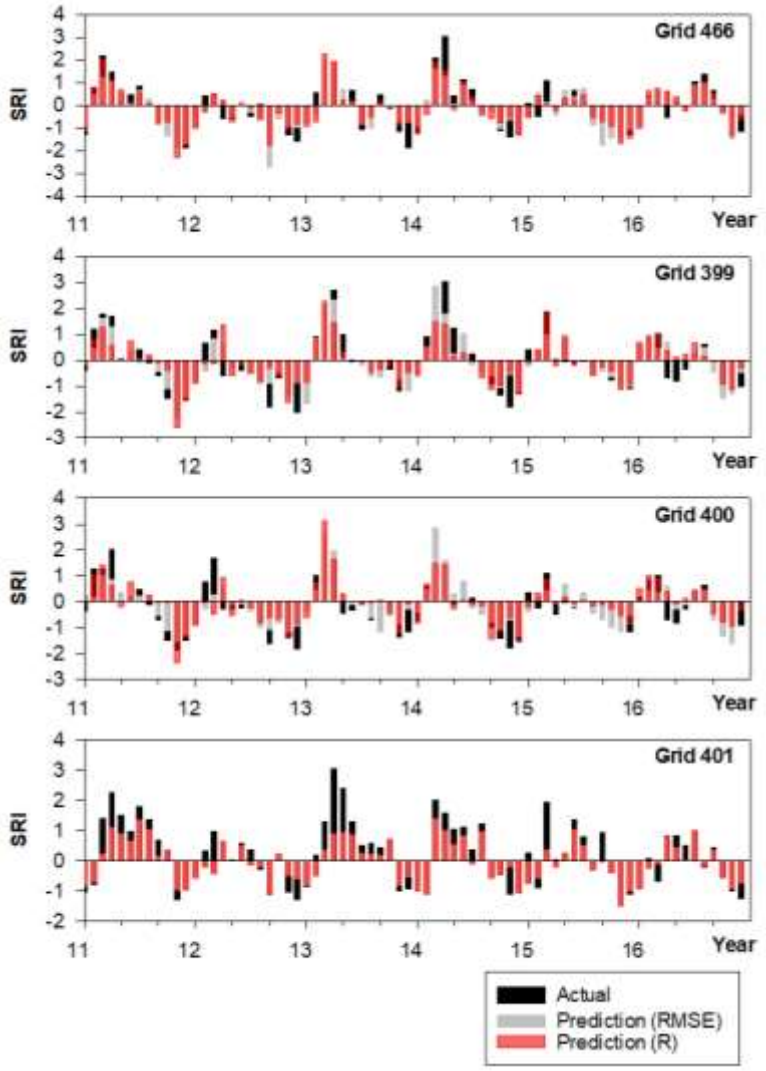

Figure 3.10. Comparison of actual and predicted values of SRI based on RMSE and R

Table 3.7 shows the results of comparison between SVC and CBS-SVR for the drought indices. According to the results, CBS-SVR outperformed SVC based on HADI, SHADI, SPEI, SMRI, SPI, SSMI, SSWEI, and SBFI. Two exceptions were observed for SRI and SSPI. Overall, CBS-SVR had better performances since a category-based scoring was used for tuning the hyperparameters for cross-validation.

Table 3.7. Comparison of the performances of SVC and CBS-SVR

Drought Index	Selected Performance Measure	AUC-ROC (Micro)		F1 Score (Weighted)		F1 Score (Micro)		F1 Score (Macro)	
		SVC	SVR	SVC	SVR	SVC	SVR	SVC	SVR
HADI	R	0.758	0.761	0.433	0.457	0.560	0.566	0.103	0.110
SHADI	R	0.719	0.723	0.394	0.415	0.490	0.497	0.115	0.124
SPEI	R	0.812	0.814	0.640	0.651	0.658	0.663	0.312	0.333
SMRI	R	0.879	0.896	0.757	0.804	0.780	0.812	0.389	0.435
SPI	R	0.980	0.987	0.960	0.975	0.964	0.977	0.522	0.551
SRI	RMSE	0.754	0.737	0.526	0.515	0.554	0.521	0.234	0.234
SSMI	RMSE	0.653	0.656	0.267	0.339	0.369	0.375	0.104	0.150
SSPI	RMSE	0.846	0.786	0.711	0.643	0.720	0.611	0.206	0.199
SSWEI	RMSE	0.747	0.748	0.527	0.543	0.540	0.542	0.176	0.197
SBFI	R	0.696	0.708	0.377	0.434	0.447	0.469	0.088	0.106

3.5. Conclusions

Using the standard performance metrics such as RMSE for scoring in cross-validation of non-categorical prediction models can result in overfitting and mis-categorization of droughts. In this study, a category-based scoring method (CBS-SVR) was proposed. Due to the crucial role of the thresholds for defining drought categories (Mishra and Singh 2010, Bazrkar et al 2020), KM and GM clustering methods were tested and compared with the traditional categorization method. Different thresholds were obtained for each drought index. When KM clustering was used, the same thresholds were derived for all standardized drought indices. For HADI and SHADI, the thresholds were close. This result was in accordance with the finding by Bazrkar and Chu (2021), where the output from a grid-based hydrologic model (GHM) (Chu et al. 2018) in a different study period (2003-2007) was used. However, the thresholds were different even for the standardized drought indices when GM was employed.

AUC-ROC and F1 score were used for evaluation of the performances of the KM, GM, and traditional categorization methods. The results indicated that depending on the employed drought index, the best categorization method was different. KM was selected as the best for SHADI and SMRI. Traditional categorization was selected as the best for most of the standardized drought indices including SPEI, SPI, SRI, SSMI, and SBFI. For HADI, the AUC-ROC and micro F1 score suggested that the traditional categorization was the best method, while the weighted and macro F1 score showed KM as the best one. In a multi-class classification, the

weighted average was preferred if there was a class imbalance (i.e., more occurrences of one class than that of other classes). Unlike other indices, the best results for SSPI were obtained when GM clustering was applied. Overall, KM and traditional categorization demonstrated a better performance than GM.

The CBS-SVR prediction models for different indices were set up based on the category-based scoring for tuning hyperparameters from the best categorization method and the results were compared with those from RMSE scoring. The CBS-SVR with R scoring outperformed the CBS-SVR with RMSE in most cases. The areal average of the AUC-ROC and F1 score suggested that R scoring was a better scoring method for tuning the hyperparameters in cross-validation of SVR if the target variables were multivariate and bivariate drought indices. Among the standardized univariate indices, SRI, SSMI, SSPI, and SSWEI showed different results and RMSE was better than R scoring. A grid-based analysis for SRI also confirmed that R was a better scoring method since it avoided overfitting and mis-categorization.

Finally, the results of CBS-SVR with the category-based scoring were compared with those of SVC. Except for SRI and SSPI, CBS-SVR performed better than SVC for all other drought indices. The results suggested using the proposed category-based scoring method for tuning hyperparameters in cross-validation of SVR successfully avoided overfitting and mis-categorization. Since this research focused on comparing the performances of the new category-based scoring method and the traditional standard performance measures in a numerical prediction model (i.e., SVR), a specific range of the hyperparameters was selected. Further analyses can be performed on other numerical prediction models with different ranges of the hyperparameters.

3.6. References

Barros, A. P., & Bowden, G. J. (2008). Toward long-lead operational forecasts of drought: An experimental study in the Murray-Darling River basin. Journal of Hydrology, 357, 349–367. https://doi.org/10.1016/j.jhydrol.2008.05.0

Barua, S., Ng, A. W. M., & Perera, B. J. C. (2012). Artificial neural network-based drought forecasting using a nonlinear aggregated drought index. Journal of Hydrologic Engineering, 17, 1408–1413. https://doi.org/10.1061/(ASCE)HE.1943-5584.0000574

Bazrkar, M. H., J. Zhang, and X. Chu. (2020). Hydroclimatic aggregate drought index (HADI): A new approach for identification and categorization of drought in cold climate regions. Stochastic Environmental Research and Risk Assessment, 34(11), 1847-1870, doi:10.1007/s00477-020-01870-5.

Bazrkar, M. H. and X. Chu. (2020). A new standardized baseflow index for identification of hydrologic drought in the Red River of the North Basin. Natural Hazards Review, 21(4), 05020011, 1-8, doi:10.1061/(ASCE)NH.1527-6996.0000414.

Belayneh, A., Adamowski, J., Khalil, B., & Ozga-Zielinski, B. (2014). Long-term SPI drought forecasting in the Awash River basin in Ethiopia using wavelet neural networks and wavelet support vector regression models. Journal of Hydrology, 508, 418–429. https://doi.org/10.1016/j.jhydrol.2013.10.052

Bergstra, J. and Bengio, Y. (2012). Random search for hyper-parameter optimization, The Journal of Machine Learning Research, 13, 281-305.

Cancelliere, A., Di Mauro, G., Bonaccorso, B., & Rossi, G. (2007). Drought forecasting using the standardized precipitation index. Water Resources Management, 21(5), 801–819. https://doi.org/10.1007/s11269-006-9062-y

Chu X, Lin Z, Tahmasebi Nasab M, Zeng L, Grimm K, Bazrkar MH, Wang N, Liu X, Zhang X, Zheng H. (2018). Macro-scale grid-based and subbasin-based hydrologic modeling: joint

simulation and cross-calibration. J Hydroinform 21(1):77–91. https://doi.org/10.2166/hydro.2018.026

Deo, R.C., O. Kisi, V. P. Singh. (2017). Drought forecasting in eastern Australia using multivariate adaptive regression spline, least square support vector machine and M5Tree model, Atmospheric Research, 184, 149-175, https://doi.org/10.1016/j.atmosres.2016.10.004.

Deo, R.C., Tiwari,M.K., Adamowski, J., Quilty, J. (2016a). Forecasting effective drought index using a wavelet extreme learning machine (W-ELM) model. Stoch. Env. Res. Risk A. http://dx.doi.org/10.1007/s00477-00016-01265-z.

Deo, R.C., Wen, X., Feng, Q. (2016b). A wavelet-coupled support vector machine model for forecasting global incident solar radiation using limited meteorological dataset. Appl. Energy 168, 568–593.

Durdu, Ö. F. (2010). Application of linear stochastic models for drought forecasting in the Büyük Menderes River basin, western Turkey. Stochastic Environmental Research and Risk Assessment, 24, 1145–1162. https://doi.org/10.1007/s00477-010-0366-3

Fawcett, T. (2001). Using rule sets to maximize ROC performance In Data Mining, 2001. Proceedings IEEE International Conference, pp. 131-138.

Fawcett, T. (2006). An introduction to ROC analysis. Pattern Recognition Letters, 27(8), pp. 861-874.

Feng, P., B. Wang, D. L. Liu, Q. Yu. (2019). Machine learning-based integration of remotely-sensed drought factors can improve the estimation of agricultural drought in South-Eastern Australia, Agricultural Systems, Volume 173, 303-316, https://doi.org/10.1016/j.agsy.2019.03.015.

Fernández, C., Vega, J. A., Fonturbel, T., & Jiménez, E. (2009). Streamflow drought time series forecasting: A case study in a small watershed in North West Spain. Stochastic

Environmental Research and Risk Assessment, 23, 1063–1070. https://doi.org/10.1007/s00477-008-0277-8

Ganguli, P., & Reddy, M. J. (2014). Ensemble prediction of regional droughts using climate inputs and the SVM–copula approach. Hydrological Processes, 28(19), 4989–5009. https://doi.org/10.1002/hyp.9966

Hao, Z., & Singh, V. P. (2016). Review of dependence modeling in hydrology and water resources. Progress in Physical Geography, 40(4), 549–578. https://doi.org/10.1177/0309133316632460

Hao, Z., Hao, F., Singh, V. P., Xia, Y., Ouyang, W., & Shen, X. (2016). A theoretical drought classification method for the multivariate drought index based on distribution properties of standardized drought indices. Advances in Water Resources, 92, 240–247. https://doi.org/10.1016/j.advwatres.2016.04.010

Hao, Z., Hao, F., Xia, Y., Singh, V. P., Hong, Y., Shen, X., & Ouyang, W. (2016). A statistical method for categorical drought prediction based on NLDAS-2. Journal of Applied Meteorology and Climatology, 55(4), 1049–1061. https://doi.org/10.1175/JAMC-D-15-0200.1

Hao, Z., Hong, Y., Xia, Y., Singh, V. P., Hao, F., & Cheng, H. (2016). Probabilistic drought characterization in the categorical form using ordinal regression. Journal of Hydrology, 535, 331–339. https://doi.org/10.1016/j.jhydrol.2016.01.074

Hao, Z., Singh, V. P., and Xia, Y. (2018). Seasonal Drought Prediction: Advances, Challenges, and Future Prospects. Reviews of Geophysics, 56(1), 108–141, doi: 10.1002/2016RG000549

Homdee, T., K. Pongput, S. Kanae. (2016). A comparative performance analysis of three standardized climatic drought indices in the Chi River basin, Thailand, Agriculture and Natural Resources 50, 211-219. http://dx.doi.org/10.1016/j.anres.2016.02.002.

Huning LS, AghaKouchak A. (2018). Mountain snowpack response to different levels of warming. Proc Natl Acad Sci U S A. 2018 Oct 23;115(43):10932-10937. doi: 10.1073/pnas.1805953115. Epub 2018 Oct 8. PMID: 30297423; PMCID: PMC6205460.

Hwang, Y., & Carbone, G. J. (2009). Ensemble forecasts of drought indices using a conditional residual resampling technique. Journal of Applied Meteorology and Climatology, 48, 1289–1301. https://doi.org/10.1175/2009JAMC2071.1

Joachims, T. (2002). Learning to Classify Text Using Support Vector Machines: Methods, Theory and Algorithms. books.google.com.

Joetzjer, E., Douville, H., Delire, C., Ciais, P., Decharme, B., Tyteca, S. (2013). Hydrologic benchmarking of meteorological drought indices at interannual to climate change timescales: a case study over the Amazon and Mississippi river basins. Hydrol. Earth Syst. Sci. 17, 4885e4895.

Kisi, O., Cimen, M. (2011). A wavelet-support vector machine conjunction model for monthly streamflow forecasting. Journal of Hydrology 399, 132–140.

Kohavi R, Provost F (1998) Glossary of terms. Mach Learn 30:271–274

Larochelle H., D. Erhan, A. Courville, J. Bergstra, and Y. Bengio. (2007). An empirical evaluation of deep architectures on problems with many factors of variation. In Z. Ghahramani, editor, Proceedings of the Twenty-fourth International Conference on Machine Learning (ICML'07), 473–480. ACM.

Liu, W., & Juárez, R. N. (2001). ENSO drought onset prediction in northeast Brazil using NDVI. International Journal of Remote Sensing, 22(17), 3483–3501. https://doi.org/10.1080/014311600100064

Liu, Y., & Hwang, Y. (2015). Improving drought predictability in Arkansas using the ensemble PDSI forecast technique. Stochastic Environmental Research and Risk Assessment, 29(1), 79–91. https://doi.org/10.1007/s00477-014-0930-3

Lohani, V. K., & Loganathan, G. (1997). An early warning system for drought management using the Palmer drought index. Journal of the American Water Resources Association, 33(6), 1375–1386. https://doi.org/10.1111/j.1752-1688.1997.tb03560.x

Lloyd-Hughes, B. (2014). "The impractically of a universal drought definition." Theoretical Applied Climatology, 117, 607-611.

Madadgar, S., & Moradkhani, H. (2013). A Bayesian framework for probabilistic seasonal drought forecasting. Journal of Hydrometeorology, 14(6), 1685–1705. https://doi.org/10.1175/JHM-D-13-010.1

McKee, T. B., Doesken, N. J., & Kleist, J. (1993). The relationship of drought frequency and duration to time scales. Paper presented at Eighth Conference on Applied Climatology, American Meteorological Society, Anaheim, CA.

Mishra, A. K., & Singh, V. P. (2010). A review of drought concepts. Journal of Hydrology, 391, 202–216. https://doi.org/10.1016/j.jhydrol.2010.07.012

Mishra, A., & Desai, V. (2005). Drought forecasting using stochastic models. Stochastic Environmental Research and Risk Assessment, 19, 326–339. https://doi.org/10.1007/s00477-005-0238-4

Mishra, A., & Desai, V. (2006). Drought forecasting using feed-forward recursive neural network. Ecological Modelling, 198, 127–138. https://doi.org/10.1016/j.ecolmodel.2006.04.017

Mishra, A., Desai, V., & Singh, V. P. (2007). Drought forecasting using a hybrid stochastic and neural network model. Journal of Hydrologic Engineering, 12, 626–638. https://doi.org/10.1061/(ASCE)1084-0699(2007)12:6(626)

Mitchell et al (2004). The multi-institution North American Land Data Assimilation System (NLDAS): Utilizing multiple GCIP products and partners in a continental distributed hydrological modeling system, J. Geophys. Res., 109, D07S90, doi: 10.1029/2003JD003823

Mo, K. C., and W. M. Thiaw. (2002). Ensemble canonical correlation prediction of precipitation over the Sahel, Geophysics Research Letter, 29(12), doi: 10.1029/2002GL015075.

Modarres, R. (2007). Streamflow drought time series forecasting. Stochastic Environmental Research and Risk Assessment, 21, 223–233. https://doi.org/10.1007/s00477-006-0058-1

Morid, S., Smakhtin, V., & Bagherzadeh, K. (2007). Drought forecasting using artificial neural networks and time series of drought indices. International Journal of Climatology, 27, 2103–2111. https://doi.org/10.1002/joc.1498

National Center for Atmospheric Research Staff (Eds). Last modified 10 Dec 2019. "The Climate Data Guide: NLDAS: North American Land Data Assimilation System." Retrieved from https://climatedataguide.ucar.edu/climate-data/nldas-north-american-land-data-assimilation-system.

NCEI (2019) <https://www.ncdc.noaa.gov/news/drought-monitoring-economic-environmental-and-social-impacts> (November 25, 2019).

NCEI: National center for Environmental Information, Retrieved from <https://www.ncdc.noaa.gov/news/drought-degrees-drought-reveal-true-picture>

NOAA National Centers for Environmental information (NCEI), Climate at a Glance: Divisional Mapping, published April 2021, retrieved on April 30, 2021 from https://www.ncdc.noaa.gov/cag/

Panu, U., & Sharma, T. (2002). Challenges in drought research: Some perspectives and future directions. Hydrological Sciences Journal, 47, S19–S30. https://doi.org/10.1080/02626660209493019

Paulo, A. A., & Pereira, L. S. (2007). Prediction of SPI drought class transitions using Markov chains. Water Resources Management, 21,1813–1827. https://doi.org/10.1007/s11269-006-9129-9

Paulo, A. A., & Pereira, L. S. (2008). Stochastic prediction of drought class transitions. Water Resources Management, 22, 1277–1296. https://doi.org/10.1007/s11269-007-9225-5

Provost, F., P. Domingos, (2000). Well-trained PETs: Improving probability estimation trees (Section 6.2), CeDER Working Paper #IS-00-04, Stern School of Business, New York University.

Rao, A. R., & Padmanabhan, G. (1984). Analysis and modeling of Palmer's drought index series. Journal of Hydrology, 68(1-4), 211–229. https:// doi.org/10.1016/0022-1694(84)90212-9

Regonda, S. K., Rajagopalan, B., & Clark, M. (2006). A new method to produce categorical streamflow forecasts. Water Resources Research, 42, W09501.

Santos, J. F., Portela, M. M., & Pulido-Calvo, I. (2014). Spring drought prediction based on winter NAO and global SST in Portugal. Hydrological Processes, 28(3), 1009–1024. https://doi.org/10.1002/hyp.9641

Sharma, T. C., & Panu, U. S. (2012). Prediction of hydrological drought durations based on Markov chains: Case of the Canadian prairies. Hydrological Sciences Journal, 57, 705–722. https://doi.org/10.1080/02626667.2012.672741

Shukla S, Wood AW. (2008). Use of a standardized runoff index for characterizing hydrologic drought. Geophys Res Lett 35(2):1–7. https://doi.org/10.1029/2007GL032487

Schölkopf, B. and A. J. Smola, (2002). Learning with Kernels: Support Vector Machines, Regularization, Optimization, and Beyond.

Smola, A.J., Schölkopf, B. (2004). A tutorial on support vector regression. Statistics and Computing 14, 199–222. https://doi.org/10.1023/B:STCO.0000035301.49549.88

Staudinger M, Stahl K, Seibert J. (2014). A drought index accounting for snow. Water Resour Res 50(10):7861–7872. https://doi.org/10.1002/2013WR015143

Stehman, S. V. (1997). Selecting and interpreting measures of thematic classification accuracy. Remote Sensing of Environment. 62 (1): 77–89. doi:10.1016/S0034-4257(97)00083-7

Sun, M., Ph, D., and Kim, G. (2016). Quantitative Monthly Precipitation Forecasting Using Cyclostationary Empirical Orthogonal Function and Canonical Correlation Analysis. Journal of Hydrologic Engineering, 21(1), 1–13.

Svoboda, M., LeComte, D., Hayes, M., Heim, R., Gleason, K., Angel, J., … Stooksbury, D. (2002). The drought monitor. Bulletin of the American Meteorological Society, 83(8), 1181–1190.

Ting K.M. (2011). Precision and Recall. In: Sammut C., Webb G.I. (eds) Encyclopedia of Machine Learning. Springer, Boston, MA. https://doi.org/10.1007/978-0-387-30164-8_652

Vapnik V. (1995). The Nature of Statistical Learning Theory. Springer, New York.

Vicente-Serrano Sergio M, Juan SB, López-Moreno I. (2010). A multiscalar drought index sensitive to global warming, the standardized precipitation evapotranspiration index. J Clim 23:1696–1718. https://doi.org/10.1175/2009JCLI2

Wang H., Zheng H. (2013). True Positive Rate. In: Dubitzky W., Wolkenhauer O., Cho KH., Yokota H. (eds) Encyclopedia of Systems Biology. Springer, New York, NY. https://doi.org/10.1007/978-1-4419-9863-7_255

Xia et al (2012). Continental-scale water and energy flux analysis and validation for the North American Land Data Assimilation System project phase 2 (NLDAS-2): 1. Intercomparison and application of model products, J. Geophys. Res., 117, D03109, 10.1029

Xu Y, Wang L, Ross KW, Liu C, Berry K. (2018). Standardized soil moisture index for drought monitoring based on soil moisture active passive observations and 36 years of North American Land Data Assimilation System data: a case study in the Southeast United States. Remote Sens. https://doi.org/10.3390/rs10020301

Yang, T., Zhou, X., Yu, Z., Krysanova, V., & Wang, B. (2015). Drought projection based on a hybrid drought index using artificial neural networks. Hydrological Processes, 29(11), 2635–2648. https://doi.org/10.1002/hyp.10394

Zhang E. and Zhang Y. (2009). F-Measure. In: LIU L., ÖZSU M.T. (eds) Encyclopedia of Database Systems. Springer, Boston, MA. https://doi.org/10.1007/978-0-387-39940-9_483

4. ENSEMBLE STATIONARY-BASED SUPPORT VECTOR REGRESSION FOR DROUGHT PREDICTION UNDER CHANGING CLIMATE[1]

4.1. Abstract

Non-stationarity due to climate change and/or variability can lower the predictive capabilities of drought prediction models. The objective of this study is to improve drought prediction by removing non-stationarity from temperature time series, a key factor in development and propagation of droughts in a changing climate. In order to relax the assumption of stationarity, an ensemble stationary-based support vector regression (ESSVR) method was developed and compared with the traditional support vector regression (SVR). Three types of drought indices in three time scales (monthly, seasonal, and semiannual) including multivariate, bivariate standardized drought indices, and univariate standardized drought indices were used as the target variables. In an application to the Red River of the North Basin (RRB), the North American Land Data Assimilation System (NLDAS) data in 1979-2016 were used for the training and testing of the prediction model. The Pearson correlation, root mean square error (RMSE), and Taylor diagram were used to evaluate the performances of the ESSVR. Remarkably, the distribution of identified change points varied by climate divisions. The results of the SVR and ESSVR in the RRB were compared, demonstrating the better performances of the ESSVR for most of the drought indices, particularly those with higher sensitivity to temperature. It was found that the extreme (high and low) values of epsilon and gamma mostly assigned by SVR caused a higher risk of overfitting for SVR. In contrast, ESSVR improved the drought prediction by removing the non-stationarity, thus providing more accurate drought predictions, especially for a warming climate.

---

[1] The material in this chapter was co-authored by Mohammad Hadi Bazrkar and Dr. Xuefeng Chu. Mohammad Hadi Bazrkar had primary responsibility for developing the new drought prediction model and drought analyses. Mohammad Hadi Bazrkar was the primary developer of the conclusions that are advanced here. Mohammad Hadi Bazrkar also drafted and revised all versions of this chapter. Dr. Xuefeng Chu served as proofreader and checked analysis conducted by Mohammad Hadi Bazrkar.

4.2. Introduction

Drought prediction is crucial not only for water resource management but also for conservation of other natural resources. Despite a large amount of literature on drought prediction, there are still fundamental limitations in drought prediction models (Wood et al. 2015). For example, the existing drought prediction methodologies lack predictive skills to predict the 2012 drought in the upper Great Plains, U.S. (Hoerling et al. 2014). Drought prediction models are generally divided into two main categories: (1) dynamical models and (2) statistical or data-driven models. The latter has the advantages of minimum data requirement and rapid development (Adamowski et al. 2008).

Various statistical methods can be employed to predict droughts. For example, Times series analysis (Durdu, 2010; Fernández et al. 2009; Mishra and Desai 2005; Modarres 2007; Rao and Padmanabhan 1984) and linear regression (Barros and Bowden 2008; Liu and Juarez 2001; Panu and Sharma 2002; Sun et al. 2012) are less applicable due to the consideration of the linear relationships between predictor(s) and predictand(s). To remove this limitation, nonlinear regression (Hwang and Carbone, 2009; Liu and Hwang, 2015) and logistic regression (Meng et al. 2017; Hao, Hao, Xia, et al., 2016; Regonda et al. 2006) have been applied. In addition, various machine learning or soft computing methods, such as artificial neural network (ANN) (Barua et al. 2012; Mishra and Desai 2006; Mishra et al. 2007; Morid et al. 2007; Santos et al. 2012; Yang et al. 2014), fuzzy logic (FL), and adaptive neuro-fuzzy inference system (ANFIS) (Ali et al. 2018; Esfahanian et al. 2016), have been used for drought prediction. To overcome the overfitting problem in the ANN method, Vapnik (1995) developed the support vector machine (SVM). Using SVM in studies by Ganguli and Reddy (2014) and Yu et al. (2006) reduced the expected error of learning models. SVM is divided into two types: support vector classification (SVC) and support vector regression (SVR). Wavelet transformation is also among the popular methods for drought prediction (Maity et al. 2016; Ozger et al. 2011). Furthermore, various hybrid methods have also been developed and employed to improve drought prediction.

They include wavelet-ANN (Deo et al. 2016; Kim and Valdes 2003), ARIMA-ANN (Mishra et al. 2007), ANN-FL (Bacanli et al. 2009), and hybrid SVM models including wavelet-SVR (Belayneh et al. 2014) and genetic algorithm and SVM (GA-SVM) (Li et al. 2010).

Some other statistical models also showed the capability in drought prediction. For example, Markov chain was employed to predict droughts using drought categories (Lohani and Loganathan 1997; Cancelliere et al. 2007; Paulo and Periera 2007; 2008; Sharma and Panu 2012). Unlike the categorical models such as Markov chain, conditional probability was used the conditional distribution of a drought indicator given multiple hydroclimatic variables. To express these multivariate variables, parametric distribution, copula models (e.g., Madadgar and Moradkhani 2013), entropy models, and nonparametric models were used (Hao and Singh 2016). The common limitation for these prediction models is that the joint distribution is hard to be obtained when a large number of variables are involved.

The ensemble techniques have been frequently used to improve prediction skills. For example, a two-phase extreme learning machine integrated with complete ensemble empirical mode decomposition with adaptive noise (CEEMDAN) was used for multi-scale runoff prediction (Wen et al. 2019). Wavelet support vector machine (WSVM) and wavelet random forest (WRF) were effective tools in the bias correction of precipitation forecasts (Xu et al. 2019). Ensemble-ANFIS (Ali et al. 2018) with ten-fold cross validation also provided better results for drought prediction after using the ensemble techniques.

Climate change has accelerated the hydrological processes, which led to severer droughts (Mukherjee et al. 2018). Natural or anthropogenic changes in climatic, hydrologic, and/or landscape processes cause non-stationary conditions in time series of hydroclimatic variables (Ryberg et al. 2019). Non-stationary time series and change points can cause violation of critical assumptions in flood/drought frequency analysis. Change points can be defined as the points in a time series where the statistical properties change (Killick et al. 2012). In frequency analysis, it is assumed that observations are independent and identically follow a particular statistical

distribution, such as the log Pearson type III distribution (England et al. 2018). Non-stationary climate information, and anthropogenic forcing can be additional challenges for a reliable drought assessment under climate change (Mukherjee et al. 2018). For instance, due to the non-stationary nature of climatic variables under future climate scenarios, the probability distribution parameters of target hydroclimatic variables will change over time. Therefore, it is important to consider non-stationarity by changing the probability distribution parameters over different time scales to improve drought assessment under climate change (Mukherjee et al. 2018). The performances of drought prediction models may not be satisfactory unless the changes in climate are captured from historical records (Hao et al. 2018, Brunner et al. 2021). Change point detection techniques can be used for drought analysis to fill this gap.

There are some studies available in investigating the impacts of non-stationarity in SVR in other fields. For example, a dynamic support vector machines (DSVMs) was proposed to model non-stationary time series (Cao et al. 2002). To deal with the structural changes in the data, the DSVMs used an exponentially increasing regularization constant and an exponentially decreasing tube size, instead of fixed values of the regularization constant and the tube size for all training data points. Fan and Tang (2013) decomposed the non-stationary time series with monotonic trend items into a finite and often small number of intrinsic mode functions and a monotone residual trend item by the Empirical Mode Decomposition (EMD) and then applied the SVR on each subset of data and finally integrated the results. Grinblat et al. (2014) introduced a time-adaptive support vector regression (TA-SVR) to improve prediction. A novel regressor as twin SVR was proposed by Peng (2010). Three different methods of transformation namely relative difference in percentages, Z-score, and natural logarithm transformations were applied to the data series (Ojemakinde 2006). In these studies, better results were obtained after accounting for the non-stationarity in time series.

Change point analysis is an active area in statistics and an area of great interest in hydrology (Ryberg et al. 2019). Tavakol et al. (2020) employed the Mann-Kendall and Pettitt

tests to identify change points and nonstationary conditions of temperature indices for the Missouri River basin. Ryberg et al. (2019) conducted a study to detect change points of annual peak streamflow in the United States. Huang et al. (2016) employed the heuristic segmentation method (Pedro et al. (2001) to detect the changing points of annual streamflow time series from 1960 to 2012 in the Columbia River basin. Duggins et al. (2010) developed a new method based on the empirical transition matrix generated by the standardized precipitation index (SPI) for identification of change point(s) in the SPI time series. Mazdiyansi and Aghakouchak (2015) employed the Cramer-von Mises change point detection method and found a significant shift in the distributions of droughts across the contiguous U.S.

To the best of our knowledge, few drought studies have been conducted to use the change point analysis for drought prediction. The objective of this research is to improve the prediction of droughts in a changing climate to overcome the non-stationarity in time series by developing a new ensemble stationary-based support vector regression (ESSVR) method. Correspondingly, a new drought identification, categorization, and prediction (DIC-Predict) system is developed for drought analyses. To highlight the importance of snow drought in the warming climate, DIC-Predict is tested in a cold climate region, in which snow, snowmelt, and snow accumulation are critical in drought identification especially in a warming climate.

4.3. Methodology

4.3.1. ESSVR Model

Figure 4.1 shows the flowchart for the ESSVR method. To overcome the nonstationary time series, a fast-approximate window-based change point detection method, window sliding (Truong et al. 2020) was used to split nonstationary time series into multiple stationary time series. SVR is further conducted on each stationary subsets of training data. An initial weight is assigned to the predicted values by SVR on each subset of data and it is updated by comparison

with the actual values and higher weights assigned to those with higher accuracy. Finally, the prediction with the higher weight is selected as the final prediction.

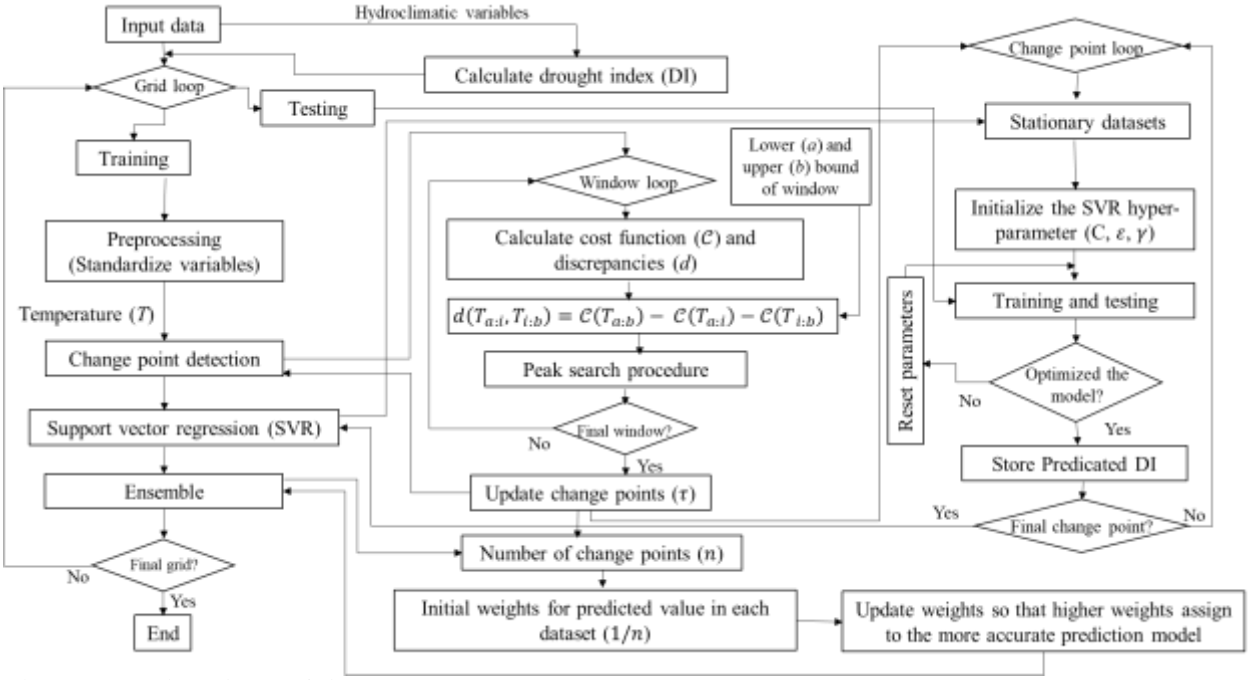

Figure 4.1. Flowchart of the ESSVR

For a temperature time series of $T_{1,j}, T_{2,j},\ldots, T_{m,j}$, if the regime switches at month τ for grid j (change point) then $T_{1,j},\ldots, T_{\tau,j}$ differ from $T_{\tau+1,j},\ldots, T_{m,j}$ in some statistical properties. For example, the means differ in series split by change points in the set of possible vectors of changepoints (i.e. $\mathcal{T}_s = \{\tau: 0 = \tau_0 < \tau_1 < \cdots \tau_m < \tau_{m+1} = s\}$).

$$T_{i,j} = \begin{cases} \mu_{j,1}^{T} & if \quad 1 \le i \le \tau_1 \\ \mu_{j,2}^{T} & if \quad \tau_1 \le i \le \tau_2 \\ \vdots & \\ \mu_{j,m}^{T} & if \quad \tau_k \le i \le \tau_m \end{cases} \tag{4.1}$$

To identify multiple change points in the temperature time series in the window-sliding algorithm, the discrepancies (d) between two adjacent windows that slide along the dataset are computed. For a given cost function C, the discrepancy between two subsets is given by (Truong et al. 2020):

$$d(T_{a:i}, T_{i:b}) = C(T_{a:b}) - C(T_{a:i}) - C(T_{i:b}) \tag{4.2}$$

where $\mathcal{C}$ is a cost (loss or error) function for a given segment; a and b is the lower and upper bounds of the sliding window. Once the computation of all discrepancies for all windows is completed, a peak search procedure is performed to find the major change points (Truong et al. 2020).

Figure 4.2 shows the SVR model (a) with and (b) without assumption of stationarity. The changing tube size, instead of a fixed tube size in all the training data points is crucial to relax the assumption of stationarity in a prediction model. The change point detection is used to identify where the changes in the tube size and the corresponding hyperparameters in the SVR should be considered.

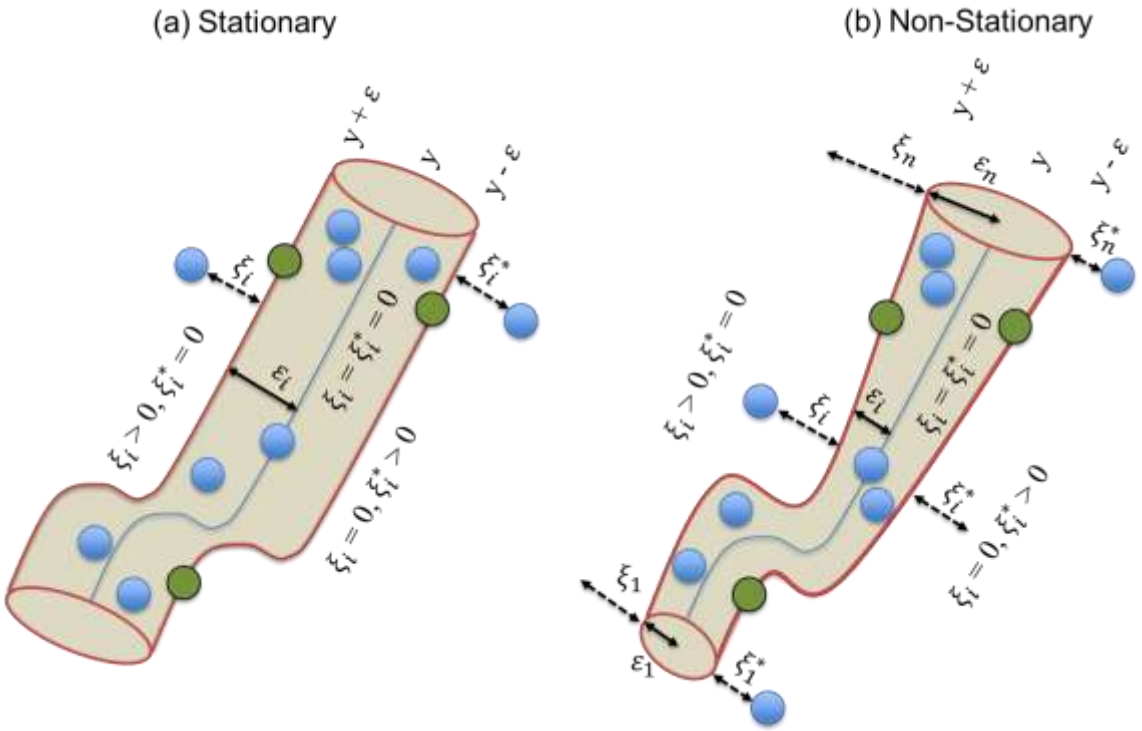

Figure 4.2. (a) Stationary SVR vs. (b) non-stationary SVR

Assume that l change points are detected in the temperature time series. Then, the dataset is divided into l time series and SVR is performed on each time series. By removing the impacts of change points, each time series is turned to l stationary time series. The SVR is a general regression model based on the relationship between predictor(s) ($X_{i,j}^{l}$) and predictand

(i.e., drought indices) ($DI_{i,j}^{l}$). $f\left(X_{i,j}^{l}\right)$, a nonlinear function, is estimated as $\hat{f}\left(X_{i,j}^{l}\right)$ by sum of a set of kernel functions. The purpose of using the kernel function is to transform the space from nonlinear to linear for input vector $X_{i,j}^{l}$.

$$DI_{i,j}^{l} = f\left(X_{i,j}^{l}\right) + e_{j}^{l} \tag{4.3}$$

where e_{j}^{l} is the error; and $\hat{f}\left(X_{i,j}^{l}\right)$ is estimated by (Vapnik 1995):

$$\hat{f}\left(X_{i,j}^{l}\right) = \langle w_{j}^{l}, X_{i,j}^{l} \rangle + b_{j}^{l} \tag{4.4}$$

where w_{j}^{l} indicates the support vector weights (basis functions); and b_{j}^{l} is a bias term (similar to the intercept in linear regression) for each stationary time series in each grid. The Angle brackets represent a dot product. The following regularized risk function needs to minimize the complexity (i.e. the magnitude of w_{j}^{l}) to estimate $\hat{f}\left(X_{i,j}^{l}\right)$ during the training (Vapnik 1995).

$$Min\left[\frac{1}{2}\left\|w_{j}^{l}\right\|^{2} + C_{j}^{l}\sum_{i=1}^{n}(\xi_{i,j}^{l} + \xi_{i,j}^{l\,*})\right] \tag{4.5}$$

Based on the ε-insensetive approach, the regularized risk function is subject to (Vapnik 1995):

$$\hat{f}\left(X_{i,j}^{l}\right) - \langle w_{j}^{l}, X_{i,j}^{l} \rangle - b_{j}^{l} \leq \varepsilon_{j}^{l} + \xi_{i,j}^{l} \tag{4.6}$$

$$\langle w_{j}^{l}, X_{i,j}^{l} \rangle + b - \hat{f}\left(X_{i,j}^{l}\right) \leq \varepsilon_{j}^{l} + \xi_{i,j}^{l\,*} \tag{4.7}$$

$$\xi_{i,j}^{l}, \xi_{i,j}^{l\,*} \geq 0 \tag{4.8}$$

where $\xi_{i,j}^{l}$ and $\xi_{i,j}^{l\,*}$ are the slack variables used to determine the degree, to which the state space samples with an error more than ε_{j}^{l} are penalized. In construction of the predictor $\hat{f}\left(X_{i,j}^{l}\right)$, errors will be tolerated to the degree of ε_{j}^{l}. This optimization problem is solved by Lagrange multipliers using scikit-learn package (Pedregosa et al. 2011).

4.3.2. Tuning Hyperparameters in Cross Validation of SVR

The hyperparameters in an SVR model play a key role in the performance of a prediction model. Therefore, the spatial distributions of C, epsilon (ε), and gamma (G) are compared in SVR and ESSVR. C, ε, and G values affect the model complexity in different ways.

Parameter C determines the tradeoff between the model complexity (flatness) and the training error (Joachims 2002), which is the degree to which deviations larger than ε are tolerated in the optimization formulation. For example, if C is too large (infinity), the objective is to minimize the empirical risk only, without considering the model complexity in the optimization formulation. A small value of C increases the training errors, while a large C leads to a behavior similar to that of a hard-margin SVM (Joachims 2002). The margin is defined as the minimum distance from the decision boundary to the training points and a hard-margin SVM makes the SVM overly sensitive to any noise in the data.

Parameter ε controls the width of the ε -insensitive zone, used to fit the training data. The value of ε has an effect on the smoothness of the SVR's response and can affect the support vectors used to construct the regression function. The bigger ε is, the fewer support vectors are selected. On the other hand, bigger ε values result in more 'flat' estimates. If ε is greater than the range of the target values, a good result cannot be obtained (Schölkopf and Smola 2002). If ε is equal to zero, overfitting occurs. The optimal value of ε scales linearly with G (variance of the Gaussian noise) (Schölkopf and Smola 2002). G is a Kernel parameter that reduces the model space and controls the complexity of the solution (Kisi and Cimen 2011).

Cherkassky and Mulier (1998) suggested the use of cross-validation for the SVM parameter choice. A gird search cross-validation approach was used for selection of the best hyperparameters in each stationary dataset. Figure 4.3 shows the cross-validation in the traditional SVR and ESSVR. The hyperparameters are tuned by splitting the training data into several stationary subsets and the cross-validation is performed on each subset. For each subset,

the drought index is predicted for the same testing period. The prediction that is closer to the actual values (based on RMSE) is selected as the final prediction.

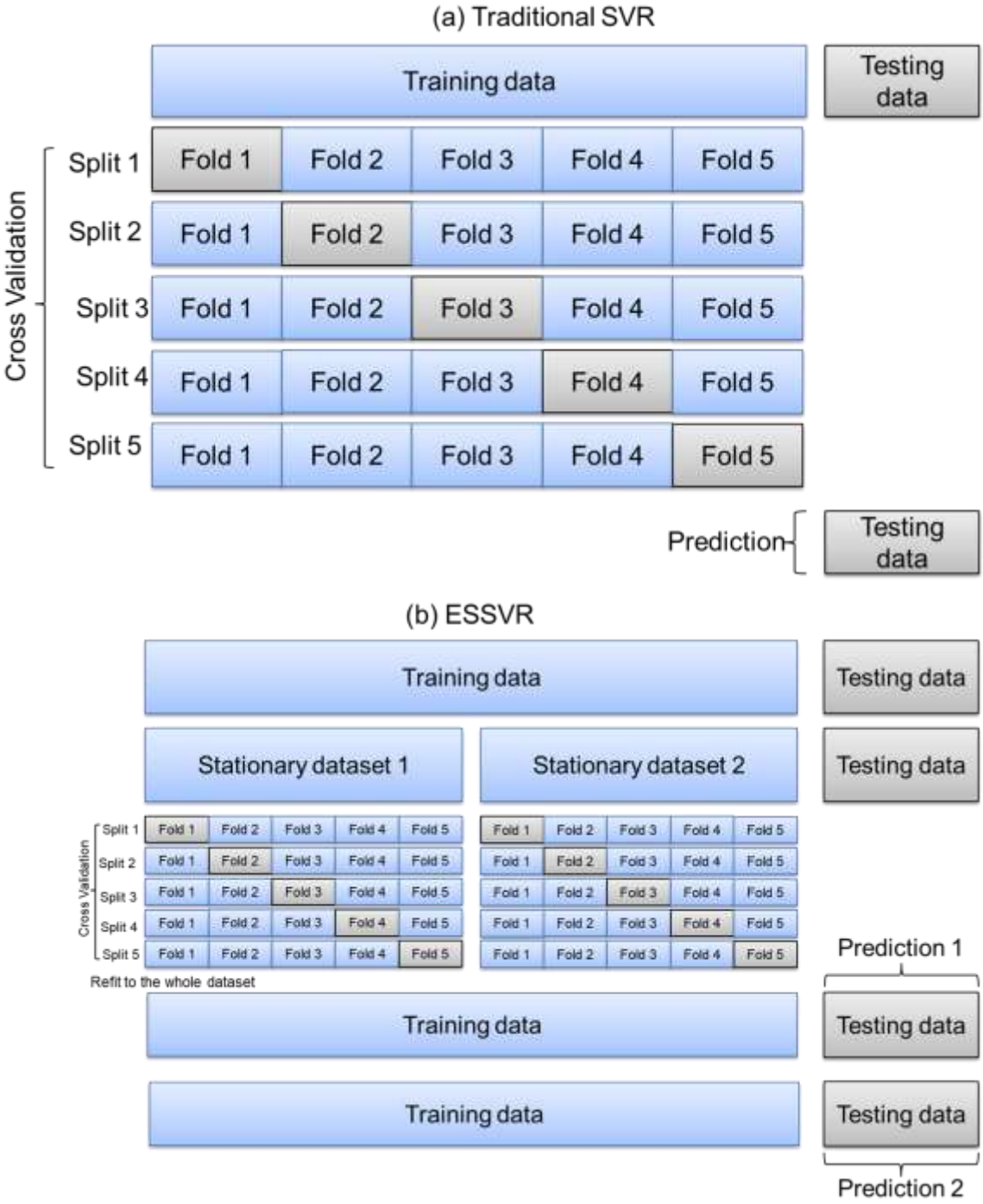

Figure 4.3. Cross-validation in (a) traditional SVR and (b) ESSVR

An ensemble technique is developed and employed on the outputs of ESSVR on stationary subsets of data ($DI_{i,j}^{l}$). The concept of this selective ensemble is based on the fact that due to the variability or change in climate, each subset of training data with different statistical properties identified and split by the change point techniques can potentially have different prediction results for a specific period. The predicted values which are closer to the actual values are selected as the final prediction result. The following algorithm is used for this selective ensemble technique on the results of the SVR on each subset:

for $l = 1,2, \dots, L$,

(1A) initialize $w_1 = w_2 = \cdots = w_L = \frac{1}{l}$.

(1B) draw a stationary subset S_l from the training data.

for time step $i = 1,2, \dots, n$,

(2A) train regressor $\hat{f}_l$ on S_l.

(2B) estimate the risk of $\hat{f}_l$ according to the probability of discrepancy between the predicted and actual values $\{p_1, p_2, \dots, p_n\}$,

$$\hat{R}_l = \sum_{i=1}^{n} p_i \left[DI_i \neq \hat{f}_l(X_i) \right] \tag{4.9}$$

(2C) update $w_l = w_l \frac{1}{1+\hat{R}_l}$.

Select the prediction with the highest weight, which has the lowest risk.

4.3.3. Assessment of ESSVR

Root mean square error (RMSE) and coefficient of determination (R^2) are used to compare the overall (areal average) performances of ESSVR and the traditional SVR (hereafter SVR). Then, a Taylor diagram (Taylor 2001) for the grid with the largest difference between RMSE values in ESSVR and SVR is created to compare the performance of these two models.

There is a challenge in selecting the best performance measures. The Taylor diagram, commonly used in climate and environment studies, facilitates the comparative assessment of

different models. It is used to quantify the degree of correspondence and correlation between the predicted and actual values in terms of three performance measures: the Pearson correlation coefficient, the root-mean-square error (RMSE), and the standard deviation. The azimuthal angle depicts the Pearson correlation coefficient. The centered RMSE in the predicted values is proportional to the distance from the actual values on the x-axis. The standard deviation of the predicted pattern is proportional to the radial distance from the origin.

4.3.4. Setup of ESSVR Model

To address different types of drought, three types of drought indices in different time scales (monthly, seasonal, and semiannual) are used to set up the ESSVR model. The target variables consist of multivariate hydroclimatic aggregate drought index (HADI) (Bazrkar et al. 2020) and snow-based hydroclimatic aggregate drought index (SHADI) (Bazrkar and Chu 2021), bivariate standardized drought indices based on the difference between precipitation and actual evapotranspiration (SPEI) and the summation of snowmelt and rainfall, and univariate standardized drought indices based on precipitation, surface runoff, baseflow, soil moisture, snowpack, and snow water equivalent. Depending on the specific drought index that is used as the target variable in the prediction model, different types of predictor(s) are used. Table 4.1 shows the predictands and their associated predictors. Precipitation (P) is used as a predictor for prediction of all drought indices. Temperature (T) is also used for prediction of SPEI, SMRI, SSPI, and SSWEI. In addition, actual evapotranspiration (ET) and the difference between precipitation and evapotranspiration (DFCT) are added in the prediction of HADI, SHADI, SSI, SRI, and SBFI.

Table 4.1. Predictands and predictors

Predictands	Reference	Type	Input	Method of calculation	Predictors
Hydroclimatic Aggregate Drought Index (HADI)	Bazrkar et al. (2020)	Multivariate	RF, SM, R, SWS	PCA	P, T, ET, DFCT
Snow-based Hydroclimatic Aggregate Drought Index (SHADI)	Bazrkar and Chu (2021)	Multivariate	P, SP, R, SWS	PCA	P, T, ET, DFCT
Standardized Soil Moisture Index (SSI)	Xu et al. (2018)	Univariate	SWS	Standardized	P, T, ET, DFCT
Standardized Runoff Index (SRI)	Shukla and Wood (2008)	Univariate	R	Standardized	P, T, ET, DFCT
Standardized Baseflow Index (SBFI)	Bazrkar et al. (2020)	Univariate	BF	Standardized	P, T, ET, DFCT
Standardized Precipitation Evapotranspiration Index (SPEI)	Vicente-Serrano et al. (2010)	Bivariate	P, ET	Standardized	P, T
Standardized Melt Rainfall Index (SMRI)	Staudinger et al. (2003)	Bivariate	SM, RF	Standardized	P, T
Standardized Snowpack Index (SSPI)	In this study	Univariate	SP	Standardized	P, T
Standardized Snow Water Equivalent Index (SSWEI)	Huning and Aghakouchak (2018)	Univariate	SWE	Standardized	P, T
Standardized Precipitation Index (SPI)	McKee (1993)	Univariate	P	Standardized	P

Notes: P: Precipitation, T: Temperature, ET: Evapotranspiration, RF: Rainfall, SM: Snowmelt, R: Runoff, SWS: Soil moisture, SP: Snowpack, BF: Baseflow, SWE: Snow water equivalent, DFCT: difference between precipitation and evapotranspiration, PCA: Principal component analysis

The training and testing periods range from 1979 to 2010 and from 2011 to 2016, respectively. The input data are obtained from the North American Land Data Assimilation System (NLDAS) (Mitchell et al., 2004; Xia et al., 2012). The goal of the NLDAS is to construct

quality-controlled, and spatially and temporally consistent land-surface model (LSM) datasets from the best available observations and model output to support modeling activities. The NLDAS products are used in modeling, research, and applications, such as drought and flood monitoring, watershed and water quality management, and case studies of extreme events. There are two phases referred to as NLDAS-1 and NLDAS-2. The latter, which spans January 1979-present, is used in this study. NLDAS integrates a large quantity of observation based and model reanalyzed data at 1/8th-degree grid spacing over Central North America (Mitchell et al., 2004; Xia et al., 2012).

4.3.5. Study Area

The Red River of the North Basin (RRB) (Figure 4.4), a typical cold climate region in the Northern Great Plain, covers over 90,000 km2 in the U.S. part of RRB. According to the NOAA (2021) data, the west part of the RRB is drier than the east part and the north part is colder than the south part. The 100-year mean dataset (Figure 4.4) shows that the order of CDs from the driest to the wettest is as follows: 3202, 3205, 3203, 3206, 3209, 3903, 2101, 2104, and 2102. The same dataset also indicates the order of CDs from the coldest to the warmest: 2101, 3203, 3202, 2101, 3205, 3206, 3209, 2104, and 3903. Drought has significant impacts on the RRB since a great portion of the RRB is covered by cultivated croplands. A variety of drought indices were used to test the ESSVR in the RRB in this study.

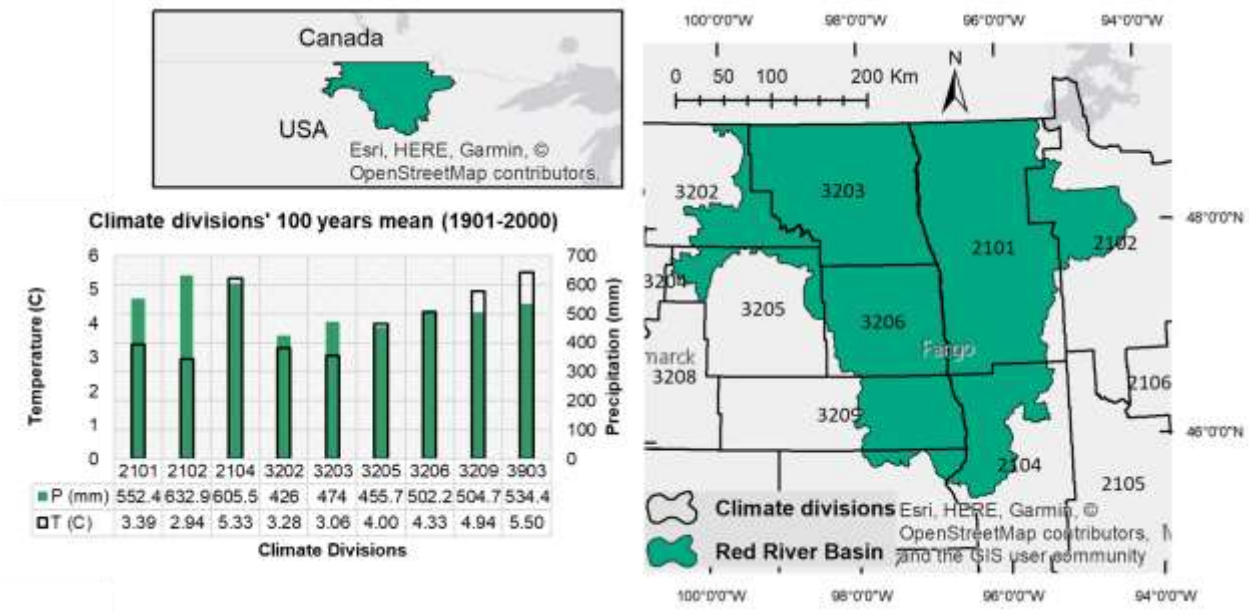

Figure 4.4. Red River of the North Basin, its associated climate divisions and 100-year mean temperature and precipitation for different climate divisions (NOAA 2021)

4.4. Results and Discussions

The spatial patterns of the first and the second identified change points on the monthly temperature time series are shown in Figure 4.5. The numbers in the legend refer to time steps starting from January 1979. 45, 160, 195, 220, 255, 260, 275, and 300 are related to September 1982, April 1992, March 1995, April 1997, March 2000, August 2000, November 2001, and December 2003, respectively. The first change point was identified in August 2000 for a great portion of the area (45%) in CDs 3206 and 3209, and CD 2101 in the southern part. In 28% of the RRB (mostly in northeast of CD 2101 and a part of CD 2102), the first change points were identified in April 1997. Grid 261, highlighted in Figure 4.5, was one of these grids. The temperature time series and the identified change points are shown in Figure 4.5. The second change point for this grid was identified in November 2001, when 65% of the RRB (CDs 3206, 3209, 3903, 2104, 2101, and 2102) had the same second change point. August 2000 was identified as the second change points in 23% of the RRB (CD 3203). The average values of monthly temperature through the entire training period, the period from January 1979 to the first change point, and the period between the first and the second change points were 4.48,

3.80, and 6.54, respectively. There also were slight changes in the standard deviation values. 12.63, 12.86, and 11.64 were the standard deviations of the entire training period, the period from January 1979 to the first change point, and the period between the first and the second change points. These changes in the statistical properties of the temperature time series confirmed the accuracy of the identified change points, and accentuated the importance of considering change points and non-stationarity for prediction of droughts in a warming climate.

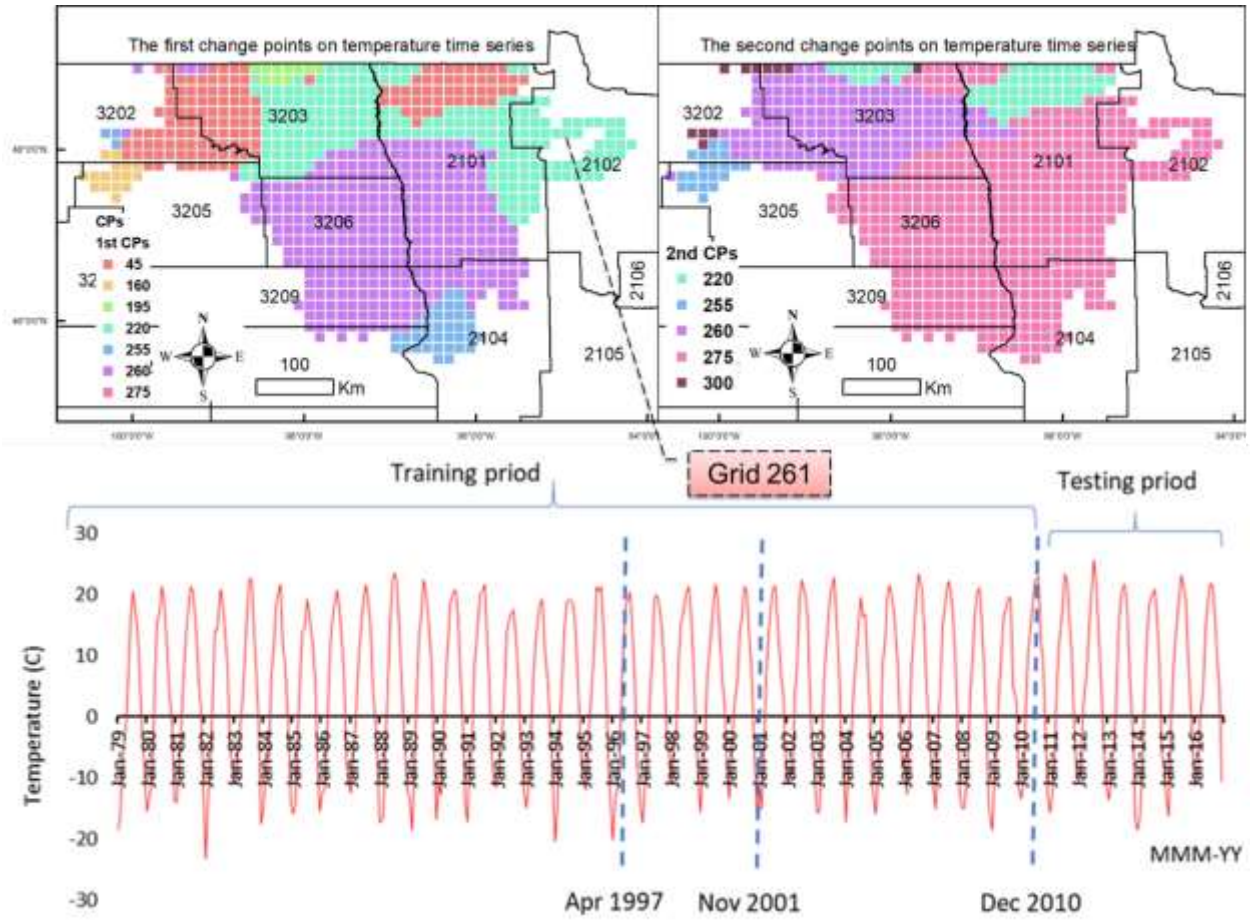

Figure 4.5. Spatial patterns of the first and second change points (CPs) on the monthly temperature time series (numbers in the legend are time steps starting from January 1979), and temperature time series and CPs for Grid 261. 45, 160, 195, 220, 255, 260, 275, and 300 are related to September 1982, April 1992, March 1995, April 1997, March 2000, August 2000, November 2001, and December 2003, respectively.

To measure the performance of ESSVR, it was compared with SVR without consideration of the non-stationarity in the temperature times series. The comparison of the performances of

ESSVR and SVR for the monthly indices was conducted based on the difference between the RMSE of the results for SVR and ESSVR (Figures 4.6-4.8). In these figures, blue spots show the points with superiority of ESSVR and the red spots depict the points with inferiority of the ESSVR. For SPI and SRI, the blue spots are accumulated in CD 3203, the 3rd driest and the 2nd coldest CD in the RRB (Figure 4.6). Since the predictor for SPI was precipitation, the impact of consideration of the non-stationarity in the temperature time series was attributed to the separation of snowfall and rainfall in this cold climate region. Thus, the superiority of ESSVR over SVR in cold and dry climate for CD 3203 was related to the higher sensitivity of SPI to temperature in a relatively colder and drier region. SRI has been suggested by Shukla and Wood (2008) to be used for the regions with prevalent snowmelt. The impact of removing the non-stationarity in temperature, as one of the predictors of SRI, was reflected on the superiority of ESSVR in a relatively colder and snowmelt-dominant region. The blue spots for SSI were mostly located in CD 2101, the 3rd wettest and the 4th coldest CD in the RRB (Figure 4.6). For SBFI, CD 2102, the wettest and coldest region showed the superiority of ESSVR over SVR due to the accumulation of the blue spots (Figure 4.6). SSI and SBFI were related to soil moisture and baseflow, respectively. The superiority of ESSVR in the wetter and colder regions for these two indices was related to the effect of frozen ground and its relation to the soil moisture and baseflow in the RRB. For SSPI, SSWEI, SPEI, and HADI, the blue spots were piled up in CD 3206, the 4th driest and the 4th warmest CD in the RRB (Figures 4.6-4.8). These indices are more sensitive to temperature, which can be the main reason for the superiority of ESSVR. CDs 3203 and 3209, the 4th wettest and the 3rd warmest CD in the RRB, had the densest accumulation of blue spots for SMRI (Figure 4.7), which was based on the summation of rainfall and snowmelt. Using ESSVR in a warmer and wetter region was more beneficial since rainfall was more dominant in such a region. For SHADI, the blue spots were gathered in CDs 3203 and 3202 (Figure 4.8). CD 3202 was the driest and the 3rd coldest CD in the RRB. The common features of CDs 3203 and 3202 were to be among the top driest and coldest CDs. SHADI has

been primarily developed to identify snow drought by considering snowpack in its calculation. The superiority of ESSVR in this cold region was related to this feature of SHADI.

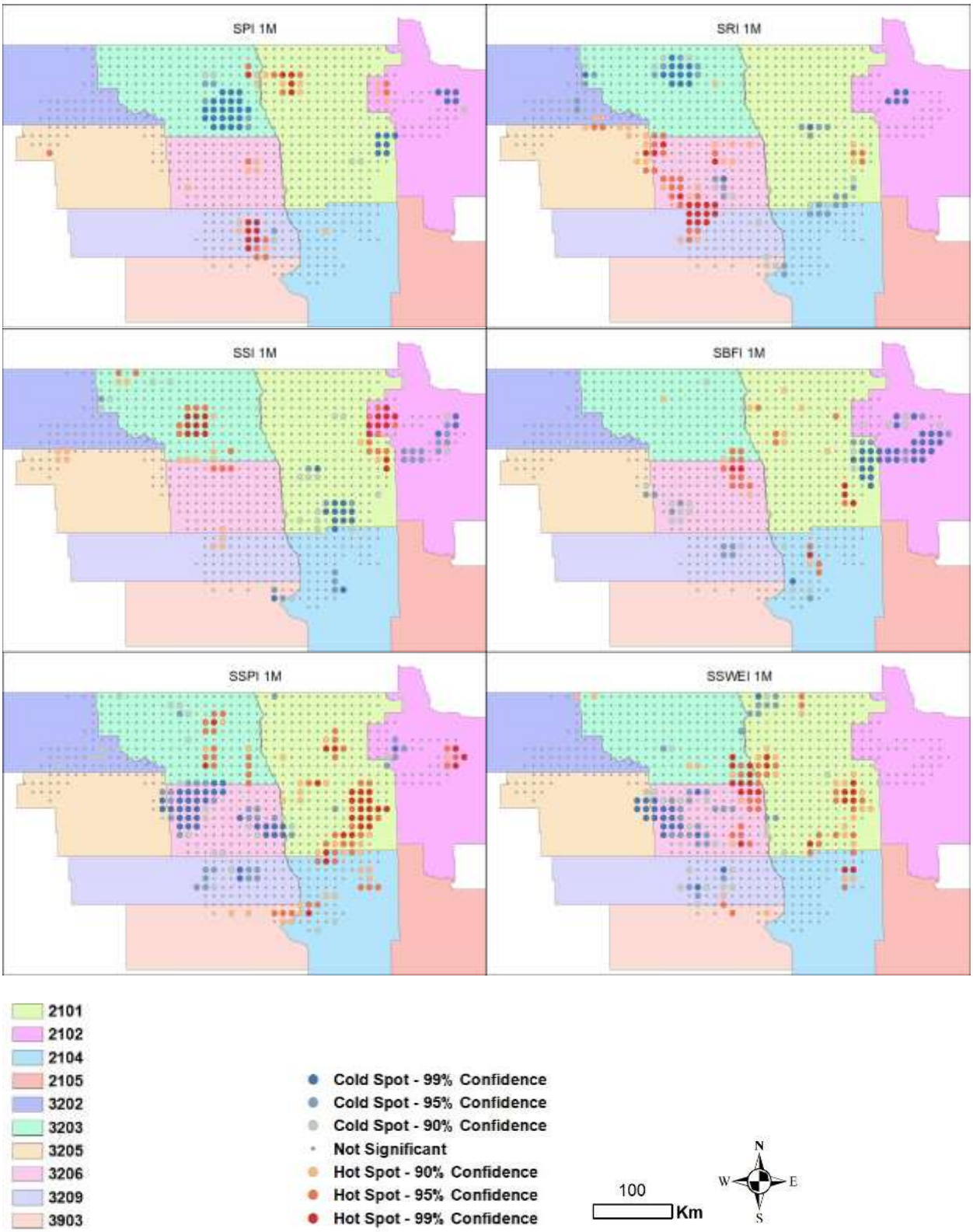

Figure 4.6. Hot and cold spot maps for comparison of the differences between the RMSE values of SVR and ESSVR for monthly standardized univariate indices

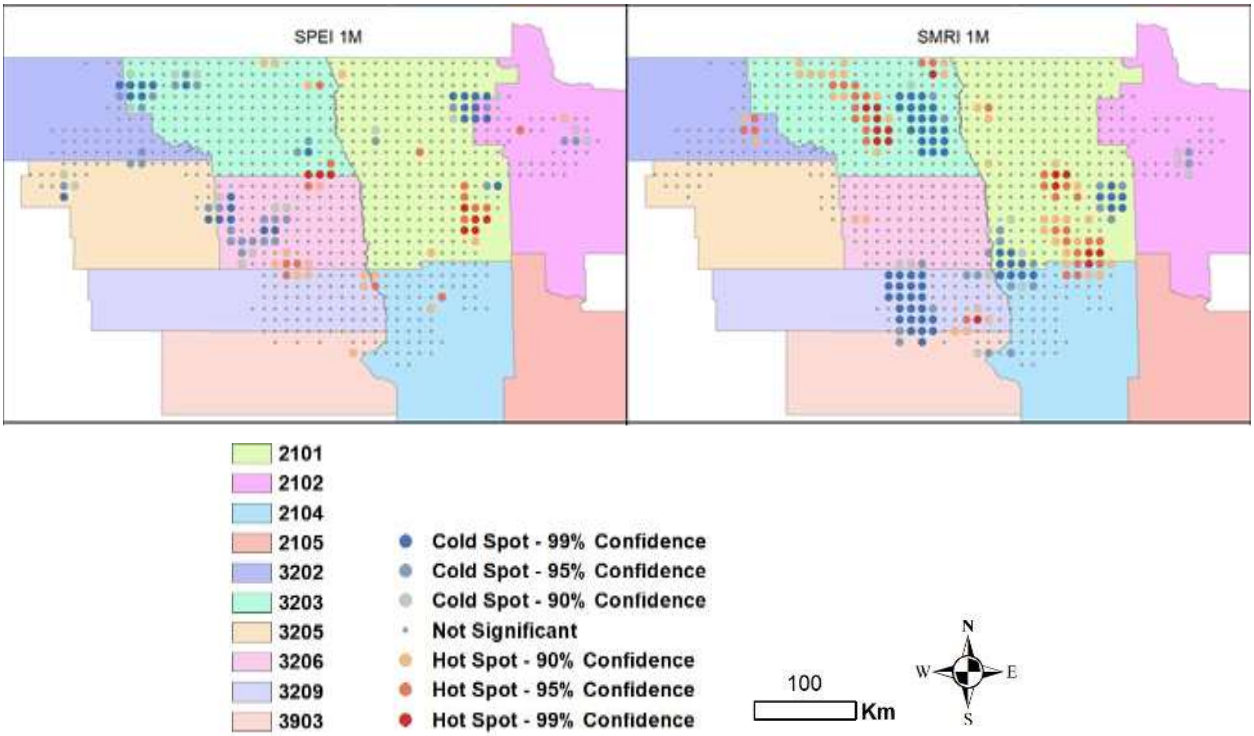

Figure 4.7. Hot and cold spot maps for comparison of the differences between the RMSE values of SVR and ESSVR for monthly standardized bivariate indices

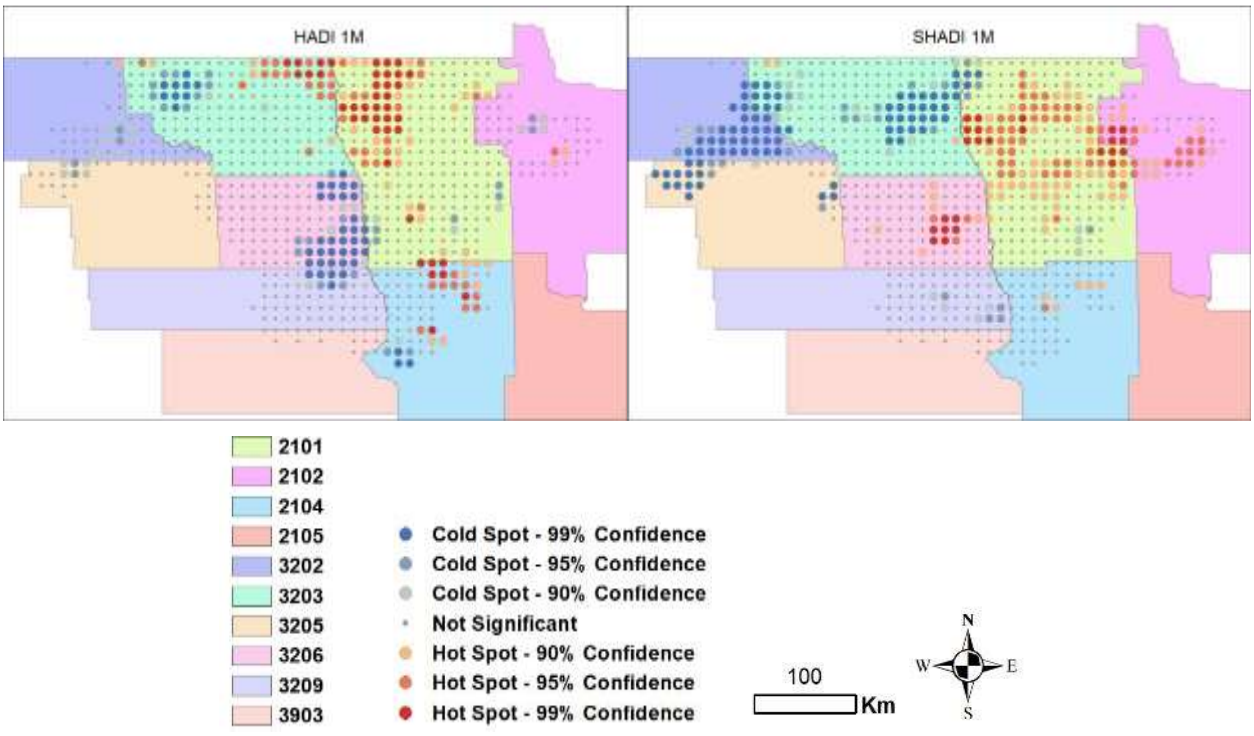

Figure 4.8. Hot and cold spot maps for comparison of the differences between the RMSE values of SVR and ESSVR for monthly multivariate indices

Figure 4.9 shows the various ranges of the differences between the RMSE values in SVR and ESSVR for monthly, seasonal, and semi-annual drought indices. Overall, ESSVR for SHADI had lower RMSE values in 71% of the RRB, which was the highest coverage among monthly drought indices. 54%, 45%, 38%, 33%, and 28% were the coverage percentages of superiority ESSVR over SVR with the ranges of the differences of RMSE higher than 0.01, 0.02, 0.03, 0.04, and 0.05, respectively. The monthly SSI and SPEI had the second largest area coverage (51%) with lower RMSE for ESSVR than that of SVR.

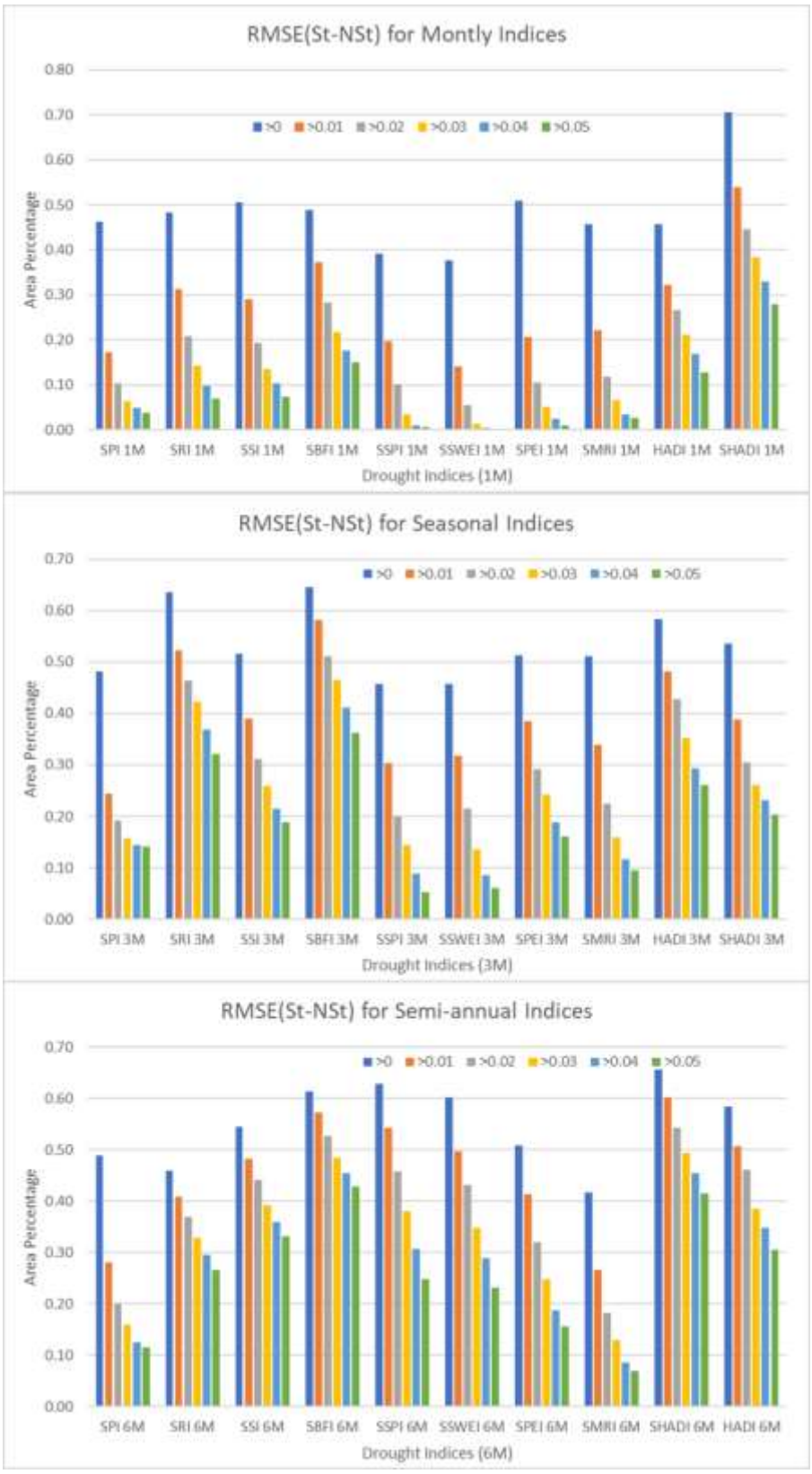

Figure 4.9. Areal coverage of different ranges of differences in RMSE of SVR (NSt) and ESSVR (St) for monthly, seasonal, and semi-annual indices

Among the seasonal indices, SRI had the highest area coverage for all ranges of the differences in the RMSE values for ESSVR and SVR except for the difference greater than 0.05. SBFI had the largest coverage for the difference greater 0.05 (36%). For SRI, 64%, 52%, 46%, 42%, 37%, and 32% were the coverage percentages of superiority of ESSVR over SVR with the range greater than 0, 0.01, 0.02, 0.03, 0.04, and 0.05, respectively. Like the monthly indices, the largest coverage of superiority of ESSVR over SVR was observed for the semi-annual SHADI. For SHADI, 66%, 60%, 54%, 49%, 46%, and 42% were the coverage percentages of superiority of ESSVR over SVR with the range greater than 0, 0.01, 0.02, 0.03, 0.04, and 0.05, respectively. Generally, the coverage percentage of superiority of ESSVR over SVR increased by increasing the time scales of drought indices.

Overall, the monthly SSI, SPEI, and SHADI and the seasonal SRI, SSI, SBFI, SPEI, SMRI, HADI, and SHADI, and the semi-annual SSI, SBFI, SSPI, SSWEI, SPEI, HADI, and SHADI were among the indices with more than 50% of the area showing better performances of ESSVR than SVR. These results suggested: (1) by increasing the time scales more drought indices showed better performance by considering the stationarity in ESSVR; and (2) regardless of the time scale, ESSVR outperformed SVR when SSI, SBFI, and SHADI were selected as the target variables. Since these indices are sensitive to temperature (considering the relation of soil moisture and baseflow to frozen ground in SSI and SBFI and snowpack in the SHADI), the stationarity of the temperature as one of the predictors improved the drought prediction.

The spatial distributions of C, epsilon (ε), and gamma (G) in SVR and ESSVR were compared (Figure 4.10) considering SHADI as the target variable. SHADI was selected since it had the largest coverage of the differences in RMSE for SVR and ESSVR (Figure 4.9). Thus, it can be helpful to investigate the reasons behind the superiority of ESSVR over SVR. The spatial patterns of C values were almost the same for SVR and ESSVR and there was only a minor discrepancy. The same percentage of RRB was assigned to the C values equal to 1 (73%) and 25 (4%) for both SVR and ESSVR. However, a slightly higher percentage of the area was covered by

C values of 15 (4%) and 20 (2%) in ESSVR comparing with 1% and 1%, respectively in SVR. 14% and 6% of the RRB were covered by C values of 5 and 10 for SVR. However, a slightly smaller percentage was assigned to the same values of C in ESSVR (12% and 5%). Overall, the difference was not significant but it can be concluded that the smaller values of C were covered by a higher percentage of the RRB in SVR and higher values of C such as 15 and 20 were assigned in a higher percentage of the RRB in ESSVR. The smaller C values in SVR can increase the training errors, while the larger C values in ESSVR can lead to a hard-margin SVM and higher sensitivity in the data noises.

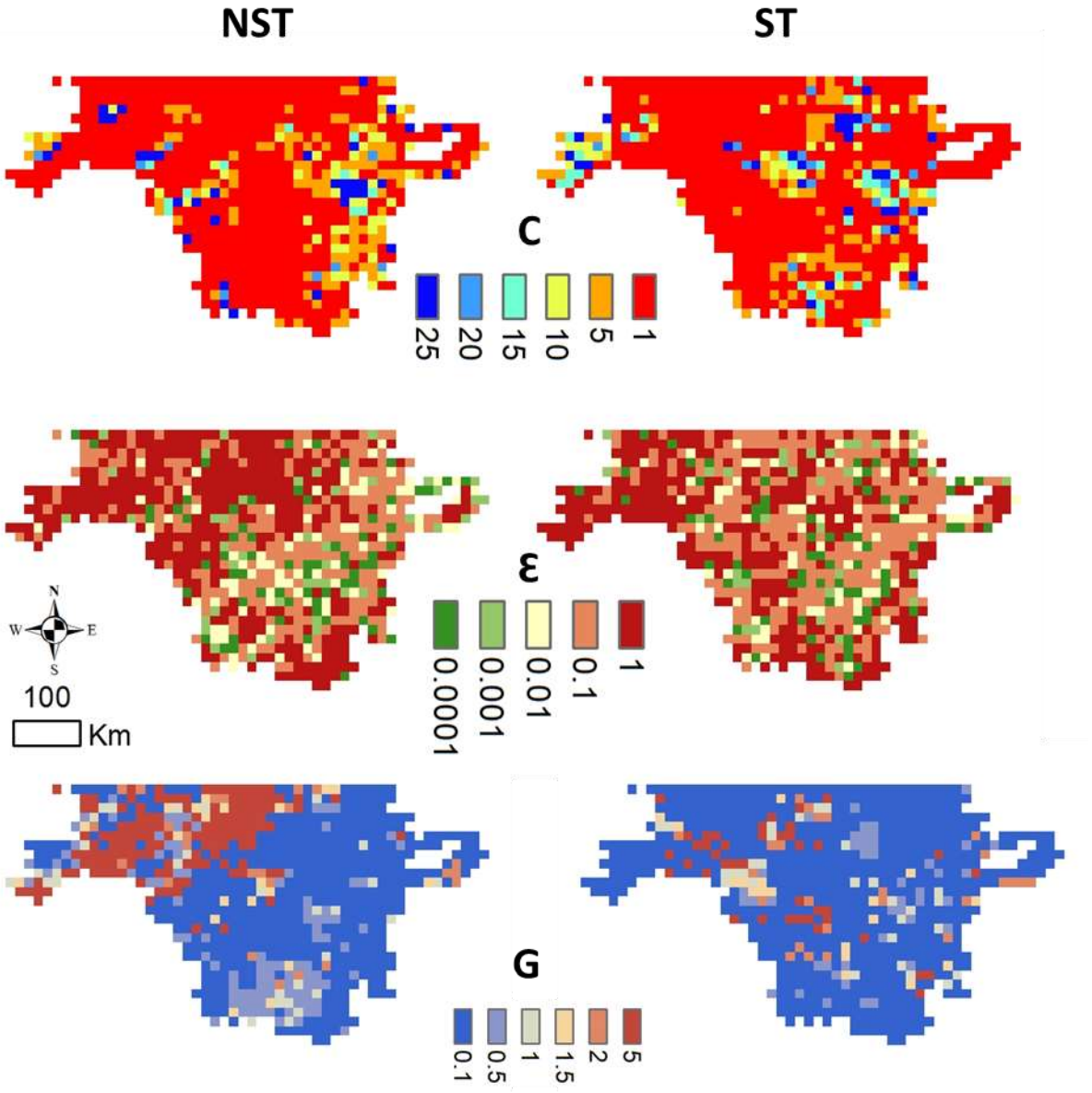

Figure 4.10. Comparison of spatial patterns and ranges of hyperparameters (Cost (C), Epsilon (ε), and Gamma (G)) in SVR (St) and ESSVR(NST) for monthly SHADI

According to Figure 4.10, for ε, a smaller area coverage (41%) in ESSVR comparing with 46% in SVR covered by ε equal to 1. A smaller coverage (i.e., 5%) for SVR comparing with 4% for ESSVR also assigned to ε of 0.001. However, a larger coverage (36%) was for a value of 0.1 for ESSVR comparing with 30% for SVR. Similar 9% coverage for 0.0001 and 10% coverage for 0.01 were observed for SVR and ESSVR. Ignoring the similar coverage for 0.0001 and 0.01, higher coverage percentages were assigned for the relatively high (e.g., 1) and low values of ε (e.g.,

0.001) for SVR. The better performance of ESSVR than SVR can be related to the fact that the bigger ε values can lead to more flat estimates and smaller ε values can cause overfitting.

Significant differences between the coverages of G values in SVR and ESSVR were observed for G equal to 0.1 and 5. 80% of the RRB was covered by G equal to 0.1 (i.e., the lowest G value in this study) for ESSVR. The corresponded percentage for SVR was 60%. However, for the highest value of G (equal to 5), a higher percentage (18%) was covered for SVR comparing with 5% for ESSVR. Thus, ESSVR was inclined to the lower values of G. According to Schölkopf and Smola (2002), G values are related to ε. While higher values of C were assigned for ESSVR, it inclined to assign lower values of G.

Finally, the grid with the largest difference in RMSE of SVR and ESSVR for each drought index was identified and a Taylor diagram was created to compare the performances of SVR and ESSVR. Among the monthly drought indices (Figure 4.11), the highest improvement was observed for SRI. The RMSE increased by 0.19 and R^2 increased from 0.06 to 0.62. Comparing ESSVR and SVR, the standard deviations of the predicted values by ESSVR were much closer to those of the observed values. For the monthly SBFI, both SVR and ESSVR were out of range of the Taylor diagram since their R2 values were negative. The application of a seasonal time scale for SBFI caused no change (Figure 4.12); while there was a slight improvement in the results after a semi-annual time scale was used (Figure 4.13). The results of SVR for HADI and SHADI were not acceptable based on the R2 values. However, the implication of ESSVR led to an improvement in the results. Generally, ESSVR outperformed SVR for all monthly standardized univariate (except SBFI), standardized bivariate, and multivariate drought indices.

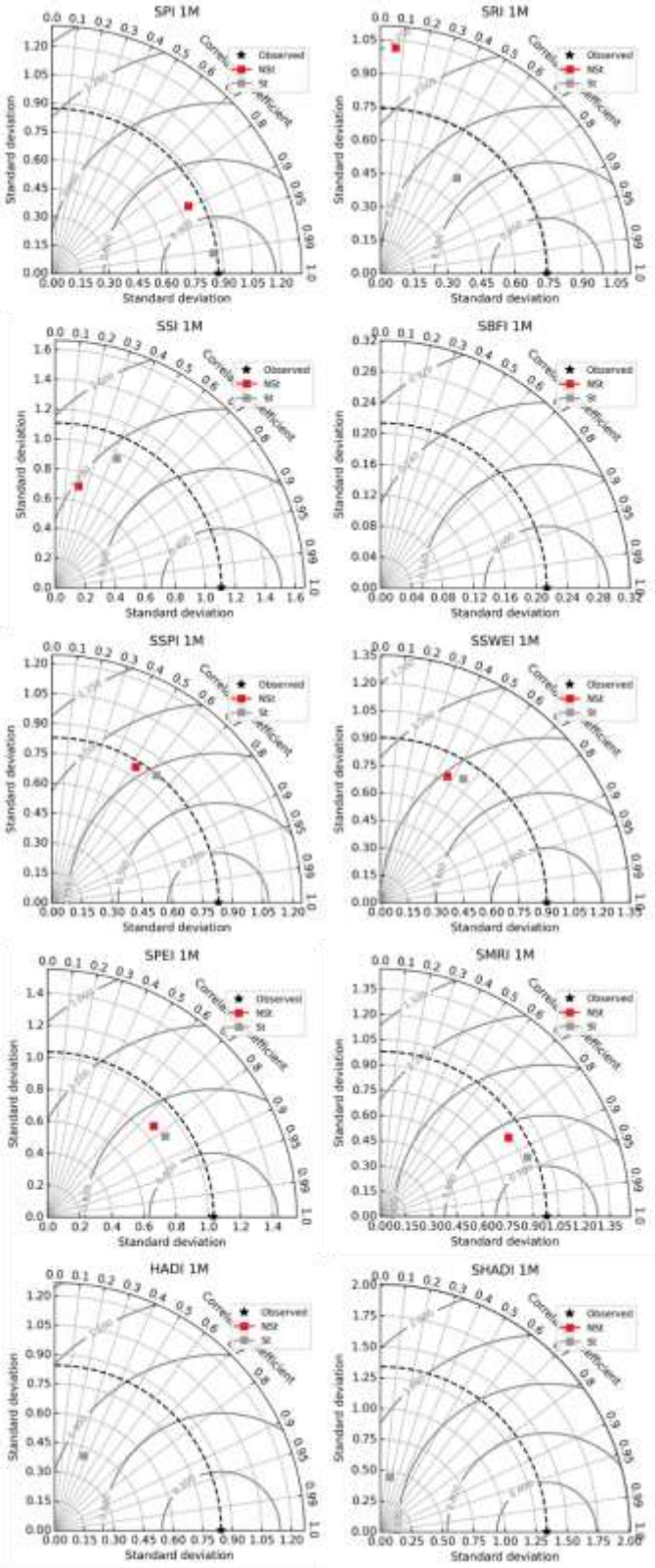

Figure 4.11. Taylor diagram for comparison of the performances of SVR (NSt) and ESSVR (St) based on monthly indices

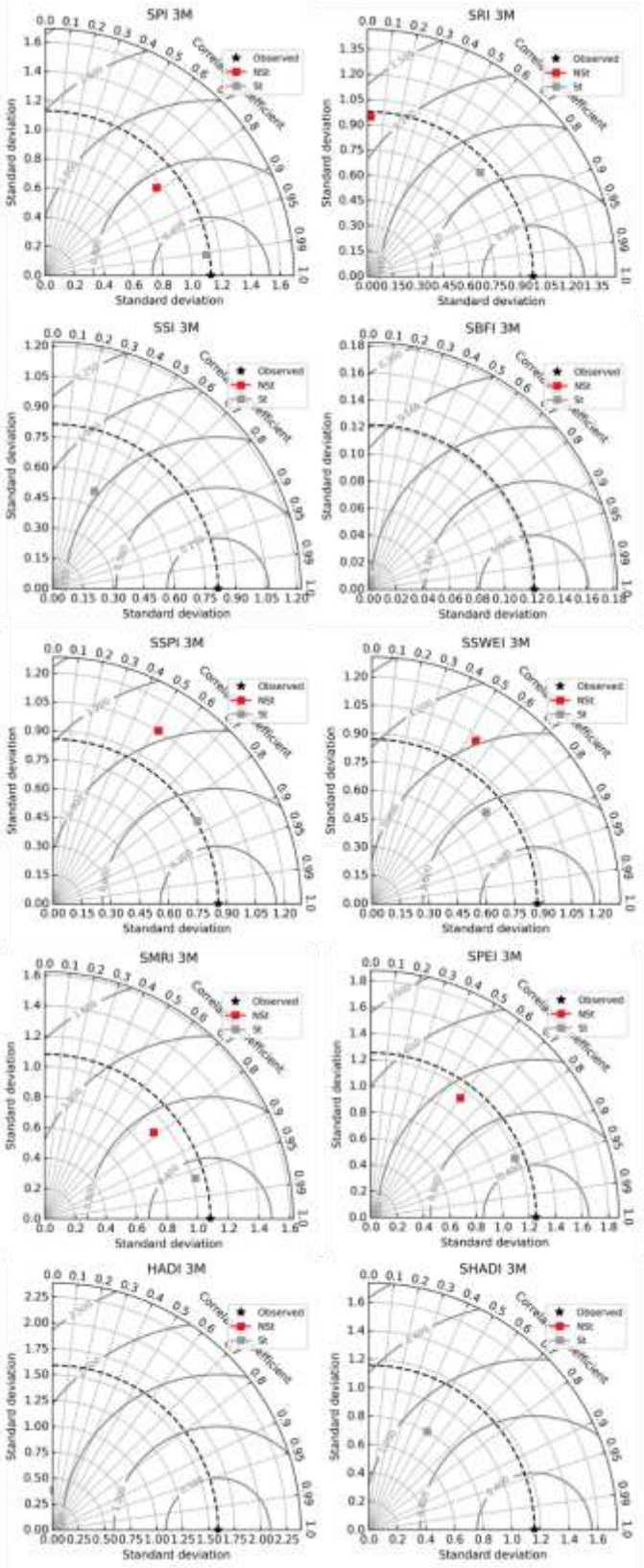

Figure 4.12. Taylor diagram for comparison of the performances of SVR (NSt) and ESSVR (St) based on seasonal indices

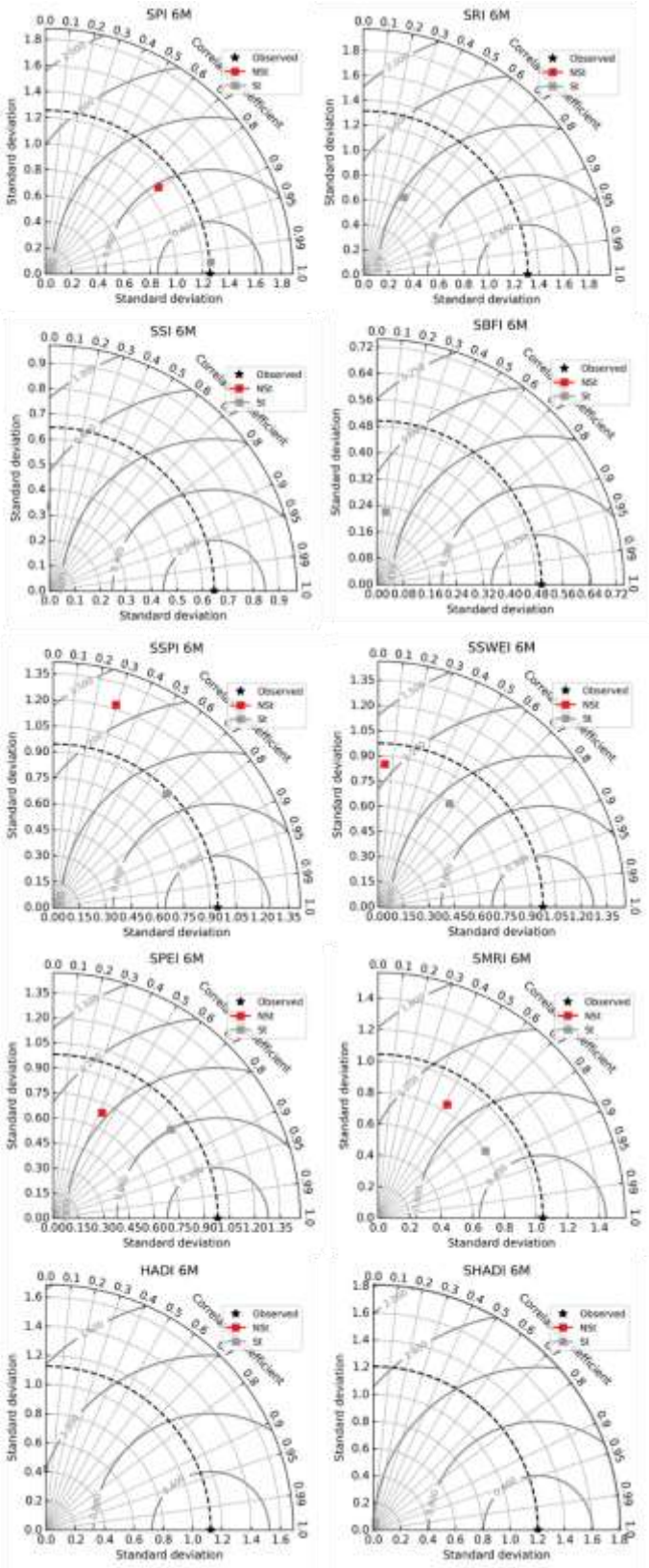

Figure 4.13. Taylor diagram for comparison of the performances of SVR (NSt) and ESSVR (St) based on semi-annual indices

Almost the same results were observed for the seasonal and semi-annual indices (Figures 4.12 and 4.13). For the seasonal indices, minor differences existed for SSI, where a negative correlation was observed for SVR. However, the application of ESSVR led to an improvement in the results. R^2 increased from -0.61 to 0.39 and RMSE had a decrease of 0.29 in RMSE. Although a similar improvement was not observed after the application of the semi-annual time scale for SSI, for all other drought indices noticeable improvements in the results were observed. For the semi-annual indices (Figure 4.13), the top three highest decreases in RMSE were for SRI, SBFI, and SHADI. For SRI, R^2 increased from -0.56 to 0.46 and RMSE decreased by 0.45. For SHADI and SBFI, decreases by 0.46 and 0.43 in RMSE were observed, respectively. Despite a decrease in RMSE of ESSVR, the R^2 values for both SVR and ESSVR were negative and not in the range of the Taylor diagram.

Although the implication of ESSVR resulted in remarkable improvements in the results for SBFI, SSI, SRI, HADI, and SHADI, the overall results were not acceptable. These indices are based on baseflow, soil moisture, and surface runoff in addition to other hydroclimatic variables, which are more complex than the observed hydroclimatic variables such as precipitation, rainfall, snowpack, snowmelt, and evapotranspiration that are required for estimation of other drought indices in this study. Thus, various reasons can justify these drawbacks: (1) The dominant hydroclimatic process such as frozen ground has been neglected in the NLDAS. Hence, the unique features of cold climate regions have not been reflected in the simulated hydroclimatic variables by the NLDAS; (2) the accumulation process of drought indices for conversion to larger time scales may cause these shortcomings especially for the bivariate and multivariate indices. It was observed that the performances of both ESSVR and SVR for HADI and SHADI, unlike other standardized univariate indices, became worse when the larger time scales were used; and (3) the employed predictors are not suitable for prediction of these drought indices and large-scale climate indices that reflect the atmosphere-ocean circulation pattern (e.g., sea surface temperature, Southern Oscillation Index, and North Atlantic

Oscillation) and local climate variables (e.g., precipitation and temperature) need to be used. Overall, according to the results, ESSVR had considerable improvements especially for the cases that the drought prediction by SVR was not acceptable. Therefore, ESSVR can improve drought prediction especially for drought indices with high sensitivity to temperature in a warming climate.

4.5. Conclusions

September 1982, April 1992, March 1995, April 1997, March 2000, August 2000, November 2001, December 2003 were identified as either the first and/or second change point(s). August 2000 in a great portion of the RRB (45%) was identified as the first change point. November 2001 was identified as the second change point in 65% of the RRB. There existed an agreement between the CDs and the first change points. The spatial pattern of the second change points can be divided into the north and south parts of the RRB. The statistical properties of the temperature time series confirmed the accuracy of the identified change points and highlighted the necessity of considering the non-stationarity for prediction of droughts in a warming climate.

ESSVR for SSI and SBFI outperformed SVR in the wetter and colder areas since the impacts of frozen ground on soil moisture and baseflow in such areas were reflected in ESSVR by removing the non-stationarity in the temperature time series. SSPI, SSWEI, SPEI, and HADI suggested the superiority by ESSVR in the relatively drier and warmer areas. Higher sensitivity of these indices to temperature was the reason for the outperformance of ESSVR in the drier and colder CDs. SHADI showed superiority of ESSVR in the colder areas due to the fact that SHADI was primarily developed to identify snow drought by considering snowpack. By increasing the time scales, ESSVR for a broader variety of drought indices outperformed SVR. Regardless of the drought indices' time scales, ESSVR outperformed SVR when SSI, SBFI, and SHADI were

selected as the target variables. These indices were more sensitive to temperature and hence using ESSVR improved the drought prediction.

Despite the noticeable similarities of spatial distributions of C values in SVR and ESSVR, smaller values of C were covered by higher percentages of the RRB in SVR and higher values of C such as 15 and 20 were assigned in a higher percentage of the RRB in ESSVR. The smaller C values in SVR increased the training errors, while the larger C values in ESSVR led to a hard-margin SVM and more sensitivity to the data noises. Despite the same coverage for ε values, a larger coverage was assigned for the relatively higher and relatively lower values of ε for SVR. Since the bigger ε values lad to more flat estimates and smaller ε values caused overfitting, the better performance of ESSVR than SVR was justified. When higher values of C were assigned by ESSVR, it inclined to assign lower values of G. This finding confirmed the results by Schölkopf and Smola 2002 about the relationship between C and G. Similar to the findings by Cao et al. (2002), ESSVR generalized better than the traditional SVR in prediction of non-stationary time series. In addition, the results indicated that ESSVR used fewer support vectors, resulting in a sparser representation of the solutions.

When ESSVR was employed, the highest improvement was observed for SRI among the monthly drought indices. A significant decrease in RMSE and a noticeable increase in R2 were observed. For the monthly HADI and SHADI for the girds with the highest improvement, the application of ESSVR led to movement for R2 from negative to positive values. The same results were observed for the seasonal indices except for SSI, where a negative correlation was observed for SVR. The top three highest decreases in RMSE values were observed for the semi-annual SRI, SBFI, and SHADI.

The results were in accordance with other studies (e.g., Xu et al. 2019, Ali et al. 2018) that reported improvements in prediction after applications of the ensemble methods. In this study, instead of using different models for the ensemble techniques, the prediction models were developed based on the stationary-based subsets and the one with the highest accuracy was

selected. In addition, like other similar studies (Cao et al. 2002, Fan and Tang 2013, Grinblat et al. 2014, Peng 2010, Ojemakinde 2006) after the application of ESSVR better results were obtained for drought prediction. The levels of improvement varied, depending upon the employed drought indices and their time scales.

In this study, by testing different change point detection methods and different numbers of change points, two change points and window-based change point detection method were used to convert a non-stationarity time series of temperature into stationary sub-datasets. Using longer time series and correspondingly more change points can be considered for further analyses. In this study a two-year period was selected as the band for sliding window for change point detection. The reason was to remove the impacts of the monthly, seasonal, and interannual variabilities of temperature and identify the major change points due to a warming climate. A wider band can be examined in the future studies.

Different values of the hyperparameters were tested in the grid search cross-validation and finally a limited number of values of the hyperparameters were selected for the prediction model based on the initial performance of the model and the suggested values in the literature. Using a wider range of the hyperparameters can be tested for further studies. In this study, the training dataset was divided into stationary sub-datasets by change points, and then each stationary dataset was further divided into k-folds for cross-validation. However, the training dataset can be divided into k-folds based on the change points in the future studies. Overall, the results suggested an improvement over the traditional SVR model for prediction of droughts by considering the non-stationarity in the temperature time series in a changing climate. The proposed ESSVR model for improvement of drought prediction is able to provide more accurate drought prediction.

4.6. References

Adamowski, J. (2008). Development of a short-term river flood forecasting method for snowmelt driven floods based on wavelet and cross-wavelet analysis. Journal of Hydrology, 353, 247–266.

Ali, M., R. C. Deo, N. J. Downs, T. Maraseni, (2018) An ensemble-ANFIS based uncertainty assessment model for forecasting multi-scalar standardized precipitation index, Atmospheric Research, 207, 155-180, https://doi.org/10.1016/j.atmosres.2018.02.024.

Bacanli, U. G., Firat, M., & Dikbas, F. (2009). Adaptive neuro-fuzzy inference system for drought forecasting. Stochastic Environmental Research and Risk Assessment, 23, 1143–1154. https://doi.org/10.1007/s00477-008-0288-5

Barros, A. P., & Bowden, G. J. (2008). Toward long-lead operational forecasts of drought: An experimental study in the Murray-Darling River basin. Journal of Hydrology, 357, 349–367. https://doi.org/10.1016/j.jhydrol.2008.05.0

Barua, S., Ng, A. W. M., & Perera, B. J. C. (2012). Artificial neural network-based drought forecasting using a nonlinear aggregated drought index. Journal of Hydrologic Engineering, 17, 1408–1413. https://doi.org/10.1061/(ASCE)HE.1943-5584.0000574

Bazrkar, M. H. and X. Chu. (2020). A new standardized baseflow index for identification of hydrologic drought in the Red River of the North Basin. Natural Hazards Review, 21(4), 05020011, 1-8, doi:10.1061/(ASCE)NH.1527-6996.0000414.

Bazrkar, M. H., J. Zhang, and X. Chu. (2020). Hydroclimatic aggregate drought index (HADI): A new approach for identification and categorization of drought in cold climate regions. Stochastic Environmental Research and Risk Assessment, 34(11), 1847-1870, doi:10.1007/s00477-020-01870-5.

Belayneh, A., Adamowski, J., Khalil, B., & Ozga-Zielinski, B. (2014). Long-term SPI drought forecasting in the Awash River basin in Ethiopia using wavelet neural networks and wavelet

support vector regression models. Journal of Hydrology, 508, 418–429. https://doi.org/10.1016/j.jhydrol.2013.10.052

Brunner, MI, Slater, L, Tallaksen, LM, Clark, M. (2021). Challenges in modeling and predicting floods and droughts: A review. WIREs Water. 8:e1520. https://doi.org/10.1002/wat2.1520

Cancelliere, A., Di Mauro, G., Bonaccorso, B., & Rossi, G. (2007). Drought forecasting using the standardized precipitation index. Water Resources Management, 21(5), 801–819. https://doi.org/10.1007/s11269-006-9062-y

Cao, L. and Gu, Q. (2002). Dynamic support vector machines for non-stationary time series forecasting. Intelligent Data Analysis, (6) 67-83.

Cherkassky, V. and F. Mulier, 1998. Learning from Data: Concepts, Theory, and Methods, John Wiley & Sons, Inc. New York, N.Y., USA.

Deo, R. C., Tiwari, M. K., Adamowski, J. F., & Quilty, J. M. (2016). Forecasting effective drought index using a wavelet extreme learning machine (W-ELM) model. Stochastic Environmental Research and Risk Assessment, 31(5), 1211–1240.

Duggins, J., Williams, M., Kim, D., Smith, E. (2010). “Changepoint detection in SPI transition probabilities.” Journal of Hydrology, 388, 456-463.

Durdu, Ö. F. (2010). Application of linear stochastic models for drought forecasting in the Büyük Menderes River basin, western Turkey. Stochastic Environmental Research and Risk Assessment, 24, 1145–1162. https://doi.org/10.1007/s00477-010-0366-3

Efron, B. (1979). Bootstrap methods: Another look at jackknife. Annals of Statistics, 7, 1-26.

England, Jr., J.F., Cohn, T.A., Faber, B.A., Stedinger, J.R., Thomas Jr., W.O., Veilleux, A. G., Kiang, J.E., Mason, R.R. (2018). Guidelines for Determining Flood Flow Frequency-Bulletin 17C (Report No. book 4, chap. B5), Techniques and Methods. U.S. Geological Survey, Reston, Virginia.

Esfahanian, E., Nejadhashemi, A.P., Abouali, M., Daneshvar, F., Ameli, A., Herman, M., Tang, Y., (2016). Defining drought in the context of stream health. Ecological Engineering 94(7):668-681. https://doi.org/10.1016/j.ecoleng.2016.06.110

Fan, J. and Tang, Y. (2013). An EMD-SVR Method for Non-Stationary Time Series Prediction. 2013 International Conference on Quality, Reliability, Risk, Maintenance, and Safety Engineering (QR2MSE), Chengdu, China, doi: 10.1109/QR2MSE.2013.6625918

Fernández, C., Vega, J. A., Fonturbel, T., & Jiménez, E. (2009). Streamflow drought time series forecasting: A case study in a small watershed in North West Spain. Stochastic Environmental Research and Risk Assessment, 23, 1063–1070. https://doi.org/10.1007/s00477-008-0277-8

Freund, Y. and Schapire, R. E. (1997). A decision-theoretic generalization of on-line learning and application to boosting. Journal of Computer and System Sciences, 55(1), 119-139.

Ganguli, P., & Reddy, M. J. (2014). Ensemble prediction of regional droughts using climate inputs and the SVM–copula approach. Hydrological Processes, 28(19), 4989–5009. https://doi.org/10.1002/hyp.9966

Grinblat, G. L., Uzal, L. C., Verdes, P. F., Granitto, P. M. (2015). Nonstationary regression with support vector machines, Neural Comput & Applic, (26) 641–649, doi: 10.1007/s00521-014-1742-6

Hao, Z., & Singh, V. P. (2016). Review of dependence modeling in hydrology and water resources. Progress in Physical Geography, 40(4), 549–578. https://doi.org/10.1177/0309133316632460

Hao, Z., Hao, F., Xia, Y., Singh, V. P., Hong, Y., Shen, X., & Ouyang, W. (2016). A statistical method for categorical drought prediction based on NLDAS-2. Journal of Applied Meteorology and Climatology, 55(4), 1049–1061. https://doi.org/10.1175/JAMC-D-15-0200.1

Hao, Z., Singh, V. P., and Xia, Y. (2018). “Seasonal Drought Prediction: Advances, Challenges, and Future Prospects.” Reviews of Geophysics, 56(1), 108–141, doi: 10.1002/2016RG000549

Hoerling, M., Eischeid, J., Kumar, A., Leung, R., Mariotti, A., Mo, K., … Seager, R. (2014). Causes and predictability of the 2012 Great Plains drought. Bulletin of the American Meteorological Society, 95(2), 269–282. https://doi.org/10.1175/BAMS-D-13-00055.1.

Huang, S., Huang, Q., Chang, J., Leng, G. (2016). “Linkages between hydrological drought, climate indices and human activities: a case study in the Columbia River basin.” International Journal of Climatology, 36, 280-290.

Huning LS, AghaKouchak A. (2018). Mountain snowpack response to different levels of warming. Proc Natl Acad Sci U S A. 2018 Oct 23;115(43):10932-10937. doi: 10.1073/pnas.1805953115. Epub 2018 Oct 8. PMID: 30297423; PMCID: PMC6205460.

Hwang, Y., & Carbone, G. J. (2009). Ensemble forecasts of drought indices using a conditional residual resampling technique. Journal of Applied Meteorology and Climatology, 48, 1289–1301. https://doi.org/10.1175/2009JAMC2071.1

Jackson, B., Sargle, J. D., Barnes, D., Arabhi, S., Alt, A., Gioumousis, P., Gwin, E., Sangtrakulcharoen, P., Tan, L., and Tsai, T. T. (2005). An Algorithm for Optimal Partitioning of Data on an Interval, IEEE Signal Processing Letters, 12, 105–108. [1590,1591]

Jalalkamali, A., Moradi, M., Moradi, N. (2015). Application of several artificial intelligence models and ARIMAX model for forecasting drought using the standardized precipitation index. International Journal of Environmental Science and Technology, 12 (4), 1201–1210.

Joachims, T., (2002). Learning to Classify Text Using Support Vector Machines: Methods, Theory and Algorithms. books.google.com.

Killick, R., Fearnhead, P., Eckley, I.A., (2012). Optimal detection of changepoints with a linear computational cost. J. Am. Stat. Assoc. 107, 1590–1598. doi:10.1080/01621459.2012.737745

Kim, T.-W., & Valdés, J. B. (2003). Nonlinear model for drought forecasting based on a conjunction of wavelet transforms and neural networks. Journal of Hydrologic Engineering, 8(6), 319–328. https://doi.org/10.1061/(ASCE)1084-0699(2003)8:6(319)

Kisi, O., Cimen, M., (2011). A wavelet-support vector machine conjunction model for monthly streamflow forecasting. Journal of Hydrology 399, 132–140.

Lau, K.-M., Kim, K.-M., and Shen, S. S. P. (2002). Potential predictability of seasonal precipitation over the United States from canonical ensemble correlation predictions. Geophysical Research Letters, 29(7), 1–4.

Lei, K.S., Wan, F. (2012). Applying Ensemble Learning Techniques to ANFIS for Air Pollution Index Prediction in Macau, International Symposium on Neural Networks. Springer, 509–516.

Li, P.-H., Kwon, H.-H., Sun, L., Lall, U. and Kao, J.-J. (2010). A modified support vector machine based prediction model on streamflow at the Shihmen Reservoir, Taiwan. Int. J. Climatol., 30: 1256-1268. https://doi.org/10.1002/joc.1954

Lim, Y., Jo, S., Lee, J., Oh, H.-S., and Kang, H.-S. (2012). “An improvement of seasonal climate prediction by regularized canonical correlation analysis.” International Journal of Climatology, 32(10), 1503–1512.

Liu, W., & Juárez, R. N. (2001). ENSO drought onset prediction in northeast Brazil using NDVI. International Journal of Remote Sensing, 22(17), 3483–3501. https://doi.org/10.1080/01431160010006430

Liu, Y., & Hwang, Y. (2015). Improving drought predictability in Arkansas using the ensemble PDSI forecast technique. Stochastic Environmental Research and Risk Assessment, 29(1), 79–91. https://doi.org/10.1007/s00477-014-0930-3

Lohani, V. K., & Loganathan, G. (1997). An early warning system for drought management using the Palmer drought index. Journal of the American Water Resources Association, 33(6), 1375–1386. https://doi.org/10.1111/j.1752-1688.1997.tb03560.x

Lloyd-Hughes, B. (2014). The impractically of a universal drought definition. Theoretical Applied Climatology, 117, 607-611.

Madadgar, S., & Moradkhani, H. (2013). A Bayesian framework for probabilistic seasonal drought forecasting. Journal of Hydrometeorology, 14(6), 1685–1705. https://doi.org/10.1175/JHM-D-13-010.1

Maity, R., Suman, M., & Verma, N. K. (2016). Drought prediction using a wavelet based approach to model the temporal consequences of different types of droughts. Journal of Hydrology, 539, 417–428. https://doi.org/10.1016/j.jhydrol.2016.05.042

Mazdiyansi, O. and Aghakouchak, A. (2015). "Substantial increase in concurrent droughts and heatwaves in the United States." Proceedings of the National Academy of Sciences of the United States of the America, 112(37), 11484-11489.

McKee, T. B., Doesken, N. J., & Kleist, J. (1993). The relationship of drought frequency and duration to time scales. Paper presented at Eighth Conference on Applied Climatology, American Meteorological Society, Anaheim, CA.

Meng, L., Ford, T. and Guo, Y. (2017). Logistic regression analysis of drought persistence in East China. Int. J. Climatol., 37: 1444-1455. https://doi.org/10.1002/joc.4789

Mishra, A., & Desai, V. (2005). Drought forecasting using stochastic models. Stochastic Environmental Research and Risk Assessment, 19, 326–339. https://doi.org/10.1007/s00477-005-0238-4

Mishra, A., & Desai, V. (2006). Drought forecasting using feed-forward recursive neural network. Ecological Modelling, 198, 127–138. https://doi.org/10.1016/j.ecolmodel.2006.04.0

Mishra, A., Desai, V., & Singh, V. P. (2007). Drought forecasting using a hybrid stochastic and neural network model. Journal of Hydrologic Engineering, 12, 626–638. https://doi.org/10.1061/(ASCE)1084-0699(2007)12:6(626)

Mitchell et al (2004). The multi-institution North American Land Data Assimilation System (NLDAS): Utilizing multiple GCIP products and partners in a continental distributed hydrological modeling system, J. Geophys. Res., 109, D07S90, doi: 10.1029/2003JD003823

Mo, K. C., and W. M. Thiaw, (2002). Ensemble canonical correlation prediction of precipitation over the Sahel, Geophysics Research Letter, 29(12), doi: 10.1029/2002GL015075.

Modarres, R. (2007). Streamflow drought time series forecasting. Stochastic Environmental Research and Risk Assessment, 21, 223–233. https://doi.org/10.1007/s00477-006-0058-1

Morid, S., Smakhtin, V., & Bagherzadeh, K. (2007). Drought forecasting using artificial neural networks and time series of drought indices. International Journal of Climatology, 27, 2103–2111. https://doi.org/10.1002/joc.1498

Moye, L. A., Kapadia, A. S., Cech, I. M., Hardy, R. J. (1988). "The theory of runs with applications to drought prediction." Journal of Hydrology, 103, 127-137.

Mukherjee S., Mishra A., Trenberth K. E. (2018). Climate Change and Drought: a Perspective on Drought Indices, Current Climate Change Reports, 4:145–163, doi: 10.1007/s40641-018-0098-x

NOAA National Centers for Environmental information, Climate at a Glance: Divisional Mapping, published April 2021, retrieved on April 29, 2021 from https://www.ncdc.noaa.gov/cag/

Ojemakinde, B. T. (2006). Support Vector Regression for Non-Stationary Time Series, Master Thesis, University of Tennessee – Knoxville.

Özger, M., Mishra, A. K., & Singh, V. P. (2011). Estimating Palmer drought severity index using a wavelet fuzzy logic model based on meteorological variables. International Journal of Climatology, 31, 2021–2032. https://doi.org/10.1002/joc.2215

Panu, U., & Sharma, T. (2002). Challenges in drought research: Some perspectives and future directions. Hydrological Sciences Journal, 47, S19–S30. https://doi.org/10.1080/02626660209493019

Paulo, A. A., & Pereira, L. S. (2007). Prediction of SPI drought class transitions using Markov chains. Water Resources Management, 21, 1813–1827. https://doi.org/10.1007/s11269-006-9129-9

Paulo, A. A., & Pereira, L. S. (2008). Stochastic prediction of drought class transitions. Water Resources Management, 22, 1277–1296. https://doi.org/10.1007/s11269-007-9225-5

Pedregosa et al. (2011). Scikit-learn: Machine Learning in Python, Journal of Machine Learning Research, 12, 2825-2830.

Pedro BG, Plamen CI, Amaral LAN. (2001). "Scale invariance in the nonstationarity of human heart rate." Physical Review Letters, 87(16): 160815.

Peng, X. (2010). Primal twin support vector regression and its sparse approximation, Neurocomputing (73) 2846–2858, doi: 10.1016/j.neucom.2010.08.013

Rao, A. R., & Padmanabhan, G. (1984). Analysis and modeling of Palmer's drought index series. Journal of Hydrology, 68(1-4), 211–229. https:// doi.org/10.1016/0022-1694(84)90212-9

Regonda, S. K., Rajagopalan, B., & Clark, M. (2006). A new method to produce categorical streamflow forecasts. Water Resources Research, 42, W09501.

Ryberg K. R., Hodgkins, G. K., Dudley R. W. (2019). Change points in annual peak streamflows: Method comparisons and historical change points in the United States, Journal of Hydrology, 1-13, doi: 10.1016/j.jhydrol.2019.124307

Santos, J. F., Portela, M. M., & Pulido-Calvo, I. (2014). Spring drought prediction based on winter NAO and global SST in Portugal. Hydrological Processes, 28(3), 1009–1024. https://doi.org/10.1002/hyp.9641

Schapire, R. E., and Freund, Y., (2012). Boosting: Foundations and Algorithms. MIT Press.

Schölkopf, B. and A. J. Smola, (2002). Learning with Kernels: Support Vector Machines, Regularization, Optimization, and Beyond. Eng. 94, 668-681.

Sharma, T. C., & Panu, U. S. (2012). Prediction of hydrological drought durations based on Markov chains: Case of the Canadian prairies. Hydrological Sciences Journal, 57, 705–722. https://doi.org/10.1080/02626667.2012.67274

Shirmohammadi, B., Moradi, H., Moosavi, V., Semiromi, M.T., Zeinali, A. (2013). Forecasting of meteorological drought using wavelet-ANFIS hybrid model for different time steps (case study: southeastern part of East Azerbaijan province, Iran). Natural Hazards, 69 (1), 389–402.

Shukla S, Wood AW (2008). Use of a standardized runoff index for characterizing hydrologic drought. Geophys Res Lett 35(2):1–7. https://doi.org/10.1029/2007GL032487

Staudinger M, Stahl K, Seibert J (2014). A drought index accounting for snow. Water Resour Res 50(10):7861–7872. https://doi.org/10.1002/2013WR015143

Sun, L., Mitchell, S. W., & Davidson, A. (2012). Multiple drought indices for agricultural drought risk assessment on the Canadian prairies. International Journal of Climatology, 32, 1628–1639. https://doi.org/10.1002/joc.2385

Sun, M., Ph, D., and Kim, G. (2016). "Quantitative Monthly Precipitation Forecasting Using Cyclostationary Empirical Orthogonal Function and Canonical Correlation Analysis." Journal of Hydrologic Engineering, 21(1), 1–13.

Tavakol A., Rahmani, V., Harrington Jr. J. (2020). Evaluation of hot temperature extremes and heat waves in the Mississippi River Basin. Atmospheric Research, 239, 1-13, doi:10.1016/j.atmosres.2020.104907

Taylor, K.E. (2001). "Summarizing multiple aspects of model performance in a single diagram". J. Geophys. Res. 106: 7183–7192. Bibcode:2001JGR...106.7183T. doi:10.1029/2000JD900719.

Truong, C., Oudre, L., & Vayatis, N. (2020). Selective review of offline change point detection methods. Signal Processing, 167. https://doi.org/10.1016/j.sigpro.2019.107299.

Vapnik V. (1995). The Nature of Statistical Learning Theory. Springer, New York.

Vicente-Serrano Sergio M, Juan SB, López-Moreno I (2010) A multiscalar drought index sensitive to global warming, the standardized precipitation evapotranspiration index. J Clim 23:1696–1718. https://doi.org/10.1175/2009JCLI2

Wen, X., Feng, Q., Deo, R.C., Wu, M., Yin, Z., Yang, L., Singh, V.P., (2019). Two-phase extreme learning machines integrated with complete ensemble empirical mode decomposition with adaptive noise for multiscale runoff prediction, Journal of Hydrology, doi: https://doi.org/10.1016/j.jhydrol.2018.12.060

Wolpert, D. H. (1992). Stacked generalization. Neural Networks, 5(2), 241-259.

Wood, E. F., Schubert, S. D., Wood, A. W., Peters-Lidard, C. D., Mo, K. C., Mariotti, A., and Pulwarty, R. S. (2015). Prospects for Advancing Drought Understanding, Monitoring, and Prediction. Journal of Hydrometeorology, 16(4), 1636–1657.

Xia et al (2012). Continental-scale water and energy flux analysis and validation for the North American Land Data Assimilation System project phase 2 (NLDAS-2): 1. Intercomparison and application of model products, J. Geophys. Res., 117, D03109, 10.1029

Xu Y, Wang L, Ross KW, Liu C, Berry K (2018). Standardized soil moisture index for drought monitoring based on soil moisture active passive observations and 36 years of North American Land Data Assimilation System data: a case study in the Southeast United States. Remote Sens. https://doi.org/10.3390/rs10020301

Xu, L., Chen, N., Zhang, X. et al. (2019). Improving the North American multi-model ensemble (NMME) precipitation forecasts at local areas using wavelet and machine learning. Clim Dyn 53, 601–615. https://doi.org/10.1007/s00382-018-04605-z

Yang, T., Zhou, X., Yu, Z., Krysanova, V., & Wang, B. (2015). Drought projection based on a hybrid drought index using artificial neural networks. Hydrological Processes, 29(11), 2635–2648. https://doi.org/10.1002/hyp.10394

Yu, P., Chen, S., Chang, I. (2006). Support vector regression for real-time flood stage forecasting. Journal of Hydrology, 328, 704-716./2011JD016048

Zhou, Z.-H., Wu, J., Tang, W. (2002). Ensembling neural networks: many could be better than all. Artificial Intelligence, 137(1–2), 239–263.

5. OVERALL SUMMARY AND CONCLUSIONS

There are some limitations in the existing methodologies for drought identification, categorization, and prediction. Neglecting the dominant hydroclimatic processes of cold climate regions can result in less accurate drought information. To improve drought identification in such regions, two drought indices, hydroclimatic aggregate drought index (HADI) and snow-based hydroclimatic aggregate drought index (SHADI) were developed. Arbitrarily defined or fixed threshold levels for categorizing droughts can lead to misleading information for stakeholders. To fill this gap, a customized drought categorization was developed to account for both spatial and temporal distributions of droughts. Moreover, using standard measures for scoring in tuning hyperparameters in non-categorical drought prediction models can cause drought mis-categorization. To avoid this problem, a category-based scoring support vector regression (CBS-SVR) was developed. Non-stationary time series due to climate change can decrease the predictability skills of drought prediction models. To minimize the impacts of non-stationary time series, an ensemble stationary-based support vector regression (ESSVR) method was developed. The proposed methodologies were applied to the Red River of the North Basin (RRB) in this dissertation research.

The HADI and SHADI improved the identification of droughts in cold climate regions. HADI integrated rainfall, snowmelt, surface runoff, and soil moisture by utilizing a correlation-based R-mode principal component analysis (PCA) to account for anomalies in available water. In contrast, SHADI accounted for stored sources of water by considering precipitation and snowpack, instead of rainfall and snowmelt in HADI. The standardized first principal component was utilized for deriving these two indices, since it had the highest percentage of eigenvalues throughout the entire study period. In addition to considering dominant hydroclimatic processes in cold climate regions, the HADI and SHADI accounted for different types of drought (e.g., meteorological, hydrologic, and agricultural droughts) by using the absolute values of loadings in PCA, responsible for addressing the target stakeholders. Drought

categorization was also improved by considering both spatial and temporal distributions of droughts by using a joint probability distribution of drought frequencies and drought classes. Conditional probability and condition expectation were used to estimate the probability of occurrence of each drought class and eventually, K-means clustering was used to categorize droughts into ten dry/wet categories. The capabilities of the HADI and SHADI in identification of drought were tested in the RRB, which was distinguished by its cold climate, and their performances were evaluated by comparing with the Palmer Drought Severity Index (PDSI) and the U.S. Drought Monitor (USDM) products. Based on the impacts of drought on agriculture, the HADI and SHADI outperformed the PDSI in the identification of droughts in the RRB. The SHADI showed the capabilities of identifying both dry and warm snow droughts, while the PDSI was able to identify dry snow drought but failed to identify dry/wet spells and warm snow drought due to its simplification in the separation of snowfall and rainfall, frozen soil, and snow accumulation processes in cold climate regions. Particularly, the SHADI facilitated a 2-month lead prediction of drought. The major differences between SHADI and HADI were observed in cold seasons and in transition periods (dry-to-wet or wet-to-dry). The derived variable threshold levels for different categories of drought based on the SHADI were close to, but different from those of the HADI. Due to the use of these variable thresholds, despite the similarities in drought onset and termination, the drought area coverages for each drought category identified by SHADI and HADI were different from that of USDM. The new HADI and SHADI are able to provide more accurate drought identification, especially for cold climate regions. The SHADI can be used for a short-term lead prediction of droughts in cold climate regions and, in particular, can provide an early drought warning in warming climate. The new customized drought categorization can be used for more accurate drought characterization since it considers both spatial and temporal distributions of droughts.

The CBS-SVR model was compared with the traditional SVR and Support Vector Classification (SVC) based on ten drought indices, including six standardized univariate indices,

two standardized bivariate indices, and two multivariate indices, to address different types of droughts. Unlike other non-categorical models that use standard measures to compare predicted values with actual values for tuning hyperparameters, the CBS-SVR model implemented a category-based scoring method by using the threshold levels derived from the novel customized drought categorization. For drought categorization, K-means clustering was compared with the traditional fixed threshold levels and the Gaussian mixture model to select the best categorization method for each drought index. The Area Under Curve of Receiver Operating Characteristics (AUC-ROC) and F1 score were used to measure the performance of the models. The CBS-SVR was applied to the RRB, and the results were compared with those from the SVR and the SVC, suggesting that the CBS-SVR model improved drought prediction. Particularly, it was found that according to the areal average of AUC-ROC and F1 score, R scoring was a better scoring method for tuning hyperparameters in cross-validation of SVR if the target variables were multivariate and bivariate drought indices. A grid-based analysis for the SRI also confirmed that R scoring was a better method since it avoided overfitting and mis-categorization. Comparing the results of the CBS-SVR with those of the SVC revealed that the CBS-SVR performed better than the SVC for eight out of ten drought indices. The results suggested that using the CBS-SVR with the proposed category-based scoring for tuning hyperparameters in the cross-validation of SVR avoided overfitting and mis-categorization.

The ESSVR improved drought prediction by reducing the impacts of non-stationarity from temperature time series in a warming climate. Comparing the results of the traditional SVR and ESSVR in the RRB demonstrated the improvements for most of the drought indices, particularly the ones with higher sensitivity to temperature. The comparison of the spatial distributions of cost parameters in ESSVR and SVR revealed that the extreme (highest and lowest) values of epsilon and gamma were mostly assigned by SVR, which increased the risk of overfitting in SVR. In contrast, ESSVR provided better results. Therefore, drought prediction

can be improved by removing the non-stationarity, thus providing a more accurate drought prediction, especially in a warming climate.

Although this dissertation research improved the identification, categorization, and prediction of droughts, especially in cold climate regions, further improvements can be made on the proposed methodologies. HADI and SHADI were tested in the RRB, which is a cold climate region in prairie type. The performances of HADI and SHADI can be tested in the mountainous cold climate regions, where dominant hydroclimatic processes have different impacts on hydroclimatic variables. The first principal component (PC) was used for deriving HADI and SHADI. Although the first PC had the highest percentage of eigenvalues in the study period, this percentage was low especially during warm seasons due to collinearity. The possibility to improve drought identification by adding the second PC can be investigated in the future studies. In addition, the customized drought categorization can be tested in different regions with various climate conditions, instead of a specific area with one type of climate. The variability of threshold levels with geographic locations and the impacts of spatial distribution of droughts on threshold levels can be examined. In this research, to convert a non-stationarity time series of temperature into many stationary time series for developing the ESSVR model, two change points and the window-based change point detection method were used after testing different change point detection methods and different numbers of change points. More change points in a longer time series can be considered for further analyses. To capture the major change points caused by a warming climate and ignore the natural change points due to monthly, seasonal, and interannual variabilities of temperature, a two-year period was selected as the band width for sliding window for change point detection in this research. Different band widths and their impacts on the results can be examined in the future studies. For tuning the hyperparameters in the ESSVR and CBS-SVR, a wider range of hyperparameters can be tested. In this study, the training dataset was divided into stationary subsets based on the identified change points, and each stationary dataset was further divided into k-fold for cross-validation.

However, the training dataset can be directly divided into k-fold based on the identified change points in the future studies.

Overall, the results and conclusions from this research accentuated the significance of the commonly-ignored hydrologic processes in cold climate regions in drought identification, the spatial distribution of droughts in drought categorization, and the impacts of non-stationarity of time series in drought prediction. The new methodologies developed in this study improved the identification, categorization, and prediction of droughts, filled the relevant research gaps, and provided more accurate drought information for stakeholders.